



UNIVERSITAT DE
BARCELONA

Novel therapeutic approaches against Head and Neck Squamous Cell Carcinoma

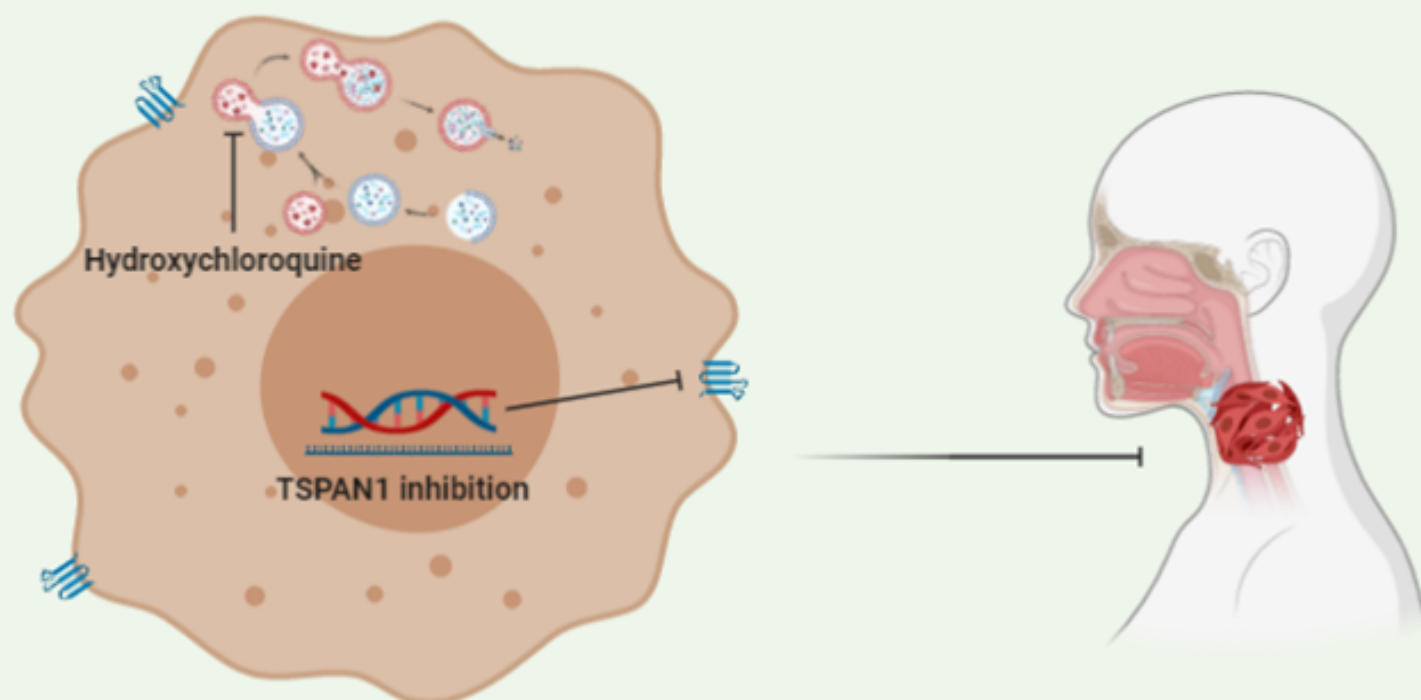
Yoelsis Garcia Mayea

ADVERTIMENT. La consulta d'aquesta tesi queda condicionada a l'acceptació de les següents condicions d'ús: La difusió d'aquesta tesi per mitjà del servei TDX (www.tdx.cat) i a través del Dipòsit Digital de la UB (diposit.ub.edu) ha estat autoritzada pels titulars dels drets de propietat intel·lectual únicament per a usos privats emmarcats en activitats d'investigació i docència. No s'autoritza la seva reproducció amb finalitats de lucre ni la seva difusió i posada a disposició des d'un lloc aliè al servei TDX ni al Dipòsit Digital de la UB. No s'autoritza la presentació del seu contingut en una finestra o marc aliè a TDX o al Dipòsit Digital de la UB (framing). Aquesta reserva de drets afecta tant al resum de presentació de la tesi com als seus continguts. En la utilització o cita de parts de la tesi és obligat indicar el nom de la persona autora.

ADVERTENCIA. La consulta de esta tesis queda condicionada a la aceptación de las siguientes condiciones de uso: La difusión de esta tesis por medio del servicio TDR (www.tdx.cat) y a través del Repositorio Digital de la UB (diposit.ub.edu) ha sido autorizada por los titulares de los derechos de propiedad intelectual únicamente para usos privados enmarcados en actividades de investigación y docencia. No se autoriza su reproducción con finalidades de lucro ni su difusión y puesta a disposición desde un sitio ajeno al servicio TDR o al Repositorio Digital de la UB. No se autoriza la presentación de su contenido en una ventana o marco ajeno a TDR o al Repositorio Digital de la UB (framing). Esta reserva de derechos afecta tanto al resumen de presentación de la tesis como a sus contenidos. En la utilización o cita de partes de la tesis es obligado indicar el nombre de la persona autora.

WARNING. On having consulted this thesis you're accepting the following use conditions: Spreading this thesis by the TDX (www.tdx.cat) service and by the UB Digital Repository (diposit.ub.edu) has been authorized by the titular of the intellectual property rights only for private uses placed in investigation and teaching activities. Reproduction with lucrative aims is not authorized nor its spreading and availability from a site foreign to the TDX service or to the UB Digital Repository. Introducing its content in a window or frame foreign to the TDX service or to the UB Digital Repository is not authorized (framing). Those rights affect to the presentation summary of the thesis as well as to its contents. In the using or citation of parts of the thesis it's obliged to indicate the name of the author.

Novel therapeutic approaches against Head and Neck Squamous Cell Carcinoma



Yoelsis Garcia Mayea
PhD Thesis 2020
University of Barcelona

UNIVERSIDAD DE BARCELONA

DEPARTAMENTO DE GENÉTICA, MICROBIOLOGÍA Y ESTADÍSTICA

PROGRAMA DE DOCTORADO EN GENÉTICA

***Novel therapeutic approaches against Head and
Neck Squamous Cell Carcinoma***

Memoria presentada por **Yoelsis Garcia Mayea** para optar al grado de **Doctor**
por la **Universidad de Barcelona**.

Trabajo realizado en el Grupo de Investigación Biomédica con Células Madre de
Cáncer, Institut de Recerca del Hospital Universitario Vall d'Hebron, bajo la
dirección de la **Dra. Matilde Esther Leonart Pajarín**.



La directora,

Dra. Matilde Esther Leonart Pajarín



El doctorando,

Yoelsis Garcia Mayea



El tutor,

Dr. Pere Martínez Serra

ABSTRACT

Head and neck squamous cell carcinoma (HNSCC) is usually diagnosed in advanced stages. The treatment has not changed much on the last decades, being limited to surgery followed by radiotherapy and/or chemotherapy [mainly cisplatin (CDDP) and 5-fluorouracil (5-FU)]. However, the acquisition of chemotherapy resistance is very common, which usually leads to recurrences and metastases. On the other hand, the role of autophagy in HNSCC is not clearly defined. This is the reason why in this thesis we have proposed: 1) to determine the role of autophagy in HNSCC models and its relationship with chemotherapy resistance and other clinical parameters; 2) to identify target proteins involved in the acquisition of chemotherapy resistance in HNSCC models whose modulation of its expression and/or activity could be of clinical and therapeutic interest.

From a retrospective immunohistochemistry (IHC) study, we found that the expression of the autophagy markers sequestosome-1 (p62/SQSTM1) and microtubule-associated proteins 1A/1B light chain 3B (LC3), as well as prostate tumor-overexpressed gene 1 protein (PTOV1), could be considered markers of poor clinical prognosis in laryngeal cancer patients. We found overexpression of PTOV1 and the autophagy-related protein 5 (ATG5) in HNSCC biopsy-derived cell lines with innate resistance to CDDP. Likewise, in general, autophagy activation and/or PTOV1 overexpression occurred in three non-metastatic HNSCC cell lines in which resistance to CDDP and 5-FU had previously been generated, as well as in cancer stem cells (CSCs). Furthermore, PTOV1 overexpression induced autophagy in JHU029 laryngeal cell line. Finally, we found that autophagy inhibition with hydroxychloroquine (HCQ), alone or in combination with CDDP or 5-FU, could be

Abstract

an attractive therapeutic alternative for HNSCC patients with chemotherapy resistance.

In addition, a comparative proteomic study revealed tetraspanin 1 (TSPAN1) as a target involved in chemotherapy resistance in HNSCC models. In this sense, TSPAN1 depletion decreased cell proliferation, induced apoptosis, and sensitized HNSCC cell lines and biopsy-derived cell lines to chemotherapeutic agents like CDDP and dasatinib. Moreover, TSPAN1 depletion reduced autophagy and blocked the activation of proto-oncogene tyrosine-protein kinase SRC (SRC), protein kinase B (AKT) and mitogen-activated protein kinase (ERK). In addition, TSPAN1 expression was associated to epithelial–mesenchymal transition (EMT) activation in mice tumors and HNSCC patient biopsies. Overall, TSPAN1 inhibition could be a promising therapeutic strategy to improve the current treatment against HNSCC patients.

INDEX

I. Introduction	25
1.1. HNSCC: incidence, risk factors, current treatments, and mortality	25
1.1.1. Laryngeal and pharyngeal cancer: incidence, mortality and anatomical parts	26
1.2. Genetic and epigenetic alterations in HNSCC	29
1.3. CSCs biology	30
1.4. Mechanisms of therapy resistance	34
1.4.1. ATP-binding cassette (ABC) transporters	37
1.4.2. Microenvironment modulation	39
1.4.3. The Hippo pathway	41
1.4.4. Epigenome	42
1.4.5. Exosomes	44
1.4.6. DNA damage response (DDR)	46
1.4.7. Unfolded protein response (UPR)/endoplasmic reticulum stress (ERS)	47
1.4.8. Metabolism	49
1.4.9. Apoptosis evasion	52
1.5. Autophagy and cancer	53
1.5.1. Types of autophagy	53
1.5.2. Autophagy is a homeostatic cell process	56
1.5.3. Autophagy flux and cancer	56
1.5.4. Autophagy inhibition as a means of anticancer therapy	58
1.6. Tetraspanin family	60
1.6.1. Structure of tetraspanins	60
1.6.2. Tetraspanins: post-translational modifications, interactions and biological relevance	61
1.6.3. Tetraspanin 1 and cancer	67
II. Hypotheses	73
III. Objectives	77
IV. Materials and methods	81
4.1. Biological samples	81

Index

4.1.1.	Patients and tissue samples.....	81
4.1.2.	Cell lines and culture conditions.....	83
4.2.	Transfections	85
4.3.	Functional assays	87
4.3.1.	Analyses of side population (SP)	87
4.3.2.	Viability assays	87
4.3.3.	Drug assays	88
4.3.4.	Proliferation assays	89
4.3.5.	Colony formation assay.....	90
4.3.6.	Apoptosis detection by flow cytometry	90
4.3.7.	Autophagy analyses by TEM	91
4.4.	RNA analyses.....	92
4.4.1.	Total RNA extraction: quality and quantification	92
4.4.2.	Reverse transcription reaction.....	93
4.4.3.	Quantitative real-time PCR.....	93
4.5.	Proteomic analysis.....	94
4.5.1.	Sample preparation and LC-MS/MS analyses	95
4.5.2.	Peptide 10-plex TMT labeling.....	96
4.5.3.	Peptide fractionation.....	96
4.5.4.	NanoLC-(Orbitrap) MS analysis	97
4.6.	Protein analyses.....	98
4.6.1.	Protein extraction and quantification	98
4.6.2.	Protein analyses by Western Blot (WB)	99
4.6.3.	Immunohistochemistry.....	101
4.6.4.	Immunocytochemistry (ICC).....	103
4.7.	Animal models.....	104
4.8.	Statistical analyses.....	105
V.	Results	109
5.1.	Autophagy inhibition as a promising therapeutic target for HNSCC	109
5.1.1.	Laryngeal cancer location distinguishes three different clinical entities	109
5.1.2.	Markers of significance in laryngeal cancer biopsies	110

5.1.3. PTOV1 and ATG5 proteins are preferentially overexpressed in those biopsy-derived cell lines that exhibit higher CDDP-resistance levels	113
5.1.4. Autophagy markers and PTOV1 are associated with drug resistance in HNSCC cancer cells	117
5.1.5. PTOV1 overexpression induces autophagy.....	122
5.1.6. Autophagy inhibition in HNSCC cell lines and biopsy-derived cell lines	124
5.2. TSPAN1: a novel protein involved in HNSCC chemoresistance	129
5.2.1. TSPAN1 protein is upregulated in CDDP-resistant HNSCC cells.....	129
5.2.2. TSPAN1 depletion induces sensitivity of HNSCC cells to chemotherapeutic agents.....	131
5.2.3. TSPAN1 depletion induces apoptosis in HNSCC cells.....	136
5.2.4. TSPAN1 depletion downregulates several signaling cascades with SRC kinase signaling as a central node	138
5.2.5. TSPAN1-depleted cells decrease tumor formation ability and metastatic capacity in mice	142
5.2.6. The expression of TSPAN1 correlate with active SRC and EMT features in patient samples.....	145
VI. Discussion	153
VII. Conclusions.....	173
VIII. References.....	177
IX. Annexes.....	203
Appendix 1. List of patients with laryngeal cancer from HUVH studied by IHC for the expression of LC3, ATG5, p62 and PTOV1 proteins.....	203
Appendix 2. Clinical and pathological characteristics of the 106 patients from HUCA.....	205
Appendix 3. Concentrations of CDDP, 5-FU and HCQ used in the combinatorial drug assays.....	207
Appendix 4. Proteins identified in the proteomic study.....	207
Appendix 5. ANOVA test.....	207
Appendix 6. <i>Post-Hoc</i> analysis.....	207
Appendix 7. Proteins commonly deregulated in CCL-138-R cells and CSCs	208
X. Publications.....	211

INDEX OF FIGURES

Figure 1. Estimated age-standardized incidence (blue) and mortality (red) rates in 2018 for different cancer types..... 27

Figure 2. Estimated age-standardized incidence (blue) and mortality (red) rates in 2018 by continent..... 28

Figure 3. Anatomy of the larynx and pharynx. 29

Figure 4. Highway toward malignancy..... 32

Figure 5. Resistance mechanisms in CSCs 38

Figure 6. Schematic representation of the Hippo signaling pathway..... 42

Figure 7. Perspectives of normal cells, cancer cells, and CSCs 51

Figure 8. Autophagy subtypes described in mammals 54

Figure 9. Schematic representation of the autophagy process in mammals. 55

Figure 10. General structure of a consensus tetraspanin protein. 60

Figure 11. Tetraspanin web and different possible interactions between partner domains. 62

Figure 12. Overall survival of laryngeal cancer patients depending on tumor location. 109

Figure 13. Expression pattern of ATG5, LC3, PTOV1 and p62 in biopsies from laryngeal cancer patients..... 111

Figure 14. Significant associations with clinical relevance in laryngeal cancer patients through IHC analyses..... 112

Figure 15. Patients with supraglottic tumors treated and not treated with chemotherapy and its association with LC3 expression and survival 113

Figure 16. CDDP-survival curves of 13 biopsy-derived cell lines from larynx and pharynx..... 114

Figure 17. Biopsy-derived cell lines from laryngeal and pharyngeal cancer patients and their relation with autophagy markers and PTOV1 115

Figure 18. CDDP-response curves and IC50 values from parental and CDDP-resistant HNSCC cell lines..... 117

Figure 19. Resistant HNSCC established cell lines show increased levels of PTOV1, autophagy-related proteins and autophagy vesicles 119

Index of figures

Figure 20. Representative images of phenotypic characteristics of the cell lines JHU029, HTB-43, CCL-138, and SCC-25 under adherent and non-adherent conditions.....	120
Figure 21. Expression of SCs and EMT genes using qRT-PCR.....	120
Figure 22. CSCs are more resistance to CDDP and 5-FU than the whole cellular population (parental cells).....	121
Figure 23. Side Population in HTB-43 and CCL-138 cell lines (parental versus CDDP-resistant cells).....	122
Figure 24. PTOV1 overexpression induces autophagy and is mainly located in the cytoplasm of CDDP-resistant cells.....	123
Figure 25. Examples of nuclear PTOV1 expression in sporadic cancer cells from laryngeal cancer biopsies	124
Figure 26. CDDP-resistant HNSCC cell lines are more sensitive to HCQ than the parental cells.....	125
Figure 27. Therapeutic benefit of HCQ in HNSCC cells regarding their CDDP-resistance levels and autophagy dependence	127
Figure 28. TSPAN1 is identified as a protein involved in HNSCC chemoresistance.....	130
Figure 29. TSPAN1 depletion inhibits cell proliferation.....	132
Figure 30. TSPAN1 depletion sensitizes HNSCC cells to CDDP	133
Figure 31. TSPAN1 depletion under an alternative specific mix of 30 siRNAs (siPool) sensitizes HNSCC cells to the effects of CDDP.....	134
Figure 32. TSPAN1 depletion sensitizes HNSCC cell lines to dasatinib treatment	135
Figure 33. TSPAN1 depletion induces apoptosis in HNSCC cells	137
Figure 34. Characterization of TSPAN1 downstream effectors	140
Figure 35. The inhibition of SRC activation (p-SRC) through dasatinib does not affect TSPAN1 expression either TSPAN1 downstream pathway	141
Figure 36. The impact of TSPAN1 depletion <i>in-vivo</i>	143
Figure 37. Phenotypic characteristics and proliferative potential of tumors formed in mice.....	144
Figure 38. <i>Ex-vivo</i> analysis of micrometastases under TSPAN1 depletion.	144
Figure 39. Protein expression assay of TSPAN1 and E-cadherin in human biopsies from HNSCC patients.....	147

Figure 40. TSPAN1 expression is associated with active SRC and tends to be associated with poorly differentiated tumors	148
Figure 41. TSPAN1 expression at mRNA level	149
Figure 42. TSPAN1 in relation to patient survival	150
Figure 43. Proposed mechanism for the acquisition of TSPAN1-mediated chemoresistance in HNSCC	166

INDEX OF TABLES

Table 1. Protein interactions with the tetraspanins family members CD9, CD53, CD81, CD82, CD151, CD63, CD37..... 65

Table 2. Clinical and pathological characteristics of the patients with laryngeal cancer from HUVH included in the IHC study..... 81

Table 3. Clinical and pathological characteristics of the patients from HUCA included in the IHC study..... 82

Table 4. Patient samples included in the IHC studies101

Table 5. Clinical information of the 13 HNSCC patients from whom the biopsy-derived cell lines were generated.116

ABBREVIATIONS

A

ABC transporters: ATP-binding cassette transporters

ABCB1/MDR1: ATP-binding cassette sub-family B member 1/ Multidrug resistance protein 1/p-glycoprotein

ABCC1/MRP1: ATP binding cassette sub-family C member 1/ multidrug resistance-associated protein 1

ABCC2/MRP2: ATP-binding cassette sub-family C member 2/multidrug resistance-associated protein 2

ABCC5/MRP5: ATP-binding cassette sub-family B member 5/multidrug resistance-associated protein 5

ABCG2: ATP-binding cassette sub-family G member 2

ADAM10: disintegrin and metalloproteinase domain-containing protein 10

AKT: protein kinase B

pAKT: active AKT

ALDH1: aldehyde dehydrogenase 1

Alix/PDCD6: programmed cell death 6-interacting protein

AMPK: AMP-activated protein kinase

APC: antigen-presenting cells

ARF6: ADP-ribosylation factor 6

ATF4: cyclic AMP-dependent transcription factor ATF-4

ATF6 α : activating transcription factor 6 α

ATG5: autophagy-related protein 5

ATM: ataxia telangiectasia mutated

ATR: ataxia telangiectasia and RAD3-related protein

B

BAI2: brain-specific angiogenesis inhibitor 2

BAK: apoptosis regulator BAK

BAX: apoptosis regulator BAX

BCA: bicinchoninic acid

B-CAM/Lu: basal cell adhesion molecule/Lutheran protein

Bcl-2: apoptosis regulator Bcl-2

BCL_{XL}: B-cell lymphoma-extra large

BID: BH3-interacting domain death agonist

BIK: Bcl-2-interacting killer

BMI1: polycomb complex protein BMI-1

BRCA1: breast cancer type 1 susceptibility protein

BSA: bovine serum albumin

C

CAF: cancer-associated fibroblasts

CAIX: carbonic anhydrase IX

CCND1: G1/S-specific cyclin-D1

CD133: CD133 antigen/ prominin-1

CD151: CD151 antigen

CD19: B-lymphocyte antigen CD19

CD44: CD44 antigen

CD55: decay-accelerating factor

Abbreviations

CD63: CD63 antigen/tetraspanin-30

CD81: CD81 antigen/tetraspanin-28

CD9: CD9 antigen/tetraspanin-29

CDDP: cisplatin

CDKN2A: cyclin-dependent kinase inhibitor 2A

CEIC: Comité Ético de Investigación Clínica

c-FLIP: cellular FLICE (FADD-like IL-1 β -converting enzyme)-inhibitory protein

CHK1: serine/threonine-protein kinase CHK1

CHK2: serine/threonine-protein kinase CHK2

CQ: chloroquine

CSCs: cancer stem cells

CUL3: cullin 3

D

DDR: DNA damage response

DDX3X: dead-box helicase 3 X-linked

DNA-PK: DNA-dependent protein kinase

DSB: double-strand breaks

E

E2F1: E2F transcription factor 1

EC1: small extracellular loop

EC2: large extracellular loop

EGFR: epidermal growth factor receptor

EMT: epithelial–mesenchymal transition

EpCAM: epithelial cell adhesion molecule

ER: endoplasmic reticulum

ERCC1: DNA excision repair protein

ERK: mitogen-activated protein kinase

pERK: active ERK

ERS: endoplasmic reticulum stress

EWI-2: Glu-Trp-Ile EWI motif-containing protein 2

F

5-FU: 5-fluorouracil

FBS: fetal bovine serum

FGFR: fibroblast growth factor receptor

G

GFR: GDNF family receptor

GLUT1: glucose transporter type 1

H

HCQ: hydroxychloroquine

HDAC1: histone deacetylases class I

HIF: hypoxia-inducible factor

HNSCC: head and neck squamous cell carcinomas

HPV: human papilloma virus

HUCA: Hospital Universitario Central de Asturias

HUVH: Hospital Universitario Vall d'Hebron

I

IAPs: inhibitors of apoptosis family proteins

IC50: half maximal inhibitory concentration

ICAM-1: intracellular cell adhesion molecule 1

IHC: immunohistochemistry

IL-10: interleukin-10

IL-17: interleukin-17

IL-1 β : interleukin 1 beta

IL-4: interleukin-4

IL-6: interleukin-6

IL-8: interleukin-8

IMP2: insulin-like growth factor mRNA-binding protein 2

IRE1 α : inositol-requiring enzyme-1 α

IRS: immunoreactive score

J

JAK: Janus kinase

K

KDM1A: lysine-specific histone demethylase 1A

KLF4: Krueppel-like factor 4

KRAS: KRAS proto-oncogene

L

LC3: microtubule-associated proteins 1A/1B light chain 3B

lncRNAs: long noncoding RNAs

LPI: lysophosphatidylinositol

M

3-MA: 3-methyladenine

Mcl-1: induced myeloid leukemia cell differentiation protein Mcl-1

MDR: multidrug resistance

MHC: major histocompatibility complex

MIIC: major histocompatibility complex class II compartments

miRNAs: microRNAs

MLL: mixed-lineage leukemia

mTOR: mammalian target of rapamycin

MMP: matrix metalloproteinase

N

NANOG: homeobox protein NANOG

NC: negative control

ncRNA: noncoding RNAs

NF- κ B: nuclear factor NF-kappa- β

Notch: neurogenic locus notch homolog protein

NOTCH1: notch receptor 1

Noxa: phorbol-12-myristate-13-acetate-induced protein 1

NSD1: nuclear receptor binding SET domain protein 1

O

OCT4: octamer-binding transcription factor 4

OXPPOS: oxidative phosphorylation

P

p53: tumor protein p53

p62/SQSTM1: sequestosome-1

PARP-1: poly [ADP-ribose] polymerase 1

Abbreviations

PBS: phosphate-buffered saline

PD-1: programmed cell death protein-1

PDK2: pyruvate dehydrogenase (acetyl-transferring)
kinase isozyme 2

PDK4: pyruvate dehydrogenase (acetyl-transferring)
kinase isozyme 4

PERK: protein kinase R-like endoplasmic reticulum
kinase

PI: propidium iodide

PI3K: phosphatidylinositol 3-kinase

PI4K: phosphatidylinositol 4-kinase

PIK3CA: phosphatidylinositol-4,5-bisphosphate 3-
kinase catalytic subunit alpha

PKC: protein kinase C

PS: phosphatidylserine

pSRC: active SRC

PTEN: phosphatidylinositol 3,4,5-trisphosphate 3-
phosphatase and dual-specificity protein
phosphatase PTEN

PTOV1: prostate tumor-overexpressed gene 1
protein

PUMA: p53 up-regulated modulator of apoptosis

Q

qRT-PCR: quantitative real-time PCR

R

RAD3: protein kinase rad3

RAD50: DNA repair protein RAD50

RAD51: DNA repair protein RAD51 homolog 1

REDD1/DDIT4: protein regulated in development
and DNA damage response 1/DNA damage-
inducible transcript 4 protein

ROS: reactive oxygen species

RT: room temperature

S

SCs: stem cells

siRNA: small interfering RNA

siTSPAN1: siRNA against TSPAN1

SNAIL1: zinc finger protein SNAIL1

SNAIL2: zinc finger protein SNAIL2

SOX2: transcription factor SOX-2

SP: side population

SRC: proto-oncogene tyrosine-protein kinase SRC

STAT: signal transducer and activator of transcription

T

TADG15: serine protease TADG-15

TAZ: Tafazzin

TEAD1-4: transcriptional enhancer factor TEF-1-4

TEM: transmission electron microscopy

TGF: transforming growth factor

TMA: tissue microarray

TMT: tandem mass tag

TNF α : tumor necrosis factor-alpha

TP53: tumor protein p53

TRAF3: TNF receptor-associated factor 3

TSG101: tumor susceptibility gene 101 protein

TSPAN1: tetraspanin 1

Abbreviations

T-TBS: 1X tween-20-tris-buffered saline

TWIST: twist-related protein

TWIST1: twist-related protein 1

U

UPR: unfolded protein response

V

VCAM-1: vascular cell adhesion molecule 1

W

WB: western blot or western blotting

WIP: WASP-interacting protein

Wnt: protein Wnt

Y

YAP1: yes1 associated transcriptional regulator

Z

ZEB1: zinc finger E-box-binding homeobox 1

ZEB2: E-box-binding homeobox 2

INTRODUCTION

I. INTRODUCTION

1.1. HNSCC: incidence, risk factors, current treatments, and mortality

Cancer treatment is constantly evolving, and life expectancy has increased for certain cancer types in the last 50 years. Nonetheless, cancer is still the third leading cause of death from non-communicable diseases worldwide ¹. The squamous cell carcinoma is the most common malignancy of head and neck location. HNSCC is the sixth most commonly diagnosed cancer worldwide, with an incidence of about 600,000 new cases per year, accounting for 1-2% of all cancer deaths worldwide (about 300,000 deaths per year) ²⁻⁵. Among the main external risk factors for the development of HNSCC are smoking, alcohol dependence and human papilloma virus (HPV) infections. HPV-positive patients tend to respond better to conventional therapy ^{6,7}. However, HPV-negative and tobacco/alcohol-related patients have a worse clinical prognosis, as well as a much higher rate of mutations in tumor protein p53 (*TP53*), G1/S-specific cyclin-D1 (*CCND1*), cyclin-dependent kinase inhibitor 2A (*CDKN2A*) and fibroblast growth factor receptor 1 (*FGFR1*) than HPV-positive patients ⁸⁻¹⁰. Risk stratification for HNSCC is determined by anatomic site, stage and histological characteristics of the tumors ¹⁰, and treatment selection is not influenced by molecular testing ⁶.

Early-stage HNSCC is generally treated with a single treatment modality (e.g., surgery or radiotherapy). Moderately advanced disease is treated with combined strategies including surgery, radiotherapy, and systemic therapies. For example, surgically resected early-stage HNSCC with risk factors of recurrence or resectable moderately advanced HNSCC receive adjuvant radiation or chemoradiation based on cisplatin; moderately advanced (resectable or unresectable) HNSCC can be treated with chemoradiation based on cisplatin for fit patients, and with

Introduction

bioradiation based on cetuximab or radiation alone for unfit or fragile patients; and metastatic patients are treated with chemotherapy and/or new systemic agents in clinical trials. Current systemic treatments include combinations of taxanes (e.g., docetaxel), platinum compounds (e.g., CDDP or carboplatin), the anti-metabolite 5-fluorouracil (5-FU), and the anti-epidermal growth factor receptor (EGFR) antibody cetuximab ^{6,11,12}. New therapeutic alternatives that have been recently approved by different regulatory agencies include *TP53*-based gene therapy (e.g., Gendicine®); oncolytic adenovirus therapy (e.g., ONYX-015 and H101); and immunotherapy (e.g., the two anti-programmed cell death protein-1 (PD-1) antibodies pembrolizumab and nivolumab) ^{5,13}.

The high mortality rate of HNSCC is mainly due to the presence of local recurrences in cervical lymph nodes, although distant metastases also occur with less frequency ¹⁴. Response rates to chemotherapeutic drugs range from 60-80%; however, there are high rates of resistance, which often leads to locoregional recurrence ¹⁵⁻¹⁷ and metastasis ². Moreover, exposure to cetuximab treatment can also develop resistance throughout the upregulation of the EGFR-downstream pathways ¹⁸. Besides, the therapeutic doses of treatments needed are often too toxic for the patients and they need to space chemotherapeutic sessions, a fact that contributes to the acquisition of resistance. Therefore, five-year survival rates for HNSCC patients have remained low (30-60%) for the past 50 years ^{5,19-21}.

1.1.1. Laryngeal and pharyngeal cancer: incidence, mortality and anatomical parts

Within the head and neck category, there are cancers of the thyroid and salivary glands, as well as in the upper aerodigestive tract. The latter represents about 90% of all cases diagnosed with HNSCC ²². Cancers of the upper aerodigestive tract

usually appear in the oral cavity, nasopharynx, oropharynx, hypopharynx, and larynx ⁶. According to data provided by the Global Cancer Observatory, International Agency for Research on Cancer (<http://gco.iarc.fr/>, 2018 report), the incidence of laryngeal and pharyngeal cancer in the Spanish population, older than 50 years, is 10 and 6 times higher in men than in women, respectively. In this regard, laryngeal cancer has a worldwide incidence of 8.7 (per 100,000 inhabitants), and a mortality rate of 4.7 (per 100,000 inhabitants), considering as reference a population older than 50 years (without differentiating between genders). However, this incidence and mortality are almost double in men of the same age range (16.1 and 8.7, respectively). Moreover, pharyngeal cancers (considering oropharynx, hypopharynx and nasopharynx cancers) have an incidence and mortality even higher than laryngeal cancers: 20.7 (per 100,000 inhabitants) and 12 (per 100,000 inhabitants), respectively (**Figure 1**).

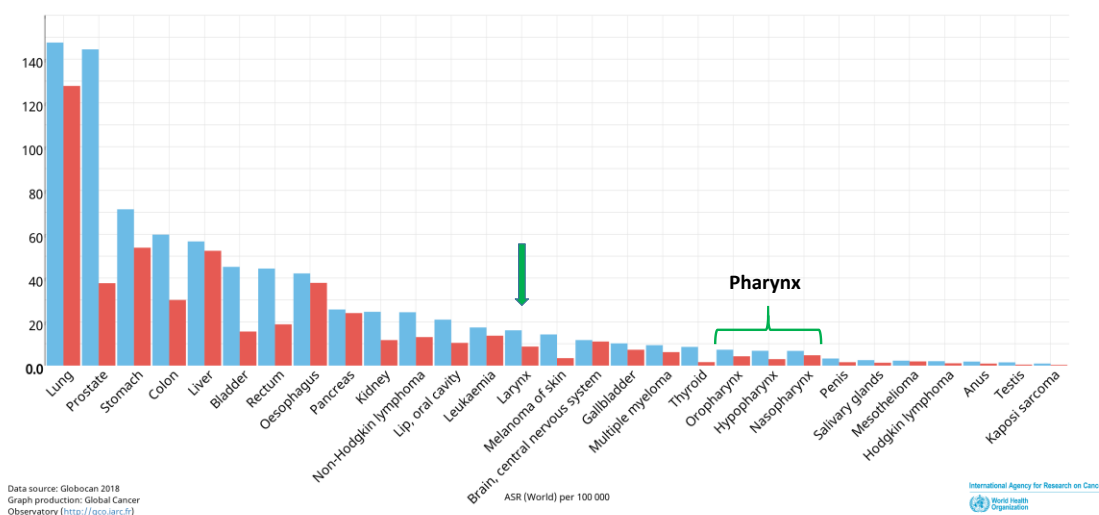


Figure 1. Estimated age-standardized incidence (blue) and mortality (red) rates in 2018 for different cancer types, worldwide, males, ages >50. Laryngeal cancer (arrow) and different subtypes of pharyngeal cancer (bracket) have been indicated in the figure. Image adapted from the Global Cancer Observatory, International Agency for Research on Cancer, [Cited on July 07, 2020]. Available in: <http://gco.iarc.fr/>.

Moreover, Europe is the continent most affected worldwide with laryngeal and pharyngeal cancer, with an incidence rate of 24.6 and 27.7 (per 100,000

Introduction

inhabitants) and a mortality rate of 12.0 and 14.8 (per 100,000 inhabitants), respectively (**Figure 2**).

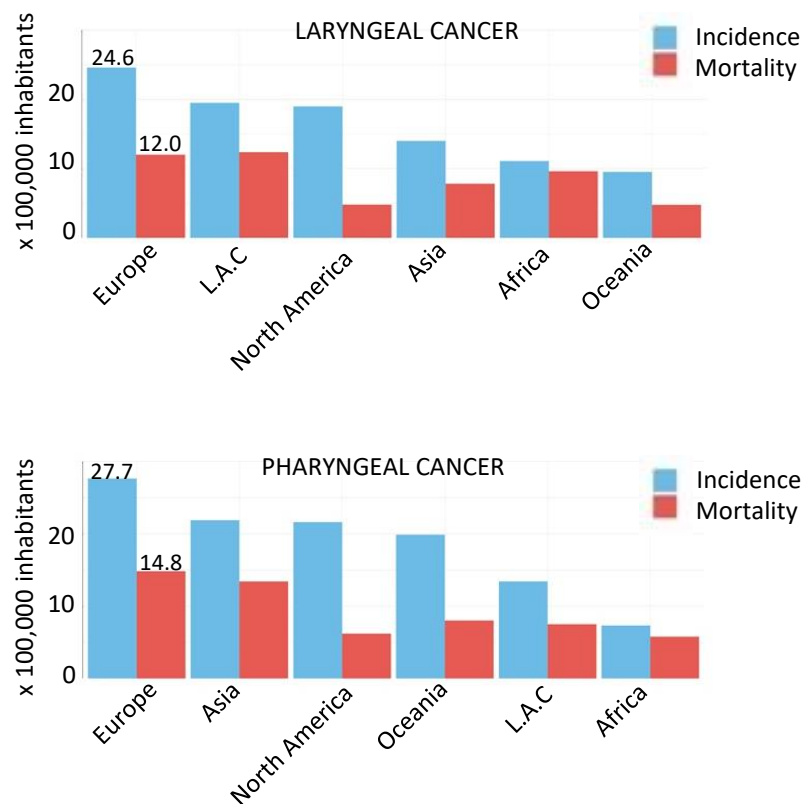


Figure 2. Estimated age-standardized incidence (blue) and mortality (red) rates in 2018 by continent, larynx (upper panel) and pharynx (bottom panel), males, ages >50. Image adapted from the Global Cancer Observatory, International Agency for Research on Cancer, [Cited on July 07, 2020]. Available in: <http://gco.iarc.fr/>. L.A.C, Latin America and the Caribbean.

The presence of early symptoms (hoarseness) in patients with laryngeal glottic tumors allows them to be usually diagnosed in the early stages of the disease. However, most patients with HNSCCs are usually diagnosed in very advanced stages, and more than half of them have cervical lymph node metastases, due to the absence of symptoms ^{19,23,24}. The main anatomical parts of the larynx and pharynx are shown in **Figure 3**.

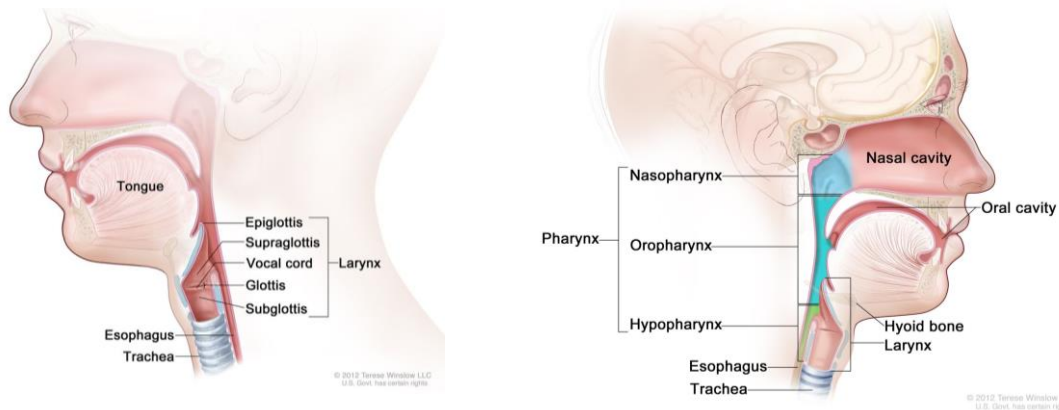


Figure 3. Anatomy of the larynx and pharynx. The figure shows the main anatomical areas related to the classification of larynx (left panel) and pharynx (right panel) cancers. Images adapted from the National Cancer Institute (USA.gov), [Cited on July 07, 2020]. Available in: <https://www.cancer.gov/types/head-and-neck>

1.2. Genetic and epigenetic alterations in HNSCC

Recent studies using next-generation sequencing have identified the genetic variability of HNSCC tumors, as well as their clinical and therapeutic implications^{10,25,26}. The most common mutations in the HPV-associated tumors group were found in the following genes: dead-box helicase 3 X-linked (*DDX3X*), fibroblast growth factor receptor (*FGFR*) 2/3, phosphatidylinositol-4,5-bisphosphate 3-kinase catalytic subunit alpha (*PIK3CA*), KRAS proto-oncogene (*KRAS*), mixed-lineage leukemia (*MLL*) 2/3 and notch receptor 1 (*Notch1*). Moreover, loss of TNF receptor-associated factor 3 (*TRAF3*) and the amplification of the cell cycle gene E2F transcription factor 1 (*E2F1*) were also common in this group of patients. On the other hand, in the group of smoking-related HNSCC (HPV-negative) the most common genetic alterations were: loss-of-function *TP53* mutations, *CDKN2A* inactivation, and mutations in *MLL 2*, cullin 3 (*CUL3*), nuclear receptor binding SET domain protein 1 (*NSD1*), *PIK3CA*, and neurogenic locus notch homolog protein (*Notch*) genes. Notably, the presence of mutated *TP53* is the most common genetic alteration in HNSCC^{10,27}. Inactivation of tumor protein p53 (p53) implies a worse

Introduction

clinical outcome due to its role in cell cycle control and induction of apoptosis in the face of DNA damage. That genetic alteration has been associated with higher tumor stages, lymphatic metastases and resistance to radiotherapy^{28,29}. Gendicine, a recombinant human p53 adenovirus used previously in clinical trials, has been shown to significantly improve the response of HNSCC patients to radiotherapy³⁰ and reduced the recurrence rates of tongue and gingival tumors (a type of oral squamous cell carcinoma)³¹. *EGFR*, *CCND1* and *FGFR1* amplifications also occurred in HPV-negative tumors and have been considered genomic alterations susceptible of being targetable²⁷.

The high rates of genetic alterations found in important pathways such as FGFR and phosphatidylinositol 3-kinase (PI3K) in HNSCC tumors constitute attractive therapeutic targets. Eliminating or counteracting the molecular changes undergone by the tumor, which are responsible for the high genetic heterogeneity, could be the key for the treatment of invasive lesions and recurrence, as well as to improve patient survival^{5,27}.

1.3. CSCs biology

CSCs present a characteristic phenotype that sets them apart from the majority of more differentiated progenies. It has been proposed that CSCs can be recognized based on their functional properties: i) the ability to self-renew, by which they are progenitors of their own population; ii) the capacity to initiate tumor formation from a limited number of cells injected in mice; iii) the capacity to differentiate into the diverse cell types present in a tumor (e.g., epithelial cells, cancer associated fibroblast); and iv) therapy resistance³²⁻³⁴. The exploitation of these characteristics makes tumors very heterogeneous³⁴⁻³⁶. In a specific tumor type, different CSCs populations coexist dictated by genetic and non-genetic factors that

contribute to modulate their differentiation and self-renewal abilities ^{34,37}. The main stem cells (SCs) signaling pathways are the Wnt/ β -catenin, Notch and Hedgehog, which govern SCs maintenance, cell differentiation, cell proliferation and tissue polarity, among others. Notch pathway has also been implicated in chemoresistance and EMT ^{38,39}. Likewise, Notch1 inhibition significantly reduces the CSCs population and its ability to self-renew both *in-vitro* and *in-vivo*, and has a synergistic effect with CDDP, docetaxel and 5-FU ⁴⁰.

It is well established that cancer arises because of mutations that accumulate with time and generate the genetic diversity of a tumor. Mutations that give some advantage in growth are recognized as “drivers” of the transformation process, while “passenger” mutations are believed to be accompanying changes without an effect *per se* but contribute to growth advantages. When a driver mutation occurs in normal cells, changes at genomic, transcription and translation levels may lead cells to acquire proliferative properties (benign tumors). Additional driver mutations, which have profound biological effects (in contrast to passenger mutations) might be acquired, converting benign into malignant cells. CSCs can originate from differentiated cancer cells (which contain a high load of mutations) or from mutations occurring in normal SCs. Given the mechanisms governing stemness by which SCs shield their DNA from external and internal damage (e.g., robust DNA damage response (DDR), high antioxidant capacity, metabolic plasticity, and other pathways mentioned here below), they show a high refractoriness to acquire *de novo* driver mutations. In this context, we propose a scenario in which CSCs derived directly from SCs that have experienced mutations would be, in principle, a “rare” event in cancer. The occurrence of this scenario

Introduction

may imply that fewer driver mutations would be necessary to convert SCs into CSCs (**Figure 4**).

Supporting this hypothesis, certain childhood cancers that appear at an early age (having a short period for the accumulation of mutations) might fit well within this scenario. A recent report analyzed somatic mutations by next-generation sequencing in childhood cancers compared to adult cancers: only 2 out of 24 types of childhood tumors (medulloblastomas and gliomas) were found hypermutated, in comparison with 10 out of 11 adult cancers studied. The majority of childhood tumors (57%) harbored only one significantly mutated driver in contrast to 76% of adult tumors with multiple mutated driver genes ⁴¹.

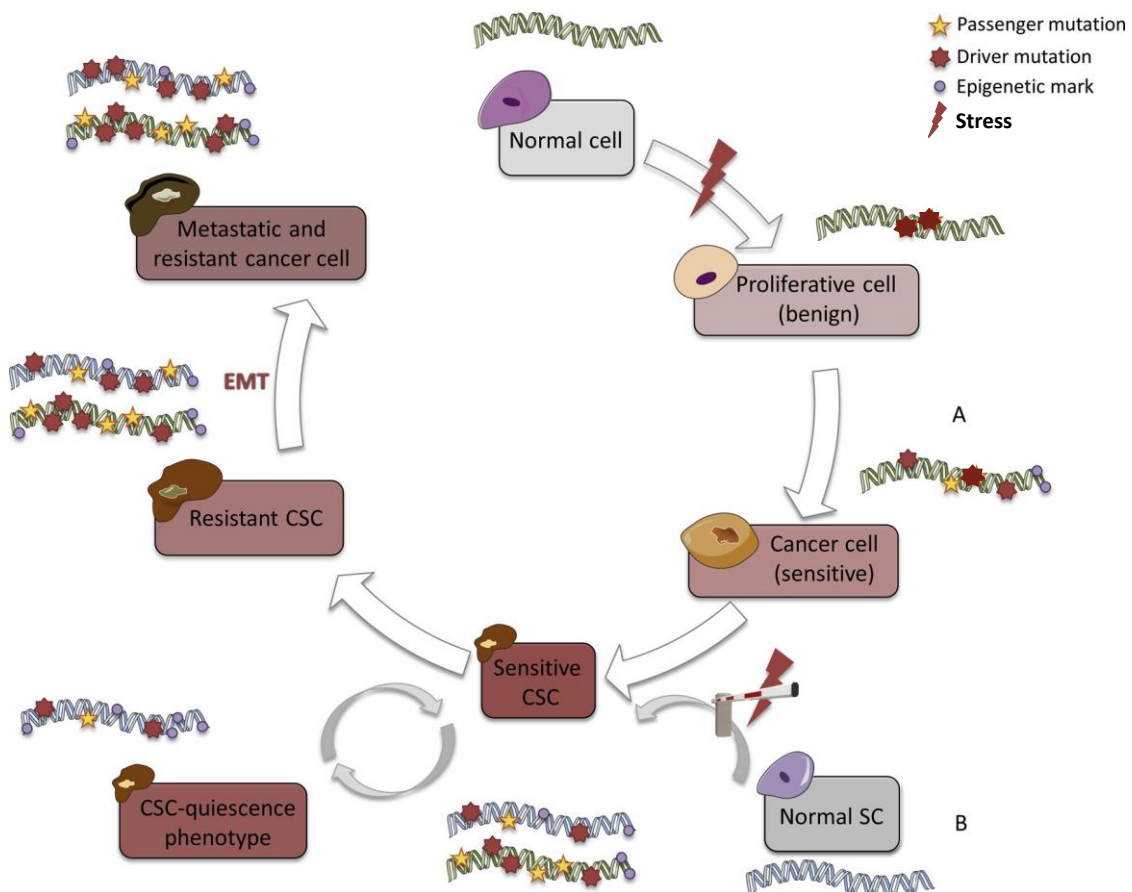


Figure 4. Highway toward malignancy. CSCs can arise from dedifferentiation of cancer cells during tumor progression caused by mutations (**A**) or may derive from mutations occurring in multipotent adult SCs (**B**). Considering that the stemness phenotype provides a survival advantage and cancer resistance, we propose a scenario in which the number of driver mutations to generate CSCs would differ depending on their origin. SCs, stem cells; CSCs, cancer stem cells. Image adapted from a recent publication of our group, Garcia-Mayea, Y. *et al.* 2019 ⁴².

Since tumors are in continuous evolution, one cancer cell clone may acquire a second driver and several passenger mutations that can be different from a cell clone in a different area of the tumor or metastatic site. These clones may respond differently to microenvironmental stress (e.g., hypoxia, immune system, chemotherapy, radiotherapy), which contributes to more genetic and epigenetic changes, tumor resistance and survival. The recent sequential genetic analyses of tumors of different origins, before and after selective stress (e.g., chemotherapeutic drugs), has shown that minor subclones became predominant after stress, suggesting that acquired mutations during tumor evolution would be a main cause of subclonal selection, disease progression and the emergence of different CSCs types ⁴³. In malignant carcinoma, most invasive tumor cells actively proliferate and are poorly differentiated, demonstrating that malignant progression is associated with a major block of the differentiation of the whole set of non-CSCs in association with the presence of CSCs ^{35,44-47}. When tumors grow after chemotherapy, evidence shows that resistance is generated by the insurgence of cells with characteristics of CSCs ^{48,49}. In support of these observations, genes whose expression is associated with stemness characteristics have been shown to play a role in tumor resistance. For example, homeobox protein NANOGP8 seems to be a key regulator of chemoresistance ⁵⁰, and downregulation of the transcription factor SOX-2 (*SOX2*) concomitantly with the ATP-binding cassette sub-family G member 2 (*ABCG2*) enhances the chemosensitivity of breast CSCs ⁵¹. These studies and others point to the crucial role of stemness properties in the generation of resistance to current anticancer therapies. In the following sections, we will focus on novel pathways and known mechanisms that have been involved in the acquisition of chemoresistance.

Introduction

1.4. Mechanisms of therapy resistance

Resistance to chemotherapy, radiation or hormonal treatment can be considered in one of these two categories: a) intrinsic or b) acquired. The first is due to preexisting factors of the tumor that are present prior to any treatment administered, thus making certain treatments useless at nontoxic doses. A few decades ago, intrinsic resistance was considered the main contributor to resistance. Instead, acquired drug resistance appears to be a relatively common issue throughout the administration of treatment and seems to be the main perpetrator of treatment failure in cancer patients, usually after a relapse⁵²⁻⁵⁴. Resistance has traditionally been considered to appear through natural selection of preexisting mutant clones. However, recent evidence points toward models that are more complex. In addition, the mechanisms of the acquisition of resistance are activated in those cancers that do not respond to therapy⁵⁵⁻⁵⁷.

Accumulated evidence shows that the expression of markers related to stemness is crucial for tumor maintenance and that they are mediators of resistance. This evidence is of special relevance since CSCs have been shown to be drivers of metastasis, and metastatic tumors are associated with a more invasive and aggressive cancer phenotype^{58,59}. In most cases, the appearance of metastasis is the result of the fate of resistant cells in the primary tumor. Such resistant phenotype has allowed cells to undergo extracellular matrix detachment, intravasation, extravasation and to reach a propitious niche^{60,61}.

Chemo and radio-therapeutic treatments are capable of inducing and selecting cell populations with stemness phenotype, which induce chemoresistance and radioresistance⁶²⁻⁶⁶. CDDP-treatment has resulted in CSCs enrichment by increasing the expression of the *TRIB* oncogene and histone deacetylases class I

(*HDAC1*), affecting DNA binding and transcription activation. Accordingly, inhibition of *TRIB1* or *HDAC1* led to a reduction of CDDP-induced CSCs⁴⁹. The activation of the nuclear factor NF-kappa- β (NF- $\kappa\beta$)/tumor necrosis factor-alpha (TNF α)/PIK3CA signaling pathway is another mechanism involved in the increase of CSCs populations provoked by CDDP action⁴⁸. After chemotherapy, glioblastoma and osteosarcoma tumors relapsed from a subset of cancer cell populations overexpressing stem-cell genes, identified as CSCs^{67,68}. It is believed that tumor regrowth after chemotherapeutic treatment could be due to the permanence of CSCs in the tumor niche, and to their unlimited self-renewal capabilities³.

Moreover, CSCs are considered responsible for the initiation, progression, invasion, metastasis, and acquisition of chemoresistance and radioresistance⁶⁹⁻⁷¹. As previously described for various types of cancer, CSCs are resistant *per se* to many of the chemotherapeutic drugs used in the clinic^{8,66,69}. Interestingly, inhibition of crucial CSCs markers such as ATP-binding cassette transporters (ABC transporters), homeobox protein NANOG (NANOG), protein Wnt (Wnt), CD44 antigen (CD44), CD133 antigen/prominin-1 (CD133), decay-accelerating factor (CD55), aldehyde dehydrogenase 1 (ALDH1), octamer-binding transcription factor 4 (OCT4), SOX-2 or Krueppel-like factor 4 (KLF4) sensitizes cancer cells to chemotherapy⁷²⁻⁷⁴.

The use of *in-vitro* chemoresistance models constitutes a fundamental tool for the study of the molecular mechanisms involved in the acquisition of resistance to current chemotherapy and for the development of new drugs against cancer¹⁵. The main strategy for establishing *in-vitro* models of chemoresistance in cell lines is the stepwise treatment with increasing concentrations of drugs until reaching a

Introduction

concentration value in which only the resistant cell population survive into the constant presence of the drug ⁷⁵⁻⁷⁸. Several multidrug resistance (MDR) cell lines have previously been generated as *in-vitro* models to study the mechanisms involved in resistance acquisition. In an *in-vitro* model of gradual MDR to docetaxel, CDDP and 5-FU in HNSCC cells, was found that the resistant cells were mostly in the G2/M phase, were capable to evade apoptosis and overexpressed multiple genes related to drugs resistance (e.g., ATP-binding cassette sub-family B member 1 (ABCB1/MDR1), ATP-binding cassette sub-family C member 2 (ABCC2/MRP2), DNA excision repair protein (ERCC1), survivin and thymidylate synthase) ¹⁵. In addition, increasing evidence demonstrates that cells with acquired resistance to a specific drug are prone to exhibit cross-resistance to other chemotherapies ^{79,80}. This could imply the existence of common mechanisms of resistance, which may be independent of the particular action of the chemotherapeutic agent.

The rapid evolution of HNSCC points to the acquisition of resistance by tumor cells that might be accompanied by the appearance of new molecular alterations in a dynamic, permanently active and mutagenic tumor microenvironment. Likewise, given that the cell populations of HNSCC tumors are very heterogeneous, such cancers type must undoubtedly be linked to cells possessing different sensitivities to radiotherapy and chemotherapy, thereby chemotherapeutic treatment exerts a selective pressure to favor the most resistant cells. Several efforts have been focused in the last few years to sensitize HNSCC cells to CDDP ^{81,82}. However, the acquisition of chemoresistance is mediated by modulations in multiple molecular pathways, including drug efflux, metabolism, DNA repair, apoptosis and cell cycle

control^{15,54}; therefore additional studies with a more global approach are necessary.

Importantly, clinical evidence shows that resistant phenotypes can be reverted to sensitive phenotypes, suggesting that cancer associated genetic alterations are not the only players in resistance^{83,84}. The need to study the mechanisms involved in the acquisition of resistance to current therapies in cancer, particularly in HNSCC⁶²⁻⁶⁶, is the focus of this thesis. In the next sections, we will describe different pathways and cellular processes that have been involved in the acquisition of resistance to current therapies.

1.4.1. ATP-binding cassette (ABC) transporters

CSCs, and in general resistance cells, express an enhanced number of ABC transporters⁸⁵ (**Figure 5 A**). It has been previously described that these proteins contribute to the MDR phenotype by exporting a wide variety of toxic drugs from the cells⁸⁶. Notably, while different ABC transporters can expel a single drug, they cannot expel all chemotherapeutic drugs. ABC transporters can be considered oncogenic proteins since most of them contribute directly to the acquisition of resistance, and the attenuation of their efflux activity reverses resistance⁸⁷. However, inhibition of specific ABC transporters does not entirely abolish the MDR phenotype. For example, tepotinib reversed the ABCB1-mediated MDR but not the ATP binding cassette subfamily C member 1/multidrug resistance-associated protein 1 (ABCC1/MRP1) or ABCG2-mediated MDR⁸⁷.

Moreover, the expression of several members of the ATP transporter family is related to CSCs in several models^{88,89}. The oncogenic protein PTOV1 increases the resistance of prostate cancer cells to docetaxel by activating the expression of ABCB1 concomitantly to the induction of stemness genes⁹⁰. In the last decade, ABC

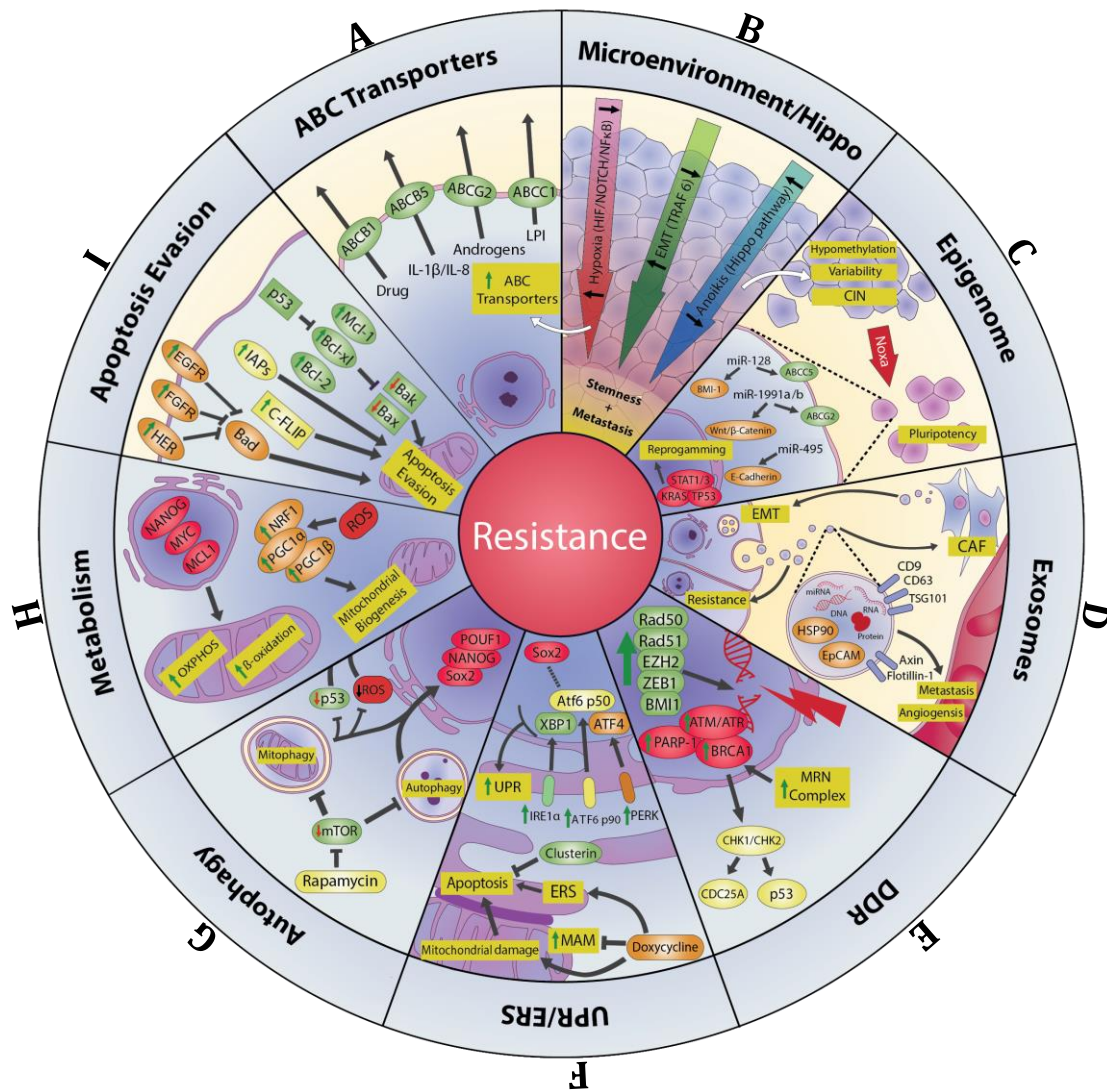


Figure 5. Resistance mechanisms in CSCs. CSCs reunite a series of characteristics that bestow upon them a natural resistance and adaptability to external insults. **A) ABC transporters:** ABC transporter overexpression confers a natural resilience to classic chemotherapeutics by decreasing cytoplasmic drug concentration and other signaling molecules, including cytokines IL-1, IL-8, androgens and lysophosphatidylinositol (LPI). **B) Microenvironment: hypoxia, anoxia resistance, and Hippo pathway inhibition** contribute to allow survival in the inhospitable tumor microenvironment and in so doing, promote pluripotency and metastatic traits in different CSCs subpopulations. **C) Epigenome:** chromosome instability (CIN), alterations of epigenetic modulators (e.g., K-RAS, TP53, STAT1, STAT3), hypomethylation and/or 3D chromatin structure instability promote different resistant phenotypes. **D) Exosomes** prime the premetastatic niche at a distance through extracellular matrix remodeling, fibroblast proliferation and transformation to cancer-associated fibroblasts (CAF). **E) DDR:** CSCs have an increased DDR due to the overexpression of proteins involved in DNA repair, such as PARP-1, ATM, ATR, BRCA1, RAD50, RAD51, EZH2, ZEB1, and BMI1, among others. **F) Unfolded protein response (UPR)/endoplasmic reticulum stress (ERS):** CSCs present increased UPR and are particularly susceptible to ERS and mitochondrial damage; **G) Autophagy deregulation:** autophagy sustains CSCs to facilitate tumor survival and resistance acquisition during chemo- and radiotherapy. **H) Metabolism:** CSCs can quickly proliferate and expand from their niche or adopt a quiescent (or dormant) phenotype. **I) Apoptosis evasion:** CSCs evade apoptosis through indirect or direct mechanisms. All of these interrelated mechanisms cooperate closely to complement each other and achieve tumor survival. Image adapted from a recent publication of our group, Garcia-Mayea, Y. *et al.* 2019 ⁴².

transporters have been described to export other signaling molecules –apart from chemotherapeutic drugs– such as hormones, which can provide an additional survival advantage. For example, ABCC1/MRP1 exports lysophosphatidylinositol (LPI), ABCG2 exports androgens, and ATP-binding cassette sub-family B member 5 (ABCB5) exports interleukin 1 beta (IL-1 β) and interleukin-8 (IL-8) ⁹¹(**Figure 5 A**).

1.4.2. Microenvironment modulation

The microenvironment may determine stemness properties and resistance phenotype. In fact, a single CSCs could not survive alone but needs other CSCs to be preserved in its niche, which is also very much influenced by the microenvironment. For example, it has been shown that myofibroblast-secreted factors, such as hepatocyte growth factor, activate the β -catenin pathway and CSCs expansion both *in-vivo* and *in-vitro* ⁹². In a colon cancer model, CSCs with a high Wnt signal activity appear to be next to stromal myofibroblasts that secrete several factors to maintain an active Wnt/ β -catenin pathway to ensure the stemness features of their neighboring cells. By designing engineered organotypic vascular niches, Ghajar *et al.* showed that thrombospondin-1 induces quiescence in disseminated breast cancer cells ⁹³. Moreover, the sprouting neovasculature accelerates cancer cell growth, favoring a quick expansion of the cells that form micrometastases ⁹³. Likewise, induced apoptosis in tumor cells due to the action of cytostatics such as CDDP, causes the release of certain cytokines in tumors-associated macrophages that stimulate the replication of CSCs and suppress apoptosis, which directly relates them with chemoresistance ⁹⁴.

Besides, EMT can promote metastasis and therapy resistance by drastically altering the microenvironment ^{95,96}. Cells that experience EMT are favored by the acquisition of migration and invasion capacities. The complex EMT process is

Introduction

regulated by known transcriptional factors: zinc finger protein SNAIL1 and SNAIL2 (SNAIL1, SNAIL2), zinc finger E-box-binding homeobox 1 and 2 (ZEB1, ZEB2), and twist-related protein (TWIST). TNF receptor-associated factor 6 (TRAF6) is a novel EMT player that facilitate the conversion into CSCs and is linked to poor prognosis in cancer patients. TRAF6 knockdown decreases stemness through EMT deregulation ⁹⁷, so TRAF6 modulation could be important to therapy of sensitization (**Figure 5 B**).

Other key factor that modulates the microenvironment and drug resistance is hypoxia. Hypoxia triggers a myriad of signaling pathways by activating mainly the hypoxia-inducible factor-1 α and 2 α (HIF1 α , HIF2 α) or alternatively the PI3K/AKT pathway, which binds to promoters containing the hypoxia-response element (HRE). As a feedback loop, activation of the PI3K/ATK pathway promotes CSCs by activating HIF1 α and HIF2 α . The cascade of activation leads to the induction of stemness and chemoresistance. This process is accompanied by the overexpression of the ABC drug transporters ABCG2, ABCB1/MDR1, and ABCC1/MRP1 ⁹⁸.

Non tumor cells harboring or surrounding the tumor microenvironment release key pro-survival signaling molecules such as NF- κ B, transforming growth factor beta (TGF- β), and IL-4, IL-6, and IL-8 cytokines with profound consequences in metastasis, resistance, and stemness properties of cancer cells ⁹⁹⁻¹⁰¹. Tumors cells have been recently described to release IL-10 and IL-17, thus modulating proliferation in neighboring cells. This, in turn, mediates the activation of NF κ B and Janus kinase (JAK)/signal transducer and activator of transcription 3 (STAT3) signaling pathways in tumor cells to nourish CSCs ¹⁰². STAT3 is a transcription factor whose activation results in the expression of several MDR genes and

consequently, in chemoresistance ¹⁰³. Therefore, changes occurring in the microenvironment can expedite and confer resistance of cancer cells and CSCs to radiotherapy and chemotherapy.

1.4.3. The Hippo pathway

The Hippo pathway is a tumor suppressor pathway mainly regulated by phosphorylation-dependent protein kinase cascade signaling. This pathway can be regulated by extracellular ligands (e.g., receptor tyrosine kinases), cell-to-cell junctions (e.g., cadherin), cell-to-matrix contact (e.g., integrins or CD44), or cell polarity. Such signaling molecules affect the tumor suppressor activity of the Merlin protein, which regulates the Hippo pathway by suppressing the transcriptional activity of Yes1 associated transcriptional regulator (YAP1)/Tafazzin (TAZ) (**Figure 6**). There are two critical tumor suppressor regulators in the Hippo pathway that belong to the family of serine-threonine protein kinases: MST1/2 and LATS1/2. The latter inhibits the interaction of the YAP1/TAZ transcription factor with a myriad of tumorigenic genes. However, upon Hippo pathway inactivation, the oncogenic transcription factors YAP1/TAZ translocate to the nucleolus and enhance gene transcription by increasing transcriptional enhancer factor TEF-1-4 (TEAD1-4) activity (**Figure 6**). Inhibition of the Hippo pathway has been involved in maintaining stemness properties in different cancers, such as lung and breast cancer ^{104,105}. Interestingly, SOX2 antagonizes the Hippo pathway to maintain CSCs ¹⁰⁶. In turn, YAP1 promotes CSCs through ABCG2. It has recently been shown that CSCs containing mutant p53 protein activate WASP-interacting protein (WIP) by enhancing PI3K/AKT pathway to control YAP1/TAZ stability ¹⁰⁷. Importantly, dysregulation of the phosphorylation status of Hippo signaling effectors (e.g., TAZ or YAP1) has been

Introduction

associated with strengthened self-renewal, proliferative properties, and chemoresistance in CSCs ¹⁰⁸.

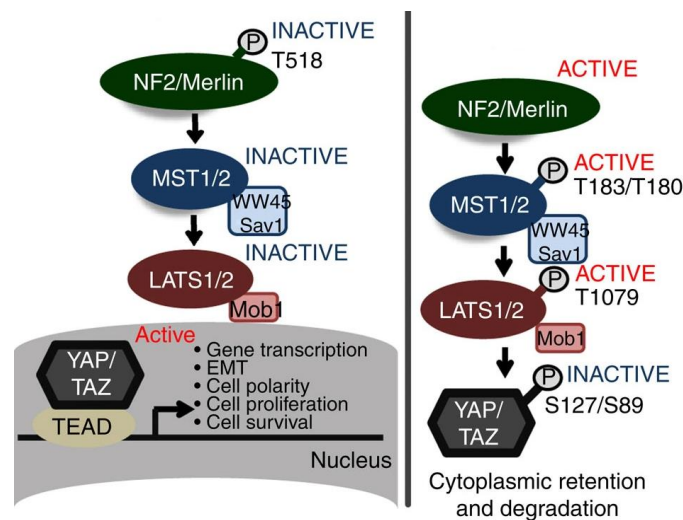


Figure 6. Schematic representation of the Hippo signaling pathway. Hippo pathway OFF provokes inactivation of Merlin/MST/LATS proteins, which induces tumor progression due the activation of the YAP/TAZ transcription factor. Hippo pathway ON results in the cytoplasmic retention and degradation of YAP/TAZ oncoproteins, and the inhibition of tumor growth. Image adapted from Serrano *et al.* 2013 ¹⁰⁹.

1.4.4. Epigenome

The term “epigenetics” introduces a new concept to consider the modulation of genes by changes in the DNA that are not hereditary. Classic mechanisms of epigenetic regulation include DNA methylation, histone modifications and nucleosome relocation. In contrast to genetic alterations, epigenetic changes are reversible and more susceptible to therapeutic options ¹¹⁰. Interestingly, some subpopulations inside tumors are capable to undergo a reversible tolerance when first challenged with drugs (and possibly other stressful stimuli) and survive to protect the whole set of the tumor population from extinction by lethal drug exposures ¹¹¹.

Deregulated methylation can be directly involved in stemness phenotype. While in general terms, a hypermethylation pattern can be detected in cancer cells –mainly to repress promoters of tumor suppressor genes– in the initial stages of

tumorigenesis, a hypomethylated pattern has also been described ¹¹². A clear hypomethylation pattern was prevalent in the CSCs grown in conditioned medium from their parental derivatives. Interestingly, one of the differentially deregulated pathways, in such conditions, involved the PI3K/AKT signaling pathway. Moreover, CSCs fate can be modulated through the activation of the Hedgehog signaling pathway by conditioned medium from macrophages ^{112,113}.

Several studies show that the acquisition of resistance is driven by increased transcriptional variability in the CSCs population. Importantly, epigenetic strategies to reverse drug resistance have been proposed for targeting CSCs in myeloma, pancreatic, breast and HNSCC cancers ¹¹⁴⁻¹¹⁶. Inhibition of lysine-specific histone demethylase 1A (KDM1A) decreases the activity of the Wnt/ β -catenin pathway to eliminate resistant CSCs from hepatocarcinoma cells ¹¹⁷.

In addition, an altered chromatin state involving the action of histone demethylases has been a common feature of different populations of cancer cells ¹¹¹. This transient resistant state might be an acute response that allows cancer cell survival until more permanent resistance mechanisms can be established. In such a case, chromatin-modifying agents can sensitize drug-tolerant cells into a more vulnerable state ⁴².

On the other hand, a hub of noncoding RNAs (ncRNA) regulates mRNA translation. Small RNA fragments, including microRNAs (miRNAs) or long noncoding RNAs (lncRNAs), are involved in chemoresistance (**Figure 5 C**). For example, miR-128 induces resistance in CSCs through the polycomb complex protein BMI-1 (BMI1) and the multidrug resistance-associated protein 5 (ABCC5/MRP5) ¹¹⁸. Upregulated levels of miR-495 in CSCs induce hypoxia resistance by downregulating E-cadherin and DNA damage-inducible transcript 4 protein (REDD1/DDIT4). In colon cancer

Introduction

cells, upregulation of miR-199a/b contributes to CDDP-resistance by activating Wnt/ β -catenin signaling pathway and ABCG2¹¹⁹ and in colorectal cancer miR-18a, miR-124 and miR-210 induce autophagy, promoting cancer progression and/or chemoresistance¹²⁰. Meanwhile, tumor suppressor microRNAs such as miR-205 or miR-99a are capable to inhibit proliferation and chemosensitize CSCs in pancreatic and lung cancer models, respectively^{121,122}. Long noncoding RNAs such as ROR and Linc-DYNC2H1-4 promote chemoresistance in CSCs, stimulating EMT^{123,124}. Transcriptome studies on CSCs are being used as pharmacodynamic markers capable to predict therapeutic responses¹²⁵.

1.4.5. Exosomes

Exosomes are biological vesicles naturally produced by cells that mediate short and long-range communications between them. Exosomes are originated from early endosomes that become integrated into multivesicular bodies that can fuse with the plasma membrane to release their contents to the extracellular matrix. Exosomes can contain DNA, RNA, ncRNA, lipids and up to 7,000 different proteins. They are usually characterized by the expression of specific cell surface markers such as CD9 antigen/tetraspanin-29 (CD9), CD63 antigen/tetraspanin-30 (CD63), CD81 antigen/tetraspanin-28 (CD81), tumor susceptibility gene 101 protein (TSG101), programmed cell death 6-interacting protein (Alix/PDCD6) and Flotillin-1¹²⁶⁻¹²⁹ (**Figure 5 D**). Their ability to carry this content to very distant parts of the body while being protected from degradation in the blood provides exosomes with an important role in cancer metastasis and drug resistance. In particular, exosomes play an essential role in cell plasticity, preserving the interaction and favoring the conversion between cancer cells and CSCs. Thus, interfering with the exosome-mediated dynamic transformation and homeostasis

between CSCs and cancer cells would be an efficient strategy to annihilate tumors^{126,127,129,130}. By using paracrine and juxtacrine signaling, exosomes release into the microenvironment chemokines, cytokines, and metalloproteinases, and stimulate angiogenesis through interactions with different cell types, preferably cancer-associated fibroblasts (CAF) and endothelial cells¹³¹. Stromal cells communicate with cancer cells using exosomes that activate STAT1 and Notch signaling¹³². The exosome communication is bidirectional, and studies have showed that CAF and adipocytes promote tumor adaptability through the induction of chemoresistance (miR-146a), EMT (miR-21, miR-278e, and miR-143), proliferation (Ephrin type-A receptor 2) and metabolic regulation (miRNA-302d, miRNA-29b, miRNA-22, and metabolites such as lactate, acetate, citrate or pyruvate). In addition, exosomes are used by resistant cells to export chemotherapeutic drugs such as CDDP¹³³.

Importantly, exosomes are novel CSCs mediators as exosomes secreted by CSCs are present in premetastatic niches, facilitating metastatic settlement a posteriori^{134,135}. CD63, a member of the tetraspanin family that is expressed in endosomes and enriched in exosomes released by CSCs, has been recently associated with CDDP-resistance. Moreover, its expression by IHC is associated with an advanced stage and poor differentiation in colorectal cancer¹³⁶⁻¹³⁸.

Notably, exosomes appear very interesting for anticancer treatments (e.g., exosome-like nanovesicles have been used to specifically target CSCs)¹³⁹. Knowledge of the content of exosomes released by resistance cells will provide us with valuable information to design therapeutic targets that prevent relapse and distant metastasis in cancer patients⁴².

Introduction

1.4.6. DNA damage response (DDR)

One of the hallmarks of cancer is the decreased ability of tumor cells to repair the damage in their DNA, thus resulting in the accumulation of mutations and genomic instability. The principle of radiotherapy is based on this defective DDR pathway and aims to selectively annihilate cancer cells with defective repair systems but not the surrounding normal cells that are capable to repair radiation adduct formation in their DNA. Instead, CSCs have an overwhelming DDR machinery that makes them extremely effective to preserve their DNA, similar to normal SCs^{140,141}. The key sensors of DNA damage are the ataxia telangiectasia mutated (ATM)- and ataxia telangiectasia and RAD3-related protein (ATR)- (ATM and RAD3)-related protein kinases. ATM recognizes and further repairs double-strand DNA breaks, while ATR recognizes single-strand DNA breaks at stalled replication forks. Briefly, upon DNA damage, ATM and ATR kinases form complexes with poly [ADP-ribose] polymerase 1 (PARP-1) -protein that detects single strand breaks and recruits DNA repair proteins- and breast cancer type 1 susceptibility protein (BRCA1) -tumor suppressor protein that detects and repairs DNA damage- to phosphorylate the serine/threonine-protein kinases CHK1 and CHK2 (CHK1, CHK2). CHK1 and CHK2 subsequently drive the activation of target proteins, including p53 and the dual specificity phosphatase CDC25A, provoking cell cycle arrest, DNA repair or apoptosis (**Figure 5 E**).

CSCs have constitutive activation of ATM and CHK1 kinases^{142,143}. The most common alteration in DNA upon treatment with DNA damaging agents is double-strand breaks (DSB), for which the MRN complex is the major sensor. The MRN complex binds and stabilizes broken DNA ends, further activating the ATM/ATR kinase axis. Overexpression of proteins that are involved in the MRN complex or in

the DSB response is linked to tumorigenesis and CSCs promotion. In particular, CSCs have a potent DDR in comparison with other cancer cells (non-CSCs), which allows them to survive in a medium with exogenous and endogenous genotoxins¹⁴⁴. For example, DNA-dependent protein kinase (DNA-PK) is a predominant DNA repair enzyme in CSCs, and targeting DNA-PK/DNA repair protein RAD50 (RAD50) is a promising approach for CSCs eradication¹⁴⁵. Additionally, the phosphorylation of CHK1 is a predictive marker of radiotherapy resistance and early local recurrence in breast cancer¹⁴⁶.

Transcription factors such as BMI1, involved in radioresistance and chemoresistance, participate in the CSCs' DNA damage response¹⁴⁷. The fact that proteins involved directly in DNA repair are constitutively active in CSCs is indicative of an efficient DNA damage response. The DNA repair proteins in CSCs that are associated directly or indirectly with resistance are CHK1, CHK2, ATR, RAD50, DNA repair protein RAD51 homolog 1 (RAD51), and RNA-binding protein Musashi homolog 1¹⁴⁸⁻¹⁵⁰. In particular, RAD51 is a mediator of CSCs resistance, with a very significant effect on the resistance to PARP inhibitors¹⁵¹.

1.4.7. Unfolded protein response (UPR)/endoplasmic reticulum stress (ERS)

Incorrect protein folding in the lumen of the endoplasmic reticulum (ER) causes stress and triggers the UPR mechanism. UPR relieves and ameliorates the ER load through the regulation of three independent branches: inositol-requiring enzyme-1 α (IRE1 α), protein kinase R-like endoplasmic reticulum kinase (PERK) and activating transcription factor 6 α (ATF6 α) (**Figure 5 F**). The activation of these pathways leads to a reduction of the protein load in the ER by regulating mRNA translation, increasing both the protein folding capacity, and the degradation of misfolded proteins¹⁵². Chronic induction of the UPR is necessary for cancer cell

Introduction

survival under the continuous challenge of the tumor microenvironment. Supporting this observation, components of the UPR pathway have been found to be overexpressed in many solid tumors ¹⁵³. Notably, recent data indicate that translation reprogramming regulates the phenotype and plasticity of melanoma cells and determines drug and immunotherapy resistance, as well as metastatic potential. The authors report that inflammation-mediated resistance to immunotherapy in melanoma activates a stress response that induces cyclic AMP-dependent transcription factor ATF-4 (ATF4), a key event to enhance tumor invasiveness ¹⁵⁴.

Interestingly, several components directly involved in protein processing in the ER are deregulated in CSCs ¹⁵⁵. Moreover, in a cervical cancer model, CSCs activate a survival signaling pathway involving IRE1-inactivation and PERK- activation, both of which are crucial in the ERS response. ERS-sensor inhibition, combined with ERS-inducible chemotherapy, shifted CSCs to apoptosis ¹⁵⁶. In addition, when prostate cancer cells are forced to grow in non-adherent conditions, they acquire CSCs-like properties that involve increased contact between mitochondria and mitochondrial associated-ER membranes. Doxycycline has been shown to specifically target CSCs and induce ERS-mediated apoptosis *in-vivo* and *in-vitro*. Consequently, the concomitant increase of ATF4 and p53 up-regulated modulator of apoptosis (PUMA) proteins induces efficient apoptosis of CSCs ¹⁵⁷. However, the expression of certain proteins in CSCs, such as Clusterin, has been shown to increase ERS tolerance, being potential targets to mitigate the intrinsic resistance of CSCs ¹⁵⁸. Moreover, the silencing of the three UPR branches had profound effects in CSCs since the levels of ATF6 α and PERK strongly correlate with SOX2

expression, which results in a reduction of sphere-forming capacity and maintenance ¹⁵⁹.

1.4.8. Metabolism

Almost one century ago, in 1927, Otto Warburg discovered that cancer cells used a distinctive metabolic pathway compared to normal cells ¹⁶⁰. The Warburg effect described in cancer cells consists of the maintenance of a high glycolytic metabolism even under normoxic conditions. It is important to clarify that this effect does not mean that tumor cells rely more on glycolysis for ATP production. What occurs instead, is an upregulation of glycolysis to support the rapid cellular growth, often (but not always) accompanied by a decreased mitochondrial ATP production. Therefore, the defining feature of the Warburg effect is increased glucose uptake and fermentation of glucose to lactate. This metabolic strategy allows cancer cells to optimally adapt to rapid fluctuations in energy demand and promote long-term survival and proliferation. Although the Warburg effect was initially attributed to defective mitochondria, this phenomenon has been observed even in the presence of completely functioning mitochondria ¹⁶¹.

It has become evident that CSCs have higher plasticity than normal cells or the whole set of cancer cells and that they modulate metabolism without losing their properties. Gene-expression studies comparing CSCs versus normal SCs found that metabolic pathways are at the top of the deregulated pathways ¹⁵⁵. Thus, CSCs undergo drastic metabolic changes that affect glycolysis, mitochondrial respiration, oxidative phosphorylation (OXPHOS) and lipid metabolism ¹⁶²⁻¹⁶⁴.

According to their metabolic status, CSCs can be classified, theoretically, as quiescent (minimal metabolic reserve state) or proliferative. However, at a biological level, different CSC metabolic populations coexist in the same tumor

Introduction

(from quiescent to several degrees of proliferation). The requirement for a quiescent CSC to originate differentiated cancer cells is to go through a proliferative state in which its dependence on OXPHOS is crucial (**Figure 7**).

Some CSC populations can even show higher OXPHOS dependence in comparison with the whole set of cancer cells ¹⁶⁵. More concretely, in quiescent CSCs, HIF1 α inhibits acetyl Co-A production through the activation of pyruvate dehydrogenase (acetyl-transferring) kinase isozyme 2 and 4 (PDK2 and PDK4) but increases the translation of glycolytic enzymes, as well as glucose transporter type 1 (GLUT1) and carbonic anhydrase IX (CAIX) (necessary to manage the lactic acidosis of glycolysis). CAIX is a powerful activator of the protein Jagged 1 and Notch1 pathways that eases pluripotency. SLC-0111, an inhibitor of CAIX, sensitizes different cancer cells to conventional chemotherapy and promotes apoptotic and necrotic programs in acidified cancer cells ¹⁶⁶. In addition, anabolism and cell proliferation are inhibited through mammalian target of rapamycin (mTOR) downregulation, which is mediated through a REDD1-HIF1 α axis. Furthermore, in the absence of glucose, CSCs will recycle the catabolites produced by CAF (such as ketone bodies, glutamine and lactic acid) to initiate the autophagy process.

In contrast, when CSCs are in the appropriate circumstances and in the presence of dioxygen, insulin-like growth factor mRNA-binding protein 2 (IMP2) promotes the proliferative phenotype through mitochondria biogenesis, the expression of complex I and IV, as well as the expression of key SCs genes (*SOX2*, *NANOG* and *OCT4*). In this state, the PI3K/AKT/mTOR pathway promotes lipogenesis, nucleic acid synthesis, mRNA translation and protein synthesis. It is from this proliferative state, mediated through the respiratory metabolic switch, that CSCs can populate the tumor through asymmetric mitosis and guarantee tumor survival ¹⁶⁶.

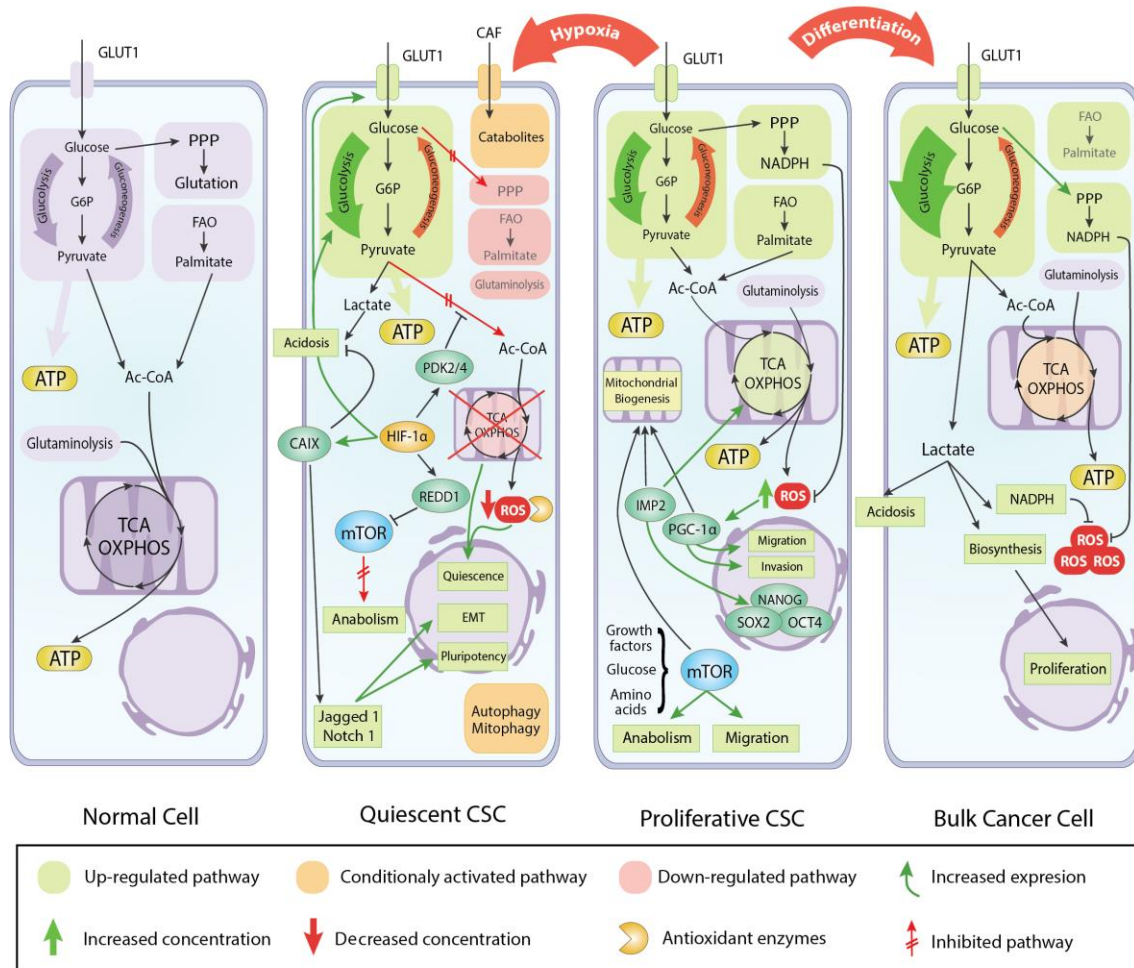


Figure 7. Perspectives of normal cells, cancer cells, and CSCs metabolism. CSCs manifest different metabolic states in response to the microenvironment. They are long-term stable in the absence of oxygen and show a quiescent phenotype that is characterized by a low metabolic rate and reduced OXPHOS. In contrast, in the presence of oxygen, CSCs have increased levels of tricarboxylic acid (TCA) cycle enzymes and OXPHOS activation, essential changes that allow CSCs to proliferate. This switch of the metabolic state generates ROS, which are eliminated through antioxidant enzymes. Image adapted from a recent publication of our group, Garcia-Mayea, Y. *et al.* 2019⁴².

Moreover, some oncogenes, such as Myc proto-oncogene protein and induced myeloid leukemia cell differentiation protein Mcl-1 (*Mcl-1*), contribute to the chemotherapeutic resistance of CSCs by regulating mitochondrial OXPHOS¹⁶⁷. Stemness genes such as *NANOG* also favor tumorigenesis through OXPHOS metabolic reprogramming and fatty acid metabolism¹⁶⁸. During the formation of spheres or spheroids, intracellular reactive oxygen species (ROS) increase and trigger the accumulation of detoxifying molecules to counteract ROS oxidation and

Introduction

maintain redox balance ¹⁶⁹⁻¹⁷¹. Interestingly, nuclear factor erythroid 2-related factor 2 (NRF2), a transcription factor that responds to oxidative stress by regulating the expression of genes involved in the cellular antioxidant response, is a mediator of CSC resistance, stimulating increased drug efflux and other functions ¹⁷². What is more, inhibition of peroxisome proliferator-activated receptor gamma coactivator 1-alpha (PGC1 α), a key transcription factor that activates antioxidant enzymes, can sensitize CSCs to the CDDP action ¹⁷³. Crucial characteristics of CSC plasticity are based on the exploitation of their cell metabolism to make versatile changes from proliferative states to other quiescent ones depending on the tumor microenvironment ⁴² (**Figure 5 H**).

1.4.9. Apoptosis evasion

CSCs can overcome death signals by several mechanisms: i) altered cell cycle regulation; ii) imbalance of programmed cell death: pro-apoptotic [*e.g.*, apoptosis regulator BAX (BAX) and BAK (BAK), BH3-interacting domain death agonist (BID), Bcl-2-interacting killer (BIK), phorbol-12-myristate-13-acetate-induced protein 1 (Noxa), and PUMA] *versus* anti-apoptotic proteins [*e.g.*, apoptosis regulator Bcl-2 (Bcl-2), B-cell lymphoma-extra large (BCL_{XL}) and Mcl-1]; iii) downregulation of death receptors and upregulation of cellular FLICE (FADD-like IL-1 β -converting enzyme)-inhibitory protein (c-FLIP); iv) increased expression of inhibitors of apoptosis family proteins (IAPs); and v) deficiency in mitochondria-mediated apoptosis (**Figure 5 I**). The fact that the CSCs have an extended G2/M phase during the cell cycle by upregulating G2/M checkpoint proteins CHK1 and CHK2 facilitates their repair of DNA damage (*e.g.*, caused by chemotherapy), which would otherwise result in apoptosis. In this case, the ability to evade apoptosis would be a display of their ability to regulate the cell cycle and adapt it to their needs. Direct

regulation of apoptosis resides in the fact that high levels of anti-apoptotic or pro-survival proteins have been associated with CSC resistance^{174,175}. The chemoresistance of CD133⁺ cells to 5-FU has been attributed to high levels of survivin, a member of the IAPs family. The death receptor-initiated pathway is suppressed by c-FLIP, which inhibits the activation of caspases, hampering the apoptotic process. Different splice variants of c-FLIP are involved in resistance to chemotherapeutical drugs^{176,177}.

In addition, to survive in circulation, the tumor cells must show resistance to cell death caused by the lack of anchoring, a process known as anoikis. This process of programmed cell death is an intrinsic mechanism activated when cells are detached from the extracellular matrix of the tissue where they grow and prevents them from migrating and colonizing other organs. In certain types of cancers (*e.g.*, cutaneous melanoma), resistance to anoikis is significantly elevated, which facilitates malignant cells metastasizing to distant organs^{178,179}. Survival factors, hypoxic conditions, or the EMT process upon contact with adverse microenvironmental conditions favors the anoikis process. Importantly, resistance to anoikis contributes to CSC survival^{180,181}. Accumulating evidence shows that the CSCs present in the circulation has an anoikis resistance phenotype, which allows them to metastasize¹⁸². It has been observed that CSCs protect the whole set of cancer cells (non-CSCs) from anoikis. They do so through integrin-associated signal transduction pathways that affect gap junctions and ERK activation¹⁸¹.

1.5. Autophagy and cancer

1.5.1. Types of autophagy

In mammals, three different subtypes of autophagy have been described: microautophagy, chaperone-mediated autophagy, and macroautophagy¹⁸³ (**Figure**

Introduction

8). Microautophagy involves direct invagination of the lysosomal/vacuolar membrane to envelop and subsequently digest nearby cytoplasmic components¹⁸⁴. The chaperone-mediated autophagy allows a more selective degradation of the autophagic cargo through the recognition by the chaperone complex of specific motifs in the target proteins and their interaction with a lysosomal receptors¹⁸⁵. Likewise, macroautophagy (hereinafter autophagy) is the main pathway for cellular autophagy. It involves both bulk degradation of cytoplasmic proteins and selective degradation of cytoplasmic organelles by double-membrane structures that end up merging to form autophagosomes. In turn, the autophagosomes fuse with lysosomes to form the autophagolysosome, where the autophagic cargo is digested^{186,187}.

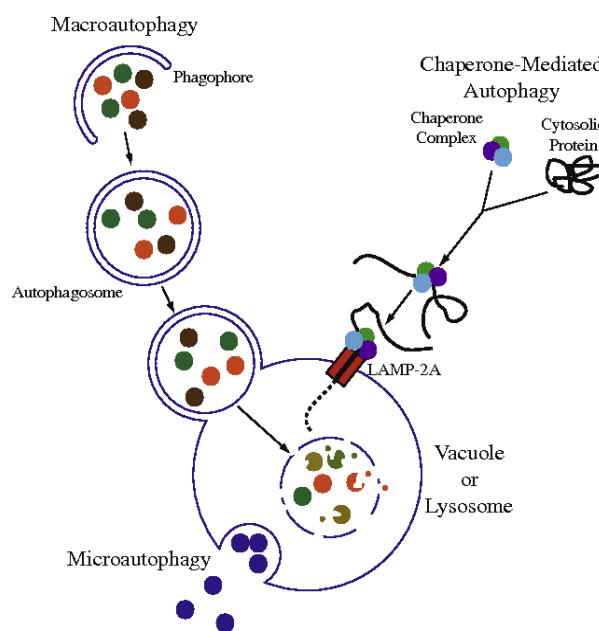


Figure 8. Autophagy subtypes described in mammals: microautophagy (by invagination of the plasma membrane), chaperone-mediated autophagy (also known as selective autophagy since it involves the participation of the chaperone complex and lysosomal receptors) and macroautophagy (it involves the selective and non-selective degradation of autophagic cargo of very different sizes, including cellular organelles). Image adapted from Lynch-Day *et al.* 2010¹⁸⁸.

Among the main autophagy-stimulating signals are nutrient or growth factor deprivation, hypoxia, oxidative stress, or protein aggregation¹⁸⁹⁻¹⁹¹ (**Figure 9**).

PI3K/AKT/mTOR, one of the main dysregulated pathways in cancer, is also the

main pathway regulating the autophagy process ¹⁹². mTOR is a highly conserved serine/threonine kinase that is part of the mTOR complex 1 (mTORC1), and together with AMP-activated protein kinase (AMPK) and HIF regulate the start of the autophagic process. The mTOR complex is inhibited under starving conditions, which causes autophagy activation ^{191,193}. On the other hand, AMPK is an energy sensor kinase that responds to the high AMP/ATP ratio at the cytoplasmic level, promoting autophagy ^{194,195}. Moreover, hypoxic signals are mediated by HIF as stress response and activate autophagy ¹⁹⁶.

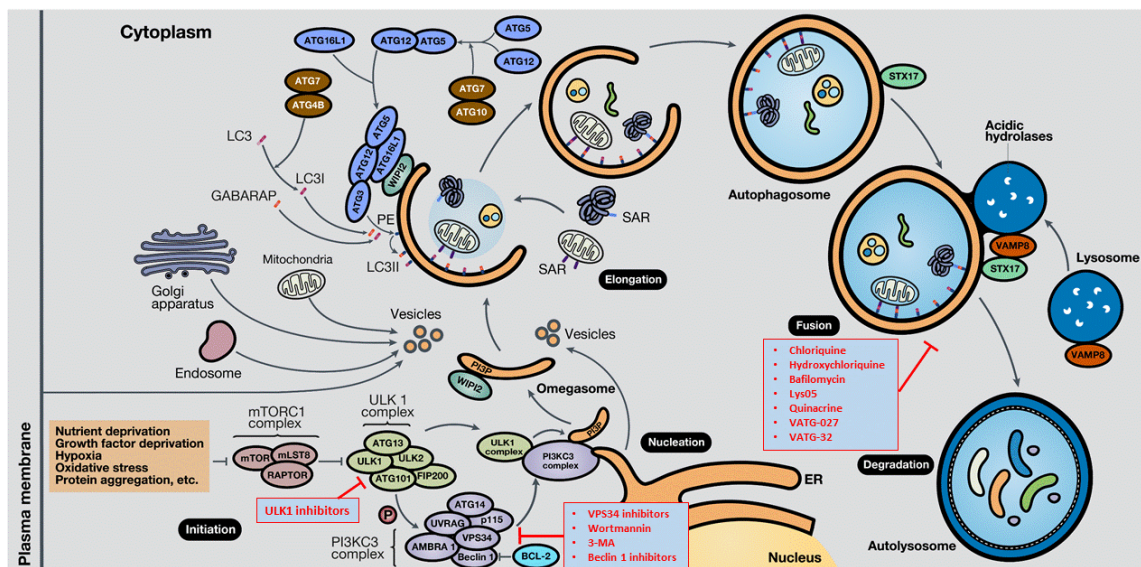


Figure 9. Schematic representation of the autophagy process in mammals. Autophagy mechanism comprises five phases: **(1) initiation** (autophagy stimulating signals inhibit the mTOR complex 1 (mTORC1), leading to ULK1 complex (ULK1C) activation), **(2) nucleation** (ULK1C phosphorylates and activates the phosphatidylinositol 3-kinase catalytic subunit type 3 (PI3KC3) complex, generating phosphatidylinositol 3-fosfato (PI3P); WD repeat domain phosphoinositide-interacting protein 2 (WIPI2) in association with PI3P induce phagophore formation), **(3) elongation** (two ubiquitin-like protein systems, ATG12-ATG5-ATG16L1 and ATG4B-ATG7-ATG3, mediate the activation of LC3 into LC3I, followed by its lipidation with phosphatidylethanolamine (PE) to form LC3II, and subsequent anchoring to the phagophore. Gamma-aminobutyric acid receptor-associated protein (GABARAP) also conjugates with PE and attaches to the membrane. LC3 and GABARAP mediate sequestering of autophagic substrates marked with selective autophagy receptors (SARs), for example p62, before phagophore closure and total autophagosome development), **(4) fusion** (autophagolysosome formation is mediated by the interaction between syntaxin-17 (STX17), present in the autophagosome, and WAMP8, present in the lysosome), and **(5) degradation** (autophagic cargo is degraded by acid lysosomal hydrolases, autophagic products are then released into the cytoplasm and recycled into metabolic and biosynthetic pathways). In addition, several autophagy inhibitors are shown at different stages of the process. 3-MA, 3-methyladenine. Figure adapted from Alvarez-Meythaler, J.G; Garcia-Mayea, Y., *et al.* 2020, currently accepted in *Frontiers in Oncology* (DOI: 10.3389/fonc.2020.586069).

Introduction

Autophagy proteins were initially identified in yeast during genetic studies ¹⁹⁷, however, the basic mechanism has been preserved in mammals ¹⁹⁸ (**Figure 9**). All phases of the autophagic mechanism are essential to complete the process, therefore the inhibition of any of the steps also affects the overall procedure ¹⁹³.

1.5.2. Autophagy is a homeostatic cell process

Autophagy is an important homeostatic catabolic process preserved in all eukaryotic organisms, allowing a high adaptive potential under stressful conditions. At basal level, autophagy maintains cellular homeostasis through cytoplasmic replacement of proteins and organelles ^{199,200}. However, macroautophagy has been described to decrease gradually during aging, with a high tendency to the accumulation of autophagic vacuoles ²⁰¹. Likewise, autophagic dysregulation has been implicated in several diseases/disorders: neurodegenerative diseases (e.g., Parkinson, Alzheimer), diseases linked to lysosomal disorders (e.g., Danon disease, Pompe disease), diseases linked to immune responses (e.g., adaptive and innate responses against *Listeria monocytogenes* and *Staphylococcus aureus* infections), muscle and cardiac disorders (e.g., chronic fatigue), and cancer ²⁰⁰. In cancer, autophagy is a process that can function, under certain conditions, either as a tumor suppressor mechanism by eliminating defective cells or as an oncogenic process allowing cancer cells to escape from chemotherapy. In fact, an increase of autophagy is associated with the acquisition of resistance to chemotherapy ^{120,200,202}.

1.5.3. Autophagy flux and cancer

Autophagic flow is defined as the rate of autophagic degradation and is usually estimated based on the degradation rate of intermediaries such as p62 and LC3 ²⁰³.

However, autophagosomes analyses and their direct quantification in cells using a transmission electron microscopy (TEM) is a useful and accurate technique to measure the state of autophagy activation ²⁰⁴. In addition, WB and IHC assays of autophagy-related proteins, such as LC3II and p62, have also been widely used and reveal useful information about autophagy activation status at a precise time ²⁰⁵⁻²⁰⁷.

Autophagy is considered a tumor-suppressive mechanism during tumor initiation and malignant transformation. During these stages, autophagy exerts its inhibitory effect on cancer because participates in the removal of damaged cells and organelles, thus avoiding genomic instability and limiting cell proliferation. This role is even more important in those cells with p53 mutated ^{190,208}.

On the other hand, there are significant evidence that autophagy has a cancer-promoting role in established tumors ²⁰⁹⁻²¹¹. Tumoral heterogeneity is the best characteristic of malignant tumors, since many different clones fight to be the main tumor driver and to prove themselves as leaders in terms of growth and resistance. Moreover, as we have previously discussed, tumor cells readjust different strategies to survive and being immortal. One of these strategies is autophagy, which is used by certain tumor populations such as resistant cancer cells and CSCs to reuse cellular organelles that maintain their functional integrity (*e.g.*, mitochondria) as an energy resource. In metastatic prostate cancer, autophagy is an important resistance mechanism that contributes significantly to ROS removal ²¹². On this matter, a recently study carried out with biopsies of nasopharyngeal carcinoma, before and after treatment with CDDP, evidenced the overexpression of Beclin-1 in all samples after treatment ²¹¹. Similar results were obtained in tongue squamous cell carcinoma (TSCC) co-cultivated with cancer-

Introduction

associated fibroblasts (CAF), and treated with CDDP, where elevated levels of LC3II and Beclin-1 were found. Moreover, treatment with the autophagy inhibitor chloroquine (CQ) and small interfering RNA (siRNA) against Beclin-1 sensitized them to CDDP and inhibited the growth of xenografted tumors ²¹³.

Likewise, the integrity of the autophagic program is crucial for CSCs as they require specific basal levels of autophagy for stemness maintenance and survival. The inhibition of OCT4 decreased CSCs pluripotency and deregulated autophagy ²¹⁴. Mitophagy, specific autophagy that affects mitochondria, represents a survival mechanism for cancer cells. More precisely, mitophagy favors the increase of the CSCs population by eliminating active p53 (p53S392) with the concomitant stimulation of NANOG by OCT4/SOX2 transcription factors ²¹⁵ (**Figure 5 G**). In addition, mutations in mitochondrial DNA or its destabilization can lead to mitophagy ²¹⁶. Besides, autophagy activators or mTOR inhibitors clearly boost pluripotency and stemness properties ²¹⁷.

Overall, autophagy should be activated to suppress cancer initiation but inhibited in established and metastatic tumors to reduce survival and tumorigenesis, and promote the efficacy of chemotherapeutic agents on resistant cancer cells.

1.5.4. Autophagy inhibition as a means of anticancer therapy

Numerous studies suggest that autophagy inhibition could be an effective cancer treatment, mainly against tumors resistant to chemo/radiotherapy. By genetic inhibition of intermediaries involved in the autophagic process, such as Beclin-1, or the autophagy proteins ATG3, ATG4, ATG5 and/or ATG12, it has been possible to improve the response to multiple current cancer treatments ^{218,219}. Furthermore, autophagy can be targeted pharmacologically upstream through ULK1, VPS34 or Beclin-1 direct inhibition, or PI3KC3 indirect inhibition, through

wortmannin and 3-methyladenine (3-MA). Downstream targets include ATG4B direct inhibitors, as well as CQ, HCQ and bafilomycin, which prevent autophagosome fusion with the lysosome¹⁹⁰ (**Figure 9**).

Although current clinical trials with autophagy inhibitors in cancer are focused on CQ and HCQ (www.clinicaltrials.gov, consulted on August 23, 2020), inhibitors of VPS34, ULK1 and ATG4B have also shown promising results in *in-vitro* and in preclinical studies with murine models²²⁰⁻²²². As well, Lys05 (a dimeric form of CQ), the antimalarial drug quinacrine, VATG-027 and VATG-032 are new next-generation lysosomal inhibitors that block autophagy more potently than CQ and HCQ (**Figure 9**). They have shown promising results in *in-vitro* and/or in preclinical mouse models of colorectal adenocarcinoma, lung cancer, ovarian cancer, and in patient-derived BRAF-mutant melanoma cell lines²²³⁻²²⁷.

Besides, previous studies from our laboratory have explored the potential benefit of autophagy inhibitors as possible therapeutic agents against certain cancer types²²⁸. In this sense, we have recently proposed that HCQ in combination with other anti-cancer drugs, might be beneficial for certain aggressive variants of breast cancer (e.g., triple-negative)²²⁹. Interestingly, autophagy inhibitors have been proposed recently in HNSCC models^{230,231}.

Furthermore, the identification of novel proteins involved in therapy resistance is very important not only at biological but also at therapeutic level. By performing a proteomic study, we identified TSPAN1, a member of the tetraspanins family, which was upregulated in CDDP-resistant cancer cells and CSCs in comparison with parental cells.

Introduction

1.6. Tetraspanin family

1.6.1. Structure of tetraspanins

In mammals, tetraspanins family comprise 33 members of transmembrane proteins. The general structure of the tetraspanins family consist of 200-350 amino acids that form four transmembrane helices. The consensus protein consist of two loops, the small EC1 and the large EC2; disulfide bonds maintain EC2. One cytoplasmic loop and both the amino (N) and the carboxyl (C) terminal tails are facing to the cytoplasmic side of the membrane (**Figure 10**)²³²⁻²³⁵.

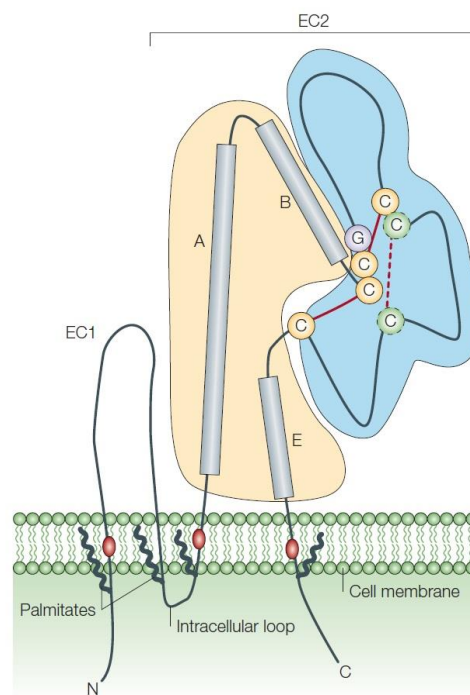


Figure 10. General structure of a consensus tetraspanin protein. Tetraspanin proteins are comprised of four transmembrane domains, two short N- and C-terminal cytoplasmic tails and two extracellular portions: EC1 domain (the smallest loop) and EC2 domain (the biggest loop). EC2 loop is stabilized by 2 to 4 disulfide bonds (red lines) and consists of four invariant Cys residues (in yellow), two of which are in a Cys-Cys-Gly (CCG) motif. In the EC2 domain there are 3 α -helices (A, B, E) that make up a highly conserved region (in yellow), as well as a variable region (in blue). Image adapted from Hemler *et al.* 2005²³².

Some evidence suggest that the four transmembrane domains form a compact bundle in the membrane, which facilitates multiple interactions with other proteins. For example, mutations in transmembrane domains affect the folding,

stability and transport capacity of numerous tetraspanins. However, structural models are only available for CD81²³⁵⁻²³⁸. Based on that information and molecular models, it has been described that there is high homology among all tetraspanins members, except in a small variable domain that is located in EC2. Nevertheless, in EC2 there are also some highly conserved motifs for all members of the family that are related to specific functions: CCG (Cys-Cys-Gly), PXSC (Phe-X-Ser-Cys) and EGC (Glu-Gly-Cys)^{236,239,240}. For example, it is widely known that EC2 regions are very important for the interactions with other family members as well as with integrins (family of cell transmembrane adhesion receptors, which form α - β heterodimers) and other signaling molecules²⁴¹⁻²⁴³.

1.6.2. Tetraspanins: post-translational modifications, interactions and biological relevance.

One of the main characteristics of tetraspanins is their high potential to establish direct or indirect interactions with multiple biomolecules, acting as molecular facilitators capable of modulating several signaling and biological processes. Tetraspanins are found anchored to the plasma membrane, to some cytoplasmic organelles (e.g., endosomes, lysosomes, ER)^{136,244-247} and to extracellular vesicles (e.g., exosomes)^{136,247}. The rod-shaped tetraspanin structure gives them a high stability in the lipid membrane, which makes them excellent candidates for forming structural/signaling networks²³⁵. They have the ability to form lateral associations with multiple proteins (including other tetraspanins), cholesterol and gangliosides, forming a dynamic assembly that has been defined as tetraspanin webs or tetraspanin-enriched microdomain membranes^{233,248-251} (**Figure 11**). The multiple possible combinations between different tetraspanins and other membrane-associated proteins generate an enormous variability of great

Introduction

biological relevance ²⁵¹. Such associations can be established through interactions of the extracellular or intracellular domains of the partners (**Figure 11**) and, in some cases, they can be originated during early stages of the biosynthetic process, in ER or Golgi compartment ²³³.

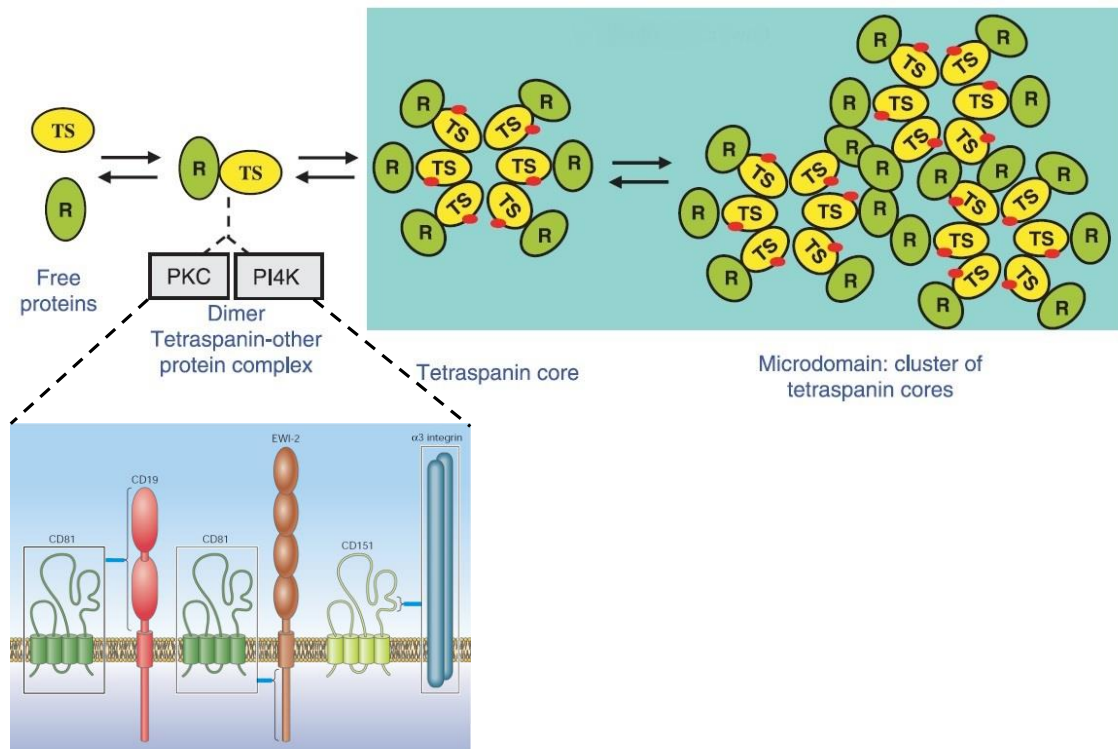


Figure 11. Tetraspanin web and different possible interactions between partner domains. A tetraspanin protein (TS, in yellow) binds to a receptor or membrane protein (R, in green; e.g., PKC, PI4K), which may be specific for each tetraspanin. This heterodimer can be incorporated into larger complexes (tetraspanin core and microdomains), then forming the tetraspanin web. The interaction among the partners can be through the extracellular or intracellular domains. For example, CD81 antigen interacts through EC2 with the extracellular domain of B-lymphocyte antigen CD19 (CD19); however, its interaction with Glu-Trp-Ile EWI motif-containing protein 2 (EWI-2) is through the intracellular domains. On the other hand, CD151 antigen (CD151) interacts with $\alpha 3$ integrins through EC2, and strong stoichiometric interactions are established. PI4K, phosphatidylinositol 4-kinase; PKC, protein kinase C; the red spots indicate post-translational modifications; brackets indicate mapped interacting domains. Figure adapted from Levy *et al.* 2005 ²³³ and Lazo 2007 ²⁵¹.

The capacity of tetraspanins to form primary interactions (that are not disrupted by harsh detergents) with different non-tetraspanin proteins (e.g., integrins, immunoglobulins and cellular receptors) may be dependent on cell lineage. For example, CD81 interact with CD19 (B-lineage-specific molecule) in B-lymphocytes, whereas in T-lymphocytes, CD81 is associated with the T-cell surface

glycoproteins CD4 and CD8^{233,252,253}. Moreover, it has been described that the presence of one or more N-glycosylations in EC2 are very common among tetraspanins, as well as palmitoylation and ubiquitination. The last two occur in the intracellular loop and at the N and C-terminal tails, in some highly conserved cysteine and lysine residues, respectively. All these post-translational modifications play a central role in the interactions within the tetraspanin webs and their downstream pathways (**Figure 11**)^{233,254}. For example, palmitoylation is necessary for the maintenance of the interactions between tetraspanin-tetraspanin (secondary interactions that are not disrupted by mild detergents)^{250,255}, tetraspanin-integrins²⁵⁰ and tetraspanin-cholesterol²⁴⁹. Furthermore, palmitoylation allows the proper structural organization of tetraspanins into exosome-like extracellular vesicle membranes²⁵⁶ and contribute to its incorporation into tetraspanins webs²⁵⁷ and B cell activation²⁵⁸. On the other hand, CD82 and CD9 N-glycosylation sites were suggested to regulate apoptosis²⁵⁹ and modulate β -catenin signaling downstream²⁵⁴, while their ubiquitination is important for the tetraspanins regulation on cell surface²⁶⁰. Finally, tertiary interactions (are not disrupted by mild detergents) are established indirectly between tetraspanins and other proteins. Functionally, these interactions allow the cross talk with intracellular signaling and cytoskeletal structures²³³.

CD9, CD81, CD82 and CD151 are the most extensively studied tetraspanins, while others such as CD53, CD63 and CD37 have also been identified in complexes but are less characterized. However, the information available about others family members is very limited^{232,251}. Through immunoprecipitation assays and proteomic analysis of tetraspanin-containing complexes, it has been possible to describe the tetraspanins interactions. They can interact with many

Introduction

transmembrane proteins such as other tetraspanins, adhesion molecules (e.g., integrins, EpCAM, VCAM-1, ICAM-1, B-CAM/Lu, and GA733 proteins), receptors and signaling molecules (e.g., BAI2, PKC, G proteins, PI4K, GFR, Notch, leucocyte receptors), proteases (ADAM10, TADG15), and membrane fusion proteins (syntaxins) ^{232,244,261-263}. However, there are fewer examples of tetraspanins interacting with cytoplasmic proteins, which could be due to the small size of the N and C-terminal tails ²⁶⁴. In **Table 1** are summarized some possible interactions between tetraspanins and other proteins.

Tetraspanin interactions have been linked to various biological processes such as antigen presentation, signal transduction pathways, proliferation, motility, adhesion, tissue differentiation, angiogenesis, tumor progression and metastasis ²⁶⁵⁻²⁶⁸. Most of the interactions reported for tetraspanins are with integrins, mainly with $\beta 1$ chain integrins, a major component for extracellular matrix binding (**Table 1**). These interactions are responsible for the modulation of multiple cellular processes, including proliferation, migration and apoptosis; as well as angiogenesis, metastasis and drug resistance ^{234,251,269,270}. For example, CD151–integrin interactions strengthen the attachment to the extracellular matrix ²⁷¹. However, the tetraspanin web formed through intracellular interactions of $\beta 1$, $\beta 2$ and $\beta 3$ integrin domains with the CD9, CD81, CD82, and CD151 tetraspanins induces high recruitment of PKCs, such as the PKC α and PKC ϵ isoforms, promoting integrin-dependent cell motility and control integrins internalization ²⁷²⁻²⁷⁵. In addition, the co-localization of CD151 with the $\alpha 6\beta 4$ integrin (**Table 1**) also triggers PKC, which promotes cell motility through integrin internalization ²⁷⁴. However, the depletion of some tetraspanins (e.g., CD151) show marked

physiological effects independent of their interactions with integrins ^{276,277}, suggesting other interactions with ligands not yet identified.

Table 1. Protein interactions with the tetraspanins family members CD9, CD53, CD81, CD82, CD151, CD63, CD37. Table adapted from Lazo, 2007 ²⁵¹.

	CD9	CD53	CD81	CD82	CD151	CD63	CD37
$\alpha 3\beta 1$	+	+	+	+	+	+	+
$\alpha 4\beta 1$	+	+	+	+	ND	+	ND
$\alpha 6\beta 1$	+	+	+	+	+	+	ND
$\alpha 5\beta 1$	+	ND	+	+	ND	+	ND
Precursor $\beta 1$	+	ND	-	-	ND	-	ND
$\alpha IIb\beta 3$	+	ND	ND	ND	ND	ND	ND
$\alpha 6\beta 4$	-	ND	-	ND	+	-	ND
CD11/CD18	ND	ND	ND	ND	ND	+	ND
HLA-DR	ND	+	+	+	ND	+	+
HLA-DM	ND	ND	ND	+	ND	+	ND
HLA-DQ	ND	+	+	+	ND	ND	ND
HLA-DO	ND	ND	ND	+	ND	+	ND
EGF-R	ND	ND	ND	+	ND	ND	ND
TGF- α	+	ND	ND	ND	ND	ND	ND
FGFR	+	ND	+	ND	ND	ND	ND
c-Met	+	ND	ND	+	ND	ND	ND
HB-EGF	+	ND	-?	-?	ND	ND	ND
FRPP	+	ND	+	ND	ND	ND	ND
EWI-2	+	ND	+	+	ND	ND	ND
EWI-F	ND	ND	+	ND	ND	ND	ND
CD36	+	ND	ND	ND	ND	ND	ND
CD9P-1	+	ND	+	+	+	+	ND
CD2	ND	+	ND	ND	ND	ND	ND
CD4	ND	ND	+	+	ND	ND	ND
CD8	ND	ND	+	+	ND	ND	ND
CD21-CD19-Leu13	ND	ND	+	ND	ND	ND	ND
CD19	+	ND	+	+	ND	ND	ND
CD20	ND	+	+	+	ND	ND	ND
CD46	+	ND	+	+	+	ND	ND
Protein kinase C	+	+	+	+	+	-	-
Phosphatidylinositol 4-kinase	+	-	+	-	+	+	ND
Dectin-1	ND	ND	ND	ND	ND	ND	+
Syntenin 1	ND	ND	ND	ND	ND	+	ND
γ -Glutamyl transpeptidase	ND	+	+	+	ND	ND	ND

(+), positive interaction; (-), no interaction; ND, not determined.

The presence of several tetraspanins related to the major histocompatibility complex (MHC) class II compartments (MIIC) in antigen-presenting cells (APC), and their association with receptors with immunoglobulin domains like Ewing (EWI) family (e.g., EWI-2 with CD81, CD9 and CD82; **Table 1**, **Figure 11**) have a relevant role during immune responses like antigens presentation and lymphocyte

Introduction

activation²⁷⁸⁻²⁸¹. EWI-2 interaction with the metastasis suppressor tetraspanin CD82 enhance its tumor-suppressing role by inhibiting cell migration²⁸⁰. Furthermore, EWI-2 interacts with growth factor receptors that poses tyrosine-kinase activity, such as c-Met, which in turn is a receptor for scatter factor or hepatocyte growth factor, and is implicated in EMT²⁸². On the other hand, CD9 interacts through its extracellular domains with TGF- α , promoting EGFR-activation and cell proliferation²⁸³. Likewise, the tetraspanins CD9, CD63, CD81, A15, and CD151 have been associated with PI4K, probably without requiring prior binding to an integrin^{251,284}. PI4K catalyzes the conversion of phosphatidylinositol (PI) to phosphatidylinositol 4-phosphate (PI4P), an important intermediate for lipid-mediated signaling and autophagy^{285,286}. In this context, it has been suggested that CD151 is a critical linker between PI4K and $\alpha 3\beta 1$ integrin, which could have important implications for cell migration²⁵⁴.

It is worth noting that in the past decade several tetraspanins have also been implicated in resistance to current therapy and/or in CSCs phenotype acquisition. For example, CD9 and CD81 mediates chemoresistance in breast cancer and small cell lung cancer. CD9 is responsible for the cross talk between bone marrow-derived mesenchymal SCs and breast cancer cells, and its inhibition trigger apoptosis^{287,288}. Furthermore, TSPAN8 overexpression in breast CSCs is responsible for promoting NANOG, OCT4, and ALDHA1 expression and is associated with resistance to therapy²⁸⁹. Finally, CD151 ablation sensitized multiple types of tumor cell to several anti-cancer drugs (e.g., gefitinib and camptothecin), increasing apoptosis and control cell migration, independently of its interactions with integrins^{276,277}.

1.6.3. *Tetraspanin 1 and cancer*

Tetraspanin 1 (also termed TSPAN1, NET-1 and C4.8) is a protein with 241 amino acid whose gene TSPAN1 is located at chromosome 1p34.1 and belongs to the tetraspanin family ²⁹⁰. TSPAN1 is still poorly studied, but its oncogenic role in cancer has recently been evidenced, mainly in digestive malignancies as pancreatic, gastric, colorectal, and esophageal cancers, but also in hepatocellular carcinoma, skin squamous cell carcinoma, prostate cancer, osteosarcoma and non-small cell lung cancer ²⁹¹⁻³⁰¹. In addition, the overexpression of TSPAN1 at mRNA and/or protein level in human tumor samples versus adjacent noncancerous tissues has been widely documented in cholangiocarcinoma ^{294,302,303}, skin squamous cell carcinoma ^{297,304}, esophageal carcinoma ²⁹⁵, ovarian carcinomas ³⁰⁵, prostate cancer ²⁹⁸, pancreatic cancer ^{292,296} and gastric carcinoma ^{293,306}.

This has inspired numerous studies focused on modulate TSPAN1 expression, as a potential target in cancer. In this way, TSPAN1 depletion with shRNA and/or siRNA decreased EMT, metastasis, proliferation, migration, and delayed tumor growth in hepatocellular carcinoma ^{291,303,307,308}. TSPAN1 inhibition has also reduced proliferation, invasion and tumor growth in human skin squamous cell carcinoma ^{304,309}, colon cancer ³¹⁰ and pancreatic cancer ³⁰¹.

Several microRNAs are capable of regulating TSPAN1 expression. Among those that have an inhibitory effect and, consequently, a tumor-suppressing role, are miRNA-194-5p and miRNA-638 in cholangiocarcinoma ^{294,303}, miRNA -491-3p in osteosarcoma ²⁹⁹, and miRNA -573 in gastric cancer ²⁹³. Contrastingly, miRNA-200a causes TSPAN1 overexpression in the lung cancer cell lines A549 and SK-MES-1, which in turn induces migration ³⁰⁰.

Introduction

Additionally, other recent studies have suggested that TSPAN1 is linked to apoptosis and autophagy. For example, silencing TSPAN1 with siRNAs markedly inhibited proliferation while increasing the caspase-3 dependent apoptosis in esophageal carcinoma cells ²⁹⁵. Likewise, multi-target siRNA against TSPAN1 and VEGF suppresses proliferation, migration, invasion, angiogenesis and induces apoptosis in hepatocellular carcinoma. These effects can be explained by the downregulation observed in cyclin D1 and Bcl-2 (an IAPs family member) ^{308,311}, which also could lead to activate beclin1-mediated autophagy (**Figure 9**) and consequently autophagy-mediated apoptosis. Furthermore, by co-immunoprecipitation and IHC analysis in skin squamous cell carcinoma, an interaction and a statistical association between TSPAN1 and survivin (another IAPs family member) were found, and both were related with metastasis. Their simultaneous and individual inhibition also inhibited proliferation and induced apoptosis. This result may be explained by the significant downregulation of VEGF, cortactin and Bcl-2, and the upregulation of caspases 3 and 8 ²⁹⁷. Downregulation of Bcl-2 could again involve autophagy-mediated apoptosis. Similar results were found in human pancreatic cancer cell lines ^{292,296}.

On the other hand, the cooperation between tetraspanins and integrins plays an important role in the regulation of cell motility and invasive capacity of tumor cells ³¹². Consequently, TSPAN1 has also been linked to EMT phenotype activation and metastasis induction. In cholangiocarcinoma, the interaction between TSPAN1 and $\alpha 6\beta 1$ integrin induces EMT via the activation of the downstream pathway PI3K/AKT/GSK-3 β /SNAIL ³⁰³. Moreover, in prostate cancer, TSPAN1 is under androgen control and the mesenchymal markers SNAIL2 and ARF6 are induced ²⁹⁸.

However, in a physiological context unrelated to cancer (dorsal root ganglion neurons), it has been described that TSPAN1 is capable of directly interacting with tropomyosin-related kinase A (TrkA)-receptor in the ER. In this way, TSPAN1 determines the surface amount of TrkA-receptor by controlling its sorting to the autophagy/lysosomal degradation pathway ²⁴⁶. This supports the possible relationship of TSPAN1 as a modulator of autophagy, while evidencing once again the important role of autophagy in cellular homeostasis, in this case controlling neuronal differentiation.

Currently we have only found one publication in HNSCC (precisely in the larynx cell line JHU029) where TSPAN1 was related to tumorigenesis. In this case, it was demonstrated that TSPAN1 interacts with the $\alpha6\beta1$ integrin and induces the activation of FAK/STAT1 α pathway and the overexpression of the matrix metalloproteinase (MMP)-2 and MMP-26. Consequently, migration and invasion were induced ³¹². However, more comprehensive studies about the role of TSPAN1 in HNSCC would be necessary in order to know if TSPAN1 could be considered in cancer therapy, particularly to eliminate chemoresistant cells.

HYPOTHESES

II. HYPOTHESES

Due to the high incidence, recurrence rates, and mortality of HNSCC, the identification of new proteins involved in chemoresistance represent key pieces for the discovery of novel molecular pathways that will allow the development of effective therapies against HNSCC. Based on this, we have formulated the following hypotheses:

- i. The establishment of HNSCC resistant cell lines (to CDDP and 5-FU), as well as the isolation of CSCs (both from sensitive cells), will represent an effective chemoresistance model.
- ii. The establishment of biopsy-derived cell lines from HNSCC patients will allow us to identify patients with innate resistance to current chemotherapy and furthermore, to test new therapeutic alternatives in those patients.
- iii. The exacerbated activation of autophagic flow has important clinical implications in cancer, particularly in HNSCC, in relation to tumor progression and chemoresistance. The analysis of autophagy activation in:
a) both sensitive and chemoresistant HNSCC cell lines, b) biopsy-derived cell lines, c) HNSCC biopsies; will allow us to establish the relationship between autophagy activation and variables with clinical relevance.
- iv. Through a comparative proteomic study among a chemosensitive cell line and their chemoresistant and CSCs derivatives, will be possible to identify target proteins responsible for the acquisition of chemotherapy resistance. The modulation of these target proteins would re-sensitize tumors to standard chemotherapeutic treatments.

OBJECTIVES

III. OBJECTIVES

The main objectives of this thesis are:

- **Objective 1:** To determine the role of autophagy in HNSCC models and its relationship with chemotherapy resistance and other clinical parameters.
- **Objective 2:** To identify target proteins involved in the acquisition of chemotherapy resistance in HNSCC models which expression and/or activity modulation could be of clinical and therapeutic interest.

In accordance with the achievement of the above-mentioned objectives, we have subdivided them into the following **specific objectives**:

- 1.1. To establish CDDP and 5-FU resistant cell lines, as well as cell cultures enriched in CSCs, both from HNSCC cell lines sensitive to these drugs.
- 1.2. To establish biopsy-derived cell lines from HNSCC patients.
- 1.3. To analyze the relationship between the expression of autophagy markers and parameters with clinical relevance in: a) HNSCC cell lines, b) biopsy-derived cell lines, and c) HNSCC biopsies.
- 1.4. To evaluate the modulation of autophagy as a possible therapeutic alternative in HNSCC.
- 2.1. To identify proteins commonly deregulated in CDDP-resistant cell lines and CSCs, respect to the corresponding CDDP-sensitive cell line (proteomic study).
- 2.2. To validate by western blot some potential target proteins identified in the proteomic study. Selection of one candidate protein.
- 2.3. To modulate the expression of this candidate protein and perform functional assays both *in-vitro* and *in-vivo*, to determinate its possible role in HNSCC tumors.

MATERIALS AND METHODS

IV. MATERIALS AND METHODS

4.1. Biological samples

4.1.1. Patients and tissue samples

HNSCC patients were diagnosed by the Otorhinolaryngology department at the Hospital Universitario Vall d’Hebron (HUVH). Patients were clinically followed for approximately 10 years and grouped by location as follows: 23 glottic, 81 supraglottic and 78 subglottic tumors. Paraffin-embedded HNSCC biopsies were studied by IHC for the expression of LC3 (84 patients), p62, ATG5 and PTOV1 (78 patients). The mean age of these 84 patients was 58 years old (range 32 to 83) and 48% of them were heavy habitual smokers (>40 pack/year). A summary of the main clinical-pathological characteristics of this group of patients is shown in **Table 2** and the raw data, including the H-scores, is shown in **Appendix 1**. Moreover, fresh biopsies of HNSCC patients undergoing surgery at the HUVH were obtained from the Pathology department.

Table 2. Clinical and pathological characteristics of the patients with laryngeal cancer from HUVH included in the IHC study. Chemo/radio-therapeutic treatments were post-surgical.

Characteristics	Classification	Number of patients	Percentage (%)
pT classification	T1-T2	18	21
	T3-T4	66	79
pN classification	N0	41	49
	N1-N3	43	51
Tumor stage	I-II	37	44
	II-IV	47	56
Histopathologic grade	Well differentiated	53	63
	Moderately differentiated	20	24
	Poorly differentiated	11	13
Surgical margins	affected	21	25
	no affected	63	75
Tumor location	glottic	8	10
	supraglottic	26	31
	subglottic	47	56
Chemotherapy	No treated	62	74
	Treated	22	26
Radiotherapy	No treated	10	12
	Treated	74	88
Total cases		84	

Materials and methods

In addition, biopsies from 106 patients with laryngeal or hypopharyngeal squamous cell carcinoma who underwent surgical treatment at the Hospital Universitario Central de Asturias (HUCA) between 1996 and 2005 were retrospectively collected in order to study them by IHC TSPAN1, active SRC (pSRC), and E-cadherin. The mean age of the Asturias's patients was 60 years (range 38 to 86 years). All patients were habitual tobacco smokers, 65 moderate (1-50 pack/years) and 41 heavy (>50 pack/year), and 98 were habitual alcohol drinkers. Some clinicopathologic features of these studied patients are summarized in **Table 3** and **Appendix 2**.

Table 3. Clinical and pathological characteristics of the patients from HUCA included in the IHC study.

Characteristics	Classification	Number of patients	Percentage (%)
pT classification	T1-T2	23	22
	T3-T4	83	78
pN classification	N0	31	29
	N1-N3	75	71
Tumor stage	I-II	8	8
	III-IV	98	92
Histopathological grade	Well differentiated	26	25
	Moderately differentiated	50	47
	Poorly differentiated	30	28
Site	Pharynx	53	50
	Larynx	53	50
Tumor recurrence	No	40	38
	Yes	66	62
Radiotherapy	No treated	49	46
	Treated	57	54
Total cases		106	

The stage of disease was determined after the surgical resection of the tumor according to the TNM system of the International Union against Cancer (Seventh Edition). The histological grade was determined according to the degree of differentiation of the tumor (Broders' classification). All patients had a single primary tumor and received no treatment prior to surgery. The experimental procedures were conducted in accordance to the Declaration of Helsinki and

approved by institutional ethics committees of the HUVH (Ref. PR[AG]342/2016) and HUCA (Ref. 70/16), and by the regionals CEIC. Written informed consents were obtained from patients.

4.1.2. Cell lines and culture conditions

Fresh samples of normal and tumoral tissue from patients surgically treated for squamous larynx and pharynx carcinoma were obtained from the Pathology department of the HUVH. One part of the tissue samples was frozen directly at -80°C until later use, and the other part was processed to establish primary long-term cultures *in-vitro*. Samples were collected in 1X phosphate-buffered saline (PBS) (Biowest, Nuaille-France) and immediately cut into very small fragments under sterile conditions. Then the samples were incubated with collagenase (200 µg/mL) and hyaluronidase (20 µg/mL) for 2 hours at 37 °C. After enzymatic digestion, independent cells and remnant tissue fragments were centrifuged and re-suspended in the appropriate culture medium and placed in optimal culture conditions. The primary cells were cultured in RPMI 1640 medium (Gibco, Life Technologies) supplemented with 20% fetal bovine serum (FBS) (Biowest, Nuaille-France), 20 U/ml penicillin and 20 µg/ml streptomycin (Gibco, Life Technologies), 2.5 µg/ml amphotericin B, 10 µg/mL gentamicin (Capricorn Scientific, Labclinics) and 2 mM L-Glutamine (Gibco, Life Technologies).

Furthermore, the following cell lines were acquired:

- HTB-43 (FaDu): human cell line derived from a primary squamous cell carcinoma of hypopharynx.
- CCL-138 (Detroit 562): human cell line derived from metastatic site (pleural effusion) whose primary tumor was a pharyngeal carcinoma.

Materials and methods

- JHU029 (RRID: CVCL_5993): human cell line derived from a primary squamous cell carcinoma of larynx.
- SCC-25 (CRL-1628): human cell line derived from a primary squamous cell carcinoma of tongue.

HTB-43 and CCL-138 were purchased from the American Type Culture Collection (ATCC, Manassas, VA, USA), and Dr. Salvador Aznar Benitah (Institute for Research in Biomedicine, Barcelona) kindly provided JHU029 LucIRES-GFP and SCC-25 LucIRES-GFP. All of them were satisfactorily authenticated based on polymorphic short tandem repeat loci (February 2019). All cell lines were cultured in MEM (HTB-43 and CCL-138), RPMI 1640 (JHU029) or DMEM F-12 (SCC-25) media (Gibco, Life Technologies) supplemented with 10% FBS, 20 U/ml penicillin, 20 µg/ml streptomycin, and 1 mM sodium pyruvate (Sigma-Aldrich, Merck).

CSCs were obtained from their respective parental cell lines (HTB-43, CCL-138, JHU029 and SCC-25) by culture under non-adherent conditions, in a CSCs selection medium (3D Tumorsphere medium XF, PromoCell), based on their ability to form tumorspheres under serum-free and xeno-free condition. Cells were seeded at 1×10^4 cells per milliliter in 6-well plates treated for suspension cell cultures (2 ml of total volume) (Sarstedt AG & Co.) and pre-coated with poly-HEMA (Poly(2-hydroxyethyl methacrylate)) (Sigma-Aldrich, Merck). CSCs were supplemented with fresh CSCs selection medium every 48 hours, and it was allowed the growth for three consecutive generations [Generation 1 (G1), Generation 2 (G2) and Generation 3 (G3)]. For that, every 7 days tumorspheres were collected in a 50 mL tube (Falcon, Corning Life Sciences, VWR) and sedimented by gravity for 10 minutes, discarding individual cells. Once sedimented, tumorspheres were treated for 10 minutes with TrypLE™ Express trypsin (Gibco, Life Technologies) at 37 °C,

and subsequently they were mechanically disaggregated using a Pasteur pipette (Labbox Labware, Spain). Individual cells were seeded again under the same initial conditions to form the next generation of CSCs. Unless otherwise stated, CSC G3 were selected for analyses, generically referred as CSC.

All cells were grown in an air flow incubator (AutoFlow UN-5510 incubator, Nuair) at 37 °C and 5% CO₂, and manipulated under sterile conditions in a vertical laminar flow hood (Bio II, Telstar, Life Science solutions). All cell lines were regularly split to keep them in sub-confluence.

On the other hand, cells were appropriately cryopreserved at 1-3 million cells per cryotube (Sarstedt AG & Co.) using FBS & 10% dimethyl sulfoxide (DMSO) (Fisher Chemical, Fisher scientific) as freezing medium. Cell pellets were re-suspended in freezing medium and immediately placed on ice, and subsequently passed at -80 °C in a Mr. Frosty freezing container (Nalgene, Thermo Scientific) with isopropanol (PanReac Applichem ITW reagents, vidra Foc), so that the freezing process was gradual (approximately at a rate of -1 °C/minute). If the cells were not going to be used for a long time, they were subsequently transferred to liquid nitrogen to maintain temperatures below -160 °C. However, during the thawing process, cells were thawed directly at 37 °C and immediately diluted in complete pre-warmed culture medium. Cells were then centrifuged at 400 xG for 5 minutes, re-suspended in complete culture medium and seeded in an appropriate culture plate.

4.2. Transfections

One of the most commonly used tools to study and control gene expression in eukaryotic cells is transfection, a process by which genetic material (DNA or RNA) is deliberately introduced into the cell. Through transient transfection, it is possible to obtain high expression levels of certain exogenous genes, and therefore

Materials and methods

to achieve high expression levels at protein level (in general). Moreover, it is also possible to block the expression of specific endogenous genes, for example by the use of siRNAs or microRNAs, often inducing a decrease in the expression of the related protein. Gene and protein expression are usually analyzed 24-96 hours after transfection.

Cells were transfected in reverse conditions with 10 nM siRNA against TSPAN1 (siTSPAN1) and other alternative siTSPAN1 (siRNA#2), 10nM DsiRNA negative control (NC) (Integrated DNA Technologies), and 4µl of lipofectamine RNAimax (Invitrogen, Thermofisher) per well of 6-well plates, in 2 mL of opti-MEM reduced serum medium (Gibco, Life Technologies). Kinesin-like protein KIF11 siPOOL (siTOOLS Biotech) and BLOCK-iT™ fluorescent oligo (Invitrogen, Thermofisher) were used as transfection positive control. Furthermore, we used an additional siTSPAN1 (siTOOLS Biotech) to demonstrate independently the biological effect of TSPAN1 inhibition. This siRNAs (siPOOLS) consist of a pool of 30 optimally-designed siRNAs that demonstrated to efficiently remove off-target effects and improve the reliability of results ³¹³.

In total 2×10^5 cells per well were seeded into 6-well plates. Next day, opti-MEM medium was replaced with the standard growth medium used for each cell line or primary cell culture. Transfected cells for the different functional assays and protein/RNA extractions were used at 48 or 72 hours after transfection.

For PTOV1 overexpression assay, JHU029 cells were transfected with plasmid pHA-PTOV1 at 2 µg/well in 6-well plates, according to the previously described protocol ³¹⁴. Reverse transfections were performed in opti-MEM (2 mL of total volume) using 6 µl/well of lipofectamine 3000 (Thermo Fisher) and 4 µL/well of

P3000. Seventy-two hours after transfection, cells were collected and lysed for protein expression.

4.3. Functional assays

4.3.1. Analyses of side population (SP)

SP assay has been widely used to detect cells with the ability to efflux the Hoechst dye via ABC family members, compared to a control population where verapamil inhibits the function of these transporters. This efflux capacity releasing compounds from the intracellular to the extracellular microenvironment (e.g., drugs or dyes) is related to the acquisition of stemness phenotype and drug resistance.

Subconfluent cells were washed with 1X PBS and re-suspended at a density of 1×10^6 cells/ml in prewarmed cell culture medium supplemented with 2% FBS and 10 mM 4-(2-hydroxyethyl)-1-piperazineethanesulfonic acid (HEPES) (Sigma-Aldrich, Merck). Then, cells were incubated at 37 °C for 2h with 5 µg/ml Hoechst 33342 dye (Thermo Scientific). Control cells were incubated with 50 µM verapamil (Sigma-Aldrich, Merck) for 15 minutes at 37 °C before the addition of Hoechst dye to validate the SP detection. For dead cell discrimination, propidium iodide (PI) (Sigma-Aldrich, Merck) at 5 µg/ml was added to the cells before analyses on FACSaria II flow cytometer (BD Biosciences). Results were confirmed in at least three independent experiments.

4.3.2. Viability assays

To determine cell viability we used two different techniques: trypan blue exclusion test (0.4% trypan blue) (Invitrogen, Thermofisher) and MTS assay (Aqueous MTS Reagent Powder, Promega Biotech Iberica):

Materials and methods

- The trypan blue exclusion test is based on the principle that living cells, having their plasma membrane intact, do not stain with this dye; however, dead cells are stained. In this way, we can determine the number of living (unstained) and dead (blue) cells during cell counts in the Neubauer chamber. We can calculate the viability of each experimental condition as the ratio of living cells and the total number of cells. During cell counts for the construction of proliferation curves and other functional assays, only the living cells were considered.
- MTS is a novel tetrazolium compound to estimate the number of viable cells in proliferation and cytotoxicity assays based on the rate of metabolic activity (in the living cells) of the previously treated cells versus control cells. The MTS stock solution is prepared at 2 mg/mL in 1X PBS. In addition, a stock solution of PMS (Phenazine methosulfate) (Sigma-Aldrich, Merck) was prepared at 200 mg/mL. A mixture of MTS:PMS (20:1, V/V) is used at the rate of 20 μ L per 80 μ L of complete medium per well of 96 well plate. Living cells produce then formazan crystals that are soluble in the cell culture medium and produce color, so after 2 hours of incubation the plates were analyzed using a spectrophotometer (Epoch, Biotek) at 490 nm. Cell viability was calculated respect to the control conditions.

4.3.3. Drug assays

The CDDP and 5-FU resistant cell lines (JHU029-R, HTB-43-R, CCL-138-R and SCC-25-R) were generated from the corresponding parental cell lines by exposure to pulses of 72-96 hours of the drugs (half-maximal inhibitory concentration (IC₅₀) or more) for 12-18 months. Cells were considered "resistant" when they were able to constantly live in the presence of the drug and achieve an IC₅₀ at least 2-3 times

higher than their corresponding parental line. To determine their respective IC₅₀, JHU029 and JHU029-R, HTB-43 and HTB-43-R, CCL-138 and CCL-138-R, and SCC-25 and SCC-25-R cell lines were seeded at 15x10³ cells per well into 96-well plates, and the biopsy-derived cell lines at 10x10³ cells per well. Twenty-four hours later, cells were exposed in triplicate to CDDP (range 0-150 μM), 5-FU (range 0-2000 μM) (Sigma Aldrich, Merck), HCQ (range 0-300 μM) (Fisher Scientific) or dasatinib (range 0-3 μM) (Sigma-Aldrich, Merck) for 48 or 72 hours. Cellular viability was measured relative to control conditions (with the drug's placebo) by MTS assay. In this way, the respective survival curves were constructed and the IC₅₀ values were determined using GraphPad Prism version 6.00 program for Windows (GraphPad Software, La Jolla California, USA).

On the other hand, to determine the appropriated concentrations (C1, C2 and C3) used in the combinatorial assay with CDDP, 5-FU and HCQ (**Figure 26, Figure 27**), the IC₅₀ of each parental cell line or biopsy-derived cell line was previously determined. Based on that, the concentration C1, C2 and C3 were chosen (**Appendix 3, Figure 27 B**), and the corresponding individual responses were determined for both parental and resistant cell lines. Results were confirmed in at least three independent experiments.

4.3.4. Proliferation assays

To determine the proliferative capacity of JHU029, JHU029-R, HTB-43, HTB-43-R, CCL-138 and CCL-138-R cell lines under TSPAN1 depletion, they were previously transfected in reversed conditions with siTSPAN1 versus NC, and 48 hours later they were seeded at the rate of 1x10⁵ cells per well in 6-well plates. For the construction of the corresponding proliferative curves, six cell counts using trypan

Materials and methods

blue and a Neubauer chamber were performed every 1-3 days up to a maximum of 12 days. Results were confirmed in at least three independent experiments.

4.3.5. Colony formation assay

The colony formation assay or clonogenic assay is an *in-vitro* cell survival assay based on the "unlimited capacity" of cell division of isolated tumor cells. These cells must be capable to form colonies of at least 50 cells (macroscopically visible). Briefly, 5×10^3 cells per well were seeded in triplicate in 6-well plates and the colony formation was allowed for 10-14 days (depending on the cell line). The quantification of the colonies was performed by fixation with 4% formaldehyde (PanReac AppliChem, ITW Reagents) for 10 minutes at room temperature (RT), and subsequent staining with crystal violet (0.5% W/V in water) (Sigma-Aldrich, Merck) for 30 minutes. After three washes, dyed colonies were diluted with 15% acetic acid (Sigma-Aldrich, Merck), and quantified colorimetrically at 595 nm in a spectrophotometer. Results were confirmed in at least three independent experiments.

4.3.6. Apoptosis detection by flow cytometry

Detection of Annexin V as a method of detecting apoptosis is based on its ability to bind phospholipids, preferably phosphatidylserine (PS). Viable cells maintain an asymmetric distribution of anionic phospholipids such as PS, which are preferably located on the cytoplasmic side of the plasma membrane. During apoptosis, the lipid bilayer loses its asymmetry and PS is translocated to the extracellular membrane as a recognition signal of phagocytosis. Thus, using fluorescently labeled Annexin V, those cells expressing apoptosis signals are identified. In early apoptosis stages, the plasma membrane excludes viability dyes such as PI,

therefore cells that display only Annexin V staining (Annexin V positive but PI negative) are in an early stages of apoptosis. However, during late apoptosis stage, loss of cell membrane integrity allows Annexin V binding to cytosolic PS, as well as cell uptake of PI (cells Annexin V and PI positives).

Apoptosis quantification was performed in HNSCC cells transfected with siTSPAN1 versus NC (72 hours post-transfection) using an Annexin V-APC detection kit (Thermo Fisher Scientific), and analyzed in a Fortessa LSR flow cytometer (Becton Dickinson, E0772; BD Biosciences, San Jose, CA, USA). Briefly, subconfluent cells were washed with 1X PBS and then trypsinized (Gibco, Life Technologies). Cells were washed twice with cold 1X PBS and centrifuged at 400 xG for 5 minutes, later they were counted using trypan blue and a Neubauer chamber. Then, 5 μ L of Annexin-V-APC was added to 1×10^5 cells previously re-suspended in 100 μ L of binding buffer, and they were incubated for 15 minutes in dark at RT. After centrifuging the cells, they were re-suspended in 400 μ L of binding buffer and 2 μ L of PI (0.5 μ g/mL) was added in the corresponding tubes (according to the design). At least 1×10^4 cells were quantified for each sample and data were subsequently analyzed using the FACS Express Flow Research Software, version 4. Results were confirmed in at least three independent experiments.

4.3.7. Autophagy analyses by TEM

Sample preparations for the TEM and the further detection of autophagic vesicles were performed in the Electronic Cryomicroscopy Unit from the Scientific and Technological Centers of the Barcelona University. Seventy-two hours after transfection, cells were fixed in 2.5% glutaraldehyde in 0.1 M phosphate buffer for 1h, washed four times with 0.1 M PBS, post-fixed with 1% osmium tetroxide (EMS, Hatfield) for 2 hours and washed with milliQ water. The samples were then

Materials and methods

dehydrated in a series of acetone (50%, 70%, 90%, 96% and 100% for 10 minutes each), and infiltrated and embedded in Epon resin (EMS, Hatfield). Ultrathin sections of 60 nm in thickness were obtained using a UC6 ultramicrotome (Leica Microsystems) and stained with 2% uranyl acetate and lead citrate. Sections were observed in a Jeol 1010 microscope (Gatan, Japan) equipped with a tungsten cathode and images were acquired at 80 kV with a CCD Megaview 1kx1k. Autophagic vesicles per cell were quantified for each group.

4.4. RNA analyses

4.4.1. Total RNA extraction: quality and quantification

For total RNA extraction we used mirVana miRNA isolation kit (Invitrogen, Thermofisher). Subsequently, samples were treated with DNase I using the DNA-free DNA removal kit (Invitrogen, Thermofisher), according to the manufacturer's instructions.

MirVana miRNA isolation kit is based on an organic extraction followed by immobilization of total RNA or RNA enriched with small RNAs in a fiberglass filter under specialized binding and wash conditions. The method isolates total RNA ranging in size from kilobases down to 10-mers. Briefly, tissues or cell pellet samples were initially exposed to a denaturing lysis solution and subsequently they were subjected to an acid-phenol:chloroform-based extraction process. Subsequently, washes were carried out with buffers containing ethanol and then the extracts were passed through the filters by means of short centrifugation cycles to immobilize the RNA into the filters. Total RNA was finally eluted using nuclease-free water (VWR Chemicals) preheated to 95 °C and quantified in a Nanodrop-2000 UV-Vis Spectrophotometer (Fisher Scientific).

RNA samples were also treated with DNase I to eliminate possible contaminations with genomic DNA. Briefly, for a typical 50 μL of total RNA eluate we added 5 μL (0.1 volume) 10X DNase I buffer and 1 μL rDNase I, and incubated the samples at 37 $^{\circ}\text{C}$ for 30 minutes. Then, we added 5 μL of DNase inactivation reagent and incubated 2 minutes at RT, mixing occasionally. Finally, we centrifuged at 10,000 $\times\text{G}$ for 1.5 minutes and transfer the DNA free-RNA to a collecting tube. The integrity index and final quantification of total RNA were obtained by analyzing the samples in a chip Bioanalyzer (Agilent Technologies). A RIN ratio ≥ 8 was considered to include the samples in the analyses.

4.4.2. Reverse transcription reaction

cDNA was obtained from PCR amplification (reverse transcription) from total RNA using the RevertAid H minus first strand cDNA synthesis kit (Thermo Scientific) and a Veriti 96-well thermal cycler (Applied Biosystems). Briefly, 11 μL including 500 ng of total RNA & 1 μL of random primer were exposed to a denaturation cycle at 65 $^{\circ}\text{C}$ for 5 minutes (to eliminate secondary structures). Subsequently, a final reaction volume of 20 μL per sample was completed: reaction buffer (4 μL), ribolock RNase inhibitor (1 μL), dNTP Mix (2 μL) and RevertAid H minus reverse transcriptase (1 μL). All samples were exposed to the following temperature cycle: 5 minutes at 25 $^{\circ}\text{C}$, 60 minutes at 42 $^{\circ}\text{C}$ and 5 minutes at 70 $^{\circ}\text{C}$. The synthesized cDNA was subsequently diluted 1:5 in nuclease-free water and stored at -20 $^{\circ}\text{C}$ until its subsequent use.

4.4.3. Quantitative real-time PCR

The expression of the following genes was analyzed by triplicates by quantitative real-time PCR (qRT-PCR) using Taqman probes (Life Technologies): TSPAN1

Materials and methods

(Hs00371661_m1), SOX2 (Hs01053049_s1); ALDH1A1 (Hs00946916_m1); KLF4 (Hs00358836_m1); CD44 (Hs01075861_m1); ABCB1/MDR1 (Hs00184500_m1) and TWIST1 (Hs01675818_s1). Furthermore, IPO8 (Hs00183533_m1) and TBP (Hs00427620_m1) were used as endogenous genes. Briefly, the following amounts per well of MicroAmp fast optical 96-well reaction plate (#4346906, Applied Biosystems) were used to carry out the qRT-PCR reaction: 6.5 μ L of nuclease-free water, 10 μ L of TaqMan Universal Master mix II no UNG (#4440040, Applied Biosystems, Life Technologies), 1 μ L of Taqman probe and 2.5 μ L of cDNA. The real-time PCR reaction was performed on an ABI Prism 7500 Fast machine (Applied Biosystems, Life Technologies) using the following temperature cycle: 2 minutes at 50 °C, 10 minutes at 95 °C, 40 cycles of 15 seconds at 95 °C, and 1 minute at 60°C. The quantification method used for all assays was $2^{-\Delta\Delta Ct}$, a relative quantification method where it is assumed that both the genes of interest and the endogenous control genes are amplified with a similar efficiency and very close to 100%. $\Delta\Delta Ct = [(CT \text{ of the interest gene} - CT \text{ of the endogenous control}) \text{ experimental condition} - (CT \text{ of the interest gene} - CT \text{ of the endogenous control}) \text{ control condition}]$.

4.5. Proteomic analysis

Recent advances in technology, instrumentation, molecular biology, and bioinformatics have made possible to begin to analyze entire units of cellular components, such as the genome, transcriptome, and more recently, the proteome³¹⁵. Proteomics is a method framed within omic technologies that allows us to identify, characterize, and comparatively quantify the relative expression levels of hundreds or thousands of proteins co-expressed in two or more experimental conditions. In the present study, we wanted to analyze the relative expression

levels of the protein profiles of three experimental conditions (in triplicate): CCL-138 (parental cells or control condition), CCL-138-R (CDDP-resistant cell line) and CSCs G3 derived from CCL-138. Through this study, we aimed to identify potential target proteins involved in the acquisition of chemoresistance in HNSCC, with a special focus on CDDP.

4.5.1. Sample preparation and LC-MS/MS analyses

The proteomic study was carried out by the technological infrastructures of the Center for Omic Sciences (COS, EURECAT, Tarragona, Spain). Cell lysis and protein solubilization was performed with modified RIPA buffer (Pierce, Thermo Scientific). Thus, 200 μ l of buffer (25 mM Tris-HCl (pH 7.6), 150 mM NaCl, 1% NP-40, 1% sodium deoxycholate, 1% SDS and protease and phosphatases inhibitors) was added to cell pellets that were sonicated (Sonics & Materials, Vibra Cell, Illkirch, France) for 3 cycles of 6 times 10 seconds with 15 seconds pause intervals. Afterwards, the suspension was centrifuged, supernatant transferred to new tubes, and protein concentration determined by Lowry method. Then, 65 μ g of protein from each sample were reduced with 4 mM dithiothreitol (DTT) for 25 minutes at 56 °C and alkylated with 8 mM iodoacetamide for 30 minutes at 25 °C in the dark, and loaded in a polyacrylamide gel (only staining process) to remove detergents. Then, the gel slice containing unresolved proteins were cut into small pieces and digested overnight at 37°C with trypsin at an enzyme:protein ratio of 1:100. After digestion, a small aliquot of 2 μ g was purified using C18 zip-tip (Millipore) to check proper protein digestion by nanoLC-Orbitrap before following sample preparation steps.

Materials and methods

4.5.2. Peptide 10-plex TMT labeling

The remaining digested protein sample was desalted on C18 Sep-Pack column (Waters, Bedford) using 80% acetonitrile, 20% water 0.1% formic acid for elution. The eluted peptides were dried in the speed-vac and labeled with tandem mass tag (TMT) 10-plex labelling (Thermo Fisher) following manufacturer's instructions. To normalize all the samples, a pool was created mixing an equal small aliquot of each sample and then, 40 µg of this pool and 40 µg of each of the 9 individual samples were labeled. Next, a small aliquot of 5 µg from each labeled sample was mixed and purified using C18 zip-tip (Millipore) and analyzed by nanoLC-Orbitrap to check the labeling reaction.

4.5.3. Peptide fractionation

The labeled peptides from each sample were mixed together and desalted on C18 Sep-Pack column (Waters, Bedford) using 80% acetonitrile, 20% water 0.1% formic acid for elution. The TMT pooled sample was dried in the speed-vac and re-suspended in rehydration buffer (5% Glycerol and 1% v/v IPG strip Buffer 3-10NL), and then fractionated by isoelectrofocusing on an Off-Gel fractionator from Agilent Technologies through 12-well IPG strips (nonlinear gradient from pH 3 to 10) according to the supplier's protocol. Initially, 13-cm-long IPG strips were hydrated with 40 µL per well of the rehydration buffer and 200 µg of TMT pooled sample was loaded on the strip (150 µL of sample in each well). The samples were focused at 50 µA, with voltages between 500 and 4500 V for a total of 20 kVh. After separation, each one of the 12 fractions obtained was desalted on C18 Sep-Pack column (Waters, Bedford) using 80% acetonitrile, 20% water 0.1% formic acid for elution. Eluted fractions were re-suspended in 50 µl of 0.1% formic acid.

4.5.4. NanoLC-(Orbitrap) MS analysis

The 12 fractions obtained from Off-Gel fractionation method were separated on a trap nano-column (100 μm I.D.; 2cm length; 5 μm particle diameter, Thermo Fisher Scientific), and next separated onto a C-18 reversed phase (RP) nano-column (75 μm I.D.; 15cm length; 3 μm particle diameter, Nikkyo Technos). The chromatographic separation was performed with a continuous acetonitrile gradient using Milli-Q water (0.1% FA) and ACN (0.1% FA) as mobile phase.

A flow rate of 300 nL/minute was used to elute peptides for real time ionization and peptide fragmentation on an LTQ-Orbitrap Velos Pro mass spectrometer (Thermo Fisher). An enhanced FT-resolution spectrum (R=30,000 FHMW) followed by two data dependent MS/MS scan events were performed. One consists of an HCD fragmentation (40% NCE) and FT-MS/MS acquisition (R=15,000 FHMW) from most intense ten parent ions with a charge state rejection of 1 and dynamic exclusion of 0.5 minutes, which is used for peptide quantification. The other event consists of a CID fragmentation (35% NCE) and IT-MS/MS acquisition from the same most intense 10 parent ions, which is used for peptide identification.

The 12 raw data files obtained were analyzed by Multidimensional Protein Identification Technology (MudPIT) on Proteome Discoverer software v.1.4.0.288 (Thermo Fisher Scientific). For protein identification all MS and MS/MS spectra were analyzed using Mascot search engine (version 2.5). Mascot was set up to search SwissProt_2017_05.fasta database (554,515 entries), restricting for human taxonomy (20,202 sequences) and assuming trypsin digestion. Two missed cleavages were allowed and an error of 0.02 Da for FT-MS/MS fragment ion mass, 0.8 Da for IT-MS/MS fragment ion mass and 10.0 ppm for a FT-MS parent ion mass

Materials and methods

were allowed. TMT-10plex on lysine and N-termini were set as quantification modifications, oxidation of methionine and acetylation of N-termini were set as dynamic modifications, whereas carbamidomethylation of cysteine was set as static modifications. The false discovery rate (FDR) and protein probabilities were calculated by Percolator.

For protein quantification, the ratios between each TMT-label against 126- TMT label were used. Protein quantification was normalized based on protein median and Log2 transformed for statistical analyses. Results regarding protein identification/quantification were detailed.

4.6. Protein analyses

4.6.1. Protein extraction and quantification

Subconfluent cells and tissue samples previously washed with 1X PBS were both lysed with RIPA buffer (25 mM TrisCl, 150 mM NaCl, 1% Igepal, 1% sodium deoxycholate, 0.1% SDS, pH 7.5) and 2 mM Halt protease (aprotinin, bestatin, E-64 and leupeptin) and phosphatases (sodium fluoride, sodium orthovanadate, sodium pyrophosphate and β -glycerophosphate) inhibitors cocktail EDTA-Free (Thermo Scientific). Lysates were collected in 1.5 mL tubes and incubated for 30 minutes on ice, while vortexing every 10 minutes. The lysates were then centrifuged at 15000 xG for 15 minutes in a microcentrifuge (Eppendorf) previously tempered at 4 °C to separate the proteins from the rest of the cellular components. Supernatants were transferred to new collecting tubes and precipitates were discarded.

Protein quantification was done using the Pierce BCA protein assay (Thermo Scientific). This assay consists of a detergent-compatible formulation based on bicinchoninic acid (BCA) for the colorimetric detection and quantitation of total protein. This method combines the well-known reduction of Cu^{+2} to Cu^{+1} by

protein in an alkaline medium (the biuret reaction) with the highly sensitive and selective colorimetric detection of the cuprous cation (Cu^{+1}) using a unique reagent containing BCA. The purple-colored reaction product of this assay is formed by the chelation of two molecules of BCA with one Cu^{+1} . This water-soluble complex exhibits a strong absorbance at 562 nm that is nearly linear with increasing protein concentrations over a broad working range (20–2000 $\mu\text{g}/\text{mL}$). Briefly, a bovine serum albumin (BSA) standard line was included in the assay, with the following BSA concentration points from a stock BSA solution of 2.0 mg/mL (Thermo Scientific): 0, 0.125, 0.250, 0.500, 0.750, 1,000, 1,500, and 2,000 mg/mL . Based on the number of samples, the total volume of reagent needed to make duplicates was determined, and a mixture of reagent A with reagent B (50:1 v/v) was prepared. Five microliters of each sample and each point of the standard line were added per well of the 96 well plate and subsequently were added 100 $\mu\text{L}/\text{well}$ of the working mixture (reagent A + B). Plates were incubated at 37 °C for 30 minutes and were subsequently read on a spectrophotometer at 562 nm.

For the subsequent western blot (WB) analyses, the samples were prediluted in lysis buffer and Bolt LDS sample buffer (Invitrogen) so that for each 30 μL of lysate mixture, we would take 40 μg of protein. Later the samples were denatured for 5 minutes at 95 °C.

4.6.2. Protein analyses by Western Blot (WB)

WB is a widely used technique to separate, identify and quantify proteins. Total proteins (40 μg) were loaded per lane of Bolt 4 to 12%, Bis-Tris, 1.0 mm mini protein gels (Invitrogen, Life Technologies) and were running 1 hour at 130 V using a mini gel tank (Life Technologies) previously fully with Bolt MES SDS running buffer (Invitrogen, Life Technologies). Proteins were separated based on

Materials and methods

their molecular weight (under denaturing conditions). As a protein ladder, we used 8 μ L/well of Spectra™ multicolor broad range protein ladder (Thermo Scientific). A semi-dry transfer system iBlot 2 gel transfer device and iBlot 2 transfer stacks with an integrated pre-activated PVDF transfer membrane (Invitrogen, Thermofisher) were used for 5 minutes at 20 V to immobilize the proteins. Membranes were subsequently blocked with 5% BSA (VWR Chemicals) in 1X tween-20-tris-buffered saline (T-TBS) (Tris-HCL 50 mM pH 7.4; NaCl 150 mM and 0.1% tween-20) for 1 hour at RT. The following primary antibodies were incubated overnight at 4 °C: anti-TSPAN1 (ab96070) (dilution 1:1000), anti-ATG5 (ab109490) (dilution 1:1000) (Abcam, Cambridge, UK); anti-LC3B (#3868) (dilution 1:600), anti-p-SRC (#6943) (dilution 1:500), anti-SRC (#2109) (dilution 1:1000), anti-p-AKT (#9271) (dilution 1:1000), anti-AKT (#9272) (dilution 1:1000), anti-PARP1 (#9542S) (dilution 1:500), anti-p-ERK (#9101L) (dilution 1:1000) (Cell Signaling Technology Europe Leiden, The Netherlands); anti-SQSTM1 (p62) (SAB3500430) (dilution 1:600) (Sigma-Aldrich, Merck); and anti-ERK (sc-514302) (dilution 1:200). The primary antibody anti-PTOV1 was obtained and used as previously described (2.3 μ g/mL)³¹⁶. Next day, membranes were washed with T-TBS and incubated 1 hour at RT with the corresponding goat anti-rabbit (BA1054) (Bosterbio, Pleasanton, CA) or anti-mouse (#31430) (Invitrogen, Thermofisher) IgG secondary antibody conjugated to HRP (both diluted at 1:10,000). Anti- β -actin (A3854)(dilution 1:20,000) (Sigma-Aldrich, Merck) and anti-vinculin (sc-73614)(dilution 1:14000) (Santa Cruz Biotechnology, Texas, USA) were used as load control. Excess antibodies was removed by 3 washes for 5 minutes with T-TBS and membranes were subsequently revealed with Super

Signal West Pico PLUS Chemiluminescent Substrate (Thermo Scientific) in a chemiluminescence emission system ImageQuant LAS 4000 (GE Healthcare).

4.6.3. Immunohistochemistry

The following table shows a summary of patient samples included in the IHC study:

Table 4. Patient samples included in the IHC studies

Origin	Number of patients	Proteins analyzed
HUVH	84	LC3, PTOV1, ATG5 and p62
HUCA	106	TSPAN1, E-Cadherin, p-SRC

In all cases, representative tissue sections were obtained to perform paraffin-embedded blocks. An experienced pathologist confirmed histological diagnosis. IHC studies in patients were performed in tissue microarrays (TMAs), which allows the staining and analyses of multiple samples, and therefore multiple patients at the same time. Each TMA was constructed using triplicates of tumor tissue from each patient, with a tumor density greater than 80%. Three morphologically representative areas were selected from each individual tumor block and furthermore each TMA contained three cores of normal epithelium as an internal control. Formalin-fixed, paraffin-embedded tissues were cut into 3 μ m sections and dried on Flex IHC microscope slides (Dako, Glostrup). The sections were deparaffinized with standard xylene and hydrated through graded alcohols into water. Endogenous peroxidase activity was quenched in 0.3% hydrogen peroxide and antigen retrieval was performed using Envision Flex Target Retrieval solution (Dako, Glostrup), high pH. Staining was done at RT on an automatic staining workstation (Dako Autostainer Plus) using the Dako EnVision Flex plus visualization system (Dako Autostainer), and the following antibodies: anti-LC3 (#3868) (dilution 1:50) (Cell Signaling Technology Europe Leiden, The Netherlands); anti-ATG5 (ab109490) (dilution 1:100) (Abcam, Cambridge, UK);

Materials and methods

anti-p62 (SAB3500430) (dilution 1:50), anti-TSPAN1 (HPA011909) (dilution 1:50) (Sigma-Aldrich, Merck); anti-E-Cadherin (610181) (dilution 1:4000) (BD Biosciences); anti-SRC (#AHO0051) (dilution 1:300) (Thermo Fisher Scientific) and anti-PTOV1 (³¹⁶) (dilution 1:50). The SRC antibody, which detects the active protein (pSRC), and PTOV1 antibody have been described previously ^{316,317}. Counterstaining with hematoxylin was the final step prior to the increasing gradient dehydration process of alcohol (70%, 96% and 100%) and xylol. Finally, crystals were mounted using a non-aqueous mounting medium (Zymed Laboratories). Immunostaining was scored blinded to clinical data by two independent observers.

TSPAN1 and E-cadherin were scored as follow: quantity scores from 0 to 3 were respectively assigned if 0%, 1% to 10%, 11% to 50%, and 51% to 100 % of the tumor cells showed cytoplasmatic staining and the staining intensity was rated on a scale of 0 to 2 (0 = negative, 1 = weak, 2 = strong). The raw data were then converted to an immunoreactive score (IRS) by multiplying the quantity and staining intensity scores. For E-cadherin, an IRS equal or above the median (score 4) was considered high expression. TSPAN1 expression was dichotomized as negative (score 0) versus positive (scores 1-6). In addition, nuclear expression of TSPAN1 was recorded as negative versus positive. Active SRC (pSRC) staining showed a homogeneous distribution and therefore a semiquantitative scoring system based in staining intensity was applied: low (0, 1+), moderate (2+), or high expression (3+). Samples that showed no immunostaining were considered negative (IRS=0), and samples that showed any positivity were grouped together as positive for statistical purposes.

LC3, PTOV1, ATG5 and p62 were evaluated using the IRS: we scored the percent of stained tumor (scores 0-100%) and the intensity of the staining (scores 1-3), which were assessed semiquantitatively. Then the IRS were calculated as follow: (percent of stained tumor) x (intensity of the staining) (scores 0-300). Patients were classified as a positive or negative base on the median values: for ATG5, PTOV1, and p62 proteins were considered positive those who scored were >50 and for LC3 protein cut off value was zero. Kaplan-Meier curves were performed to time-to-event analyses. **Appendix 1** and **Appendix 2** show clinicopathological characteristics of the patients and the quantifications of each protein analyzed by IHC.

4.6.4. Immunocytochemistry (ICC)

We used the ICC technique to analyze the cellular localization/distribution of PTOV1 and its possible modulation in CDDP-resistant cell lines and CDDP-resistant patients versus controls. We used confocal microscope to analyze PTOV1 localization in HTB-43 (CDDP-sensitive) versus HTB-43-R (CDDP-resistant) cells, and a biopsy-derived cell line from patient 7 (P7: CDDP-sensitive) and patient 33 (P33: CDDP-resistant). Cells were treated with NH₄Cl (50 mM) and subsequently with Saponin (0.1%) and BSA (3%) in 1X PBS for 1 hour at RT. The primary antibody PTOV1 was used as described for 1 hour and detected with the secondary antibody goat anti-rabbit IgG (H+L) Highly Cross-Adsorbed Secondary Antibody Alexa Fluor 488 (A11034) (Invitrogen, Thermofisher) at 2 µg/ml³¹⁸. SlowFade™ Diamond Antifade Mountant with DAPI (S36964) (Invitrogen, Thermofisher) was used to stain nuclei and to assemble crystals.

Materials and methods

4.7. Animal models

Five week old female mice from NMRI-FOXn1 nu/nu strain (Janvier Labs, Saint Berthevin Cedex, France) were used for *in-vivo* studies. JHU029 and JHU029-R cell lines had been labeled with LucIRES-GFP following the protocol previously described³⁷. They were transfected in reverse with siTSPAN1 and siRNA negative control (NC). Forty-eight hours post-transfection, 1×10^6 cells were injected in each flank of the animals, at a final volume of 200 μ L of 1X PBS and matrigel (1:1, V:V) (Corning, Life Sciences). Sixteen mice were included in the study, 4 mice for each of the following experimental groups: JHU029 NC, JHU029 siTSPAN1, JHU029-R NC, JHU029-R siTSPAN1. Tumor volume was measured using an electronic calibrator every 2-4 days, for 42 days. At the end point, animals were analyzed by IVIS spectrum (Perkin Elmer. 940 Winter St. Waltham, Massachusetts. USA) as an alternative method of tumor volume determination and for *in-vivo* micrometastasis analyses.

Optical imaging studies were carried out by the Preclinical Imaging Platform technicians (Lab Animal Service, Campus Vall d'Hebron, Barcelona). For bioluminescence studies, animals were injected with an intraperitoneal injection of luciferin at 150 mg/kg body weight. Then, animals were anesthetized prior to the scans with an isoflurane mixture (5% for induction, 2% for maintenance). Air flow was 0.8 L/minute. After images acquisition, animals were brought back to their cages for recovery. All the procedures were performed following institutional ethic committee (Ref. CEEA 42/15).

Mice were sacrificed by cervical dislocation. A portion of each primary tumor was immediately fixed in 4% formaldehyde and subsequently paraffin-embedded, while the other section was frozen in liquid nitrogen for later protein extraction

and WB analyses. In parallel, necropsies of all the animals were done and the liver, spleen, kidneys, lungs and heart were collected, which were analyzed by IVIS Spectrum together with the remains of the animal, for *ex vivo* detection of micrometastases.

Images were analyzed by the Preclinical Imaging Platform staff with Living Image software (Perkin Elmer). The analyses consist in light radiance quantification. Signals from the light sources were isolated and characterized. The kinetic curve of bioluminescence chemical reaction was examined looking for the highest signals in each light source. These signals are theoretically proportional to the amount of cells involved in bioluminescence reaction. Analyses units were photons(p)/second(s)/centimeter(cm²)/stereoradian(sr). These units were technically corrected and allowed comparisons between different studies.

4.8. Statistical analyses

For the proteomic study, statistical analyses to find the significant protein changes between conditions included in the present study were performed by using Mass Profiler Professional software v.14.5 (Agilent Technologies). One-way ANOVA followed by a *Post-Hoc* analyses were performed to cover the experimental conditions. Benjamini-Hochberg p-value correction for multiple comparisons was applied to reduce false-positive findings. Only those proteins that were quantified in at least two replicates per experimental group were considered for statistical purposes.

On the other hand, all other statistical analyses executed on patients, mice and cell lines samples were performed using SPSS 15.0 software package (SPSS Inc., Chicago, IL). Kruskal-Wallis test and Mann-Whitney U-test were used to analyze the possible associations between continuous quantitative variables with tumor

Materials and methods

stage. The χ^2 test and Fisher's exact test were used for the analyses of categorical variables. Correlation analyses were performed using Pearson correlation test. For time-to-event analyses, Kaplan-Meier curves were plotted and the differences between survival times were analyzed by the Log-rank test. Wilcoxon test was used as a non-parametric test for medians ranks comparisons. Paired or unpaired Student's t-test were performed to compare means between two related or unrelated groups, respectively. All tests were two-tailed. A p value < 0.05, 0.01 or 0.001 (indicated in the plots as *, ** and ***, respectively) was considered statistically significant.

RESULTS

V. RESULTS

5.1. Autophagy inhibition as a promising therapeutic target for HNSCC

The results included in this chapter have been previously published in the Journal Carcinogenesis, Garcia-Mayea, Y. *et al.* 2019 ³¹⁹.

5.1.1. Laryngeal cancer location distinguishes three different clinical entities

Laryngeal cancer has been classified as supraglottic (above the glottis), glottic, and subglottic (below the glottis) (**Figure 3**), as these are different entities based on clinical presentation, etiology and prognosis. For example, glottic tumors are usually diagnosed in early stages because relatively early changes in the voice occur, since the vocal cords are the most commonly affected site. Therefore, this type of tumor usually has a good response and survival rate ³²⁰. We found that supraglottic and glottic tumors had better survival rates than subglottic tumors (**Figure 12**). However, fortunately, subglottic tumors have a very low incidence according to laryngeal cancer statistics ^{321,322}.

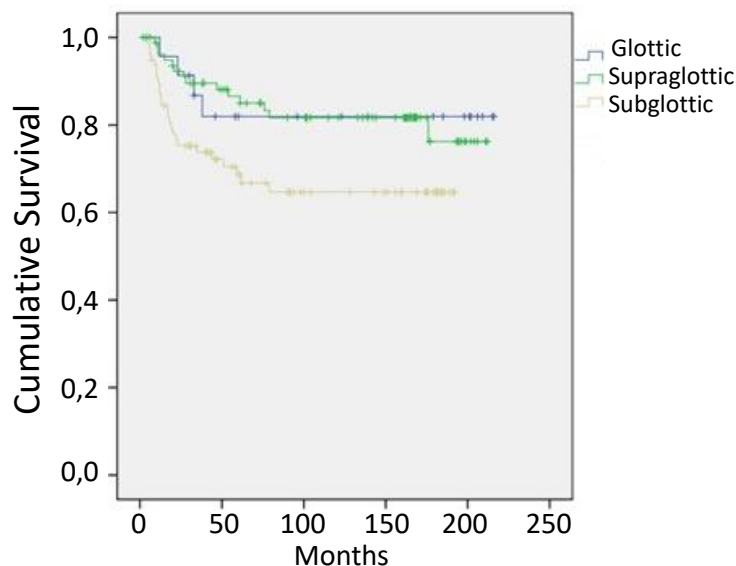


Figure 12. Overall survival of laryngeal cancer patients depending on tumor location. Laryngeal cancers patients were studied and clinically followed for approximately 10 years. They were grouped by location: glottic, supraglottic and subglottic tumors. Note that patients with subglottic tumors have the worst prognosis. Log-rank test, $p < 0.05$.

Results

5.1.2. Markers of significance in laryngeal cancer biopsies

To study if autophagy might be involved in HNSCC, a retrospective series of laryngeal tumors biopsies was analyzed by IHC for the expression of LC3, p62, ATG5, and PTOV1. While p62 showed both nuclear and cytoplasmic localization, ATG5, LC3 and PTOV1 showed a cytoplasmic expression pattern (**Figure 13 A-B**). **Figure 13 C** summarizes the total number of patients analyzed for the expression of the four studied proteins, as well as the number and percentage of positive and negative patients for each protein. The high percentage of PTOV1 positive patients (85%) is especially notable. LC3 and p62 protein expression correlated between them, and ATG5 protein correlated with PTOV1 (**Figure 14 A-B**). The expression of both cytoplasmic p62 and PTOV1 were associated with tumor stage. Of note, as tumor stage increased (T1-T4), the levels of PTOV1 and p62 also tended to be expressed more intensively at cytoplasmic level (**Figure 14 C-E**). The expression levels of ATG5, LC3, p62 and PTOV1 proteins were studied in relation to the clinical evolution of the patients. The study was performed considering all patients or grouped by tumor location (each group independently: glottic, supraglottic or subglottic). We found that the positive expression of LC3 was associated with worse overall survival in supraglottic cancers (**Figure 14 G**).

Finally, patients were grouped as treated and not treated with chemotherapy after surgery, specifically CDDP. Although the differences were not statistically significant ($p > 0.05$), a trend was observed in patients with supraglottic tumors treated with CDDP. LC3 positive patients tend to have a worse clinical prognosis than those who did not express LC3 (**Figure 15**).

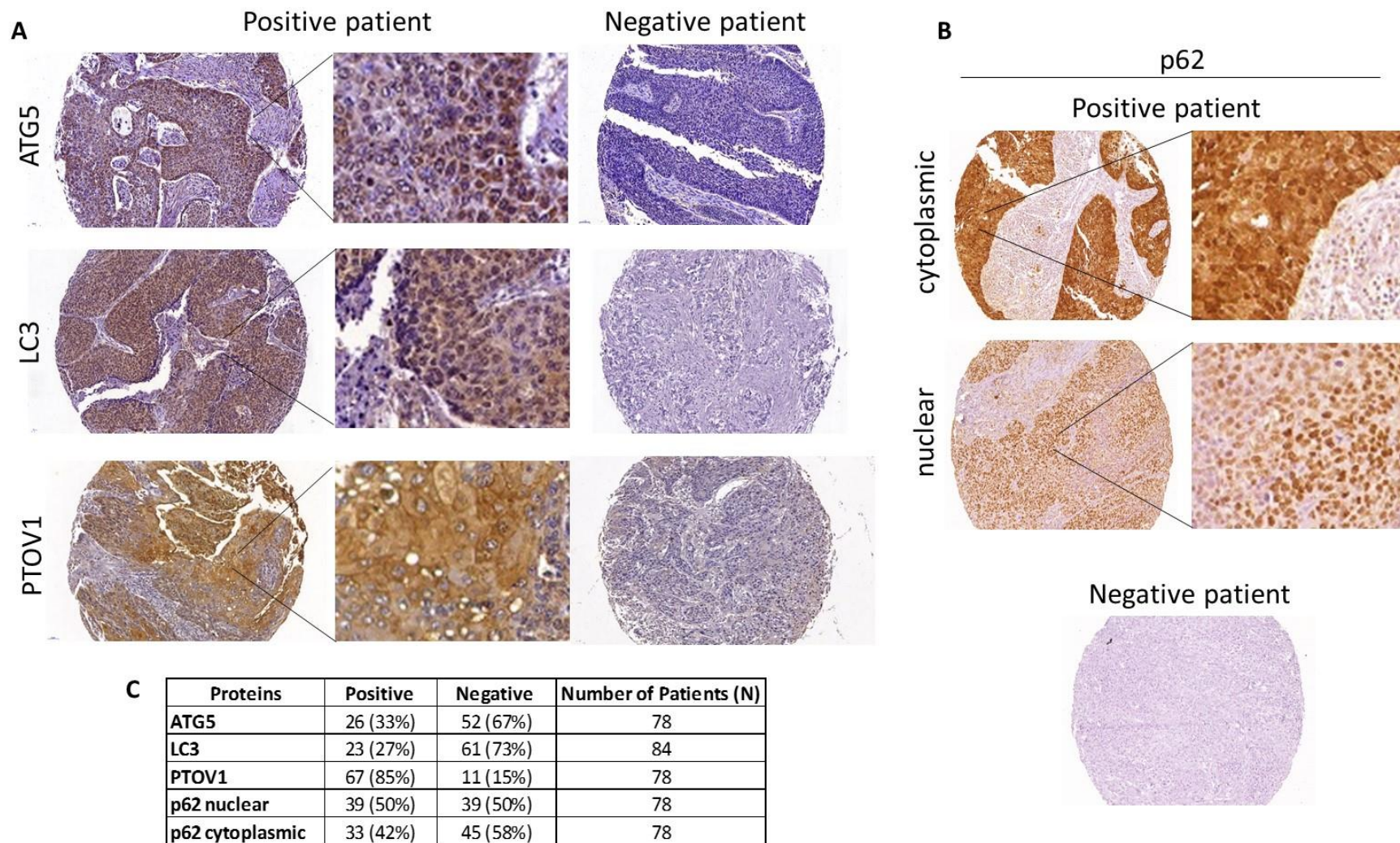


Figure 13. Expression pattern of ATG5, LC3, PTOV1 and p62 in biopsies from laryngeal cancer patients. A) IHC representative pictures of ATG5, LC3 and PTOV1 protein expression in tumoral tissues of laryngeal cancer patients. **B)** Expression of nuclear and cytoplasmic p62 protein in tumoral tissues of laryngeal cancer patients. **C)** Number and percentages of patients expressing the indicated proteins.

Results

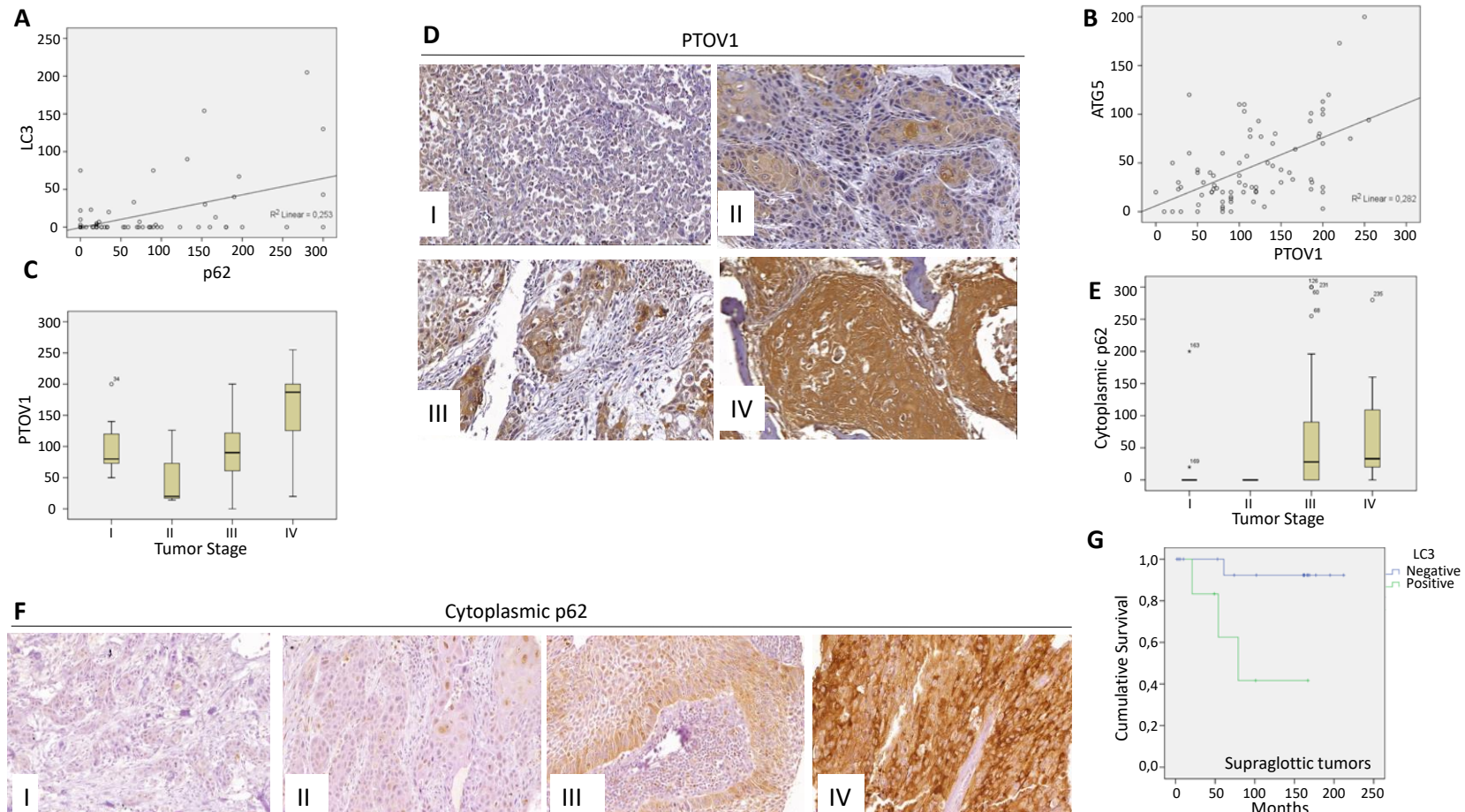


Figure 14. Significant associations with clinical relevance in laryngeal cancer patients through IHC analyses. A) Significant correlation between LC3 and p62 expression. Pearson correlation test, $p < 0.05$; $R^2 = 0.253$. **B)** Significant correlation between ATG5 and PTOV1 expression. Pearson correlation test, $p < 0.05$; $R^2 = 0.262$. **C)** PTOV1 expression is associated with tumor stage. Tumor stage represents how much the tumor has grown into the larynx and nearby structures (I, early tumor stage; IV, late tumor stage). Kruskal-Wallis test, $p < 0.05$, Mann-Whitney U-test (I vs IV), $p < 0.001$. **D)** Representative pictures of the increase in PTOV1 expression according to tumor stage. Note that PTOV1 tends to accumulate more in the cytoplasm in III and IV stages in comparison with I and II stages. **E)** Cytoplasmic p62 is associated with tumor stage. Kruskal-Wallis test, $p < 0.05$, Mann-Whitney U-test (I, II vs III; I, II vs IV), $p < 0.001$. **F)** Representative pictures of the increase in cytoplasmic p62 protein expression according to tumor stage. Cytoplasmic p62 protein expression increases in III and IV stages. **G)** Positive LC3 expression is associated with poorer overall survival in supraglottic tumors. Log-rank test, $p < 0.05$.

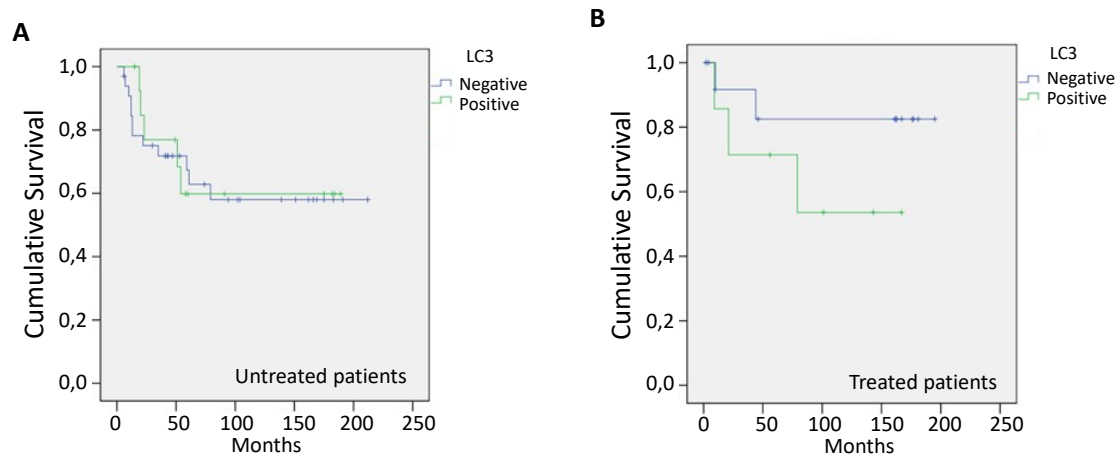


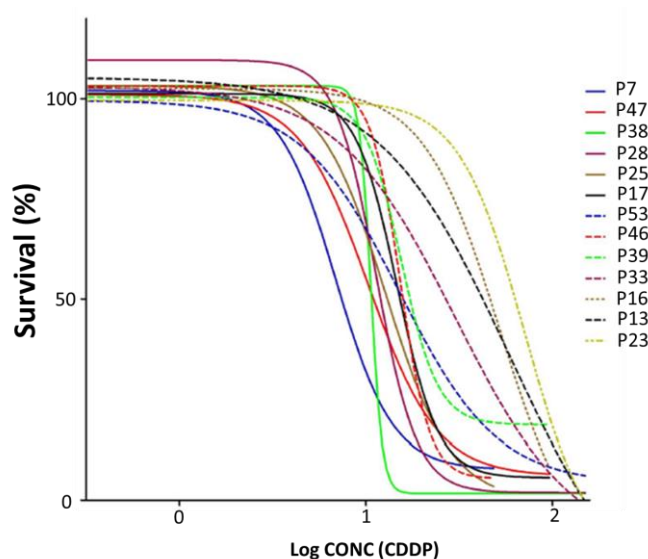
Figure 15. Patients with supraglottic tumors treated and not treated with chemotherapy and its association with LC3 expression and survival. A) LC3 expression is not associated with survival in those patients untreated with chemotherapy (only surgery was performed). **B)** High LC3 expression tends to be associated with worse survival in those patients who received CDDP treatment. Log-rank test, $p > 0.05$.

5.1.3. PTOV1 and ATG5 proteins are preferentially overexpressed in those biopsy-derived cell lines that exhibit higher CDDP-resistance levels

We established 13 biopsy-derived cell lines from laryngeal and pharyngeal cancer patients and calculated their IC₅₀ value for CDDP (**Figure 16**). The cell lines were grouped into two separate categories according to their intrinsic level of resistance (none of them had previously received chemotherapy treatment). Those biopsy-derived cell lines with IC₅₀ > 15 μ M (median value) were considered resistant, while those with IC₅₀ \leq 15 μ M were considered sensitives. Sensitive patients were P7, P47, P38, P28, P25, and P17; and resistant patients were P53, P46, P39, P33, P16, P13, and P23 (**Figure 16** and **Figure 17 A**). Observe that those biopsy-derived cell lines with higher CDDP-resistance levels, in general, tended to show higher 5-FU-resistance levels. We studied PTOV1, p62, ATG5, and LC3 expression by WB in these groups of patients and vinculin was used as load control (**Figure 17 B**). LC3 protein quantification was based upon the LC3II (bottom)/LC3I (upper) levels (lipidated/non-lipidated form), as a high LC3II/LC3I ratio is indicative of

Results

autophagy activation ³²³. Analyzing the LC3 expression pattern respect to the levels of CDDP-innate resistance, we found no differences between the groups of sensitive versus CDDP-resistant patients. However, the overexpression of PTOV1 and ATG5 were significantly associated with the group of the most resistant patients. Furthermore, ATG5 expression significantly correlated with p62 and PTOV1 expression (**Figure 17 C**).



	P7	P47	P38	P28	P25	P17	P53	P46	P39	P33	P16	P13	P23
CDDP (μM)	6,90	10,30	10,64	11,36	12,72	14,69	15,12	15,31	15,49	30,30	51,77	59,12	70,91

Figure 16. CDDP-survival curves of 13 biopsy-derived cell lines from larynx and pharynx. The Y-axis represents cell survival and the X-axis represents the concentration of CDDP on a logarithmic scale. The IC50 values (μM) for each cell line are shown in the table below. Sensitive patients (solid lines), resistant patients (dashed lines).

To determine autophagy deregulation by an independent technique, TEM was used in biopsy-derived cell lines from patients: P46 (resistant patient with high LC3II/LC3I) and P47 (sensitive patient with low LC3II/LC3I). The presence of autophagic vesicles was calculated for each patient, being significantly higher in P46 than in P47 (**Figure 17 D-E**). Of note, only 33% (2/6) of the sensitive patients (IC50≤15) died after standard treatment versus 57% (4/7) of resistant patients who died due to cancer recurrence (**Figure 17 A-B, Table 5**).

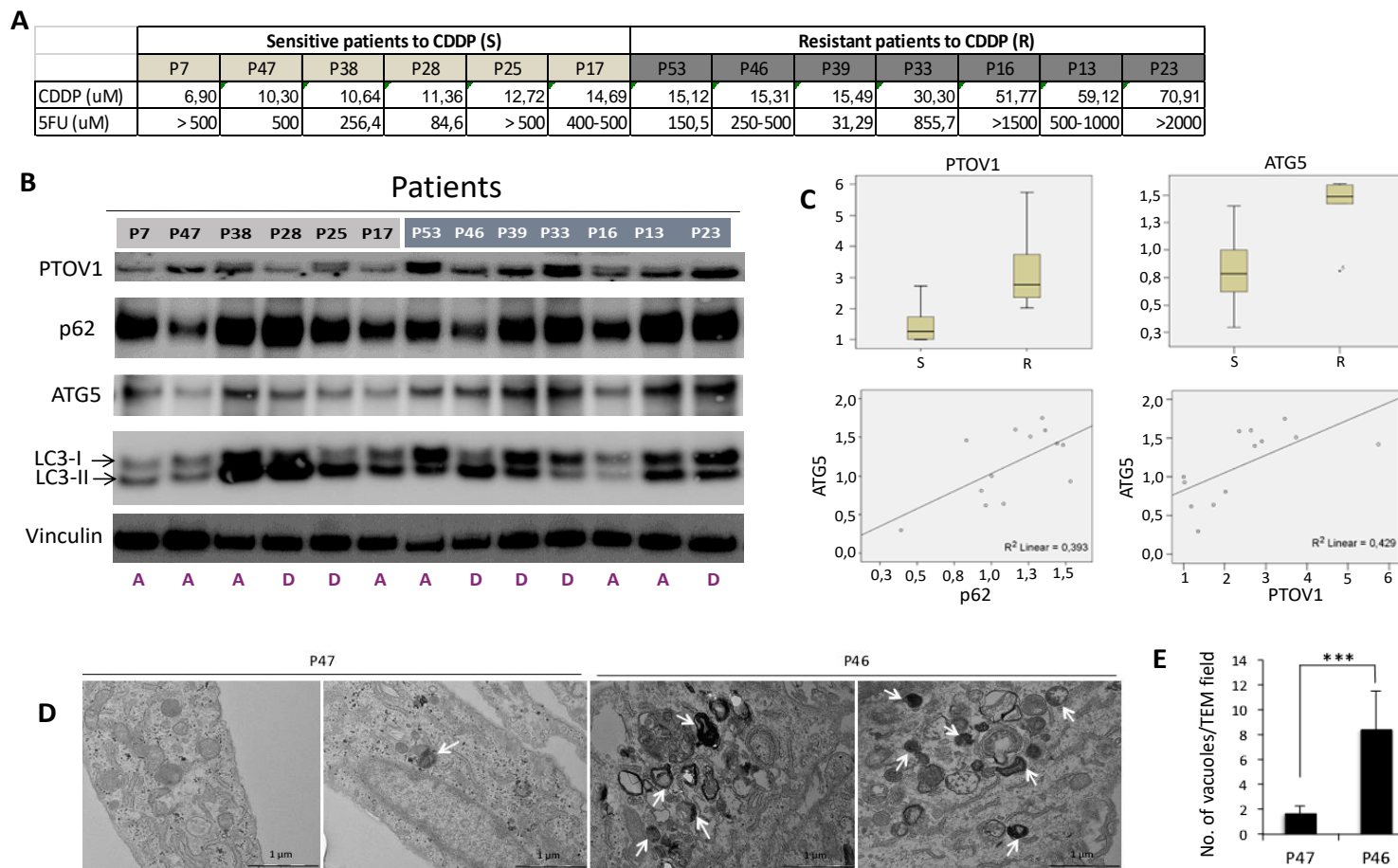


Figure 17. Biopsy-derived cell lines from laryngeal and pharyngeal cancer patients and their relation with autophagy markers and PTOV1. **A)** The IC50 values (μM) for CDDP and 5-FU for the patients P7, P47, P38, P28, P25, P17, P53, P46, P39, P33, P16, P13, and P23, are shown. **B)** PTOV1, p62, ATG5, and LC3 expression by WB in the 13 biopsy-derived cell lines obtained. Status of patients are indicated as A (Alive) or D (Dead). **C)** Proteins from panel B were quantified and analyzed respect to the groups of sensitive versus resistant patients. The plots show a significant association of PTOV1 and ATG5 with the resistant patients (upper panel). Mann-Whitney U-test, $p < 0.05$, $p < 0.001$, respectively; sensitive (S), resistant (R). Moreover, ATG5 correlates with p62 and PTOV1 expression (lower panel). Pearson correlation test, $p < 0.05$, $R^2 = 0.393$, $R^2 = 0.429$; respectively. **D)** Representative TEM images showing the presence of autophagy vesicles (see arrows) in the biopsy-derived cell lines P47 and P46. **E)** Quantification of autophagy vesicles in the indicated biopsy-derived cell lines. Data are expressed as mean \pm SD. Unpaired Student's t-test, *** ($p < 0.001$).

Results

Overall, these results indicate that high PTOV1 and ATG5 levels are associated with the intrinsic resistance of biopsy-derived cell lines from laryngeal and pharyngeal patients, and represent good markers for this type of resistance. The correlation of ATG5 with p62 and PTOV1 expression supports previous observations regarding the IHC study (**Figure 14 B**) and suggest a putative link between PTOV1 and autophagy.

Table 5. Clinical information of the 13 HNSCC patients from whom the biopsy-derived cell lines were generated. Notice that P7, P47, P38, P28, P25 and P17 were classified as sensitive patients while P53, P46, P39, P33, P16, P13 and P23 were classified as resistant patients (with P7 and P23 classified as the most sensitive and most resistant to CDDP, respectively). RT, radiotherapy.

	Patient Code	Age	Sex	Primary tumor	Stage	Post-surgical treatment	Clinical Status
Sensitive	P7	58	Female	SCC Transglottic	pT3pN0	CDDP + RT	Healthy
	P47	85	Male	SCC Supraglottic	pT4aNx	NO	Healthy
	P38	54	Male	SCC Supraglottic	pT4apN0	RT	Healthy
	P28	71	Female	SCC Glottic	pT3pNx	RT	Exitus
	P25	74	Male	SCC Glottic	rT4N0	CDDP + RT	Exitus
	P17	58	Male	SCC Supraglottic	pT2pN1	RT	Healthy
Resistant	P53	45	Male	SCC Hypopharynx	pT4apN2b	RT	Healthy
	P46	69	Male	SCC Supraglottic	pT4apN0	RT	<u>Exitus</u>
	P39	74	Male	SCC Glottic	pT4aNx	RT	Exitus
	P33	72	Female	SCC Supraglottic	pT4apN0	RT	Exitus
	P16	50	Male	SCC Supraglottic	pT3pN1	RT	Healthy
	P13	45	Male	SCC Glottic	pT3pN0	NO	Healthy
	P23	81	Male	SCC Glottic	pT2Nx	RT	Exitus

5.1.4. *Autophagy markers and PTOV1 are associated with drug resistance in HNSCC cancer cells*

We developed and characterized eight different HNSCC chemoresistant cell lines, namely, JHU029-R, HTB-43-R, CCL-138-R, and SCC-25-R, which are individually resistant to CDDP and 5-FU. These resistant variants were generated from the corresponding parental cell lines by means of exposure pulses to the drugs at doses equal to or higher than the IC₅₀ of each respective drug for 12-18 months. The IC₅₀ values to CDDP and 5-FU for each cell line are shown in **Figure 18** and **Figure 19 A**.

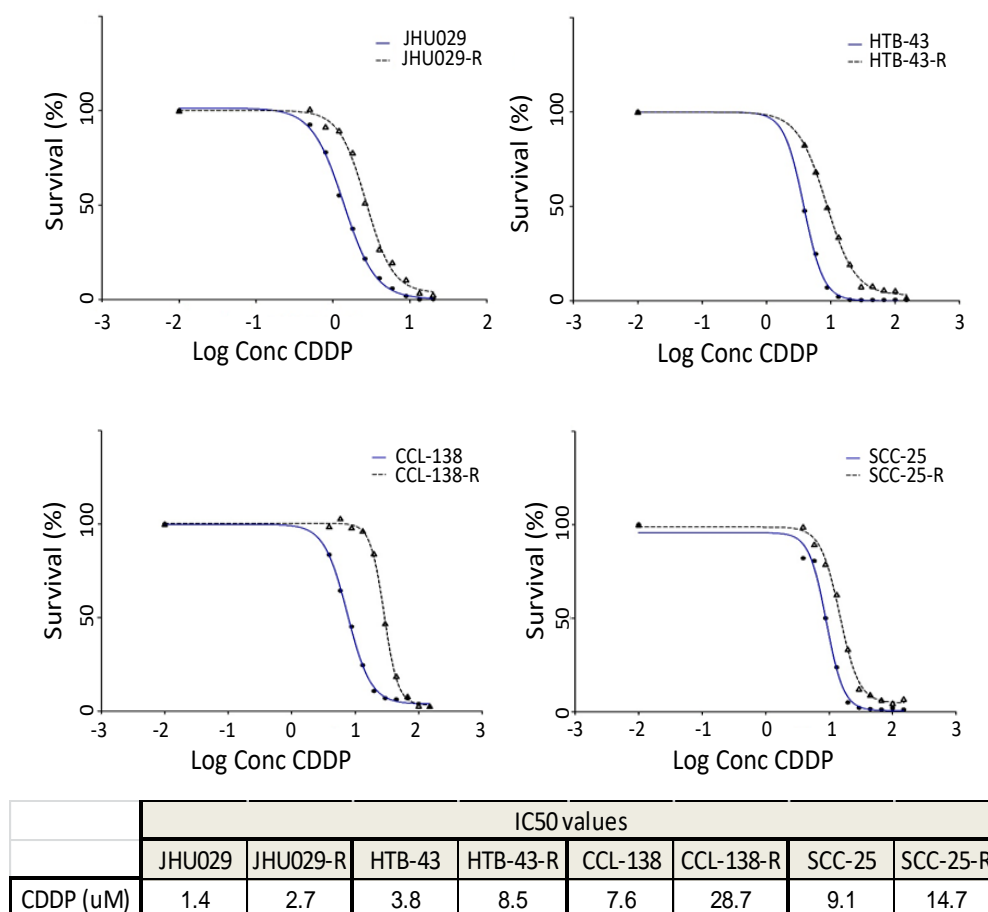


Figure 18. CDDP-response curves and IC₅₀ values from parental and CDDP-resistant HNSCC cell lines. The CCL-138 and CCL-138-R cell lines showed the greatest differences in IC₅₀ values (μM). The Y-axis represents cell survival and the X-axis represents the concentration of CDDP on a logarithmic scale.

Results

In general, the comparison between resistant versus sensitive cell lines showed an increased expression of autophagy-related proteins in the resistant cells (**Figure 19 B**). PTOV1, p62 and LC3II/LC3I proteins were increased in JHU029-R, HTB-43-R and SCC-25-R cells (especially in those resistant to CDDP). ATG5 was overexpressed in JHU029-R (in both CDDP- and 5-FU-resistant cells) and HTB-43-R (only in 5-FU-resistant cells). Autophagy activation in the CDDP-resistant cell line JHU029-R versus the parental cell line JHU029 was further corroborated by TEM image analyses (**Figure 19 C-D**). However, the CCL-138-R cell line, derived from a metastatic tumor from pharyngeal origin, did not show significant changes in autophagy-related proteins or PTOV1 (**Figure 19 B**).

On the other hand, the acquisition of resistance to chemotherapy has often been attributed to the presence of CSCs in the tumor ^{324,325}, therefore, we studied the expression of PTOV1 and autophagy-related proteins in CSCs derived from HNSCC cell lines (**Figure 19 B**). For this purpose, CSCs derived from each parental cell line were enriched through sphere formation up to 3 generations (**Figure 20**) and characterized for the expression of the SC markers *SOX2*, *ALDH1A1*, *KLF4*, *CD44*, *ABCB1*, and the EMT marker *TWIST1* (**Figure 21**). *SOX2*, *ALDH1A1*, *KLF4* and *ABCB1* were overexpressed in the 3 generations of CSCs (G1-G3) in the cell lines HTB-43 and CCL-138. Remark that several of these CSCs markers were also overexpressed in CDDP-resistant cell lines, supporting a connection between CSCs and chemoresistance. Indeed, CSCs were more resistant to CDDP and 5-FU than the whole cell population (parental cells) (**Figure 22**). Moreover, we observed that the CDDP-resistant cell lines HTB-43-R and CCL-138-R contained a slightly increase in the percentage of CSCs (side population) respect to their parental cells when they were analyzed by flow cytometry (**Figure 23**).

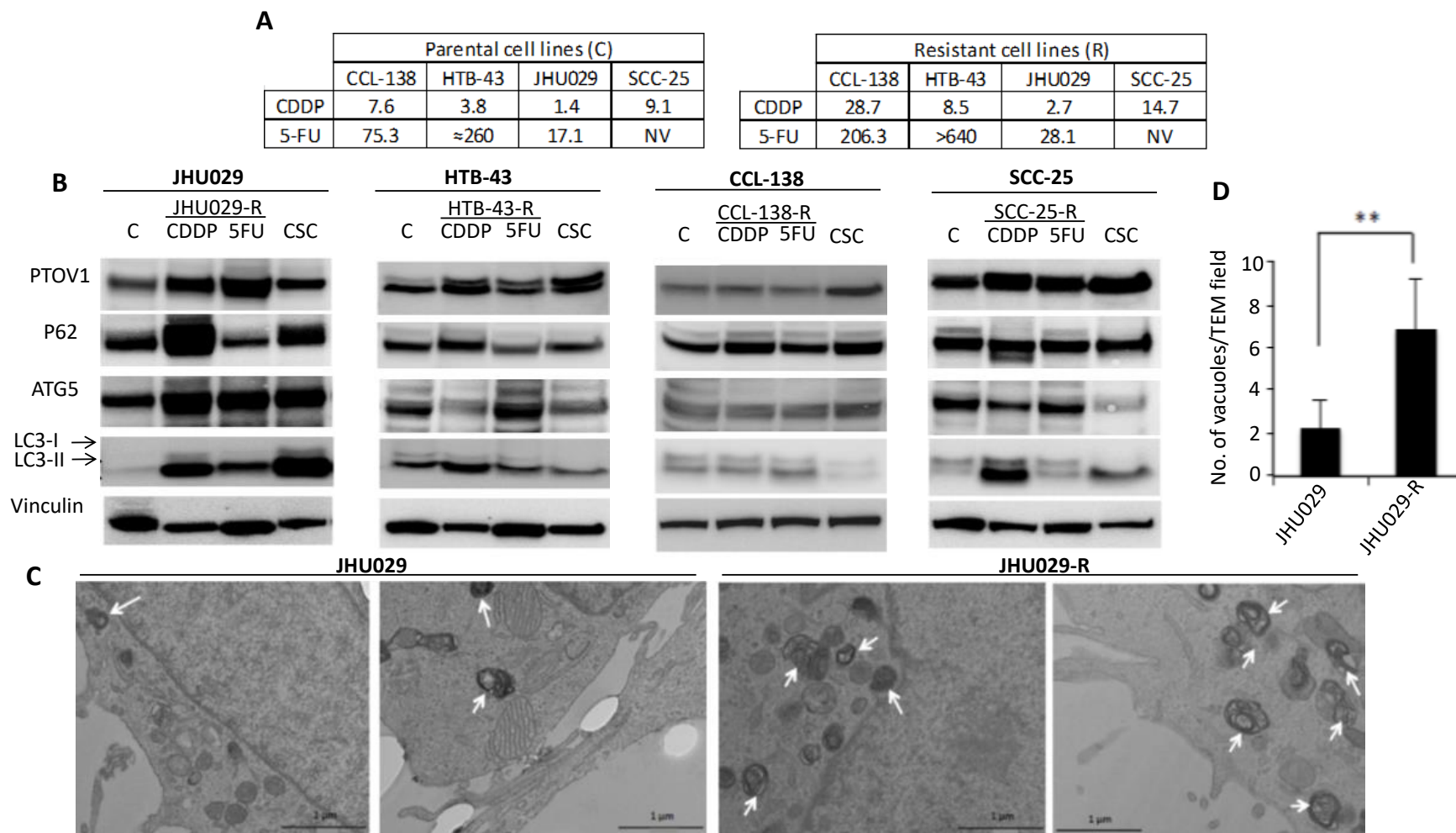


Figure 19. Resistant HNSCC established cell lines show increased levels of PTOV1, autophagy-related proteins and autophagy vesicles. A) Tables of the IC50 values (μM) to CDDP and 5-FU for each cell line (parental versus resistant cells). NV, IC50 was an undetermined value. **B)** JHU029, HTB43, CCL-138, and SCC-25 cell lines (control, resistant cells to CDDP & 5-FU, and CSCs) were analyzed by WB for the expression of PTOV1, p62, ATG5, and LC3II/LC3I proteins. **C)** Representative TEM images showing the presence of autophagy vesicles (see arrows) in JHU029 and JHU029-R. **D)** Quantification of autophagy vesicles in the indicated cells, statistical differences were found. Data are expressed as mean \pm SD. Paired Student's t-test, **($p < 0.01$).

Results

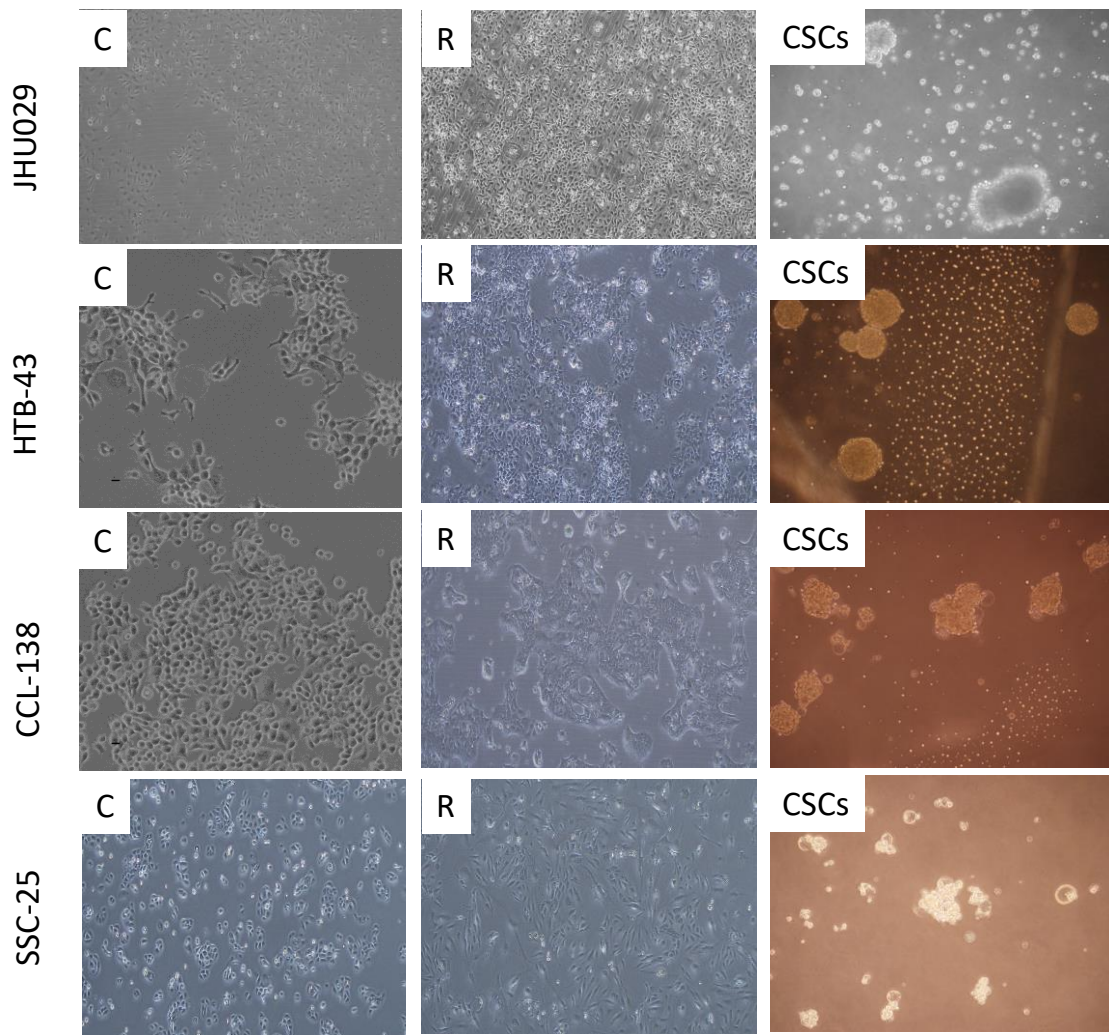


Figure 20. Representative images of phenotypic characteristics of the cell lines JHU029, HTB-43, CCL-138, and SSC-25 under adherent and non-adherent conditions. C, control cells (parental cells); R, CDDP-resistant cells; both in adherent conditions; and CSCs at generation 3 (CSCs cultures in non-adherent conditions to form spheroids).

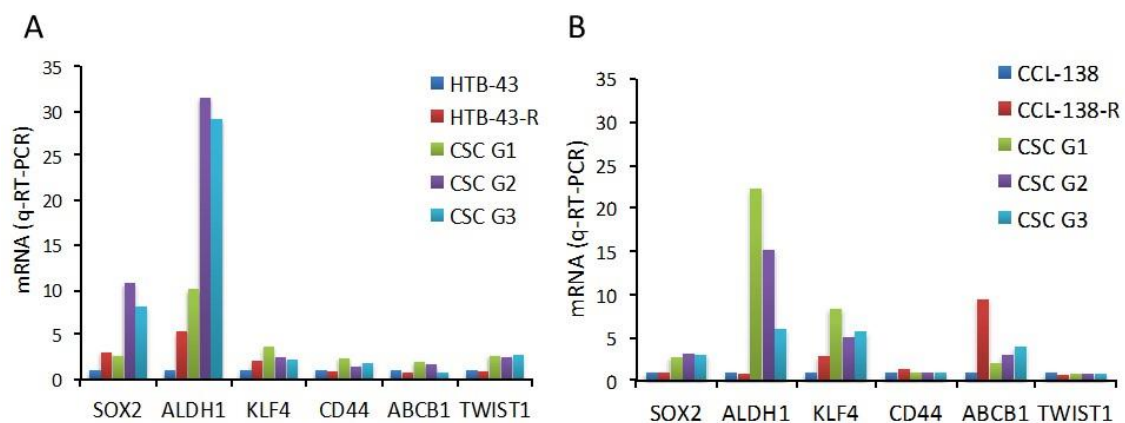


Figure 21. Expression of SCs and EMT genes using qRT-PCR. Figures show the expression of SOX2, ALDH1, KLF4, CD44, ABCB1, and TWIST1 in HTB-43 (A) and CCL-138 (B) cells and their corresponding CDDP-resistant variants and CSCs in consecutive generations (G1, G2, and G3).

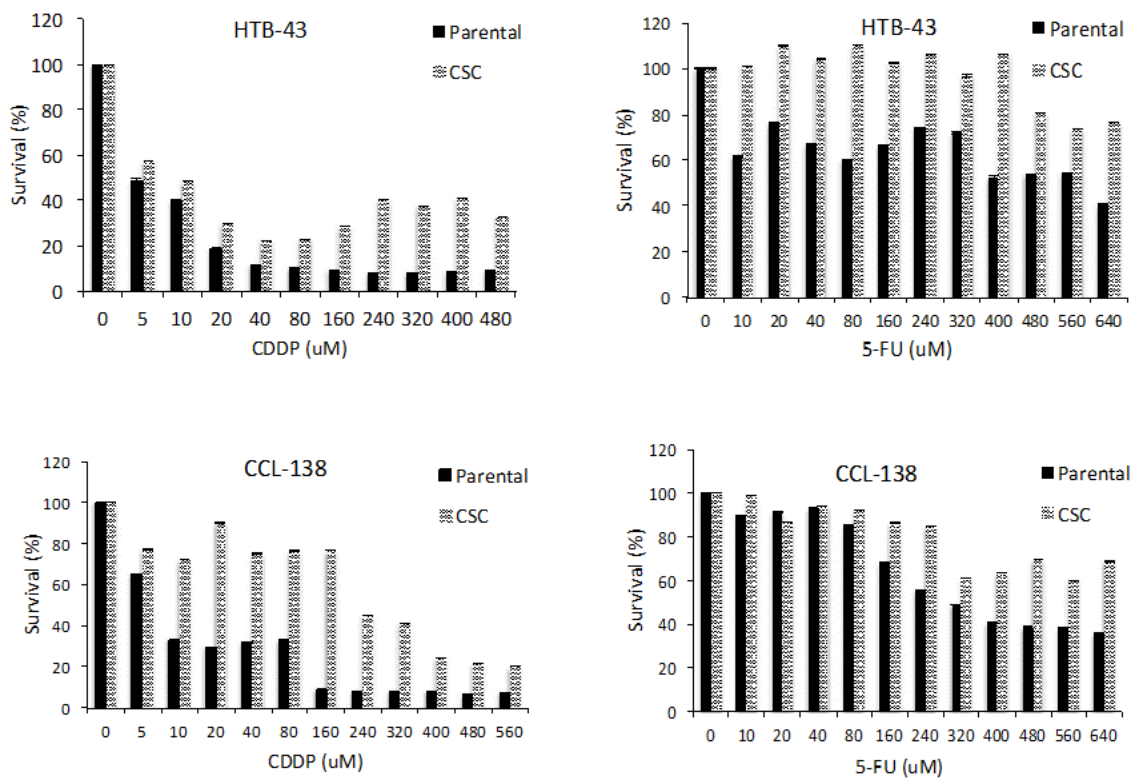


Figure 22. CSCs are more resistance to CDDP and 5-FU than the whole cellular population (parental cells). The response to CDDP and 5-FU was assessed in the CSCs G3 (generated from HTB-43 and CCL-138) with regard to their respective parental cell lines. Note the resistance of the CSCs (increased viability, Y-axis) for the indicated drug concentrations (X-axis).

Interestingly, CSCs from JHU029 and SCC-25 cell lines had higher LC3II/LC3I levels than the control cells, while PTOV1 increased in all CSCs derived from different HNSCC cell lines (**Figure 19 B**). These results support those observed in biopsy-derived cell lines, confirming that higher expression of autophagy markers and PTOV1 might be indicative of resistant phenotypes. Moreover, the results suggest once again an association between PTOV1 and autophagy activation, and corroborate the critical role of autophagy and PTOV1 in certain CSCs models, such as laryngeal (JHU029) and tongue (SCC-25).

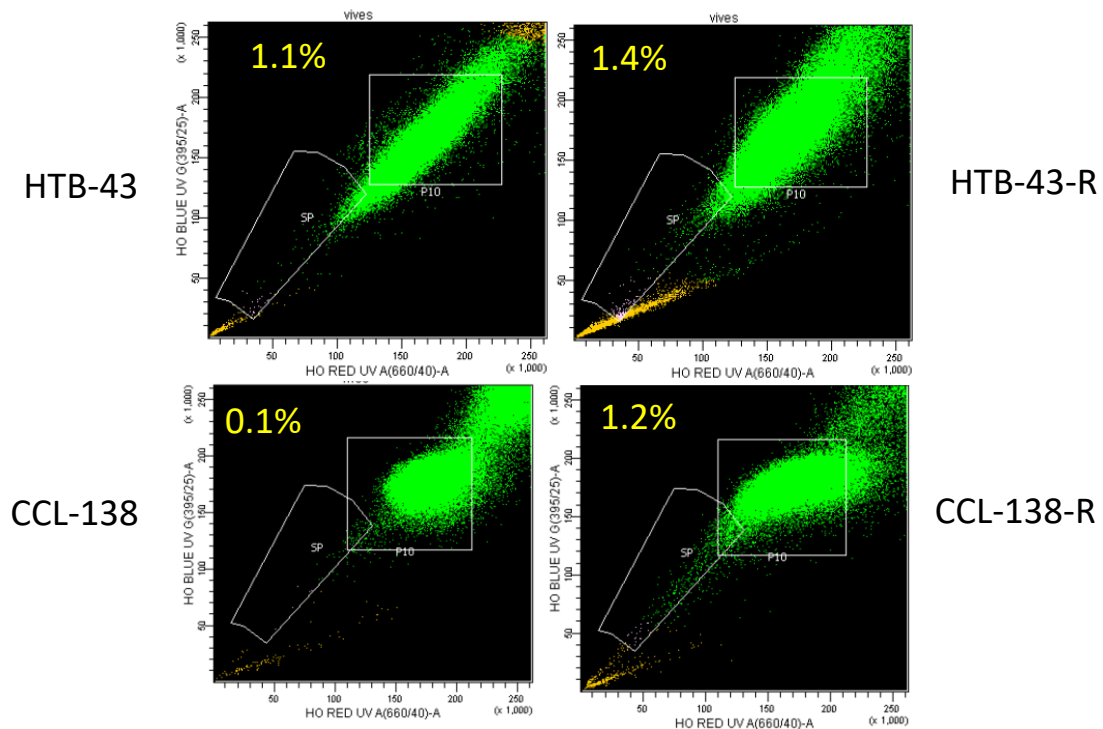


Figure 23. Side Population in HTB-43 and CCL-138 cell lines (parental versus CDDP-resistant cells). The CSCs percentage was determined by the Side Population profile given by flow cytometry. The percentages are indicated for each control case (left panel) and their CDDP-resistant cell variants (right panel).

5.1.5. PTOV1 overexpression induces autophagy

To define the role of PTOV1 in HNSCC, we overexpressed PTOV1 in JHU029 cells. An increase in LC3II/LC3I and p62 proteins was clearly observed in cells where PTOV1 was overexpressed when compared to the control cells (**Figure 24 A**). Moreover, a TEM study was performed for detection of autophagy vesicles. Cells overexpressing PTOV1 showed a higher number of autophagy vesicles than control cells (**Figure 24 B, C**).

Although in the IHC study the majority of PTOV1 proteins were located at cytoplasmic level, in some sporadic cancer cells PTOV1 was located in the nucleus (**Figure 25**). In order to determine if the differences, observed by WB, regarding the PTOV1 expression in sensitive versus resistant cells were related to a different subcellular localization of PTOV1, we studied PTOV1 expression by immunocytochemistry in biopsy-derived cell lines from patients

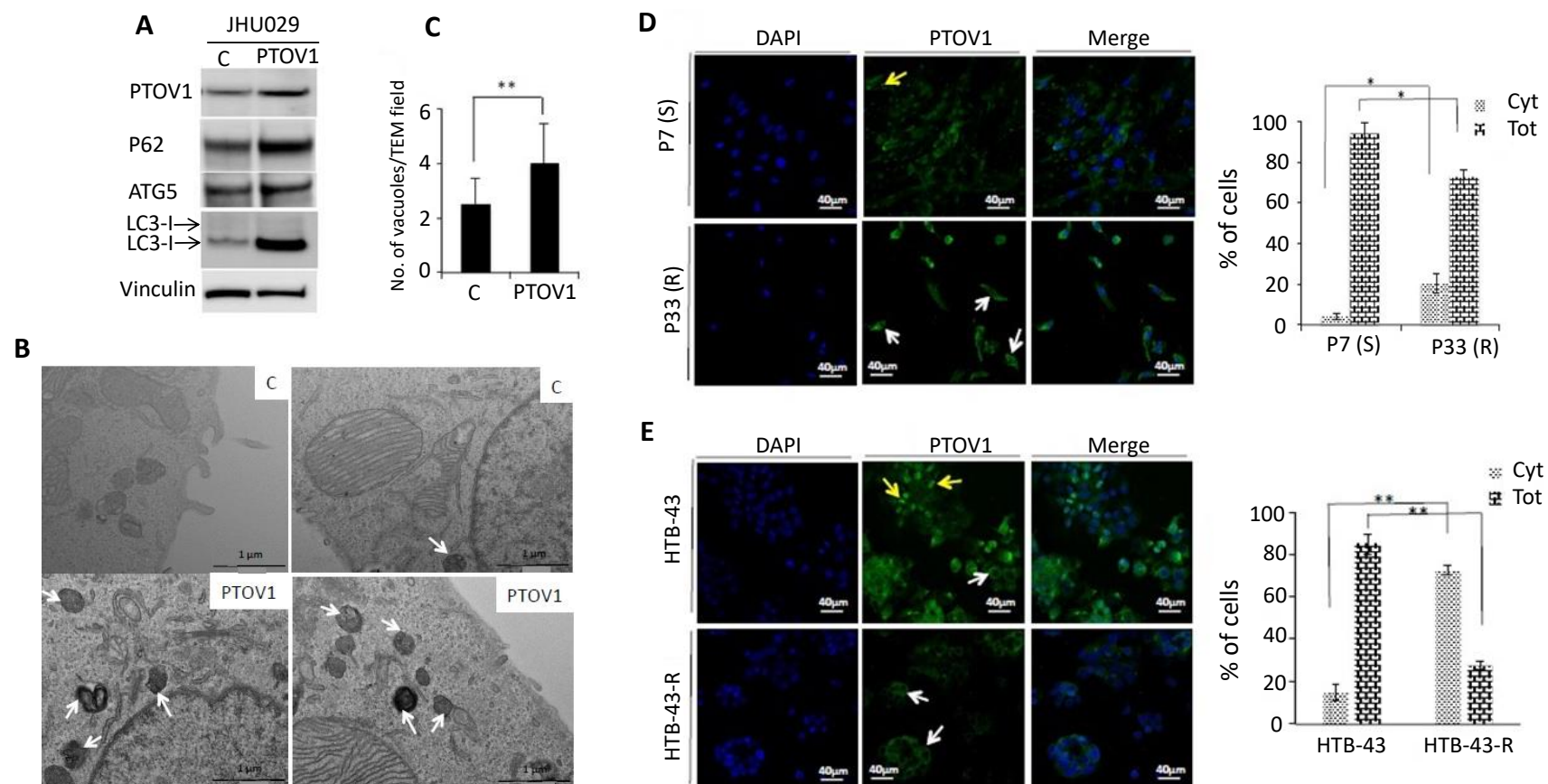


Figure 24. PTOV1 overexpression induces autophagy and is mainly located in the cytoplasm of CDDP-resistant cells. **A)** WB showing the PTOV1 overexpression in JHU029. P62 and LC3II/LC3I ratio were increased in PTOV1-overexpressing cells. **B)** Representative TEM images from the cells represented in panel A to quantify autophagy vesicles. C, control cells; PTOV1, PTOV1-overexpressing cells. **C)** Autophagic events quantification from TEM images of PTOV1-overexpressing cells versus control cells. Paired Student's t-test, **($p < 0.01$). **D)** Confocal microscopy pictures of PTOV1 protein in the resistant biopsy-derived cell line from patient P33 (R) versus the sensitive biopsy-derived cell line from patient P7 (S). Quantification of the proportion of cells expressing PTOV1 exclusively in the cytoplasm versus total location (nucleus and cytoplasm) is shown in the right panel. Unpaired Student's t-test, *($p < 0.05$). **E)** Confocal microscopy pictures of PTOV1 protein in HTB-43 cells. Note the PTOV1 accumulation in the cytoplasm of CDDP-resistant cells (HTB-43-R) versus control cells (HTB-43). Quantification of the proportion of cells expressing PTOV1 exclusively in the cytoplasm versus total location (nucleus and cytoplasm) is shown in the right panel. Unpaired Student's t-test, **($p < 0.01$). Yellow arrows indicate total PTOV1; white arrows indicate cytoplasmic PTOV1. Cyt, cytoplasmic; Tot, total PTOV1 distribution.

Results

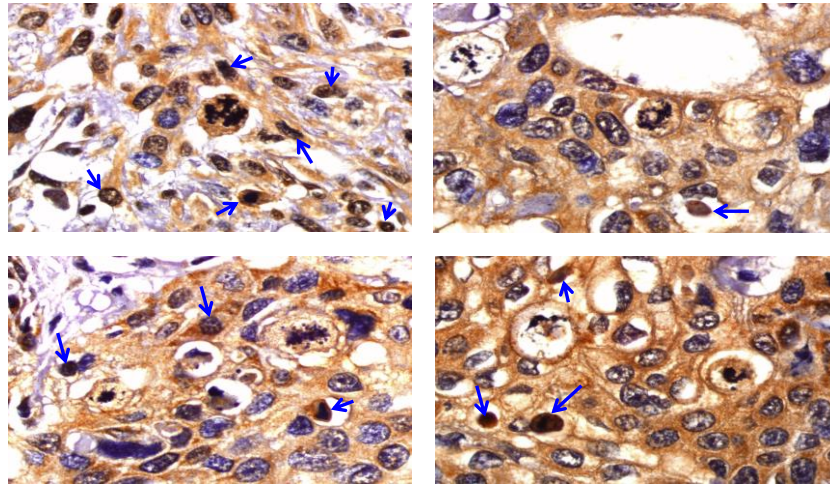


Figure 25. Examples of nuclear PTOV1 expression in sporadic cancer cells from laryngeal cancer biopsies. Arrows indicate nuclear PTOV1.

P7 (CDDP-sensitive, S) and P33 (CDDP-resistant, R). In P7, PTOV1 was located in the nucleus and cytoplasm in most cells and a minor fraction of cells expressed PTOV1 solely in the cytoplasm. In contrast, in P33, the number of cells that expressed PTOV1 solely in the cytoplasm was significantly increased, suggesting a shift of PTOV1 location to the cytoplasm in resistant cells (**Figure 24 D**). To corroborate these results, we performed the same analysis in HTB-43 cells, comparing sensitive (HTB-43) versus CDDP-resistant cells (HTB-43-R). Similarly, the number of cells expressing PTOV1 solely in the cytoplasm increased considerably in the resistant cells (**Figure 24 E**). These results support the notion that PTOV1 expression can be associated with resistance in our HNSCC models by activating autophagy. Moreover, the cytoplasmic location of PTOV1 seems to be important for such resistance acquisition.

5.1.6. Autophagy inhibition in HNSCC cell lines and biopsy-derived cell lines

In order to determine if autophagy inhibition could provide a therapeutic benefit, particularly for CDDP-resistant HNSCC, we performed different cell proliferation assays in response to the autophagy inhibitor HCQ. In general, we found that in the CDDP-resistant cells from all tested HNSCC cell lines (note that they do not

respond to CDDP), the autophagy inhibitor HCQ was more effective in causing cell death than in the corresponding parental cells (**Figure 26**).

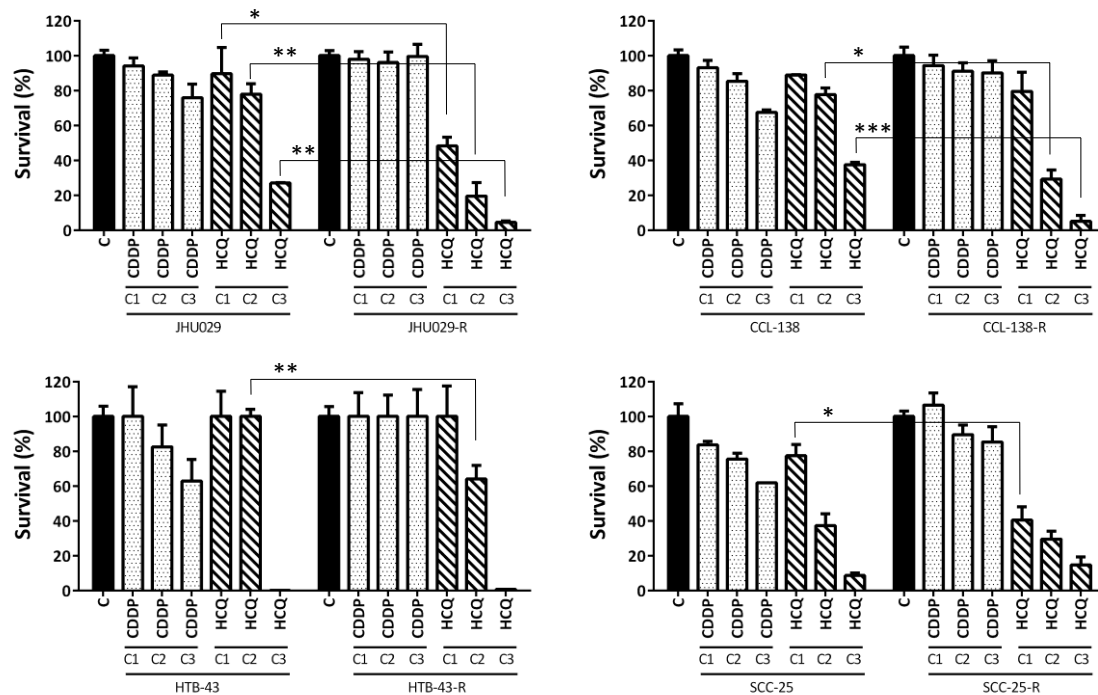


Figure 26. CDDP-resistant HNSCC cell lines are more sensitive to HCQ than the parental cells. The Y-axis represents cell survival and the X-axis represents the concentration of CDDP or HCQ. C1, C2 and C3 concentration values for each drug can be found in the **Appendix 3**. Data are expressed as mean \pm SD. Paired Student's t-test, * ($p < 0.05$); ** ($p < 0.01$); *** ($p < 0.001$).

In order to explore the concomitant action of HCQ with CDDP and 5-FU, we performed combinatorial assays in response to CDDP & HCQ versus the standard treatment with CDDP, and 5-FU & HCQ versus 5-FU. For these purpose, we used CDDP-resistant HNSCC cell lines and autophagy-dependent and independent patients, both sensitive and resistant to CDDP. JHU029-R and SCC-25-R cells (note their high levels of LC3II/I, p62 and autophagy vesicles in **Figure 19 B-D**) showed better response to the concomitant action of CDDP & HCQ (and 5-FU & HCQ for SCC-25-R) than HTB-43-R (which showed less increment in the autophagy markers respect to control cells) (**Figure 19 B, Figure 27 A**). Interestingly, CCL-138-R cells, the single cell line where autophagy-related proteins and autophagy vesicles were not significantly increased in the resistant cells when compared with

Results

control cells (**Figure 19 B** and **Figure 34 B-C**), did not respond efficiently to the concomitant action of HCQ & CDDP, or HCQ & 5-FU, when compared with only CDDP or 5-FU, respectively (**Figure 27 A**). However, the metastatic cell line CCL-138-R responds efficiently to the action of HCQ alone (**Figure 26**).

The following four biopsy-derived cell lines were also included in this assay: P47 (CDDP-sensitive patient, autophagy independent), P28 (CDDP-sensitive patient, autophagy dependent -A-), P46 (CDDP-resistant patient -R-, autophagy dependent -A-) and P33 (CDDP-resistant patient -R-, autophagy independent). Autophagy dependence was mainly considered based on LC3II/LC3I ratio and autophagy vesicles quantification by TEM (**Figure 17**). The concomitant action of CDDP & HCQ was significantly observed in P46 (R, A) but not in P47 (**Figure 27 B**). P33 (R) responds less efficiently to the concomitant action of CDDP & HCQ (except C3), in comparison with P46 (R, A) that respond efficiently to the three different concentrations (**Figure 27 B**). Interestingly, those patients considered autophagy dependent (P28 and P46), respond well to the concomitant action of CDDP & HCQ. Furthermore, a strong concomitant effect was observed between 5-FU and HCQ in P28 (A) and P33 (R).

Overall, these results suggest that the inhibition of autophagy by the autophagy inhibitor HCQ significantly affect the cell viability in resistant HNSCC cells. This effect is more prominent in those resistant cell lines where there is also autophagy activation. The fact that the metastatic pharyngeal cell line CCL-138-R, where autophagy is not altered in relation to CCL-138, does not respond to CDDP & HCQ confirms these observations.

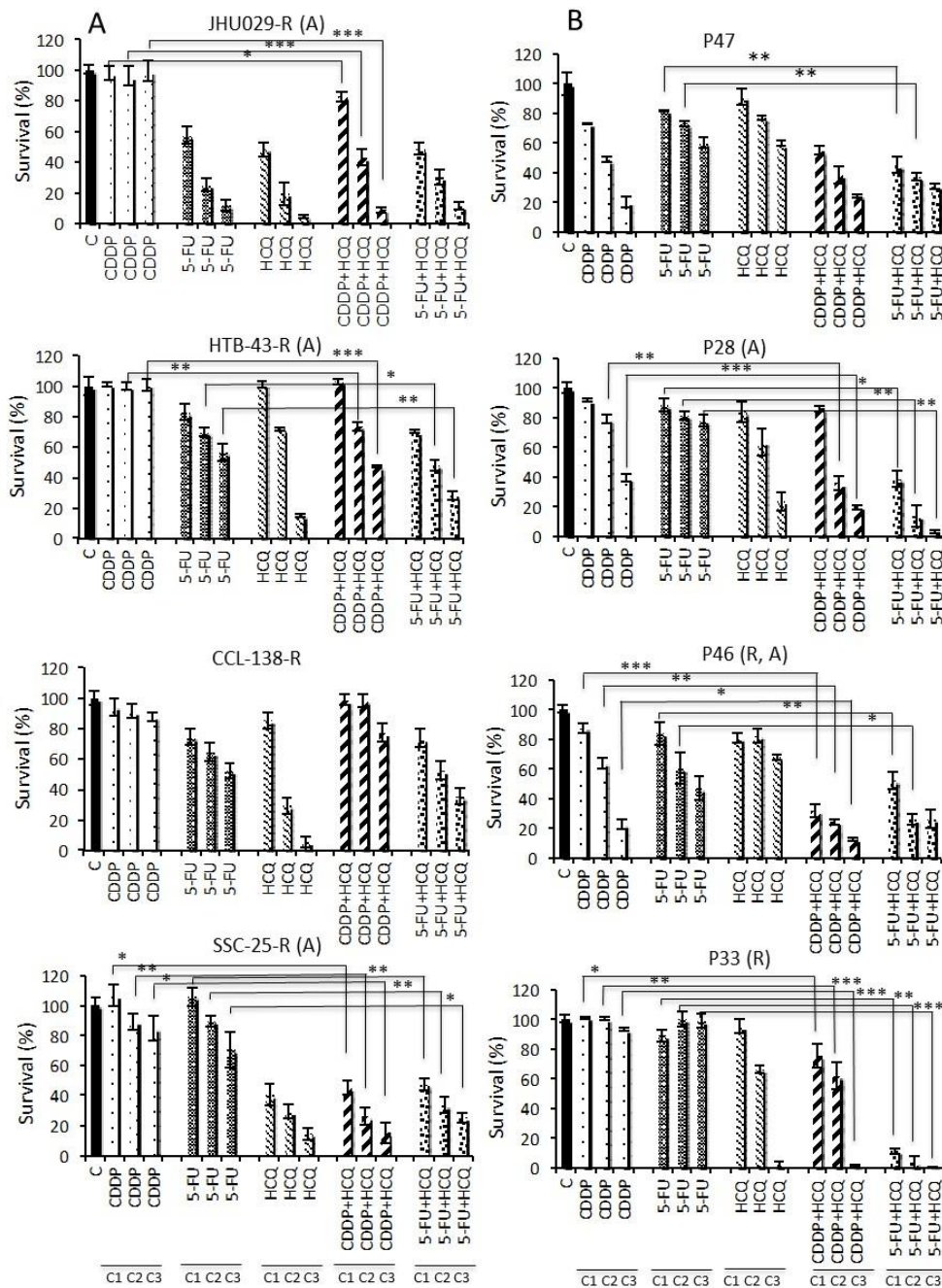


Figure 27. Therapeutic benefit of HCQ in HNSCC cells regarding their CDDP-resistance levels and autophagy dependence. **A)** The action of CDDP and 5-FU concomitantly to HCQ was studied in JHU029-R, HTB-43-R, CCL-138-R and SCC-25-R cells. Note the stronger effect of HCQ alone or in combination with CDDP in the indicated resistant cells. The concomitant effect of 5-FU & HCQ is observed in HTB-43-R and SCC-25-R cells. Note the lack of effect of HCQ & CDDP, and 5-FU & HCQ, in the CCL-138-R cells that did not show autophagy-related protein upregulation relative to parental cells. The concentrations (C1, C2 and C3) used for CDDP, 5-FU and HCQ are described in Appendix 3. **B)** The response of CDDP and 5-FU concomitantly to HCQ was also studied in P47 (sensitive and autophagy independent), P28 (sensitive and autophagy dependent -A-), P46 (resistant -R- and autophagy dependent -A-) and P33 (resistant -R- and autophagy independent). Note the major combinatory effect of HCQ in those patients who show autophagy-related protein upregulation. The concentrations used for biopsy-derived cell lines were: CDDP (C1 5 μ M, C2 10 μ M and C3 15 μ M), 5-FU (C1 15 μ M, C2 30 μ M and C3 60 μ M), HCQ (C1 30 μ M, C2 45 μ M and C3 60 μ M); and C1 + C1, C2 + C2 and C3 + C3 of each drug. Data are expressed as mean \pm SD. Paired Student's t-test, * ($p < 0.05$); ** ($p < 0.01$); *** ($p < 0.001$).

5.2. TSPAN1: a novel protein involved in HNSCC chemoresistance

The results included in this chapter are currently under review in the Journal "Cancers". Reference: cancers-942889. Garcia-Mayea, Y. *et al.* 2020.

5.2.1. TSPAN1 protein is upregulated in CDDP-resistant HNSCC cells

To identify proteins that might, potentially, have a relevant role in chemoresistance, a proteomic analysis was performed to compare the protein profile expressed in the parental cells CCL-138 versus CSCs and CCL-138-R (CDDP-resistant cells). In total 1535 proteins were identified in the three groups of cells mentioned above (**Appendix 4**). One-way ANOVA showed that 476 proteins were differentially expressed among at least two of these groups (**Appendix 5**). A *Post-Hoc* analysis revealed which of these proteins were dysregulated between groups, by comparing CCL-138-R versus CCL-138 (262 proteins), and CCL-138 CSCs versus CCL-138 (363 proteins) (**Appendix 6**). Finally, 36 proteins were commonly and differentially expressed in CCL-138-R and CSCs compared to the parental cells CCL-138: 12 proteins were upregulated and 24 proteins were downregulated (**Figure 28 A, Appendix 7**). One of the most upregulated proteins was TSPAN1, a member of the tetraspanin family, which was selected to perform functional assays because its potential clinical interest in various cancer models ^{298,326}. In order to explore the putative relevance of TSPAN1 in HNSCC, TSPAN1 protein levels were assessed in the following HNSCC cell lines: CCL-138, JHU029, HTB-43 and SSC-25. The metastatic cell line CCL-138 derived from pharyngeal cancer showed the highest TSPAN1 levels (**Figure 28 B**). To verify the proteomic results, TSPAN1 expression was evaluated by WB in the aforementioned HNSCC cell lines confirming that TSPAN1 was upregulated in the resistant variants of CCL-138-R, JHU029-R and HTB-43-R (**Figure 28 C**). Moreover, TSPAN1 was upregulated in the

Results

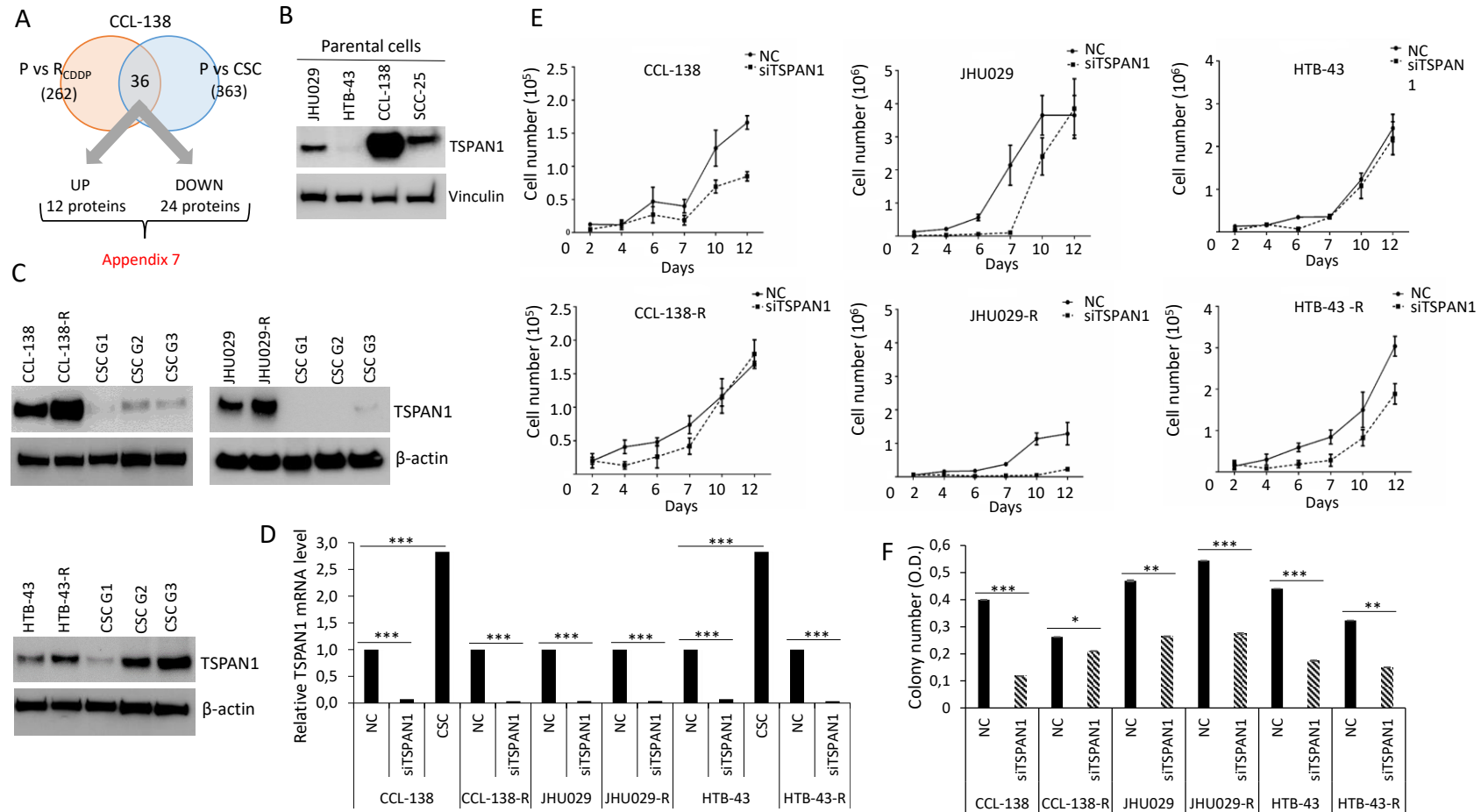


Figure 28. TSPAN1 is identified as a protein involved in HNSCC chemoresistance. A) A proteomic study identified 36 proteins commonly deregulated in CSCs and CDDP-resistant cells compared with parental cells (P), TSPAN1 was one of the most upregulated proteins. **B)** WB analysis of TSPAN1 in four different HNSCC cell lines (CCL-138, JHU029, HTB-43 and SCC-25). **C)** WB analyses confirmed proteomic data verifying the increased TSPAN1 expression in CDDP-resistant cells; and CSCs G2 and G3 from HTB-43 cell line. **D)** TSPAN1 mRNA levels in parental and CDDP-resistant HNSCC cells (-R) upon TSPAN1 depletion. Data were normalized to IPO8 expression (endogenous control) and relativized to NC (negative control or scramble). Furthermore, TSPAN1 mRNA levels for CSCs from HTB-43 and CCL-138 cell lines were assessed. Data are expressed as mean \pm SEM. Paired Student's t-test, ***($p < 0.001$). **E)** The proliferation curves from HNSCC cells transduced with the siTSPAN1 versus NC are shown. Note that the most drastic inhibitory effect on proliferation occurs in JHU029-R cells. Data are expressed as mean \pm SD. **F)** Colony number quantification of HNSCC cell lines transduced with siTSPAN1 compared to the respective NC. Data are expressed as mean \pm SD. Paired two-tailed Student's t-test, *($p < 0.05$), **($p < 0.01$), ***($p < 0.001$). OD: optical density measured at 595 nm (crystal violet).

second and third generation (G2 and G3) of CSCs in HTB-43 cells at protein level and in HTB-43 and CCL-138 at mRNA level (**Figure 28 C-D**).

The functional relevance of TSPAN1 was assessed by siRNA depletion in HNSCC cells. The parental cells JHU029, HTB-43, CCL-138, and their respective CDDP-resistant variants were transfected with siTSPAN1. All of them robustly decreased TSPAN1 mRNA levels by approximately 90% (**Figure 28 D**) and the protein levels were also effectively reduced except in CCL-138-R (**Figure 33 A, Figure 34 A**). Cell proliferation decreased in TSPAN1-depleted cells, and more significantly, this reduction was observed in the CDDP-resistant cells JHU029-R and HTB-43-R compared to parental cells (**Figure 28 E, Figure 29**). Consistently, colony formation capacity was also significantly reduced upon TSPAN1 depletion in CDDP-resistant and parental HNSCC cells (**Figure 28 F**).

5.2.2. TSPAN1 depletion induces sensitivity of HNSCC cells to chemotherapeutic agents

The effects of TSPAN1 depletion on drug responses were analyzed in the parental cells CCL-138, JHU029, and HTB-43, and their respective CDDP-resistant variants. These cell lines showed levels of sensitization to CDDP that vary between 14-43% in IC₅₀ reductions in relation to the control cells (**Figure 30 A-B**). Sensitization to CDDP was observed in all cell lines due to TSPAN1 depletion, with a higher effect in the respective resistant variants. Considering the IC₅₀ values, HTB-43-R cells showed the highest sensitization (**Figure 30 A-B**). The role of TSPAN1 on CDDP response was also assessed in laryngeal and pharyngeal biopsy-derived cell lines. We chose four biopsy-derived cell lines with high levels of resistance to CDDP (IC₅₀ values ranging 39-53 μ M). According to our previous report, IC₅₀ values >15 μ M were considered as highly resistant to CDDP ³¹⁹. The four biopsy-derived cell

Results

lines showed CDDP-sensitization upon TSPAN1 depletion, with a range of 29-59% in IC50 reductions in comparison with control cells (**Figure 30 C-D**). Therefore, TSPAN1 depletion sensitizes both biopsy-derived cell lines and established CDDP-resistant HNSCC cell lines to the effects of CDDP.

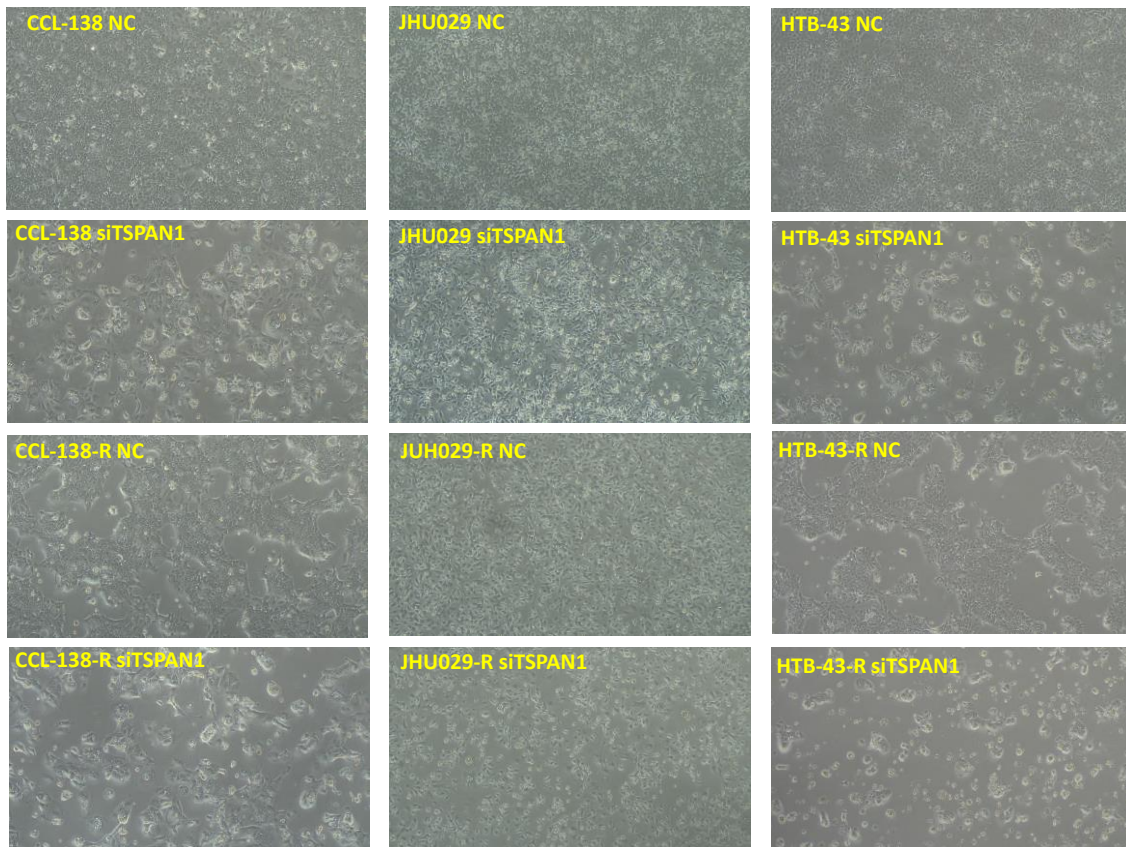


Figure 29. TSPAN1 depletion inhibits cell proliferation. Pictures show the decrease in cell number in conditions where TSPAN1 was depleted (pictures were acquired 72 hours after transfections).

In addition, we tested two independent siRNA against TSPAN1 (the siRNA#2 (Integrated DNA Technologies) and siRNA siPool (siTOOLS Biotech)) to demonstrate that the phenotypic effects observed under TSPAN1 depletion were not due to off-target effects. We found that TSPAN1 depletion with the new siRNAs (siRNA#2 and siPool), decreased cell proliferation and sensitized HNSCC cells to the effects of CDDP, corroborating previous results (**Figure 31**, data not shown).

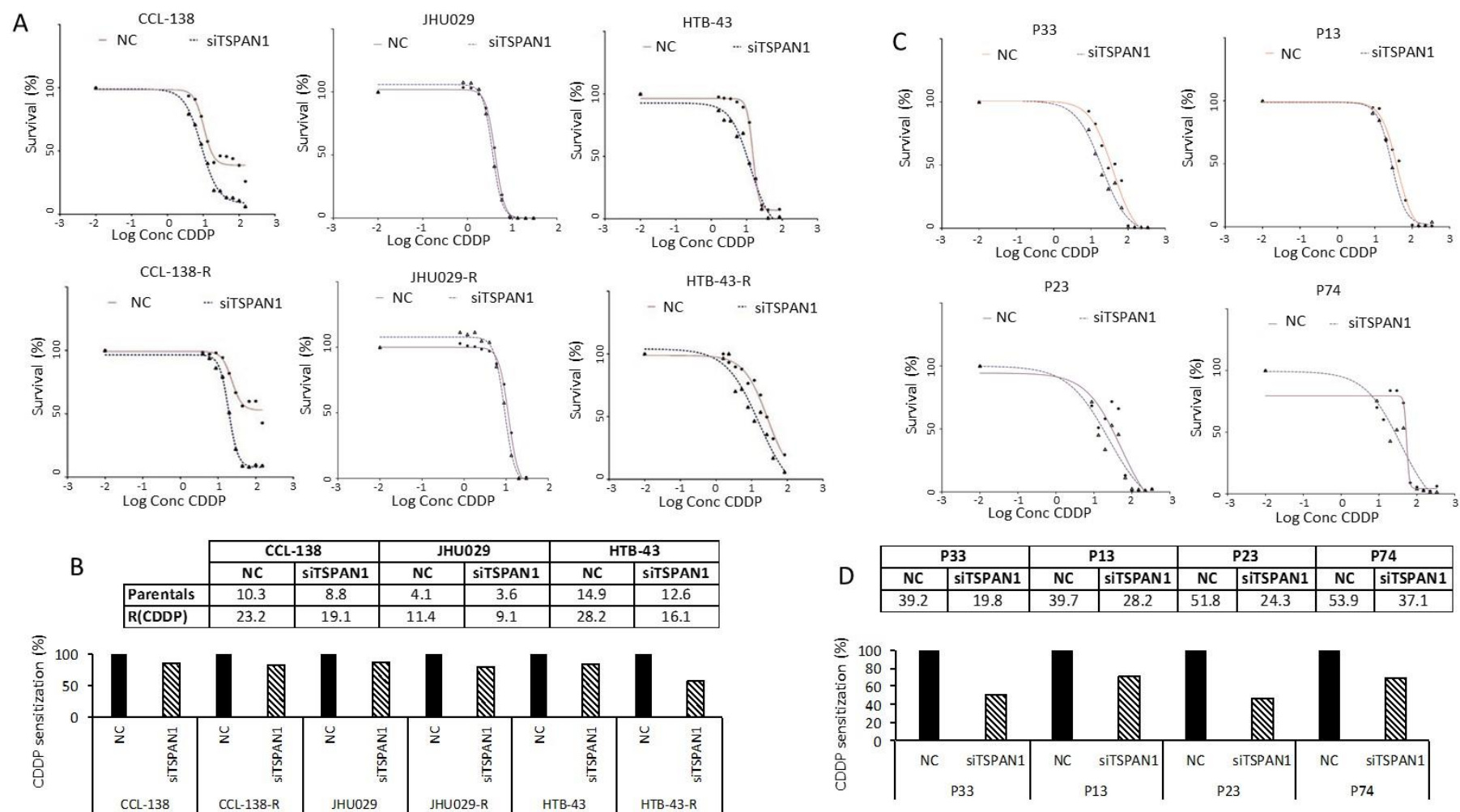


Figure 30. TSPAN1 depletion sensitizes HNSCC cells to CDDP. **A)** TSPAN1 depletion sensitizes both parental and CDDP-resistant cells CCL-138, JHU029 and HTB-43 to the effects of CDDP. A representative experiment from at least three independent experiments is shown. **B)** Table includes the IC₅₀ values (μM) from the plots shown in panel A, the IC₅₀ values are represented graphically as the percentage of sensitization relative to control cells (assigned a 100% value). **C)** TSPAN1 depletion sensitizes four biopsy-derived cell lines resistant to CDDP to the effects of CDDP: P33, P13 and P74 (larynx) and P23 (pharynx). A representative experiment from at least three independent experiments is shown. **D)** Table include the IC₅₀ values (μM) from the plots shown in panel C, the IC₅₀ values are represented graphically as the percentage of sensitization relative to control cells (assigned a 100% value).

Results

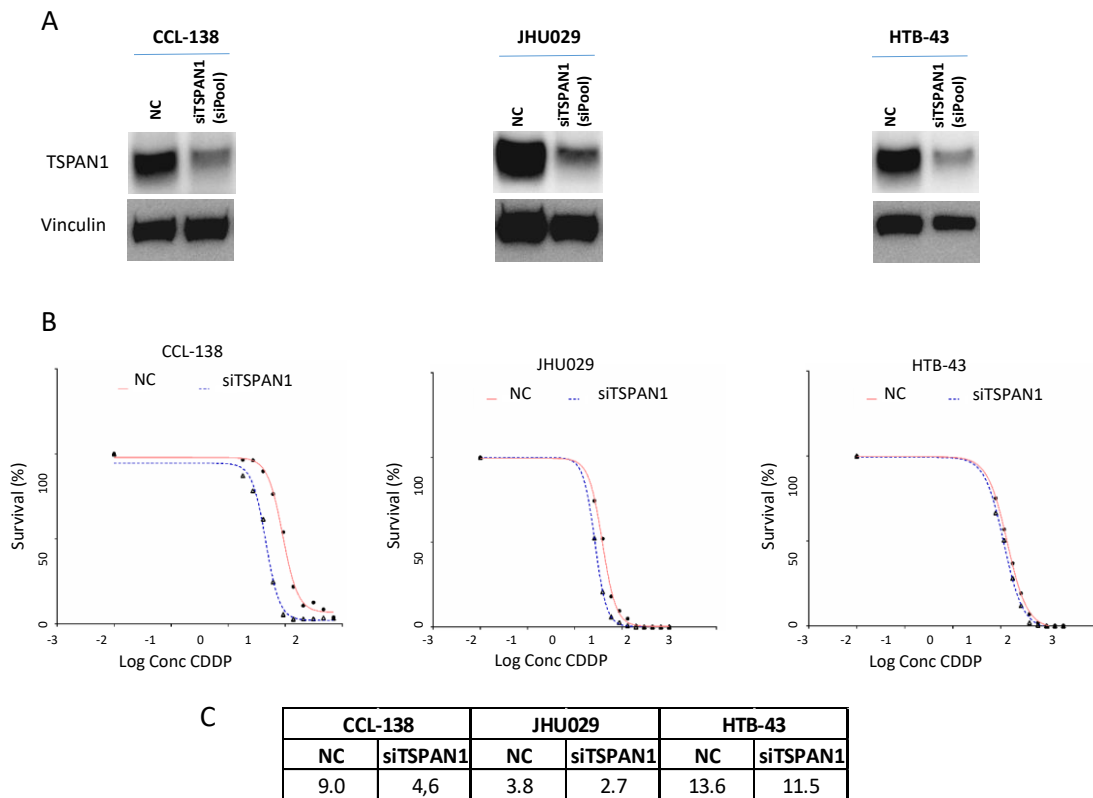
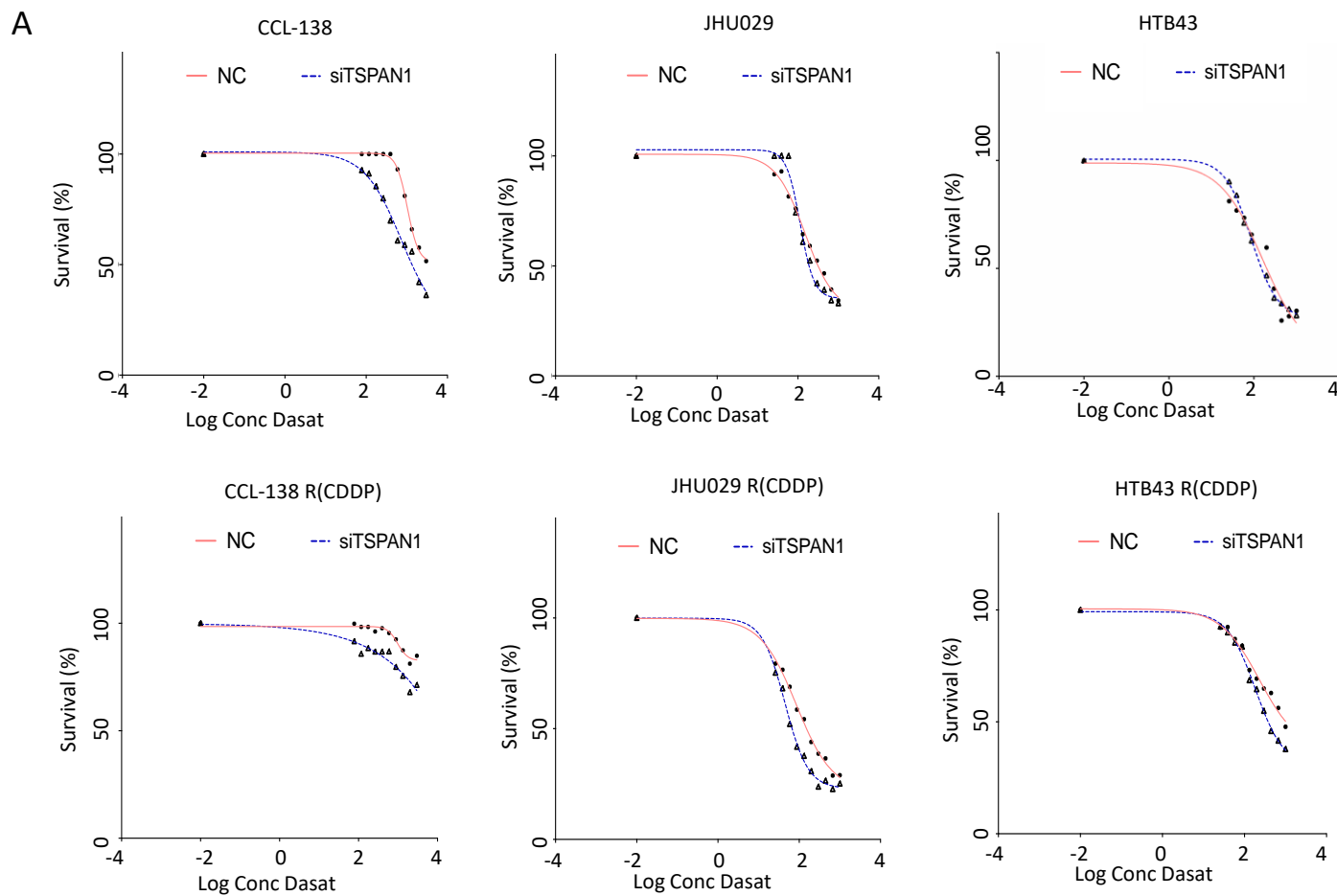


Figure 31. TSPAN1 depletion under an alternative specific mix of 30 siRNAs (siPool) sensitizes HNSCC cells to the effects of CDDP. A) TSPAN1 is depleted by the siRNA against TSPAN1 (siPool) in CCL-138, JHU029 and HTB-43 cell lines. **B)** siRNA against TSPAN1 (siPool) induces CDDP sensitization in this HNSCC cell lines. **C)** IC50 values to CDDP (μM) from panel B.

Next, we investigated if the sensitizing action of TSPAN1 depletion could be extended to other therapeutic drugs, such as dasatinib, a dual SRC/ABL kinase inhibitor actively tested in various clinical trials, including HNSCC (www.clinicaltrials.gov)^{327,328}. TSPAN1 depletion sensitized HNSCC cells to dasatinib (**Figure 32**). Hence, the effect of TSPAN1 depletion on drug sensitization is not restricted to CDDP and, beyond dasatinib, could also affect other chemotherapeutic drugs.



B

	CCL-138		JHU029		HTB-43	
	NC	siTSPAN1	NC	siTSPAN1	NC	siTSPAN1
Parentals	1035	748.0	150.1	114.3	159.9	86.6
R(CDDP)	982.0	----	85.33	44.85	230.2	185.4

Figure 32. TSPAN1 depletion sensitizes HNSCC cell lines to dasatinib treatment. A) The figure shows that TSPAN1 depletion induces dasatinib sensitization in HNSCC cell lines, mainly in the CDDP-resistant cell lines. **B)** IC50 values to dasatinib (nM) from the indicated cell lines in panel A.

Results

5.2.3. *TSPAN1* depletion induces apoptosis in HNSCC cells

Evidence of apoptosis induction upon TSPAN1 depletion emerged from PARP1 cleavage analyses by WB (**Figure 33 A**). It was found that the active form of PARP1, cleaved PARP1 -indicative of apoptosis-, increased in all TSPAN1-depleted cell lines. To corroborate these results, we further evaluated apoptosis by Annexin V detection through flow cytometry (FACS). Upon TSPAN1 depletion, apoptosis increased in all cell lines except HTB-43-R -which was only observed in early apoptosis- (**Figure 33 B**). In CCL-138 cells, the early and late apoptosis represent 1.4% and 4.4% (5.8% total) respectively, whereas these numbers increased up to 1.9% and 5.2% (7.1% total) in the corresponding TSPAN1-depleted cells. For CCL-138-R cells, early and late apoptosis represent 1.5% and 2.1% respectively (3.6% total) while apoptosis increased up to 2.2% and 4.1% (6.3% total) in TSPAN1-depleted cells. In the parental cells JHU029, early and late apoptosis were 7.7% and 15.4% (23.1% total), robustly increasing in the TSPAN1-depleted cells up to 3.5% and 53.9% (57.4% total). Similarly, early and late apoptosis in the resistant cells JHU029-R represent 7.1% and 27.9% (35% total) respectively, and apoptosis was markedly induced in the TSPAN1-depleted cells, reaching 7.4% and 42.2% (49.6% total). For the parental cells HTB-43, the early and late apoptosis represent 2.4% and 1.9% respectively (4.3% total), increasing to 3.3% and 4.2% (7.5% total) due to TSPAN1 depletion. For HTB-43-R cells, early and late apoptosis represent 4.0% and 6.1% respectively (10.1%), while in the TSPAN1-depleted cells these numbers represent 5.3% and 4% (9.3%) (**Figure 33 B**). These results show that TSPAN1 depletion induces apoptosis in HNSCC cells.

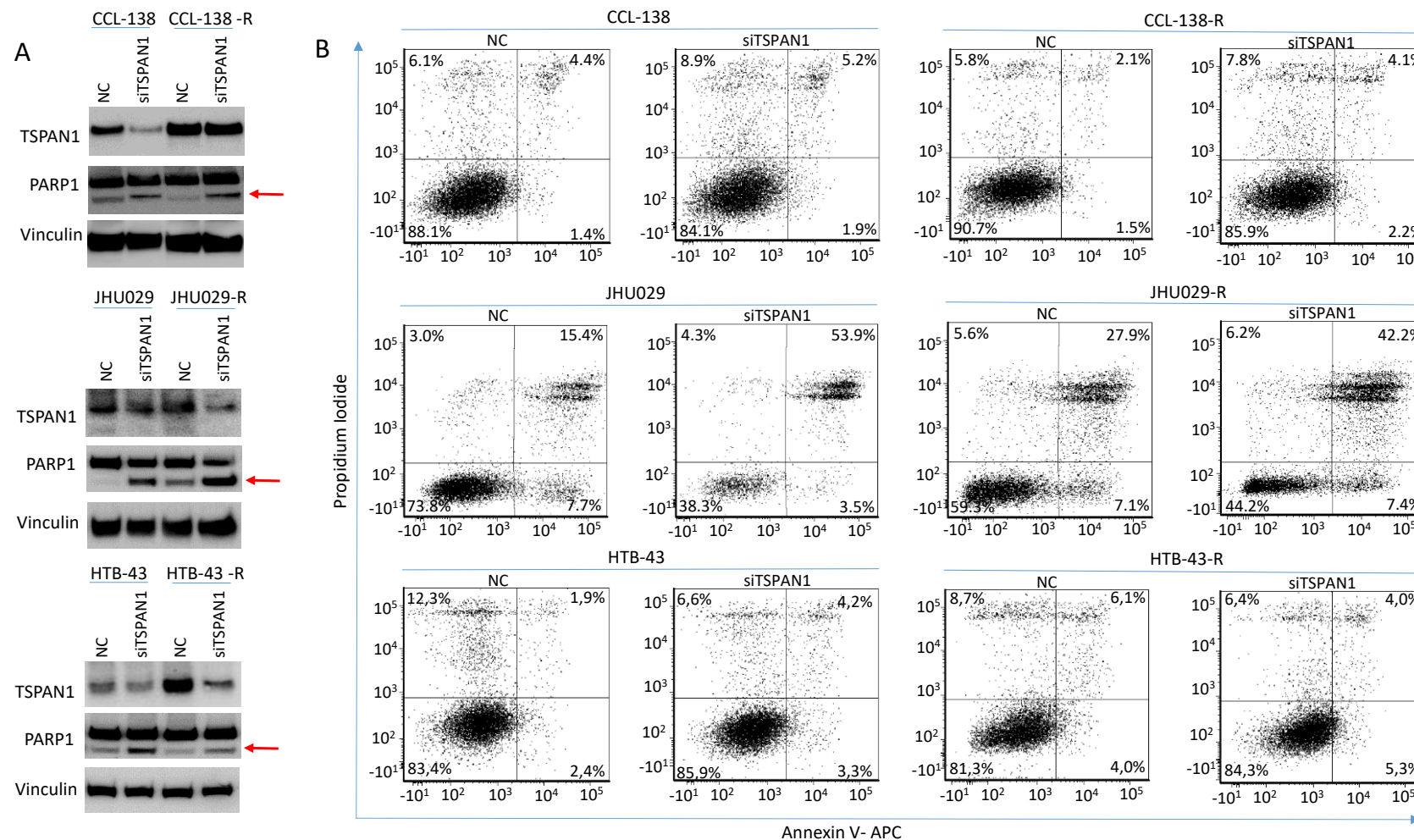


Figure 33. TSPAN1 depletion induces apoptosis in HNSCC cells. A) WB analyses of TSPAN1 and PARP1 cleavage in parental and CDDP-resistant HNSCC cell lines upon TSPAN1 depletion. PARP-1 cleavage was induced in all cases under TSPAN1 depletion. In the CCL-138-R cell line, despite not observing TSPAN1 inhibition at protein level (but it was inhibited at the mRNA level, **Figure 28 D**), an induction of PARP1 was observed. Note: the lower band corresponds to cleaved PARP1 (red arrows). Vinculin was used as protein loading normalization. **B)** Apoptosis analyses by FACS using an Annexin V expression kit, comparing NC versus TSPAN1 depleted cells. The figure shows representative scatter plots of propidium iodide (y-axis) versus Annexin V-APC (x-axis) to detect early (right bottom quadrant) and late (right upper quadrant) apoptosis in parental and their respective CDDP-resistant cells.

Results

5.2.4. *TSPAN1* depletion downregulates several signaling cascades with SRC kinase signaling as a central node

Based on our previous report linking HNSCC chemoresistance with autophagy³¹⁹, the possible relationship between TSPAN1 and autophagy was investigated. LC3II/LC3I and p62 proteins decreased at protein level in cells depleted for TSPAN1 (ATG5 only decreased in the parental cells CCL-138) (**Figure 34 A**). Autophagy inhibition was confirmed by TEM (**Figure 34 B-C**). This inhibitory effect on autophagy might be associated with: i) the suppressive effect of TSPAN1 depletion on cell proliferation and ii) apoptosis induction. Given the fact that TSPAN1 depletion sensitized both the parental cells JHU029, HTB-43, and CCL-138, and their CDDP-resistance derivatives to dasatinib (**Figure 32**), we wonder if the phosphorylation of SRC kinase (p-SRC or active SRC) -a direct target of dasatinib-, could be a mediator of TSPAN1 function in our HNSCC models. In fact, p-SRC levels (an indicator of SRC activation) consistently decreased in all 6 cell lines tested upon TSPAN1 depletion: JHU029, JHU029-R, HTB-43, HTB-43-R, CCL-138, CCL-138-R (**Figure 34 A**). Notably, p-SRC levels were co-expressed with TSPAN1: both proteins were upregulated in JHU029-R and HTB-43-R compared to their respective parental cells and, although expressions were low in CSCs at G1, both proteins were increased in CSCs at G3 (**Figure 35 A-B**). Interestingly, dasatinib robustly inhibited SRC activity and its major target p-SRC in our HNSCC models; however, dasatinib did not alter the expression of various autophagy-related proteins or TSPAN1 (**Figure 35 B**). These findings indicate that TSPAN1 inhibition efficiently targets SRC-dependent and -independent signaling pathways, beyond merely mimicking the action of dasatinib as SRC inhibitor.

Recently, it has also been described in a cholangiocarcinoma model that TSPAN1 promotes epithelial-to-mesenchymal transition (EMT) and metastasis, acting through the p-ERK and p-AKT pathways ³⁰³. This prompted us to study the link between TSPAN1 and EMT in our HNSCC models. For this purpose, EMT-related proteins vimentin, E-cadherin and N-cadherin were analyzed by WB in TSPAN1-depleted cells. Only the expression of vimentin –a mesenchymal-related protein-, decreased upon TSPAN1 inhibition in the JHU029 and JHU029-R cells, but no clear differences were observed in E-cadherin or N-cadherin, neither in the other HNSCC cell lines (data not shown). WB analyses of p-ERK and p-AKT were performed to explore if the ERK and AKT pathways were involved in our model. p-AKT levels were found to decrease in CCL-138, JHU029-R, HTB-43, and HTB-43-R cells upon TSPAN1 depletion, while p-ERK1/2 decreased in all 6 conditions (CCL-138, CCL-138-R, JHU029, JHU029-R, HTB-43, and HTB-43-R cells) at variable levels (**Figure 34 A**). In JHU029-R, CCL-138 and HTB-43 cells, dasatinib treatment decreased p-ERK1/2, but only decreased p-AKT in HTB-43-R (**Figure 35 B**).

Results

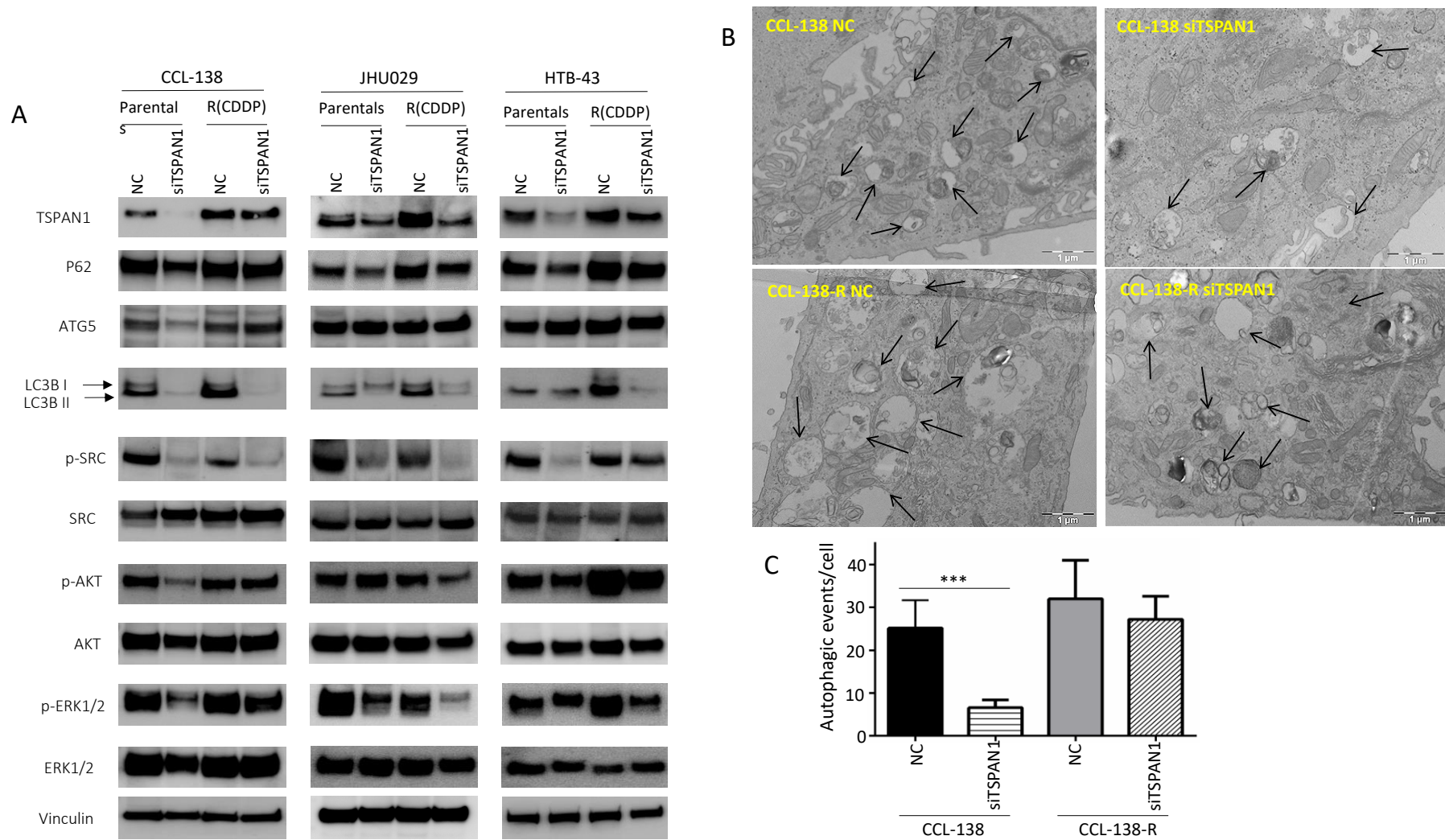


Figure 34. Characterization of TSPAN1 downstream effectors. **A)** WB analyses of proteins modulated by TSPAN1 depletion in parental and CDDP-resistant HNSCC cells, including various key proteins related to autophagy and SRC/AKT/ERK signaling pathways. **B)** Representative TEM images from TSPAN1-depleted cells versus control cells (NC) in CCL-138 and CCL-138-R cells. TEM images revealed autophagosomes and autophagolysosomes, features characteristic of autophagic cells. **C)** Quantification of autophagic vesicles from each experimental group defined in panel B. Note that autophagy vesicles decrease in CCL-138 cells upon TSPAN1 depletion. Data are expressed as mean±SD. Paired Student's t-test, ***($p < 0.001$).

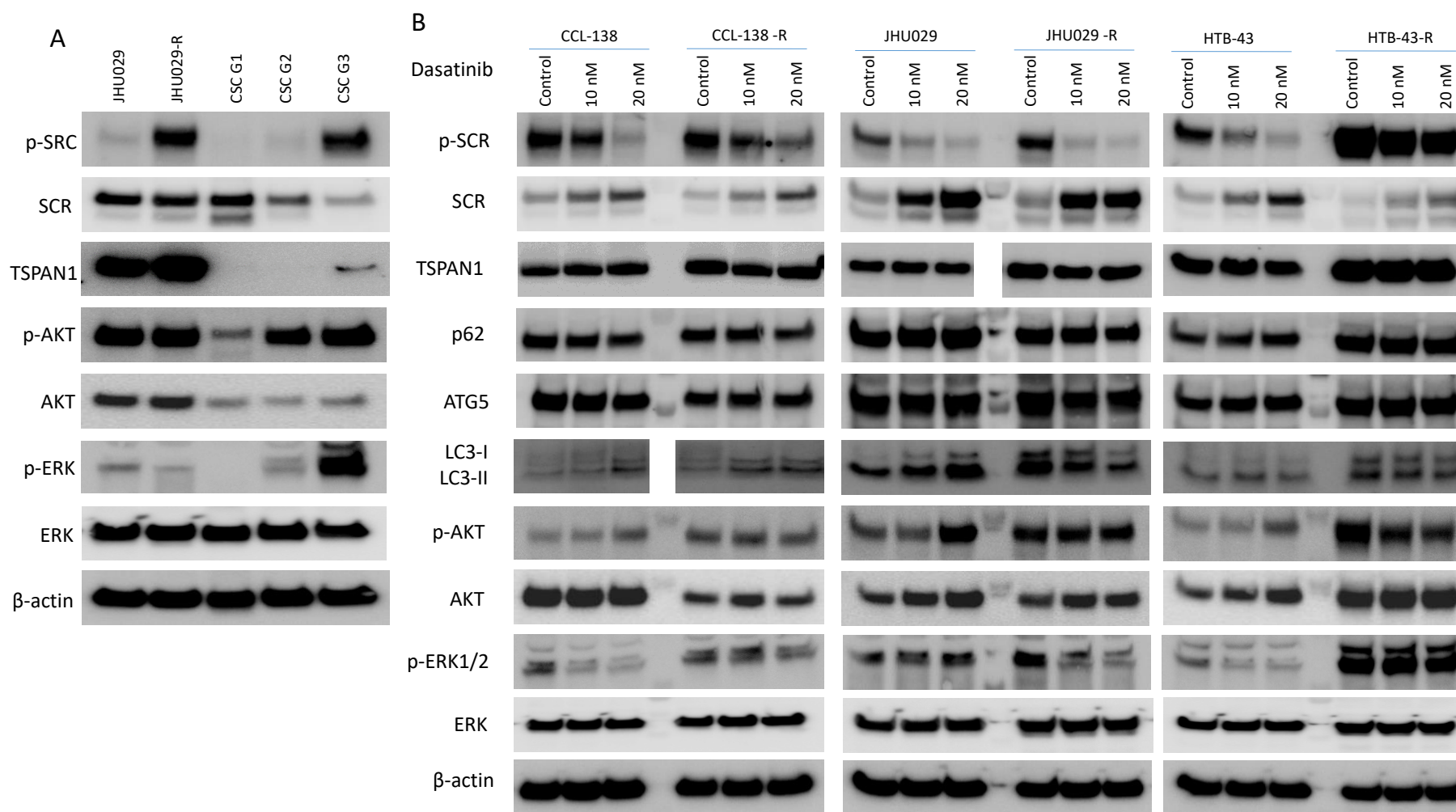


Figure 35. The inhibition of SRC activation (p-SRC) through dasatinib does not affect TSPAN1 expression either TSPAN1 downstream pathway. A) p-SRC, TSPAN1, p-AKT and p-ERK expression in JHU029, JHU029-R cells and different generations of CSCs (G1, G2 and G3). Note that G1 derives directly from parental cells growing in non-adherent conditions and G3 is the most enriched CSCs population. **B)** The inhibition of p-SRC through dasatinib does not affect TSPAN1 expression or its downstream targets.

Results

5.2.5. *TSPAN1-depleted cells decrease tumor formation ability and metastatic capacity in mice*

The role of TSPAN1 was investigated *in-vivo* in HNSCC models, inducing mice tumors with JHU029 and the CDDP-resistant cells JHU029-R, both depleted for TSPAN1 versus control cells (NC). In such cells, TSPAN1 depletion was confirmed at protein level (**Figure 36 A**). Tumors formed in mice phenotypically reproduced the characteristics observed in HNSCC tumors from patients (**Figure 37 A**). Tumor sizes were significantly lower in the tumors generated from TSPAN1-depleted cells compared to those formed by control cells (**Figure 36 B-C, Figure 37 B**). Measurement of tumor size by IVIS bioluminescence imaging further confirmed these results (**Figure 36 D-E**). Notably, tumors formed by the resistant cells JHU029-R, despite being smaller in size, showed EMT features (a fusocellular morphology) (**Figure 36 F**, arrows). However, that EMT phenotype was reversed in those tumors formed by the TSPAN1-depleted cells.

The pathological examination of the primary tumors from mice did not show significant differences of Ki-67 staining regardless depletion of TSPAN1 (**Figure 37 C**). The impact of TSPAN1 depletion on metastasis formation was also assessed *ex-vivo*, thereby monitoring the presence of luciferin-positive cells in various organs extracted from the different experimental groups of mice, using the IVIS bioluminescence imaging system. A significant decrease in bone and liver metastasis was measured in tumors originated from JHU029-R cells under TSPAN1 depletion compared to control cells, and a trend to significance for lung metastasis was also observed (**Figure 38, Figure 36 G**). Overall, TSPAN1 depletion renders smaller tumors with lower proliferative rates and less metastatic capacity.

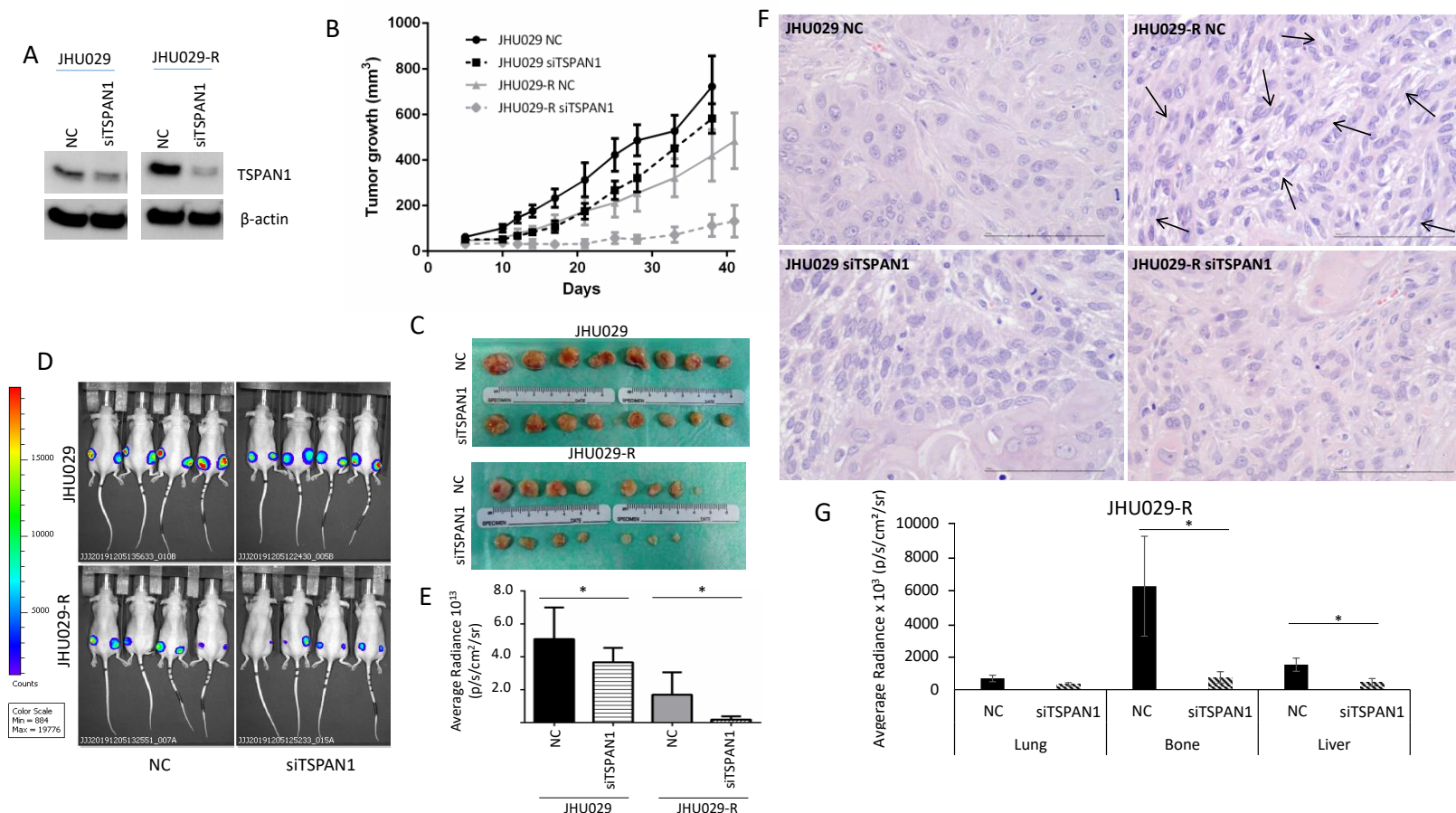


Figure 36. The impact of TSPAN1 depletion *in-vivo*. JHU029 and JHU029-R cells were transduced with siTSPAN1 and injected into immunosuppressed mice. **A)** TSPAN1 depletion was monitored in cultured cells 48 hours after transfection. **B)** Graph representing the growth of the tumor originated in mice. Data are expressed as mean \pm SD. Significant differences were found, JHU029 NC vs siTSPAN1 (days 10-28), and JHU029-R NC vs siTSPAN1 (days 12-41). Paired Student's t-test. **C)** Pictures of the tumors formed in the indicated group of mice. **D)** Pictures of the mice tumors at the end point of the experiment. The luminescent signal was taken by the IVIS apparatus. **E)** Quantifications of the luminescent signals of the tumors were acquired by Living Image software and were graphed. Data are expressed as mean \pm SD. Paired Student's t-test, *($p < 0.05$). **F)** Representative images of H&E staining of the indicated mice tumors are shown. Note the presence of a fusocellular pattern in the resistant cells but not in those parental cells. The fusocellular pattern, indicating the activation of an EMT program was reverted in the animals where TSPAN1 has been inhibited (JHU029-R-NC versus JHU029-R-siTSPAN1). **G)** Quantification of micrometastases based upon the luminescent signals acquired by Living Image software in the indicated organs of the JHU029-R mice tumors. Data are expressed as mean \pm SD. Paired Student's t-test, *($p < 0.05$).

Results

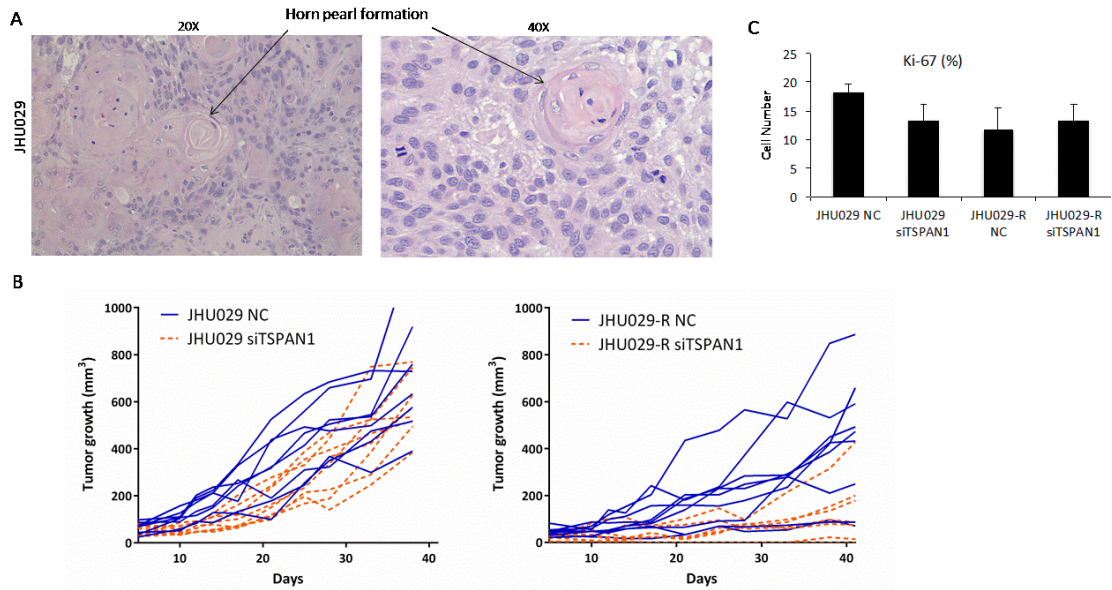


Figure 37. Phenotypic characteristics and proliferative potential of tumors formed in mice. **A)** Laryngeal tumors formed by the injection of JHU029 cells mimicking the horn pearls characteristic of human head and neck squamous carcinomas. **B)** Plots indicating the tumor growth (JHU029 and JHU029-R tumors) in each individual mouse. Data are expressed as mean \pm SD. **C)** Percentage of Ki-67 positive cells in the indicated tumor types. Note the presence of proliferative cells given by the positivity of the proliferative marker Ki-67.

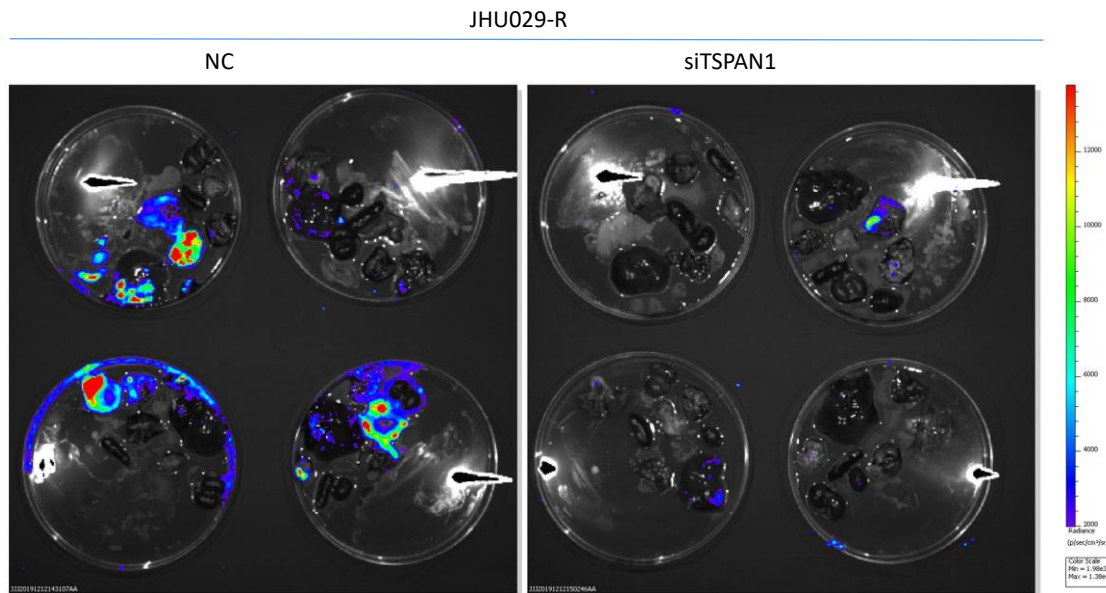


Figure 38. Ex-vivo analysis of micrometastases under TSPAN1 depletion. Pictures of the presence of luminescent tumoral cells detected by IVIS showing the presence of micrometastases in several organs including liver, lung, heart, spleen and kidneys.

5.2.6. *The expression of TSPAN1 correlate with active SRC and EMT features in patient samples.*

The relevance of TSPAN1 expression was further investigated in tumors from HNSCC patients. TSPAN1 levels were assessed by WB in paired samples of laryngeal and pharyngeal tumors (T) and patient-matched normal mucosa (N). TSPAN1 overexpression was detected in 8 out of 12 tumor samples compared to the normal counterparts (**Figure 39 A**). Of note, high TSPAN1 levels were also observed in some normal tissues comparable to the matched tumor. To further and significantly extend these data, IHC analyses of TSPAN1 was performed in a cohort of 106 laryngeal and pharyngeal cancer patients and correlated with clinical data and disease outcome. TSPAN1 protein expression in tumors exhibited cytoplasmic and nuclear patterns that were scored separately, whereas TSPAN1 expression was negligible in matched adjacent normal epithelia and stromal cells (**Figure 39 B**). Forty-eight out of 106 patients (45.2%) showed cytoplasmic TSPAN1, and 34 cases out of 48 patients showed concomitant cytoplasmic and nuclear staining (32.1% of total) (**Figure 39 C**). Based on our data from HNSCC models, possible associations of TSPAN1 expression with p-SRC and E-cadherin were assessed. Interestingly, cytoplasmic and nuclear TSPAN1 were both inversely and significantly associated with E-Cadherin expression (**Figure 39 D**), confirming a possible link between TSPAN1 and EMT in HNSCC. In agreement with our results in HNSCC cells, TSPAN1 expression was associated with active SRC (**Figure 40 A-B**). Although the differences did not reach statistical significance (in fact, they are in the limit of significance, $p=0.055$), we found that TSPAN1 expression tends to be associated with a poor degree of histological differentiation of tumors (**Figure 40C-D**).

Results

On the other hand, normal and tumor tissue samples from 16 HNSCC patients were analyzed by qRT-PCR for the expression of TSPAN1. Eight patients overexpressed TSPAN1 at mRNA level (**Figure 41 A**). However, non-significant differences were observed between normal and tumor tissues comparing the median expression levels of TSPAN1 (**Figure 41 B**). *In silico* analysis of TCGA database was performed to explore TSPAN1 expression more extensively in different cancer types at the mRNA level ³²⁹. It was revealed that TSPAN1 mRNA is upregulated in various cancers compared to the corresponding normal counterparts, including HNSCC (**Figure 41 C**). Finally, the role of TSPAN1 on prognosis was assessed in our HNSCC patient cohort (at protein level) and TCGA databases (at mRNA level). However, we did not find any association of TSPAN1 with overall survival or disease-specific survival (**Figure 42 A-B**) ³²⁹.

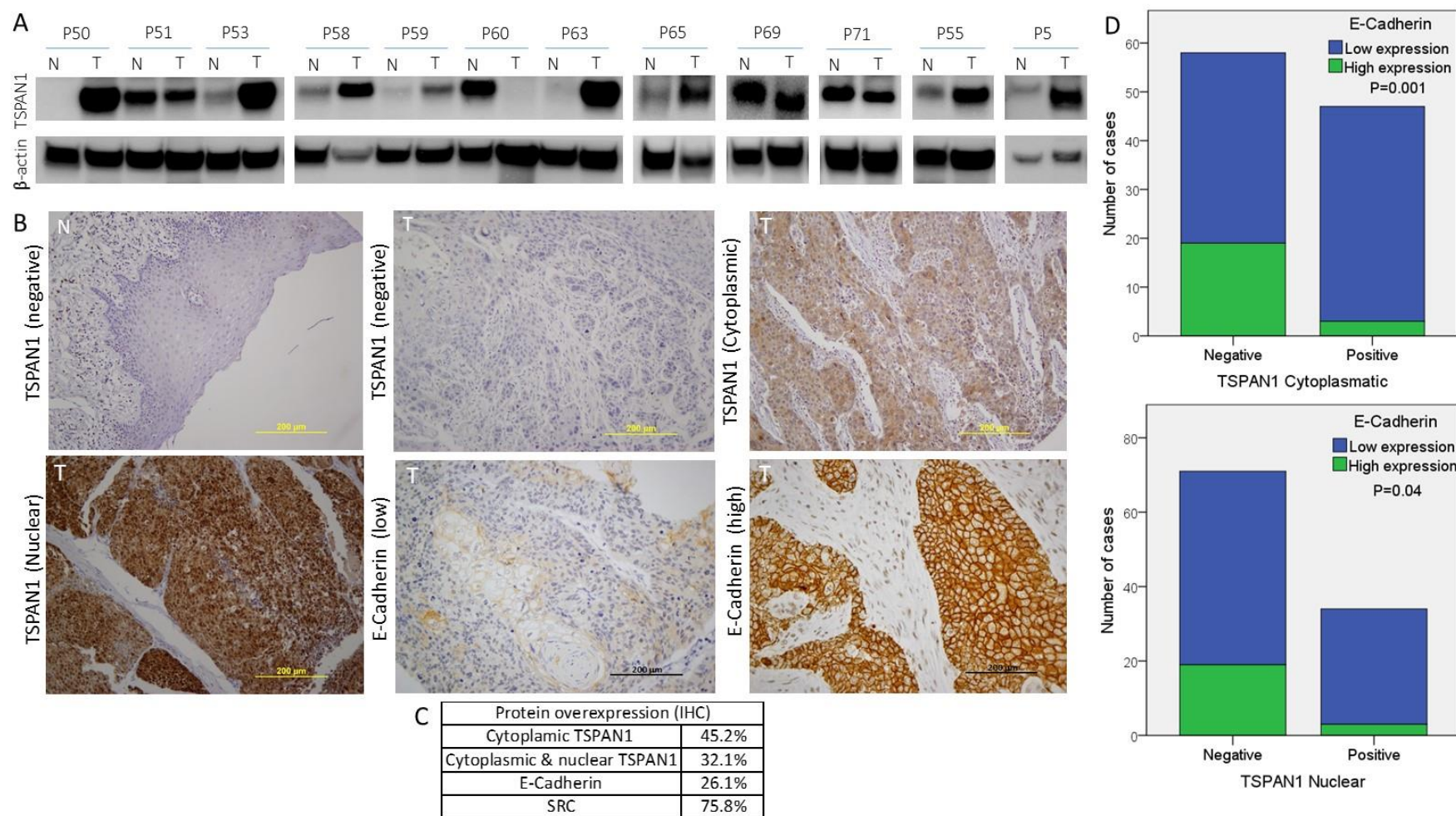


Figure 39. Protein expression assay of TSPAN1 and E-cadherin in human biopsies from HNSCC patients. A) WB of TSPAN1 protein in laryngeal cancer biopsies comparing tumor (T) versus normal tissue (N). Note the overexpression of TSPAN1 in 8 out of 12 patients. **B)** Representative images of IHC expression of TSPAN1 and E-Cadherin proteins. The expression of TSPAN1 was only observed in the tumor tissue. TSPAN1 expression can be at cytoplasmic level or at cytoplasmic and nuclear level. **C)** Table indicating the percentage of positive patients for the analyzed proteins in the TMs that include 106 patients from HUCA. **D)** Association between E-Cadherin and TSPAN1 expression. Note that patients showing TSPAN1 expression have low expression of E-Cadherin. The plots show the expression of TSPAN1 at cytoplasmic level (upper panel) and at cytoplasmic & nuclear level (lower panel, designated as Nuclear). χ^2 test and Fisher's exact test, $p < 0.05$.

Results

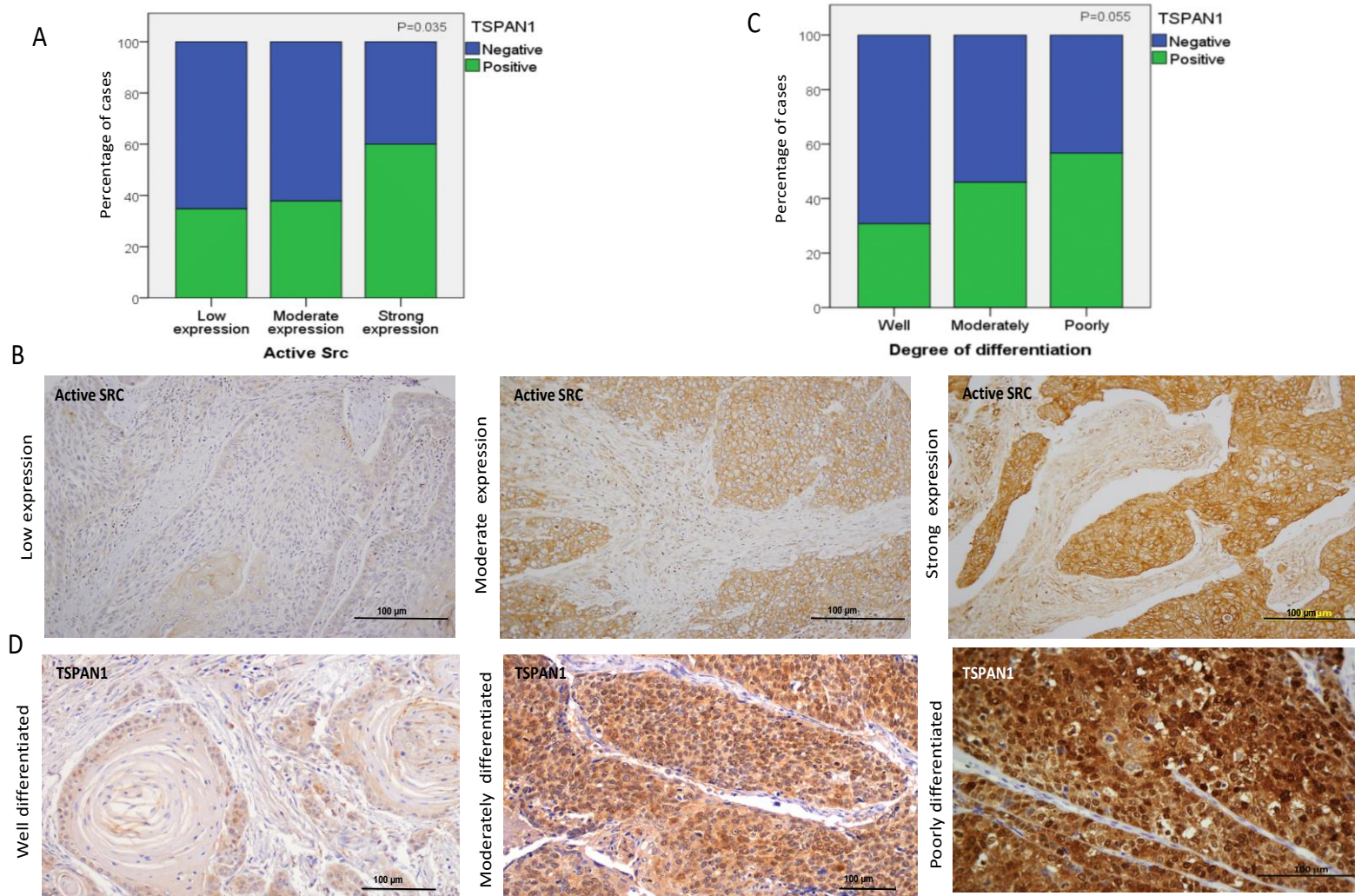


Figure 40. TSPAN1 expression is associated with active SRC and tends to be associated with poorly differentiated tumors. A) Direct association of TSPAN1 with active SRC (p-SRC). χ^2 test and Fisher's exact test, $p < 0.05$. **B)** Representative IHC images of pSRC expression at different levels (low, moderate and high) as classified. **C)** TSPAN1 expression tends to be associated with the degree of tumor differentiation. Note that TSPAN1 expression tends to be higher in those patients with HNSCC tumors of poor differentiation. χ^2 test and Fisher's exact test, $p > 0.05$. **D)** Representative IHC images of TSPAN1 expression at different levels of differentiation (well, moderately and poorly) as classified.

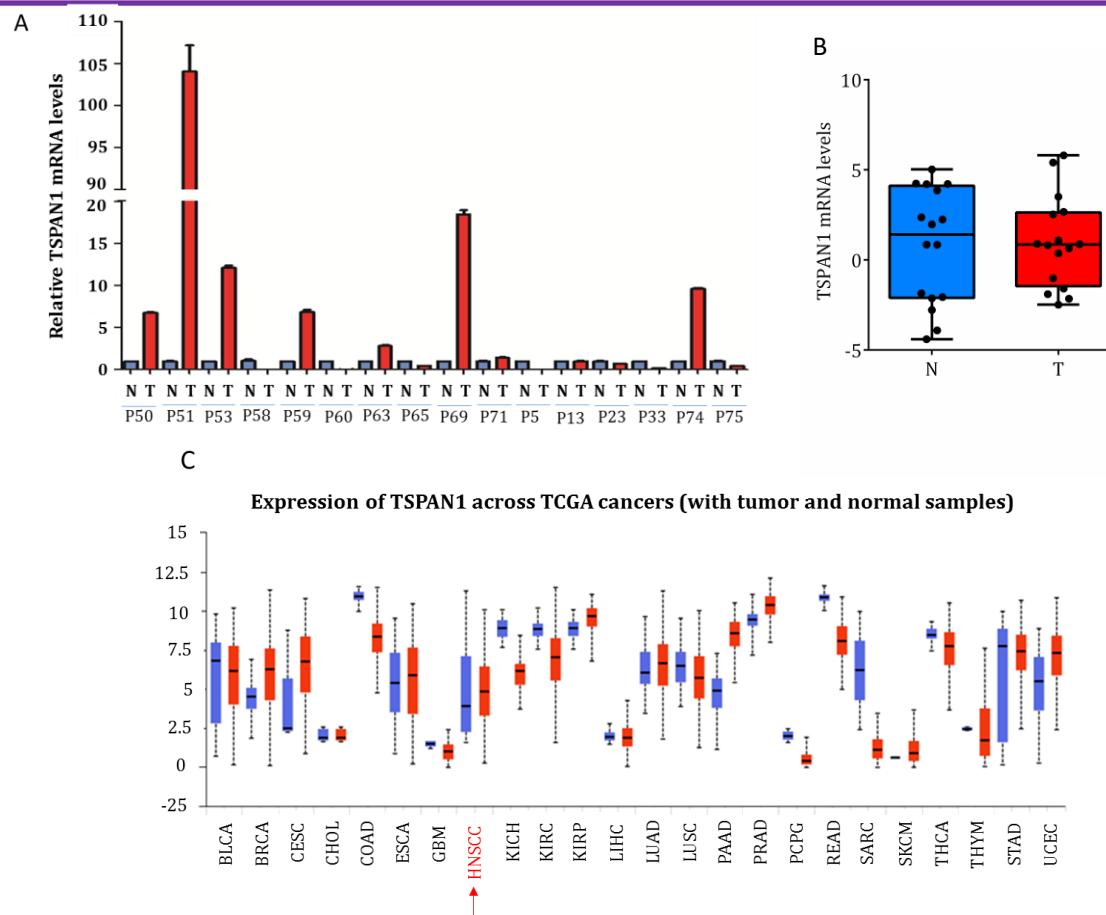


Figure 41. TSPAN1 expression at mRNA level. A) TSPAN1 mRNA expression levels in normal (N) and tumor tissue (T) in biopsies from 16 patients with HNSCC. **B)** TSPAN1 mRNA expression levels considering the 16 patients included in panel A, non-significant difference between both groups were found (Wilcoxon test, $p > 0.05$). **C)** TSPAN1 mRNA levels in different tumor types according to the TCGA databases. Normal (blue) and tumor tissue (red) are indicated for each tumor type. Note that pancreatic adenocarcinoma, prostate adenocarcinoma and cervical squamous cell carcinoma showed the most increment of TSPAN1 in tumor tissue versus normal tissue. BLCA, Bladder Urothelial Carcinoma; BRCA, Breast Carcinoma; CESC, Cervical Squamous Cell Carcinoma; CHOL, Cholangiocarcinoma; COAD, Colon Adenocarcinoma; ESCA, Esophageal Carcinoma; GBM, Glioblastoma Multiform; HNSC, Head and Neck Squamous Cell Carcinoma; KICH, Kidney Chromophobe; KIRC, Kidney Renal Clear Cell Carcinoma; KIRP, Kidney Renal Papillary Cell Carcinoma; LIHC, Liver Hepatocellular Carcinoma; LUAD, Lung Adenocarcinoma; LUSC, Lung Squamous Cell Carcinoma; PAAD, Pancreatic Adenocarcinoma; PRAD, Prostate Adenocarcinoma; PCPG, Pheochromocytoma and Paraganglioma; READ, Rectum Adenocarcinoma; SARC, Sarcoma; SKCM, Skin Cutaneous Melanoma; THCA, Thyroid Carcinoma; THYM, Thymoma; STAD, Stomach Adenocarcinoma; UCEC, Uterine Corpus Endometrial Carcinoma.

Results

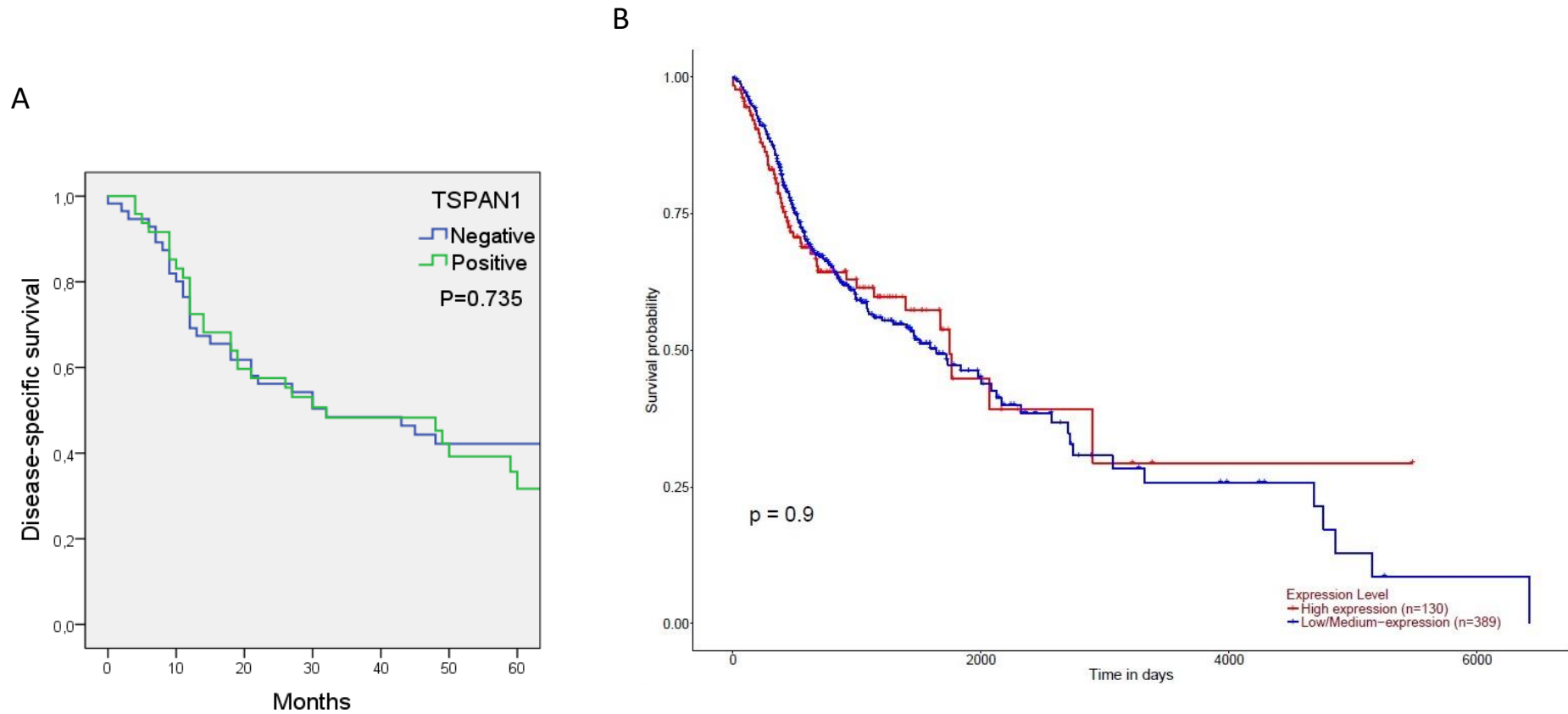


Figure 42. TSPAN1 in relation to patient survival. A) TSPAN1 expression at the protein level is not associated with disease-specific survival in our series of HNSCC patients. Log-rank test, $p > 0.05$. **B)** According to the TCGA databases, there is no association of TSPAN1 at mRNA level with overall survival in HNSCC tumors. Log-rank test, $p > 0.05$.

DISCUSSION

VI. DISCUSSION

In the last decades, the few advances in the treatment of patients with HNSCC, together with the high rates of recurrence and local metastases, are the main reasons for the high death rate of this type of cancer ^{10,14,330}. Despite the efforts devoted to finding markers of resistance to categorize patients ³³¹, the MDR phenotype remains a great hurdle for efficient cancer treatments. It has been demonstrated that the activation of stemness-associated genes confers chemoresistance in HNSCC ^{8,332}. Undoubtedly, CSCs provide the best explanation for radio and chemoresistance. Due to the fact that multiple CSCs subpopulations may coexist within a tumor, this adds further complexity to therapeutic approaches based on proliferative transcriptomic patterns that consider the whole set of cancer cells ³³³.

Under therapeutic treatments, CSCs and other cancer cells with the potential to acquire resistance to current treatments, are capable of activating different molecular mechanisms that allow them to survive. One of these survival strategies is autophagy (**Figure 5 G**). Autophagic flow overactivation, and its association with the stemness phenotype and resistance acquisition to the current therapy, have previously been described in several cancer types ^{209,210,212}, including HNSCC ^{211,213,334-336}. These associations were also corroborated in this thesis for laryngeal, pharyngeal, and tongue cancer models. Studies about the role of autophagy activation and autophagy-associated proteins (e.g., LC3, p62, and ATG5) in tumor growth are increasing. In general, a positive correlation between autophagy activation and poor clinical prognosis has been found in several cancer models ³³⁷⁻³⁴¹. Moreover, some autophagy-associated proteins like Beclin-1, ULK1, ATG5, ATG7, ATG12, ATG14, and p62 have been implicated in HNSCC ³³⁴⁻³³⁶.

Discussion

To study if autophagy disruption could have a role in chemotherapy resistance in HNSCC, we analyzed autophagy-related proteins in biopsies derived from patients with laryngeal cancer. In addition, the oncogenic protein PTOV1 has recently been implicated in HNSCC ³⁴²⁻³⁴⁴ and autophagy ^{345,346}, therefore it was also included in this study. Indeed, we observed that a proportion of laryngeal cancer patients were positive for the expression of ATG5 (33%), LC3 (27%), nuclear p62 (50%), cytoplasmic p62 (42%) and PTOV1 (85%) (**Figure 13**). Besides, we found a significant correlation between LC3 and p62, and positive cytoplasmic p62 was more commonly observed in patients with advanced tumor stage (III and IV) (**Figure 14 A, E-F**). Interestingly, p62 translocation from the nucleus to cytoplasm has been detected in cancerous cells, but not in normal epithelial cells (e.g., esophageal or urothelial carcinoma). This is associated with a worse prognosis and an increased risk of developing metastasis ^{338,347,348}, which could be explained by its participation in the autophagic process (cytoplasmic). Our IHC results agree with such studies, as cytoplasmic p62 (but not nuclear p62) is associated with advanced tumor stage in our series of patients.

Furthermore, our results confirm previous IHC studies in which PTOV1 expression was associated with advanced tumor stage in some cancers ^{349,350}, including laryngeal cancer ³⁴² and others HNSCC ^{343,344}. We also proposed a link between PTOV1 and autophagy, as suggested by a network proteomic study ³⁴⁶ and a breast cancer model ³⁴⁵. However, we have not found any previous report describing the concomitant expression of ATG5 and PTOV1 as we found in the patients herein analyzed (**Figure 14 B, C-D**). Thus, our results suggest that high expression levels of cytoplasmic p62 and PTOV1 could be considered as prognosis markers for more aggressive laryngeal tumors.

We also found that LC3 positive expression was capable to distinguish a subgroup of patients with supraglottic tumors with worse overall survival. Moreover, that subgroup of patients trend to respond worse under chemotherapy treatment (**Figure 14 G, Figure 15**), suggesting the potential use of LC3 expression at IHC level to predict patient survival in this specific subgroup of patients. Accordingly, LC3 has been suggested as a poor prognostic marker in various IHC studies in HNSCC ^{206,351,352} and other aggressive cancers, such as triple-negative breast cancers ³⁵³.

Interestingly, the 13 biopsy-derived cell lines established from laryngeal and pharyngeal tumors showed that the intrinsic resistance of cancer cells to CDDP (IC₅₀>15 μM) was significantly associated with a higher expression of ATG5 and PTOV1 proteins. Again, an association between PTOV1 and ATG5 was found, suggesting an autophagy role of PTOV1 in HNSCC. The classification of these patients as dependent or independent of autophagy based on the results obtained by WB was also validated through the analysis and quantification of the autophagic vesicles using a TEM (**Figure 17**). In agreement with our results, metastatic melanoma patients with activated autophagy were associated with therapy resistance and poor clinical prognosis, in both 3D cultures and *in-vivo* models ³⁵⁴.

Importantly, 4 out of 7 (57%) of the patients considered intrinsically resistant to CDDP (based on the IC₅₀ values from their biopsy-derived cell lines) experienced cancer relapse and death upon standard clinical treatment. In contrast, only 2 out of 6 (33%) patients defined as sensitive to CDDP are currently died (**Table 5**). Therefore, by determining the intrinsic grade of CDDP-resistance (IC₅₀ values) of biopsy-derived cell lines, from laryngeal and pharyngeal cancer patients, could be possible to predict the group of non-responder patients to conventional therapy,

Discussion

thus providing sufficient time for an alternative treatment in the clinic. These results also support the feasibility of culturing biopsy-derived cell lines from HNSCC tumors in order to predict the clinical response, as technically described by other authors ^{355,356}. However, to our knowledge, there are currently no commercial laryngeal cell lines in the world (ATCC does not currently sell JHU029 or other laryngeal cell lines), so we have pioneered the establishment of these cultures.

Of interest, the HNSCC cell lines in which chemotherapy resistance was progressively induced, showed an increase in LC3II/LC3I, PTOV1, ATG5 (JHU029) and p62 (JHU029) in the resistant cells JHU029-R, HTB-43-R, and SCC-25-R (especially in the CDDP-resistant variants), but not in the metastatic CCL-138-R cell line (**Figure 19**). This could be explained because the CCL-138 cell line derives from a pleural effusion metastasis from a pharyngeal carcinoma, and during this complex metastatic process, such tumor might have already activated resistance mechanisms (e.g., the overactivation of the autophagic flow). In this way, when CCL-138 was exposed to CDDP and 5-FU during the generation of the respective resistant cell lines (CCL-138-R), autophagy markers were not overexpressed. Note that the cell line CCL-138 showed more than 12 times more autophagic events by TEM analysis than the cell line JHU029. Furthermore, CCL-138 is more than five times more resistant to CDDP than JHU029 if we compare the IC50 values from both parental cell lines (**Figure 19**; **Figure 24 B-C**; **Figure 34 B-C**). We hypothesize that autophagy might not be the main regulator of chemoresistance in already established metastatic cells that have a higher resistance than pharyngeal and laryngeal cells derived from primary tumors (**Figure 19 A-B**). In addition, since autophagy-related proteins were also activated in CSCs generated from

established HNSCC cell lines (particularly in the laryngeal and tongue cell lines JHU029 and SCC-25; **Figure 19 B**), we hypothesize that an autophagy inhibitor treatment (e.g., HCQ) would also target CSCs in HNSCC tumors –apart from chemoresistant cells- as had been proposed for other cancer models ³⁵⁷. Note that the acquisition of the CSCs phenotype was corroborated based on: i) their ability to grown in suspension cultures (3D) under serum deprivation to form spheroids, ii) the overexpression of various CSCs genes, and iii) their innate resistance to CDDP in relation to parental cells. The results obtained from HNSCC cell lines (**Figure 19**) corroborate the previous data from biopsy-derived cell lines (**Figure 17**), suggesting an association between autophagy activation and chemoresistance.

Our results are consistent with a recent study conducted on the cell line HTB-43 where several autophagic markers (Beclin-1, Ulk1, ATG5, ATG7, and ATG14) were overexpressed in a model of CDDP-resistant cell line (HTB-43-R). The cell surface receptor and resistant marker CD44 (characteristic of HNSCC CSCs) was decreased in ATG14-deficient HTB-43 cells, which also supports a link between the CSCs phenotype and CDDP-resistance ³³⁴. Moreover, ATG5-mediated autophagy was also associated with 5-FU resistance in gastric cancer ³⁵⁸.

Regarding the expression of PTOV1, although most cancerous cells expressed PTOV1 at the cytoplasmic level (IHC study), a minor fraction of malignant cells showed nuclear PTOV1 (**Figure 25**). Confocal microscopy examination of the cell lines HTB-43 and HTB-43-R, as well as the biopsy-derived cell lines P7 and P33, support the notion that a shift in PTOV1 location -particularly from the nucleus to the cytoplasm- is associated with a resistance phenotype (**Figure 24 D-E**). Increased cytoplasmic PTOV1 might be related to its action promoting mRNA translation in aggressive cancer cells ^{314,359}, but also support its role inducing

Discussion

autophagy, as has been suggested in this thesis (**Figure 14 B**; **Figure 17 C**; **Figure 24**). This novel role for PTOV1 described here, as autophagy activator, could anticipate the early acquisition of resistant phenotypes. PTOV1 has also been linked to the acquisition of chemotherapy resistance (e.g., CDDP and docetaxel), SCs phenotype and poor clinical prognosis in non-small cell lung cancer ³⁶⁰ and prostate cancer ⁹⁰. However, to our knowledge, this is the first time that such associations and its possible role as autophagy activator have been described in HNSCC.

Previous studies from our group and others have suggested that autophagy inhibitors are particularly effective against resistant cancer cells, while autophagy induction contributes to resistance in different cancer cell models ^{229,361,362}. Currently, several clinical trials in different cancer types are underway (e.g., breast, pancreas, and liver cancers), specifically exploiting the use of autophagy inhibitors for cancer therapy. Twenty-two out of 85 clinical trials using HCQ in cancer are still actively recruiting patients (www.clinicaltrials.gov, consulted on August 23, 2020), however there are no studies involving HNSCC patients. To explore if HNSCC cancers could potentially benefit from autophagy inhibitors –specifically HCQ- we analyzed individual and combined treatments of HCQ in HNSCC cells and biopsy-derived cell lines. The treatments were: 1) only HCQ, and HCQ & CDDP, *versus* CDDP alone; 2) only HCQ, and HCQ & 5-FU, *versus* 5-FU alone. Considering the individual effect of HCQ on cell proliferation, CDDP-resistant cell lines were significantly more sensitive to HCQ when compared with corresponding parental cell lines (**Figure 26**). Note that even CCL-138-R (which neither autophagic markers nor PTOV1 were overexpressed compared to the parental cell line CCL-138, **Figure 19 B**) responded well to HCQ treatment. This could be due to their

high basal levels of autophagic activation in both CCL-138 and CCL-138-R. Subsequently, analyzing the combined use of HCQ & CDDP, and HCQ & 5-FU, we found that JHU029-R (only for HCQ & CDDP), HTB-43-R and SCC-25-R responded significantly better to the combined treatment of both drugs compared to the treatment with CDDP or 5-FU alone. However, CCL-138-R, despite responding well to the treatment with HCQ alone, does not respond adequately to HCQ & CDDP, or HCQ & 5-FU. In our opinion, this could be due to two main causes:

1) As we commented before, during the acquisition of CDDP and 5-FU-resistance this cell line was not capable of overactivating autophagy as a mechanism to acquire resistance, because CCL-138 already had very high basal levels of autophagic activation.

2) The cellular stress that CDDP and 5-FU cause in the cells, triggering even autophagy activation during standard treatments ^{213,363-366}, implies that higher doses of HCQ would be required to counteract such side effects.

The second hypothesis is evident for the four HNSCC cell lines analyzed here, since they all respond similarly or even better to the treatment with HCQ alone than to the combined treatments with CDDP and 5-FU (**Figure 27A**). Accordingly, it has been described that paclitaxel and hypoxia also trigger the autophagy activation ^{367,368}.

The biopsy-derived cell lines P47, P28, P33 and P46 were chosen based on their basal autophagic activation (mainly considering LC3II/LC3I ratio, and autophagy vesicles by TEM) and CDDP-resistance (**Figure 17**). Then, they were classified as dependent or independent of autophagy, and sensitive or resistant to CDDP. In this sense, P46 and P28, classified as autophagy-dependent patients, responded significantly better to the combined treatment of HCQ & CDDP, and HCQ & 5-FU,

Discussion

than P47 (autophagy-independent patient). On the other hand, P33, initially classified as a CDDP-resistant patient and autophagy independent (based on LC3II/LC3I ratio), also responded well to both combined treatments. This could be because P33, despite having a low LC3II/LC3I ratio, has high levels of ATG5 and p62, so perhaps P33 could have been classified as an autophagy-dependent patient (**Figure 17 B**). In consequence, independently of the level of CDDP-resistance in both HNSCC cell lines and biopsy-derived cell lines, those cells that display autophagy upregulation respond significantly better to HCQ, and HCQ & CDDP (and usually also for HCQ & 5-FU) than those autophagy-independent cells (**Figure 26, Figure 27**). Note that the four CDDP-resistant cell lines included here –previously exposed to CDDP for a long time– respond significantly better to the individual treatment with HCQ than the combined treatment with HCQ & CDDP; while the four biopsy-derived cell lines –not exposed to CDDP or 5-FU before– respond better to the combined treatment of HCQ & CDDP, and HCQ & 5-FU, than to HCQ alone.

Our results confirm the statement that autophagy activation play an important role as a survival mechanism used by HNSCC cells in response to chemotherapeutic drugs. Moreover, two possible therapeutic options for those HNSCC patients who do not respond to current treatments are suggested:

- 1) Treatment based on autophagy inhibitors (e.g., HCQ) for recurrent and/or metastatic patients who have become resistant to current treatments, probably because autophagy overactivation.
- 2) Combined treatment of HCQ & CDDP, and/or HCQ & 5-FU, for those patients who have not previously been treated with CDDP or 5-FU, but have high basal levels of autophagy.

In this regard, we suggest that the group of patients with supraglottic laryngeal tumors that overexpress LC3 protein and has bad prognosis (**Figure 14 G**) would be one of the most benefits from a HCQ combined treatment. In this regard, it has been described that some cancer cells can develop autophagy addiction, even in the absence of stress stimuli. For example, a subtype of breast cancer with STAT3-mediated autophagy dependence, responds well to pharmacological autophagy inhibition *in-vivo* ³⁶⁹. However, the same combination of one autophagy inhibitor with one anticancer drug can show a synergistic effect on autophagy-dependent tumor cells, and in turn, show an antagonistic effect on autophagy-independent tumor cells ^{369,370}. This reinforces the need to find reliable diagnostic methods capable of detecting autophagy-dependent cancers before making therapeutic decisions that include autophagy inhibitors.

In clinical treatments, the maximum tolerated dose for HCQ has been reported as 600 mg daily ^{371,372}. Considering an average person with 5 liters of blood, the theoretical concentration of HCQ sulfate in blood would be 120 µg/mL (275 µM, $MW_{\text{HCQ sulfate}} = 433.95 \text{ g/mol}$). Therefore, we can consider that our *in-vitro* functional assays were performed within an adequate physiologically range (0-300 µM). The chronic use of HCQ for the treatment of rheumatological disorders and CQ for the treatment of cancer show no adverse toxicity ³⁷⁰, suggesting that long-term treatments with lysosomal autophagy inhibitors are feasible. Most importantly, cancer cells are more autophagy-dependent than normal tissues ¹⁹⁰. However, we must consider that the uptake of CQ in tumor tissue is affected by the tumor's pH, which makes it difficult to block autophagy in more acidic tumors ³⁷³. Although most of the studies related to autophagy inhibition as a method of chemotherapy sensitization are involved with CQ or HCQ treatments, other

Discussion

promising and potent pharmacological inhibitors of lysosomal fusion have been described (**Figure 9**). For example, the use of Lys05, quinacrine, VATG-027, and VATG-032 have shown promising results both in *in-vitro* and in preclinical models in various cancer types ²²³⁻²²⁷. On the other hand, a large number of studies that have focused on the genetic inhibition of key intermediaries of the autophagic process (e.g., beclin1, ATG3, ATG4, ATG5, and/or ATG12), have also improved the response to current treatments ^{218,219}. However, autophagosomes are known to function as scaffolds during the induction of apoptosis and necroptosis under certain physiological conditions ^{374,375}. Therefore, downstream inhibition of the autophagic flow is generally preferred for clinical purposes ¹⁹⁰.

Moreover, we proposed to find target proteins that could be involved in the acquisition of resistance to current chemotherapeutic treatments. Then, we performed a comparative proteomic study where the HNSCC cell lines CCL-138 (parental), CCL-138-R (resistant to CDDP), and CCL-138 CSCs G3 were included. From this study, we were capable to identify TSPAN1, a protein member of the tetraspanin family that was overexpressed in CCL-138-R and CCL-138 CSCs, in comparison to the parental cell line CCL-138. TSPAN1 has been described as a typical cell surface receptor that, like other tetraspanin family members, could be involved in the activation of various signaling cascades through interactions with other tetraspanins, integrins, receptors and cytoplasmic proteins (associations known as tetraspanin web).

WB validation demonstrated TSPAN1 overexpression in the three CDDP-resistant cell lines CCL-138-R, JHU029-R, and HTB-43- R, as well as in HTB-43 CSCs G2 and G3. Regardless of the endogenous level of TSPAN1 expression in different HNSCC cell lines (CCL-138, JHU029, HTB-43 or SCC-25), its inhibition by siRNAs –

evidenced at RNA and protein level (except for CCL-138-R that just was evidenced at RNA level)-, consistently caused a decrease in proliferation and colony formation capacity, as well as apoptosis induction. Moreover, the apoptosis induction was concomitantly accompanied by a decrease in autophagy (**Figure 28, Figure 29, Figure 33, and Figure 34**). Accordingly, similar results in which TSPAN1 inhibition has been linked to decreased cell proliferation and apoptosis induction have previously been reported for various cancer types. The upregulation of caspases 3 and 8, and Bcl-2 downregulation, have been suggested as the common molecular mechanism responsible for the apoptosis activation observed under TSPAN1 inhibition in these studies ^{292,295-297}. Mechanistically, the downregulation of Bcl-2 would suggest the activation of beclin1-mediated autophagy, which is contrary to the effect found by us in our HNSCC models. However, the activation of BAX-mediated apoptosis in the absence of Bcl-2 seems to prevail in this context ³⁷⁶, since there are currently no other studies involving TSPAN1 with autophagy. These results support our previous findings indicating that autophagy activation is a feature associated with chemoresistant phenotypes in HNSCC cells and tumors ³¹⁹.

Importantly, TSPAN1 depletion was found to sensitize parental and resistant cells to the action of different therapeutic drugs (e.g., CDDP and dasatinib) (**Figure 30, Figure 31, Figure 32**), and this sensitization was more pronounced in biopsy-derived cell lines from larynx and pharynx in comparison to established HNSCC cell lines. Although studies involving some tetraspanin family members (e.g. CD9, CD81, TSPAN8, CD51) with the acquisition of CSCs characteristics and/or resistance to current therapy have emerged in the last decade for various cancer

Discussion

models^{276,277,287-289}, to our knowledge, this is the first time that it is suggested that TSPAN1 could be involved in chemotherapy resistance.

Upon TSPAN1 depletion, a decrease in SRC activation (p-SRC) occurred as a common feature in all different HNSCC cell lines tested, which was usually accompanied by a decrease in p-AKT and p-ERK1/2 levels (**Figure 34 A**). TSPAN1 depletion decreased p-ERK1/2 in both CCL-138 and JHU029 parental and CDDP-resistant cells, and in HTB-43-R; while p-AKT levels only diminished in CCL-138, JHU029-R and HTB-43-R cells. Moreover, vimentin was reduced in both JHU029 and JHU029-R cells upon TSPAN1 depletion, suggestive of a link between TSPAN1 and the EMT process. However, vimentin reduction was not accompanied by an induction of E-Cadherin or a decrease in N-Cadherin expression (data not shown). Therefore, our results suggest that SRC signaling is an important effect of TSPAN1 in these HNSCC models, with p-SRC emerging as a central node. However, the effects of TSPAN1 depletion extend beyond the exclusive regulation of SRC activation to also effectively target p-AKT and p-ERK1/2 levels, and the autophagy pathway. In marked contrast, the action of a SRC inhibitor (dasatinib) in JHU029-R and CCL-138 cells was restricted to decrease p-SRC and p-ERK1/2 levels but did not affect p-AKT levels nor autophagy-related genes (**Figure 35 B**).

Due to its various interactions and locations, TSPAN1 could activate additional effectors, apart from p-SRC, to contribute to the carcinogenesis process, facilitating the acquisition of therapy resistance. Wang *et al.* described that TSPAN1-integrin $\alpha 6 \beta 1$ interaction caused PI3K/AKT/GSK-3 β /SNAIL pathway amplification, which induced EMT and metastasis, and predicted poor prognosis in cholangiocarcinoma patients³⁰³. The activation of the PI3K/AKT/mTOR pathway is key for the induction of the biosynthetic metabolism (dependent on oxidative

phosphorylation) in CSCs that go into the proliferative state ¹⁶⁸, in agreement with our results (**Figure 35 A**). In this sense, Moon *et al.* have recently described that the activation of integrins $\beta 1$ has a significant role in stemness regulation, chemoresistance, and *in-vivo* tumor-forming capacity in HNSCC ³⁷⁷.

TSPAN1-integrin $\alpha 6\beta 1$ interaction has been described previously in HNSCC, where it was also associated with cell migration and invasion mediated by FAK/STAT1 α pathway activation, and MMP2 and MMP26 overexpression ³¹². These statements are especially relevant considering that a recent report in breast cancer showed that integrin $\alpha 5\beta 3$ and Fak/PI3K/AKT signaling pathway overactivation were responsible for CDDP-resistance and EMT *in-vivo* and *in-vitro*, as well as migration and proliferation in *in-vitro* assays ³⁷⁸. In addition, in response to high levels of oxidative stress (e.g., elevated levels of ROS caused by chemotherapy), SRC is activated, which can stimulate the RAS/RAF/ERK pathway and trigger autophagy ²⁰². Consequently, the inhibition of SRC activation through TSPAN1 inhibition could help to the effect of CDDP by decreasing the autophagy activation. On the other hand, if the interaction between TSPAN1 and survivin recently described in skin squamous cell carcinoma also occurs in our HNSCC model, this could induce apoptosis evasion ²⁹⁷. In addition, survivin interacts with Beclin 1 and LC3, resulting in inhibition of autophagy-mediated apoptosis ³⁷⁹⁻³⁸¹.

It will be of great interest to investigate in the future, which are the ligands that interact with TSPAN1 in our HNSCC models, as well as the association between each of them with the acquisition of chemoresistance and SCR activation. However, based on the currently available information about the interactions described for TSPAN1 in relation to cancer promotion, and the results presented in this thesis,

Discussion

we have proposed the following mechanism for the acquisition of TSPAN1-mediated chemoresistance (**Figure 43**).

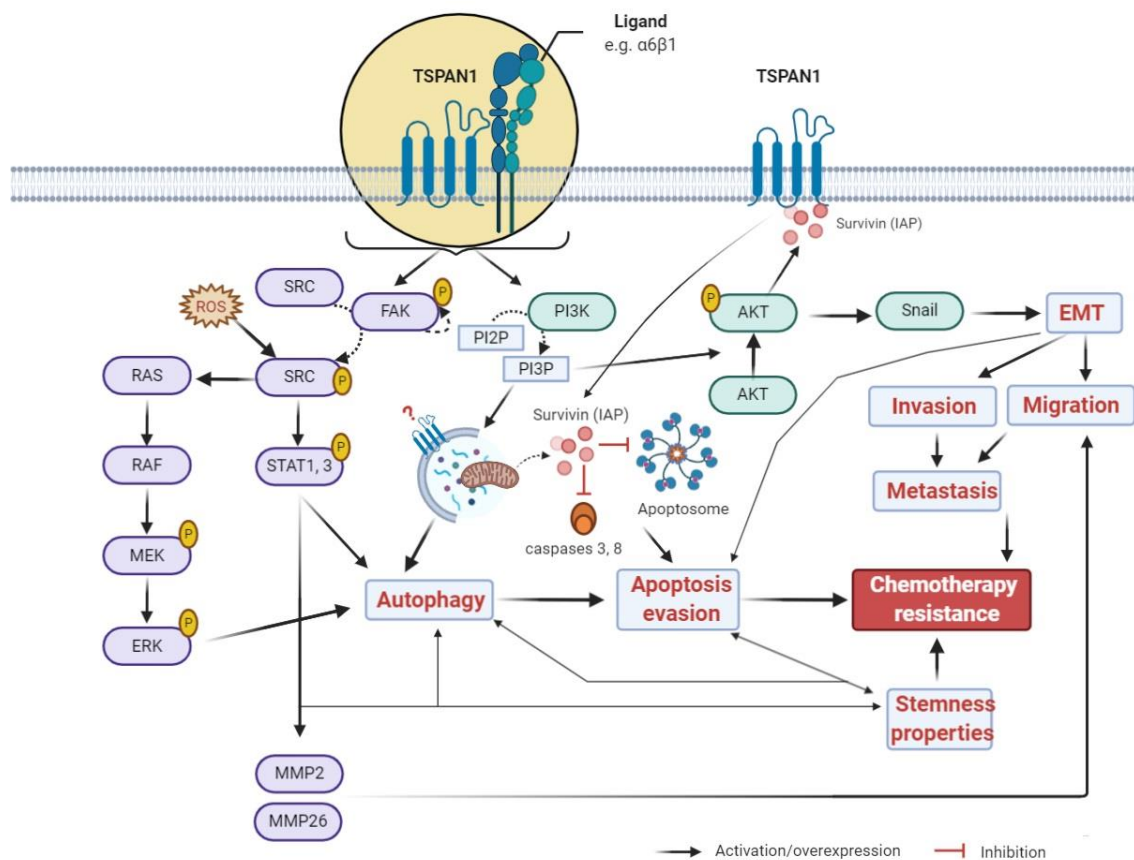


Figure 43. Proposed mechanism for the acquisition of TSPAN1-mediated chemoresistance in HNSCC. TSPAN1 could interact with multiple ligands, including integrins (e.g., $\alpha6\beta1$). TSPAN1- $\alpha6\beta1$ interaction induces the recruitment of FAK and PI3K. FAK activation causes phosphorylation-mediated SRC activation, which ultimately induces autophagy and promotes cell migration and invasion through the activation of ERK and STAT1/3. On the other hand, PI3K recruitment catalyzes PI3P formation, which is important in EMT induction (through AKT/SNAIL pathway) and promotes autophagy. TSPAN1 may also interact with survivin, a small protein capable of inhibiting apoptosis. All these pathways converge in the induction of chemotherapy resistance. Figure created with BioRender.com

Interestingly, the biological effects of TSPAN1 depletion observed *in-vitro* were also corroborated *in-vivo* (**Figure 36**, **Figure 37**). In the xenografted mice, we found that tumors formed from TSPAN1 depleted cells were smaller than their respective control tumors (in both, JHU029 and JHU029-R). Moreover, we found that tumors formed from the CDDP- resistant cells JHU029-R were smaller in size but developed more metastasis than those formed from the parental cells JHU029

(data not shown). Accordingly, all resistant HNSCC cell lines showed reduced proliferate capacity in culture than the corresponding parental cells (**Figure 28 E**). This can be explained because resistant cells have a higher proportion of CSCs and autophagy upregulation, as previously reported by us ³¹⁹. This supports the notion that resistant tumors –that presumably are enriched in number and features of CSCs and autophagy activation- are not necessarily bigger in size or more proliferative (instead they are more aggressive), a characteristic frequently observed in the clinic ³⁸². Specifically, CSCs subpopulations are quite quiescent. Moreover, dynamic changes and complex interactions in the tumor microenvironment play a relevant role during tumor progression and metastasis, as an adaptive response to enhance CSCs survival ³⁸³. In this line of evidence, tumors formed from the slowly growing resistant cells JHU029-R showed a fusocellular pattern compared to tumors formed from the parental cells JHU029. Such pattern is associated with EMT features, which is typically predominant in aggressive and resistant tumor phenotypes ³⁸⁴. Moreover, in tumors formed by JHU029-R, TSPAN1 depletion was capable to revert the fusocellular pattern to an epithelial morphology and decreased the capacity of tumors to metastasize (**Figure 36 G, Figure 38**). These results confirm the oncogenic role of TSPAN1 *in vivo* in our laryngeal cancer model and suggest a putative role of TSPAN1 in EMT, supporting the observations described by Wang *et al.* in a cholangiocarcinoma model ³⁰³ (**Figure 43**).

Importantly, the IHC and WB analyses of TSPAN1 in patient biopsies, further confirm the potential oncogenic role of TSPAN1 in HNSCC pathogenesis. TSPAN1 overexpression by WB was detected in 67% of tumor samples compared to the normal counterparts. Besides, TSPAN1 expression by IHC was detected in

Discussion

approximately 45% of laryngeal and pharyngeal tumors, a percentage similar to the upregulation of TSPAN1 at mRNA level (50% of the patients) (**Figure 39**, **Figure 41 A**). TSPAN1 protein showed predominantly a cytoplasmic and nuclear pattern in tumor cells, whereas TSPAN1 expression was negligible in stromal cells and adjacent normal epithelia. Although the cytoplasmic expression of TSPAN1 has been reported, we have not found previous reports describing its nuclear expression^{298,303,385}.

IHC analyses on patient biopsies also corroborate the association between TSPAN1 and p-SRC previously observed in the HNSCC cell models. An inverse association of cytoplasmic and nuclear TSPAN1 with E-cadherin expression was also demonstrated, which reinforces our *in vitro* findings and suggests a possible link between TSPAN1 and EMT. In addition, TSPAN1 expression was more frequently detected in poorly differentiated tumors (with higher EMT features) than in those well-differentiated (57% versus 31%) (**Figure 39 D**, **Figure 40**). All together, these results strongly support the involvement of TSPAN1 in EMT promotion in HNSCC.

In agreement, TSPAN1 overexpression at RNA and/or protein level in different human cancers, including HNSCC, has also been widely documented^{292-298,302-306}. However, in our series of 16 patients, we found no significant difference between the expression of TSPAN1 in normal versus tumor tissues at the mRNA level, neither did we find any association with survival (**Figure 41 B-C**, **Figure 42**). Despite the clinical evidence that HNSCC HPV-positive patients tend to respond better to conventional therapies than HPV-negative patients, a subset of these patients who do not respond adequately has recently been described. Surprisingly, within an expression profile of six potential genetic biomarkers described for this

group of patients, the downregulation of TSPAN1 at the mRNA level was found ³⁸⁶. Although apparently these data contradict our hypothesis about the tumor promotion role of TSPAN1 in HNSCC, on the other hand, they show another possible link between TSPAN1 and therapy response in that subgroup of HPV-positive patients. Likewise, that could explain, at least in part, why 50% of our patient series presented lower expression levels of TSPAN1 mRNA in tumor tissue and why there was no association between TSPAN1 and survival. However, in HPV-associated cervical carcinomas, TSPAN1 is considered an important diagnostic and prognostic marker. A strong expression of TSPAN1 was found in a subset of high-grade cervical neoplasia and in most of the undifferentiated squamous cell cancers ³⁸⁷⁻³⁸⁹.

Hence, all these observations lead us to propose for the first time TSPAN1 as an oncogenic protein involved in HNSCC chemoresistance, with p-SRC emerging as a predominant downstream effector. Moreover, TSPAN1 expression is associated to the development of an EMT program as consistently observed in mice tumors and HNSCC patient biopsies. Our findings support the notion that SRC activation may contribute to metastatic dissemination in HNSCC ³¹⁷ and provide additional evidence extending the association of SRC activation with EMT to other HNSCC subtypes, apart from nasopharyngeal cancers (e.g., laryngeal and tongue carcinomas) ³⁹⁰.

Based on the data presented here, we propose that TSPAN1 inhibition could represent a promising candidate to improve the therapy against laryngeal and pharyngeal cancer, and possibly other HNSCC. The fact that inhibition of TSPAN1 was able to sensitize resistant cells to different chemotherapeutic agents has an important added value to be considered as a potential target for cancer therapy.

CONCLUSIONS

VII. CONCLUSIONS

Based on the results obtained in this thesis, we have reached the following conclusions:

1. Cytoplasmic p62 and PTOV1 expression could be considered prognosis markers for the most aggressive laryngeal tumors.
2. LC3 expression could be a poor prognostic marker for supraglottic laryngeal tumors.
3. The establishment of laryngeal and pharyngeal biopsy-derived cell lines is feasible and could be useful to predict the clinical response of patients to current treatments.
4. Autophagy activation occurs during chemotherapy resistance and CSCs phenotype acquisition in non-metastatic HNSCC cell lines.
5. PTOV1 is related to chemoresistance and CSCs phenotype in HNSCC, possibly mediating autophagy activation.
6. Treatment with HCQ (alone or in combination with CDDP or 5-FU) could be an efficient therapeutic option for HNSCC patients, including recurrent or metastatic patients.
7. TSPAN1 emerges for the first time as a potential target involved in HNSCC chemoresistance.
8. TSPAN1 depletion decreases cell proliferation, induces apoptosis, and sensitizes HNSCC cell lines and biopsy-derived cell lines to chemotherapeutic agents.
9. TSPAN1 depletion reduces pSRC and autophagy activation.
10. TSPAN1 expression is associated to EMT activation in mice tumors and HNSCC patient biopsies.

Conclusions

11. TSPAN1 inhibition could be a good strategy to improve the current treatment against laryngeal and pharyngeal cancers, and possibly other types of HNSCC tumors.

REFERENCES

VIII. REFERENCES

1. Bray, F., *et al.* Global cancer statistics 2018: GLOBOCAN estimates of incidence and mortality worldwide for 36 cancers in 185 countries. *CA Cancer J Clin* **68**, 394-424 (2018).
2. Chen, D., *et al.* Targeting BMI1(+) Cancer Stem Cells Overcomes Chemoresistance and Inhibits Metastases in Squamous Cell Carcinoma. *Cell stem cell* **20**, 621-634 e626 (2017).
3. Peitzsch, C., Nathansen, J., Schniewind, S.I., Schwarz, F. & Dubrovskaya, A. Cancer Stem Cells in Head and Neck Squamous Cell Carcinoma: Identification, Characterization and Clinical Implications. *Cancers* **11**(2019).
4. Ferlay, J., *et al.* Cancer incidence and mortality worldwide: sources, methods and major patterns in GLOBOCAN 2012. *International journal of cancer* **136**, E359-386 (2015).
5. Devaraja, K. Current Prospects of Molecular Therapeutics in Head and Neck Squamous Cell Carcinoma. *Pharmaceutical medicine* **33**, 269-289 (2019).
6. Marur, S. & Forastiere, A.A. Head and Neck Squamous Cell Carcinoma: Update on Epidemiology, Diagnosis, and Treatment. *Mayo Clinic proceedings* **91**, 386-396 (2016).
7. Ang, K.K., *et al.* Human papillomavirus and survival of patients with oropharyngeal cancer. *The New England journal of medicine* **363**, 24-35 (2010).
8. Gunduz, M., Gunduz, E., Tamagawa, S., Enomoto, K. & Hotomi, M. Identification and chemoresistance of cancer stem cells in HPV-negative oropharyngeal cancer. *Oncology letters* **19**, 965-971 (2020).
9. Biktasova, A., *et al.* Demethylation Therapy as a Targeted Treatment for Human Papillomavirus-Associated Head and Neck Cancer. *Clin Cancer Res* **23**, 7276-7287 (2017).
10. Cancer Genome Atlas, N. Comprehensive genomic characterization of head and neck squamous cell carcinomas. *Nature* **517**, 576-582 (2015).
11. Steuer, C.E., El-Deiry, M., Parks, J.R., Higgins, K.A. & Saba, N.F. An update on larynx cancer. *CA Cancer J Clin* **67**, 31-50 (2017).
12. Forastiere, A.A., *et al.* Concurrent chemotherapy and radiotherapy for organ preservation in advanced laryngeal cancer. *The New England journal of medicine* **349**, 2091-2098 (2003).
13. Cohen, E.E.W., *et al.* The Society for Immunotherapy of Cancer consensus statement on immunotherapy for the treatment of squamous cell carcinoma of the head and neck (HNSCC). *J Immunother Cancer* **7**, 184 (2019).
14. Holohan, C., Van Schaeybroeck, S., Longley, D.B. & Johnston, P.G. Cancer drug resistance: an evolving paradigm. *Nat Rev Cancer* **13**, 714-726 (2013).
15. Govindan, S.V., *et al.* Establishment and characterization of triple drug resistant head and neck squamous cell carcinoma cell lines. *Molecular medicine reports* **12**, 3025-3032 (2015).
16. Salama, J.K., Seiwert, T.Y. & Vokes, E.E. Chemoradiotherapy for locally advanced head and neck cancer. *Journal of clinical oncology : official journal of the American Society of Clinical Oncology* **25**, 4118-4126 (2007).

References

17. Chinn, S.B. & Myers, J.N. Oral Cavity Carcinoma: Current Management, Controversies, and Future Directions. *Journal of clinical oncology : official journal of the American Society of Clinical Oncology* **33**, 3269-3276 (2015).
18. Hollebecque, A., *et al.* Phase I study of temsirolimus in combination with cetuximab in patients with advanced solid tumours. *European journal of cancer* **81**, 81-89 (2017).
19. Hedberg, M.L., *et al.* Genetic landscape of metastatic and recurrent head and neck squamous cell carcinoma. *The Journal of clinical investigation* **126**, 169-180 (2016).
20. Razzaghi, H., *et al.* Five-year relative survival for human papillomavirus-associated cancer sites. *Cancer* **124**, 203-211 (2018).
21. Taghavi, N. & Yazdi, I. Prognostic factors of survival rate in oral squamous cell carcinoma: clinical, histologic, genetic and molecular concepts. *Archives of Iranian medicine* **18**, 314-319 (2015).
22. Curry, J.M., *et al.* Tumor microenvironment in head and neck squamous cell carcinoma. *Seminars in oncology* **41**, 217-234 (2014).
23. Coca-Pelaz, A., *et al.* Head and Neck Cancer: A Review of the Impact of Treatment Delay on Outcome. *Advances in therapy* **35**, 153-160 (2018).
24. Marur, S. & Forastiere, A.A. Head and neck cancer: changing epidemiology, diagnosis, and treatment. *Mayo Clinic proceedings* **83**, 489-501 (2008).
25. Keck, M.K., *et al.* Integrative analysis of head and neck cancer identifies two biologically distinct HPV and three non-HPV subtypes. *Clin Cancer Res* **21**, 870-881 (2015).
26. Walter, V., *et al.* Molecular subtypes in head and neck cancer exhibit distinct patterns of chromosomal gain and loss of canonical cancer genes. *PLoS One* **8**, e56823 (2013).
27. Seiwert, T.Y., *et al.* Integrative and comparative genomic analysis of HPV-positive and HPV-negative head and neck squamous cell carcinomas. *Clin Cancer Res* **21**, 632-641 (2015).
28. Zhou, G., Liu, Z. & Myers, J.N. TP53 Mutations in Head and Neck Squamous Cell Carcinoma and Their Impact on Disease Progression and Treatment Response. *J Cell Biochem* **117**, 2682-2692 (2016).
29. Perrone, F., *et al.* TP53 mutations and pathologic complete response to neoadjuvant cisplatin and fluorouracil chemotherapy in resected oral cavity squamous cell carcinoma. *Journal of clinical oncology : official journal of the American Society of Clinical Oncology* **28**, 761-766 (2010).
30. Pan, J.J., *et al.* Effect of recombinant adenovirus-p53 combined with radiotherapy on long-term prognosis of advanced nasopharyngeal carcinoma. *Journal of clinical oncology : official journal of the American Society of Clinical Oncology* **27**, 799-804 (2009).
31. Liu, S., *et al.* Randomized, controlled phase II study of post-surgery radiotherapy combined with recombinant adenoviral human p53 gene therapy in treatment of oral cancer. *Cancer Gene Ther* **20**, 375-378 (2013).
32. Medema, J.P. Cancer stem cells: the challenges ahead. *Nat Cell Biol* **15**, 338-344 (2013).
33. Friedmann-Morvinski, D. & Verma, I.M. Dedifferentiation and reprogramming: origins of cancer stem cells. *EMBO Rep* **15**, 244-253 (2014).

34. Eun, K., Ham, S.W. & Kim, H. Cancer stem cell heterogeneity: origin and new perspectives on CSC targeting. *BMB reports* **50**, 117-125 (2017).
35. Meacham, C.E. & Morrison, S.J. Tumour heterogeneity and cancer cell plasticity. *Nature* **501**, 328 (2013).
36. Lan, X., *et al.* Fate mapping of human glioblastoma reveals an invariant stem cell hierarchy. *Nature* **549**, 227-232 (2017).
37. Pascual, G., *et al.* Targeting metastasis-initiating cells through the fatty acid receptor CD36. *Nature* **541**, 41-45 (2017).
38. Capaccione, K.M. & Pine, S.R. The Notch signaling pathway as a mediator of tumor survival. *Carcinogenesis* **34**, 1420-1430 (2013).
39. Hassan, K.A., *et al.* Notch pathway activity identifies cells with cancer stem cell-like properties and correlates with worse survival in lung adenocarcinoma. *Clin Cancer Res* **19**, 1972-1980 (2013).
40. Zhao, Z.L., *et al.* NOTCH1 inhibition enhances the efficacy of conventional chemotherapeutic agents by targeting head neck cancer stem cell. *Sci Rep* **6**, 24704 (2016).
41. Grobner, S.N., *et al.* The landscape of genomic alterations across childhood cancers. *Nature* **555**, 321-327 (2018).
42. Garcia-Mayea, Y., Mir, C., Masson, F., Paciucci, R. & ME, L.L. Insights into new mechanisms and models of cancer stem cell multidrug resistance. *Seminars in cancer biology* (2019).
43. Ding, L., *et al.* Clonal evolution in relapsed acute myeloid leukaemia revealed by whole-genome sequencing. *Nature* **481**, 506-510 (2012).
44. Jopling, C., Boue, S. & Belmonte, J.C.I. Dedifferentiation, transdifferentiation and reprogramming: three routes to regeneration. *Nature Reviews Molecular Cell Biology* **12**, 79 (2011).
45. Elster, J.D., McGuire, T.F., Lu, J. & Prochownik, E.V. Rapid In Vitro Derivation of Endothelium Directly From Human Cancer Cells. *PLOS ONE* **8**, e77675 (2013).
46. Lamouille, S., Xu, J. & Derynck, R. Molecular mechanisms of epithelial-mesenchymal transition. *Nature Reviews Molecular Cell Biology* **15**, 178 (2014).
47. Vlashi, E. & Pajonk, F. Cancer stem cells, cancer cell plasticity and radiation therapy. *Seminars in cancer biology* **31**, 28-35 (2015).
48. Thakur, B. & Ray, P. Cisplatin triggers cancer stem cell enrichment in platinum-resistant cells through NF-kappaB-TNFalpha-PIK3CA loop. *Journal of experimental & clinical cancer research : CR* **36**, 164 (2017).
49. Wang, L., *et al.* Cisplatin-enriching cancer stem cells confer multidrug resistance in non-small cell lung cancer via enhancing TRIB1/HDAC activity. *Cell Death Dis* **8**, e2746 (2017).
50. Ma, X., Wang, B., Wang, X., Luo, Y. & Fan, W. NANOGP8 is the key regulator of stemness, EMT, Wnt pathway, chemoresistance, and other malignant phenotypes in gastric cancer cells. *PLoS One* **13**, e0192436 (2018).
51. Das, S., Mukherjee, P., Chatterjee, R., Jamal, Z. & Chatterji, U. Enhancing chemosensitivity of breast cancer stem cells by down regulating SOX2 and ABCG2 using Wedelolactone-encapsulated nanoparticles. *Mol Cancer Ther* (2018).

References

52. Prieto-Vila, M., Takahashi, R.U., Usuba, W., Kohama, I. & Ochiya, T. Drug Resistance Driven by Cancer Stem Cells and Their Niche. *Int J Mol Sci* **18**(2017).
53. Schmidt, F. & Efferth, T. Tumor Heterogeneity, Single-Cell Sequencing, and Drug Resistance. *Pharmaceuticals* **9**(2016).
54. Naik, P.P., *et al.* Implications of cancer stem cells in developing therapeutic resistance in oral cancer. *Oral oncology* **62**, 122-135 (2016).
55. Bristow, R.G., *et al.* Resistance to DNA-damaging agents is discordant from experimental metastatic capacity in MEF ras-transformants-expressing gain of function MTP53. *Oncogene* **22**, 2960-2966 (2003).
56. Morelli, M.P., *et al.* Characterizing the patterns of clonal selection in circulating tumor DNA from patients with colorectal cancer refractory to anti-EGFR treatment. *Annals of oncology : official journal of the European Society for Medical Oncology* **26**, 731-736 (2015).
57. Hata, A.N., *et al.* Tumor cells can follow distinct evolutionary paths to become resistant to epidermal growth factor receptor inhibition. *Nat Med* **22**, 262-269 (2016).
58. Alonso-Alconada, L., *et al.* Molecular profiling of circulating tumor cells links plasticity to the metastatic process in endometrial cancer. *Mol Cancer* **13**, 223 (2014).
59. Lawson, D.A., *et al.* Single-cell analysis reveals a stem-cell program in human metastatic breast cancer cells. *Nature* **526**, 131-135 (2015).
60. Jolly, M.K., *et al.* Hybrid epithelial/mesenchymal phenotypes promote metastasis and therapy resistance across carcinomas. *Pharmacology & therapeutics* **194**, 161-184 (2019).
61. Hao, Y., Baker, D. & Ten Dijke, P. TGF-beta-Mediated Epithelial-Mesenchymal Transition and Cancer Metastasis. *Int J Mol Sci* **20**(2019).
62. Liu, L., *et al.* Chemotherapy Induces Breast Cancer Stemness in Association with Dysregulated Monocytosis. *Clin Cancer Res* **24**, 2370-2382 (2018).
63. Chen, X., Liao, R., Li, D. & Sun, J. Induced cancer stem cells generated by radiochemotherapy and their therapeutic implications. *Oncotarget* **8**, 17301-17312 (2017).
64. Jandial, R., Waters, D.J. & Chen, M.Y. Cancer stem cells can arise from differentiated neoplastic cells. *Neurosurgery* **69**, N22 (2011).
65. Lagadec, C., Vlashi, E., Della Donna, L., Dekmezian, C. & Pajonk, F. Radiation-induced reprogramming of breast cancer cells. *Stem cells* **30**, 833-844 (2012).
66. Saha, S., *et al.* Aspirin Suppresses the Acquisition of Chemoresistance in Breast Cancer by Disrupting an NFkappaB-IL6 Signaling Axis Responsible for the Generation of Cancer Stem Cells. *Cancer Res* **76**, 2000-2012 (2016).
67. Chen, J., *et al.* A restricted cell population propagates glioblastoma growth after chemotherapy. *Nature* **488**, 522-526 (2012).
68. Martins-Neves, S.R., *et al.* Chemotherapy induces stemness in osteosarcoma cells through activation of Wnt/beta-catenin signaling. *Cancer Lett* **370**, 286-295 (2016).
69. Sheng, I.Y., *et al.* Blood Myeloid-Derived Suppressor Cells Correlate with Neutrophil-to-Lymphocyte Ratio and Overall Survival in Metastatic Urothelial Carcinoma. *Targeted oncology* (2020).

70. Esquivel, N., Garcia, Y., Lores, B., Gutierrez, M. & Rodriguez, C. Characterization of aged male BALB/cenp mice as a model of dementia. *Laboratory animal research* **36**, 7 (2020).
71. Albers, A.E., *et al.* Stem cells in squamous head and neck cancer. *Critical reviews in oncology/hematology* **81**, 224-240 (2012).
72. Saygin, C., *et al.* CD55 regulates self-renewal and cisplatin resistance in endometrioid tumors. *J Exp Med* **214**, 2715-2732 (2017).
73. Kozovska, Z., *et al.* ALDH1A inhibition sensitizes colon cancer cells to chemotherapy. *BMC cancer* **18**, 656 (2018).
74. Rodrigues, M., *et al.* Prognostic implications of CD44, NANOG, OCT4, and BMI1 expression in tongue squamous cell carcinoma. *Head & neck* **40**, 1759-1773 (2018).
75. Fukusumi, T., *et al.* CD10 as a novel marker of therapeutic resistance and cancer stem cells in head and neck squamous cell carcinoma. *British Journal of Cancer* **111**, 506-514 (2014).
76. Ma, J., *et al.* FaDu cell characteristics induced by multidrug resistance. *Oncol Rep* **26**, 1189-1195 (2011).
77. Chen, D., *et al.* FOX-A1 contributes to acquisition of chemoresistance in human lung adenocarcinoma via transactivation of SOX5. *EBioMedicine* **44**, 150-161 (2019).
78. Ayers, D., Mestdagh, P., Van Maerken, T. & Vandesompele, J. Identification of miRNAs contributing to neuroblastoma chemoresistance. *Computational and structural biotechnology journal* **13**, 307-319 (2015).
79. Chen, J., *et al.* Characteristics of doxorubicin-selected multidrug-resistant human leukemia HL-60 cells with tolerance to arsenic trioxide and contribution of leukemia stem cells. *Oncology letters* **15**, 1255-1262 (2018).
80. Luzhna, L., Lykkesfeldt, A.E. & Kovalchuk, O. Altered radiation responses of breast cancer cells resistant to hormonal therapy. *Oncotarget* **6**, 1678-1694 (2015).
81. Tian, L., *et al.* Overexpression of miR-26b decreases the cisplatin-resistance in laryngeal cancer by targeting ATF2. *Oncotarget* **8**, 79023-79033 (2017).
82. Yuan, Z., *et al.* Long non-coding RNA AFAP1-AS1/miR-320a/RBPJ axis regulates laryngeal carcinoma cell stemness and chemoresistance. *J Cell Mol Med* **22**, 4253-4262 (2018).
83. Easwaran, H., Tsai, H.C. & Baylin, S.B. Cancer epigenetics: tumor heterogeneity, plasticity of stem-like states, and drug resistance. *Molecular cell* **54**, 716-727 (2014).
84. Obenauf, A.C., *et al.* Therapy-induced tumour secretomes promote resistance and tumour progression. *Nature* **520**, 368-372 (2015).
85. Ohashi, R., *et al.* Expression of MRP1 and ABCG2 is associated with adverse clinical outcomes of papillary thyroid carcinoma with a solid component. *Hum Pathol* **67**, 11-17 (2017).
86. Hou, Y., *et al.* The FOXM1-ABCC5 axis contributes to paclitaxel resistance in nasopharyngeal carcinoma cells. *Cell Death Dis* **8**, e2659 (2017).
87. Wu, Z.X., *et al.* Tepotinib reverses ABCB1-mediated multidrug resistance in cancer cells. *Biochemical pharmacology* (2019).

References

88. Sasaki, N., *et al.* Stemness and anti-cancer drug resistance in ATP-binding cassette subfamily G member 2 highly expressed pancreatic cancer is induced in 3D culture conditions. *Cancer Sci* **109**, 1135-1146 (2018).
89. Wang, N., *et al.* Dietary compound isoliquiritigenin targets GRP78 to chemosensitize breast cancer stem cells via beta-catenin/ABCG2 signaling. *Carcinogenesis* **35**, 2544-2554 (2014).
90. Canovas, V., *et al.* Prostate Tumor Overexpressed-1 (PTOV1) promotes docetaxel-resistance and survival of castration resistant prostate cancer cells. *Oncotarget* **8**, 59165-59180 (2017).
91. Wilson, B.J., *et al.* ABCB5 maintains melanoma-initiating cells through a proinflammatory cytokine signaling circuit. *Cancer Res* **74**, 4196-4207 (2014).
92. Vermeulen, L., *et al.* Wnt activity defines colon cancer stem cells and is regulated by the microenvironment. *Nat Cell Biol* **12**, 468-476 (2010).
93. Ghajar, C.M., *et al.* The perivascular niche regulates breast tumour dormancy. *Nat Cell Biol* **15**, 807-817 (2013).
94. Shore, N.D., *et al.* CD8(+) T Cells Impact Rising PSA in Biochemically Relapsed Cancer Patients Using Immunotherapy Targeting Tumor-Associated Antigens. *Molecular therapy : the journal of the American Society of Gene Therapy* (2020).
95. Boulding, T., *et al.* LSD1 activation promotes inducible EMT programs and modulates the tumour microenvironment in breast cancer. *Sci Rep* **8**, 73 (2018).
96. Sahu, S.K., *et al.* FBXO32 promotes microenvironment underlying epithelial-mesenchymal transition via CtBP1 during tumour metastasis and brain development. *Nature communications* **8**, 1523 (2017).
97. Chen, L., *et al.* TRAF6 regulates tumour metastasis through EMT and CSC phenotypes in head and neck squamous cell carcinoma. *J Cell Mol Med* **22**, 1337-1349 (2018).
98. Giuntoli, S., *et al.* Hypoxia suppresses BCR/Abl and selects imatinib-insensitive progenitors within clonal CML populations. *Leukemia* **20**, 1291-1293 (2006).
99. Francipane, M.G., *et al.* Crucial role of interleukin-4 in the survival of colon cancer stem cells. *Cancer Res* **68**, 4022-4025 (2008).
100. Nakano, M., *et al.* Dedifferentiation process driven by TGF-beta signaling enhances stem cell properties in human colorectal cancer. *Oncogene* (2018).
101. Shimizu, M. & Tanaka, N. IL-8-induced O-GlcNAc modification via GLUT3 and GFAT regulates cancer stem cell-like properties in colon and lung cancer cells. *Oncogene* (2018).
102. Luo, Y., *et al.* Non-CSCs nourish CSCs through interleukin-17E-mediated activation of NF-kappaB and JAK/STAT3 signaling in human hepatocellular carcinoma. *Cancer Lett* **375**, 390-399 (2016).
103. Abubaker, K., *et al.* Inhibition of the JAK2/STAT3 pathway in ovarian cancer results in the loss of cancer stem cell-like characteristics and a reduced tumor burden. *BMC cancer* **14**, 317 (2014).
104. Lu, T., *et al.* The Hippo/YAP1 pathway interacts with FGFR1 signaling to maintain stemness in lung cancer. *Cancer Lett* **423**, 36-46 (2018).
105. Cordenonsi, M., *et al.* The Hippo transducer TAZ confers cancer stem cell-related traits on breast cancer cells. *Cell* **147**, 759-772 (2011).

106. Basu-Roy, U., *et al.* Sox2 antagonizes the Hippo pathway to maintain stemness in cancer cells. *Nature communications* **6**, 6411 (2015).
107. Escoll, M., Gargini, R., Cuadrado, A., Anton, I.M. & Wandosell, F. Mutant p53 oncogenic functions in cancer stem cells are regulated by WIP through YAP/TAZ. *Oncogene* **36**, 3515-3527 (2017).
108. Bartucci, M., *et al.* TAZ is required for metastatic activity and chemoresistance of breast cancer stem cells. *Oncogene* **34**, 681-690 (2015).
109. Serrano, I., McDonald, P.C., Lock, F., Muller, W.J. & Dedhar, S. Inactivation of the Hippo tumour suppressor pathway by integrin-linked kinase. *Nature communications* **4**, 2976 (2013).
110. Reiter, J.G., *et al.* Minimal functional driver gene heterogeneity among untreated metastases. *Science* **361**, 1033-1037 (2018).
111. Sharma, S.V., *et al.* A chromatin-mediated reversible drug-tolerant state in cancer cell subpopulations. *Cell* **141**, 69-80 (2010).
112. Oo, A.K.K., *et al.* Up-Regulation of PI 3-Kinases and the Activation of PI3K-Akt Signaling Pathway in Cancer Stem-Like Cells Through DNA Hypomethylation Mediated by the Cancer Microenvironment. *Transl Oncol* **11**, 653-663 (2018).
113. Fan, F., *et al.* Macrophage conditioned medium promotes colorectal cancer stem cell phenotype via the hedgehog signaling pathway. *PLoS One* **13**, e0190070 (2018).
114. Issa, M.E., *et al.* Epigenetic strategies to reverse drug resistance in heterogeneous multiple myeloma. *Clin Epigenetics* **9**, 17 (2017).
115. Pathania, R., *et al.* Combined Inhibition of DNMT and HDAC Blocks the Tumorigenicity of Cancer Stem-like Cells and Attenuates Mammary Tumor Growth. *Cancer Res* **76**, 3224-3235 (2016).
116. Giudice, F.S., Pinto, D.S., Jr., Nor, J.E., Squarize, C.H. & Castilho, R.M. Inhibition of histone deacetylase impacts cancer stem cells and induces epithelial-mesenchyme transition of head and neck cancer. *PLoS One* **8**, e58672 (2013).
117. Huang, M., *et al.* Targeting KDM1A attenuates Wnt/beta-catenin signaling pathway to eliminate sorafenib-resistant stem-like cells in hepatocellular carcinoma. *Cancer Lett* **398**, 12-21 (2017).
118. Zhu, Y., *et al.* Reduced miR-128 in breast tumor-initiating cells induces chemotherapeutic resistance via Bmi-1 and ABCC5. *Clin Cancer Res* **17**, 7105-7115 (2011).
119. Chen, B., *et al.* Upregulation of miR-199a/b contributes to cisplatin resistance via Wnt/beta-catenin-ABCG2 signaling pathway in ALDHA1(+) colorectal cancer stem cells. *Tumour Biol* **39**, 1010428317715155 (2017).
120. Fesler, A., *et al.* Autophagy regulated by miRNAs in colorectal cancer progression and resistance. *Cancer translational medicine* **3**, 96-100 (2017).
121. Chaudhary, A.K., Mondal, G., Kumar, V., Kattel, K. & Mahato, R.I. Chemosensitization and inhibition of pancreatic cancer stem cell proliferation by overexpression of microRNA-205. *Cancer Lett* **402**, 1-8 (2017).
122. Feliciano, A., *et al.* miR-99a reveals two novel oncogenic proteins E2F2 and EMR2 and represses stemness in lung cancer. *Cell Death Dis* **8**, e3141 (2017).

References

123. Gao, Y., *et al.* Linc-DYNC2H1-4 promotes EMT and CSC phenotypes by acting as a sponge of miR-145 in pancreatic cancer cells. *Cell Death Dis* **8**, e2924 (2017).
124. Pan, Y., *et al.* Long noncoding RNA ROR regulates chemoresistance in docetaxel-resistant lung adenocarcinoma cells via epithelial mesenchymal transition pathway. *Oncotarget* **8**, 33144-33158 (2017).
125. Prabhu, V.V., *et al.* Cancer stem cell-related gene expression as a potential biomarker of response for first-in-class imipridone ONC201 in solid tumors. *PLoS One* **12**, e0180541 (2017).
126. Walker, N.D., *et al.* Exosomes from differentially activated macrophages influence dormancy or resurgence of breast cancer cells within bone marrow stroma. *Cell Death Dis* **10**, 59 (2019).
127. Xu, J., Liao, K. & Zhou, W. Exosomes Regulate the Transformation of Cancer Cells in Cancer Stem Cell Homeostasis. *Stem cells international* **2018**, 4837370 (2018).
128. Meister, M. & Tikkanen, R. Endocytic trafficking of membrane-bound cargo: a flotillin point of view. *Membranes* **4**, 356-371 (2014).
129. Mashouri, L., *et al.* Exosomes: composition, biogenesis, and mechanisms in cancer metastasis and drug resistance. *Mol Cancer* **18**, 75 (2019).
130. Steinbichler, T.B., *et al.* Therapy resistance mediated by exosomes. *Mol Cancer* **18**, 58 (2019).
131. Kholia, S., *et al.* Extracellular vesicles as new players in angiogenesis. *Vascul Pharmacol* **86**, 64-70 (2016).
132. Boelens, M.C., *et al.* Exosome transfer from stromal to breast cancer cells regulates therapy resistance pathways. *Cell* **159**, 499-513 (2014).
133. Safaei, R., *et al.* Abnormal lysosomal trafficking and enhanced exosomal export of cisplatin in drug-resistant human ovarian carcinoma cells. *Mol Cancer Ther* **4**, 1595-1604 (2005).
134. Hardin, H., *et al.* Thyroid cancer stem-like cell exosomes: regulation of EMT via transfer of lncRNAs. *Lab Invest* **98**, 1133-1142 (2018).
135. Sun, Z.P., *et al.* MicroRNA expression profiling in exosomes derived from gastric cancer stem-like cells. *Oncotarget* **8**, 93839-93855 (2017).
136. Kaprio, T., Hagstrom, J., Andersson, L.C. & Haglund, C. Tetraspanin CD63 independently predicts poor prognosis in colorectal cancer. *Histol Histopathol*, 18209 (2020).
137. Tanaka, N., *et al.* Single-cell RNA-seq analysis reveals the platinum resistance gene COX7B and the surrogate marker CD63. *Cancer medicine* **7**, 6193-6204 (2018).
138. Aaberg-Jessen, C., *et al.* Co-expression of TIMP-1 and its cell surface binding partner CD63 in glioblastomas. *BMC cancer* **18**, 270 (2018).
139. Kumar, D., Gupta, D., Shankar, S. & Srivastava, R.K. Biomolecular characterization of exosomes released from cancer stem cells: Possible implications for biomarker and treatment of cancer. *Oncotarget* **6**, 3280-3291 (2015).
140. Skvortsov, S., Debbage, P., Lukas, P. & Skvortsova, I. Crosstalk between DNA repair and cancer stem cell (CSC) associated intracellular pathways. *Seminars in cancer biology* **31**, 36-42 (2015).

141. Carruthers, R.D., *et al.* Replication Stress Drives Constitutive Activation of the DNA Damage Response and Radioresistance in Glioblastoma Stem-like Cells. *Cancer Res* **78**, 5060-5071 (2018).
142. Min, W., *et al.* Poly(ADP-ribose) binding to Chk1 at stalled replication forks is required for S-phase checkpoint activation. *Nature communications* **4**, 2993 (2013).
143. Zhang, J., *et al.* Chk2 phosphorylation of BRCA1 regulates DNA double-strand break repair. *Mol Cell Biol* **24**, 708-718 (2004).
144. Manic, G., *et al.* Replication stress response in cancer stem cells as a target for chemotherapy. *Seminars in cancer biology* **53**, 31-41 (2018).
145. Wang, Y., *et al.* Temporal DNA-PK activation drives genomic instability and therapy resistance in glioma stem cells. *JCI Insight* **3**(2018).
146. Alsubhi, N., *et al.* Chk1 phosphorylated at serine345 is a predictor of early local recurrence and radio-resistance in breast cancer. *Mol Oncol* **10**, 213-223 (2016).
147. Facchino, S., Abdouh, M., Chato, W. & Bernier, G. BMI1 confers radioresistance to normal and cancerous neural stem cells through recruitment of the DNA damage response machinery. *J Neurosci* **30**, 10096-10111 (2010).
148. Venere, M., *et al.* Therapeutic targeting of constitutive PARP activation compromises stem cell phenotype and survival of glioblastoma-initiating cells. *Cell death and differentiation* **21**, 258-269 (2014).
149. Manic, G., *et al.* CHK1-targeted therapy to deplete DNA replication-stressed, p53-deficient, hyperdiploid colorectal cancer stem cells. *Gut* **67**, 903-917 (2018).
150. Gallmeier, E., *et al.* Inhibition of ataxia telangiectasia- and Rad3-related function abrogates the in vitro and in vivo tumorigenicity of human colon cancer cells through depletion of the CD133(+) tumor-initiating cell fraction. *Stem cells* **29**, 418-429 (2011).
151. Liu, Y., *et al.* RAD51 Mediates Resistance of Cancer Stem Cells to PARP Inhibition in Triple-Negative Breast Cancer. *Clin Cancer Res* **23**, 514-522 (2017).
152. Spriggs, K.A., Bushell, M. & Willis, A.E. Translational regulation of gene expression during conditions of cell stress. *Molecular cell* **40**, 228-237 (2010).
153. Wang, M. & Kaufman, R.J. The impact of the endoplasmic reticulum protein-folding environment on cancer development. *Nat Rev Cancer* **14**, 581-597 (2014).
154. Falletta, P., *et al.* Translation reprogramming is an evolutionarily conserved driver of phenotypic plasticity and therapeutic resistance in melanoma. *Genes Dev* **31**, 18-33 (2017).
155. Po, A., *et al.* Sonic Hedgehog Medulloblastoma Cancer Stem Cells Mirnome and Transcriptome Highlight Novel Functional Networks. *Int J Mol Sci* **19**(2018).
156. Fujimoto, A., *et al.* Inhibition of endoplasmic reticulum (ER) stress sensors sensitizes cancer stem-like cells to ER stress-mediated apoptosis. *Oncotarget* **7**, 51854-51864 (2016).

References

157. Matsumoto, T., *et al.* Doxycycline induces apoptosis via ER stress selectively to cells with a cancer stem cell-like properties: importance of stem cell plasticity. *Oncogenesis* **6**, 397 (2017).
158. Arumugam, P., Samson, A., Ki, J. & Song, J.M. Knockdown of clusterin alters mitochondrial dynamics, facilitates necrosis in camptothecin-induced cancer stem cells. *Cell Biol Toxicol* **33**, 307-321 (2017).
159. Li, C., *et al.* The three branches of the unfolded protein response exhibit differential significance in breast cancer growth and stemness. *Exp Cell Res* **367**, 170-185 (2018).
160. Warburg, O., Wind, F. & Negelein, E. The Metabolism of Tumors in the Body. *J Gen Physiol* **8**, 519-530 (1927).
161. Liberti, M.V. & Locasale, J.W. The Warburg Effect: How Does it Benefit Cancer Cells? *Trends in biochemical sciences* **41**, 211-218 (2016).
162. Shen, Y.A., Wang, C.Y., Hsieh, Y.T., Chen, Y.J. & Wei, Y.H. Metabolic reprogramming orchestrates cancer stem cell properties in nasopharyngeal carcinoma. *Cell Cycle* **14**, 86-98 (2015).
163. Peiris-Pages, M., Martinez-Outschoorn, U.E., Pestell, R.G., Sotgia, F. & Lisanti, M.P. Cancer stem cell metabolism. *Breast Cancer Res* **18**, 55 (2016).
164. Sancho, P., Barneda, D. & Heeschen, C. Hallmarks of cancer stem cell metabolism. *British Journal of Cancer* **114**, 1305-1312 (2016).
165. Gao, C., Shen, Y., Jin, F., Miao, Y. & Qiu, X. Cancer Stem Cells in Small Cell Lung Cancer Cell Line H446: Higher Dependency on Oxidative Phosphorylation and Mitochondrial Substrate-Level Phosphorylation than Non-Stem Cancer Cells. *PLoS One* **11**, e0154576 (2016).
166. Andreucci, E., *et al.* The carbonic anhydrase IX inhibitor SLC-0111 sensitises cancer cells to conventional chemotherapy. *Journal of enzyme inhibition and medicinal chemistry* **34**, 117-123 (2019).
167. Lee, K.M., *et al.* MYC and MCL1 Cooperatively Promote Chemotherapy-Resistant Breast Cancer Stem Cells via Regulation of Mitochondrial Oxidative Phosphorylation. *Cell Metab* **26**, 633-647 e637 (2017).
168. Chen, C.L., *et al.* NANOG Metabolically Reprograms Tumor-Initiating Stem-like Cells through Tumorigenic Changes in Oxidative Phosphorylation and Fatty Acid Metabolism. *Cell Metab* **23**, 206-219 (2016).
169. Mizuno, T., *et al.* Cancer stem-like cells of ovarian clear cell carcinoma are enriched in the ALDH-high population associated with an accelerated scavenging system in reactive oxygen species. *Gynecologic oncology* **137**, 299-305 (2015).
170. Chandimali, N., Jeong, D.K. & Kwon, T. Peroxiredoxin II Regulates Cancer Stem Cells and Stemness-Associated Properties of Cancers. *Cancers* **10**(2018).
171. Kim, D., Choi, B.H., Ryoo, I.G. & Kwak, M.K. High NRF2 level mediates cancer stem cell-like properties of aldehyde dehydrogenase (ALDH)-high ovarian cancer cells: inhibitory role of all-trans retinoic acid in ALDH/NRF2 signaling. *Cell Death Dis* **9**, 896 (2018).
172. Ryoo, I.G., Lee, S.H. & Kwak, M.K. Redox Modulating NRF2: A Potential Mediator of Cancer Stem Cell Resistance. *Oxid Med Cell Longev* **2016**, 2428153 (2016).

173. Kim, B., *et al.* PGC1alpha induced by reactive oxygen species contributes to chemoresistance of ovarian cancer cells. *Oncotarget* **8**, 60299-60311 (2017).
174. Schwickart, M., *et al.* Deubiquitinase USP9X stabilizes MCL1 and promotes tumour cell survival. *Nature* **463**, 103-107 (2010).
175. Liu, G., *et al.* Analysis of gene expression and chemoresistance of CD133+ cancer stem cells in glioblastoma. *Mol Cancer* **5**, 67 (2006).
176. Safa, A.R., Day, T.W. & Wu, C.H. Cellular FLICE-like inhibitory protein (c-FLIP): a novel target for cancer therapy. *Curr Cancer Drug Targets* **8**, 37-46 (2008).
177. Safa, A.R. Roles of c-FLIP in Apoptosis, Necroptosis, and Autophagy. *Journal of carcinogenesis & mutagenesis Suppl* **6**(2013).
178. Paoli, P., Giannoni, E. & Chiarugi, P. Anoikis molecular pathways and its role in cancer progression. *Biochim Biophys Acta* **1833**, 3481-3498 (2013).
179. Fofaria, N.M. & Srivastava, S.K. Critical role of STAT3 in melanoma metastasis through anoikis resistance. *Oncotarget* **5**, 7051-7064 (2014).
180. Frisch, S.M., Schaller, M. & Cieply, B. Mechanisms that link the oncogenic epithelial-mesenchymal transition to suppression of anoikis. *J Cell Sci* **126**, 21-29 (2013).
181. Kim, S.Y., *et al.* Cancer Stem Cells Protect Non-Stem Cells From Anoikis: Bystander Effects. *J Cell Biochem* **117**, 2289-2301 (2016).
182. Huang, Y.T., Lan, Q., Lorusso, G., Duffey, N. & Rugg, C. The matricellular protein CYR61 promotes breast cancer lung metastasis by facilitating tumor cell extravasation and suppressing anoikis. *Oncotarget* **8**, 9200-9215 (2017).
183. Klionsky, D.J. & Schulman, B.A. Dynamic regulation of macroautophagy by distinctive ubiquitin-like proteins. *Nature structural & molecular biology* **21**, 336-345 (2014).
184. Uttenweiler, A., Schwarz, H. & Mayer, A. Microautophagic vacuole invagination requires calmodulin in a Ca²⁺-independent function. *The Journal of biological chemistry* **280**, 33289-33297 (2005).
185. Massey, A.C., Zhang, C. & Cuervo, A.M. Chaperone-mediated autophagy in aging and disease. *Current topics in developmental biology* **73**, 205-235 (2006).
186. Klionsky, D.J. Autophagy: from phenomenology to molecular understanding in less than a decade. *Nature reviews. Molecular cell biology* **8**, 931-937 (2007).
187. du Toit, A., Hofmeyr, J.S., Gniadek, T.J. & Loos, B. Measuring autophagosome flux. *Autophagy* **14**, 1060-1071 (2018).
188. Lynch-Day, M.A. & Klionsky, D.J. The Cvt pathway as a model for selective autophagy. *FEBS letters* **584**, 1359-1366 (2010).
189. Dikic, I. & Elazar, Z. Mechanism and medical implications of mammalian autophagy. *Nature reviews. Molecular cell biology* **19**, 349-364 (2018).
190. Levy, J.M.M., Towers, C.G. & Thorburn, A. Targeting autophagy in cancer. *Nat Rev Cancer* **17**, 528-542 (2017).
191. White, E., Mehnert, J.M. & Chan, C.S. Autophagy, Metabolism, and Cancer. *Clin Cancer Res* **21**, 5037-5046 (2015).

References

192. Jung, C.H., Ro, S.H., Cao, J., Otto, N.M. & Kim, D.H. mTOR regulation of autophagy. *FEBS letters* **584**, 1287-1295 (2010).
193. Ravanan, P., Srikumar, I.F. & Talwar, P. Autophagy: The spotlight for cellular stress responses. *Life sciences* **188**, 53-67 (2017).
194. Alers, S., Löffler, A.S., Wesselborg, S. & Stork, B. Role of AMPK-mTOR-Ulk1/2 in the regulation of autophagy: cross talk, shortcuts, and feedbacks. *Mol Cell Biol* **32**, 2-11 (2012).
195. Meley, D., *et al.* AMP-activated protein kinase and the regulation of autophagic proteolysis. *The Journal of biological chemistry* **281**, 34870-34879 (2006).
196. Bellot, G., *et al.* Hypoxia-induced autophagy is mediated through hypoxia-inducible factor induction of BNIP3 and BNIP3L via their BH3 domains. *Mol Cell Biol* **29**, 2570-2581 (2009).
197. Nakatogawa, H., Suzuki, K., Kamada, Y. & Ohsumi, Y. Dynamics and diversity in autophagy mechanisms: lessons from yeast. *Nature reviews. Molecular cell biology* **10**, 458-467 (2009).
198. Mizushima, N., Yoshimori, T. & Ohsumi, Y. The role of Atg proteins in autophagosome formation. *Annual review of cell and developmental biology* **27**, 107-132 (2011).
199. Komatsu, M., *et al.* Impairment of starvation-induced and constitutive autophagy in Atg7-deficient mice. *J Cell Biol* **169**, 425-434 (2005).
200. Saha, S., Panigrahi, D.P., Patil, S. & Bhutia, S.K. Autophagy in health and disease: A comprehensive review. *Biomedicine & pharmacotherapy = Biomedecine & pharmacotherapie* **104**, 485-495 (2018).
201. Cuervo, A.M., *et al.* Autophagy and aging: the importance of maintaining "clean" cells. *Autophagy* **1**, 131-140 (2005).
202. Lorente, J., *et al.* The interplay between autophagy and tumorigenesis: exploiting autophagy as a means of anticancer therapy. *Biol Rev Camb Philos Soc* **93**, 152-165 (2018).
203. Lumkwana, D., du Toit, A., Kinnear, C. & Loos, B. Autophagic flux control in neurodegeneration: Progress and precision targeting-Where do we stand? *Progress in neurobiology* **153**, 64-85 (2017).
204. Tooze, S.A. & Yoshimori, T. The origin of the autophagosomal membrane. *Nat Cell Biol* **12**, 831-835 (2010).
205. Liu, J.L., *et al.* Prognostic significance of p62/SQSTM1 subcellular localization and LC3B in oral squamous cell carcinoma. *British Journal of Cancer* **111**, 944-954 (2014).
206. Tang, J.Y., *et al.* High LC3 expression correlates with poor survival in patients with oral squamous cell carcinoma. *Hum Pathol* **44**, 2558-2562 (2013).
207. Lin, C.W., *et al.* Autophagy-related gene LC3 expression in tumor and liver microenvironments significantly predicts recurrence of hepatocellular carcinoma after surgical resection. *Clinical and translational gastroenterology* **9**, 166 (2018).
208. Cordani, M., Butera, G., Pacchiana, R. & Donadelli, M. Molecular interplay between mutant p53 proteins and autophagy in cancer cells. *Biochimica et biophysica acta. Reviews on cancer* **1867**, 19-28 (2017).
209. Lu, R., *et al.* Inhibition of CD133 Overcomes Cisplatin Resistance Through Inhibiting PI3K/AKT/mTOR Signaling Pathway and Autophagy in CD133-

- Positive Gastric Cancer Cells. *Technology in cancer research & treatment* **18**, 1533033819864311 (2019).
210. Zhu, Z., *et al.* Lovastatin Enhances Cytotoxicity of Temozolomide via Impairing Autophagic Flux in Glioblastoma Cells. *BioMed research international* **2019**, 2710693 (2019).
211. Aga, T., *et al.* Inhibition of autophagy by chloroquine makes chemotherapy in nasopharyngeal carcinoma more efficient. *Auris, nasus, larynx* **46**, 443-450 (2019).
212. Balvan, J., *et al.* Oxidative Stress Resistance in Metastatic Prostate Cancer: Renewal by Self-Eating. *PLoS One* **10**, e0145016 (2015).
213. Liao, J.K., *et al.* Cancer-associated fibroblasts confer cisplatin resistance of tongue cancer via autophagy activation. *Biomedicine & pharmacotherapy = Biomedecine & pharmacotherapie* **97**, 1341-1348 (2018).
214. Sharif, T., *et al.* Autophagic homeostasis is required for the pluripotency of cancer stem cells. *Autophagy* **13**, 264-284 (2017).
215. Liu, K., *et al.* Mitophagy Controls the Activities of Tumor Suppressor p53 to Regulate Hepatic Cancer Stem Cells. *Molecular cell* **68**, 281-292 e285 (2017).
216. Wu, S., Akhtari, M. & Alachkar, H. Characterization of Mutations in the Mitochondrial Encoded Electron Transport Chain Complexes in Acute Myeloid Leukemia. *Sci Rep* **8**, 13301 (2018).
217. Bhola, N.E., *et al.* Treatment of Triple-Negative Breast Cancer with TORC1/2 Inhibitors Sustains a Drug-Resistant and Notch-Dependent Cancer Stem Cell Population. *Cancer Res* **76**, 440-452 (2016).
218. Chittaranjan, S., *et al.* Autophagy inhibition augments the anticancer effects of epirubicin treatment in anthracycline-sensitive and -resistant triple-negative breast cancer. *Clin Cancer Res* **20**, 3159-3173 (2014).
219. Apel, A., Herr, I., Schwarz, H., Rodemann, H.P. & Mayer, A. Blocked autophagy sensitizes resistant carcinoma cells to radiation therapy. *Cancer Res* **68**, 1485-1494 (2008).
220. Akin, D., *et al.* A novel ATG4B antagonist inhibits autophagy and has a negative impact on osteosarcoma tumors. *Autophagy* **10**, 2021-2035 (2014).
221. Petherick, K.J., *et al.* Pharmacological inhibition of ULK1 kinase blocks mammalian target of rapamycin (mTOR)-dependent autophagy. *The Journal of biological chemistry* **290**, 11376-11383 (2015).
222. Ronan, B., *et al.* A highly potent and selective Vps34 inhibitor alters vesicle trafficking and autophagy. *Nature chemical biology* **10**, 1013-1019 (2014).
223. McAfee, Q., *et al.* Autophagy inhibitor Lys05 has single-agent antitumor activity and reproduces the phenotype of a genetic autophagy deficiency. *Proc Natl Acad Sci U S A* **109**, 8253-8258 (2012).
224. Cechakova, L., *et al.* A Potent Autophagy Inhibitor (Lys05) Enhances the Impact of Ionizing Radiation on Human Lung Cancer Cells H1299. *Int J Mol Sci* **20**(2019).
225. Goodall, M.L., *et al.* Development of potent autophagy inhibitors that sensitize oncogenic BRAF V600E mutant melanoma tumor cells to vemurafenib. *Autophagy* **10**, 1120-1136 (2014).

References

226. Jung, D., *et al.* Quinacrine upregulates p21/p27 independent of p53 through autophagy-mediated downregulation of p62-Skp2 axis in ovarian cancer. *Sci Rep* **8**, 2487 (2018).
227. Das, S., *et al.* TRAIL enhances quinacrine-mediated apoptosis in breast cancer cells through induction of autophagy via modulation of p21 and DR5 interactions. *Cellular oncology* **40**, 593-607 (2017).
228. Artero-Castro, A., *et al.* Disruption of the ribosomal P complex leads to stress-induced autophagy. *Autophagy* **11**, 1499-1519 (2015).
229. Abad, E., *et al.* Common metabolic pathways implicated in resistance to chemotherapy point to a key mitochondrial role in breast cancer. *Mol Cell Proteomics* (2018).
230. Cai, J., Sun, M., Ge, X. & Sun, Y. EGFR tyrosine kinase inhibitors differentially affect autophagy in head and neck squamous cell carcinoma. *Biochem Biophys Res Commun* **486**, 1027-1033 (2017).
231. Fan, T.F., *et al.* Tumor growth suppression by inhibiting both autophagy and STAT3 signaling in HNSCC. *Oncotarget* **6**, 43581-43593 (2015).
232. Hemler, M.E. Tetraspanin functions and associated microdomains. *Nature reviews. Molecular cell biology* **6**, 801-811 (2005).
233. Levy, S. & Shoham, T. Protein-protein interactions in the tetraspanin web. *Physiology* **20**, 218-224 (2005).
234. Berditchevski, F., *et al.* Analysis of the CD151-alpha3beta1 integrin and CD151-tetraspanin interactions by mutagenesis. *The Journal of biological chemistry* **276**, 41165-41174 (2001).
235. Min, G., Wang, H., Sun, T.T. & Kong, X.P. Structural basis for tetraspanin functions as revealed by the cryo-EM structure of uroplakin complexes at 6-A resolution. *J Cell Biol* **173**, 975-983 (2006).
236. Kovalenko, O.V., Metcalf, D.G., DeGrado, W.F. & Hemler, M.E. Structural organization and interactions of transmembrane domains in tetraspanin proteins. *BMC structural biology* **5**, 11 (2005).
237. Florin, L. & Lang, T. Tetraspanin Assemblies in Virus Infection. *Frontiers in immunology* **9**, 1140 (2018).
238. van Deventer, S.J., Dunlock, V.E. & van Spriël, A.B. Molecular interactions shaping the tetraspanin web. *Biochemical Society transactions* **45**, 741-750 (2017).
239. Shoham, T., Rajapaksa, R., Kuo, C.C., Haimovich, J. & Levy, S. Building of the tetraspanin web: distinct structural domains of CD81 function in different cellular compartments. *Mol Cell Biol* **26**, 1373-1385 (2006).
240. Seigneuret, M., Delaguillaumie, A., Lagaudriere-Gesbert, C. & Conjeaud, H. Structure of the tetraspanin main extracellular domain. A partially conserved fold with a structurally variable domain insertion. *The Journal of biological chemistry* **276**, 40055-40064 (2001).
241. Yanez-Mo, M., Mittelbrunn, M. & Sanchez-Madrid, F. Tetraspanins and intercellular interactions. *Microcirculation* **8**, 153-168 (2001).
242. Yu, J., *et al.* The CD9, CD81, and CD151 EC2 domains bind to the classical RGD-binding site of integrin alphavbeta3. *The Biochemical journal* **474**, 589-596 (2017).
243. Zou, Y., *et al.* Determination of protein regions responsible for interactions of amelogenin with CD63 and LAMP1. *The Biochemical journal* **408**, 347-354 (2007).

244. Wright, M.D., Moseley, G.W. & van Spriël, A.B. Tetraspanin microdomains in immune cell signalling and malignant disease. *Tissue antigens* **64**, 533-542 (2004).
245. Starodubova, E.S., Kuzmenko, Y.V., Latanova, A.A., Preobrazhenskaya, O.V. & Karpov, V.L. [C-terminal lysosome targeting domain of CD63 modifies cellular localization of rabies virus glycoprotein]. *Molekuliarnaia biologii* **51**, 460-463 (2017).
246. Ferrero Restelli, F., *et al.* Tetraspanin1 promotes NGF signaling by controlling TrkA receptor proteostasis. *Cell Mol Life Sci* **77**, 2217-2233 (2020).
247. Zitvogel, L., *et al.* Eradication of established murine tumors using a novel cell-free vaccine: dendritic cell-derived exosomes. *Nat Med* **4**, 594-600 (1998).
248. Rubinstein, E., *et al.* CD9, CD63, CD81, and CD82 are components of a surface tetraspan network connected to HLA-DR and VLA integrins. *European journal of immunology* **26**, 2657-2665 (1996).
249. Charrin, S., *et al.* A physical and functional link between cholesterol and tetraspanins. *European journal of immunology* **33**, 2479-2489 (2003).
250. Berditchevski, F., Odintsova, E., Sawada, S. & Gilbert, E. Expression of the palmitoylation-deficient CD151 weakens the association of alpha 3 beta 1 integrin with the tetraspanin-enriched microdomains and affects integrin-dependent signaling. *The Journal of biological chemistry* **277**, 36991-37000 (2002).
251. Lazo, P.A. Functional implications of tetraspanin proteins in cancer biology. *Cancer Sci* **98**, 1666-1677 (2007).
252. Levy, S. Function of the tetraspanin molecule CD81 in B and T cells. *Immunologic research* **58**, 179-185 (2014).
253. Todd, S.C., Lipps, S.G., Crisa, L., Salomon, D.R. & Tsoukas, C.D. CD81 expressed on human thymocytes mediates integrin activation and interleukin 2-dependent proliferation. *J Exp Med* **184**, 2055-2060 (1996).
254. Termini, C.M. & Gillette, J.M. Tetraspanins Function as Regulators of Cellular Signaling. *Frontiers in cell and developmental biology* **5**, 34 (2017).
255. Charrin, S., *et al.* Differential stability of tetraspanin/tetraspanin interactions: role of palmitoylation. *FEBS letters* **516**, 139-144 (2002).
256. Romancino, D.P., *et al.* Palmitoylation is a post-translational modification of Alix regulating the membrane organization of exosome-like small extracellular vesicles. *Biochimica et biophysica acta. General subjects* **1862**, 2879-2887 (2018).
257. Yang, X., *et al.* Palmitoylation supports assembly and function of integrin-tetraspanin complexes. *J Cell Biol* **167**, 1231-1240 (2004).
258. Cherukuri, A., *et al.* B cell signaling is regulated by induced palmitoylation of CD81. *The Journal of biological chemistry* **279**, 31973-31982 (2004).
259. Ono, M., Handa, K., Withers, D.A. & Hakomori, S. Motility inhibition and apoptosis are induced by metastasis-suppressing gene product CD82 and its analogue CD9, with concurrent glycosylation. *Cancer Res* **59**, 2335-2339 (1999).
260. Lineberry, N., Su, L., Soares, L. & Fathman, C.G. The single subunit transmembrane E3 ligase gene related to anergy in lymphocytes (GRAIL)

References

- captures and then ubiquitinates transmembrane proteins across the cell membrane. *The Journal of biological chemistry* **283**, 28497-28505 (2008).
261. Saint-Pol, J., *et al.* Regulation of the trafficking and the function of the metalloprotease ADAM10 by tetraspanins. *Biochemical Society transactions* **45**, 937-944 (2017).
262. Andre, M., *et al.* Proteomic analysis of the tetraspanin web using LC-ESI-MS/MS and MALDI-FTICR-MS. *Proteomics* **6**, 1437-1449 (2006).
263. Le Naour, F., *et al.* Profiling of the tetraspanin web of human colon cancer cells. *Mol Cell Proteomics* **5**, 845-857 (2006).
264. Stipp, C.S., Kolesnikova, T.V. & Hemler, M.E. Functional domains in tetraspanin proteins. *Trends in biochemical sciences* **28**, 106-112 (2003).
265. Ang, J., Fang, B.L., Ashman, L.K. & Frauman, A.G. The migration and invasion of human prostate cancer cell lines involves CD151 expression. *Oncol Rep* **24**, 1593-1597 (2010).
266. Tardif, M.R. & Tremblay, M.J. Tetraspanin CD81 provides a costimulatory signal resulting in increased human immunodeficiency virus type 1 gene expression in primary CD4+ T lymphocytes through NF-kappaB, NFAT, and AP-1 transduction pathways. *Journal of virology* **79**, 4316-4328 (2005).
267. Tiwari-Woodruff, S.K., *et al.* OSP/claudin-11 forms a complex with a novel member of the tetraspanin super family and beta1 integrin and regulates proliferation and migration of oligodendrocytes. *J Cell Biol* **153**, 295-305 (2001).
268. Otsubo, C., *et al.* TSPAN2 is involved in cell invasion and motility during lung cancer progression. *Cell reports* **7**, 527-538 (2014).
269. Gesierich, S., *et al.* Colocalization of the tetraspanins, CO-029 and CD151, with integrins in human pancreatic adenocarcinoma: impact on cell motility. *Clin Cancer Res* **11**, 2840-2852 (2005).
270. Li, J., *et al.* MGAT3-mediated glycosylation of tetraspanin CD82 at asparagine 157 suppresses ovarian cancer metastasis by inhibiting the integrin signaling pathway. *Theranostics* **10**, 6467-6482 (2020).
271. Nishiuchi, R., *et al.* Potentiation of the ligand-binding activity of integrin alpha3beta1 via association with tetraspanin CD151. *Proc Natl Acad Sci U S A* **102**, 1939-1944 (2005).
272. Detchokul, S., Williams, E.D., Parker, M.W. & Frauman, A.G. Tetraspanins as regulators of the tumour microenvironment: implications for metastasis and therapeutic strategies. *British journal of pharmacology* **171**, 5462-5490 (2014).
273. Berditchevski, F. Complexes of tetraspanins with integrins: more than meets the eye. *J Cell Sci* **114**, 4143-4151 (2001).
274. Zhang, X.A., Bontrager, A.L. & Hemler, M.E. Transmembrane-4 superfamily proteins associate with activated protein kinase C (PKC) and link PKC to specific beta(1) integrins. *The Journal of biological chemistry* **276**, 25005-25013 (2001).
275. Ivaska, J., Whelan, R.D., Watson, R. & Parker, P.J. PKC epsilon controls the traffic of beta1 integrins in motile cells. *The EMBO journal* **21**, 3608-3619 (2002).
276. Hwang, S., Takimoto, T. & Hemler, M.E. Integrin-independent support of cancer drug resistance by tetraspanin CD151. *Cell Mol Life Sci* **76**, 1595-1604 (2019).

277. Palmer, T.D., *et al.* Integrin-free tetraspanin CD151 can inhibit tumor cell motility upon clustering and is a clinical indicator of prostate cancer progression. *Cancer Res* **74**, 173-187 (2014).
278. Kropshofer, H., *et al.* Tetraspan microdomains distinct from lipid rafts enrich select peptide-MHC class II complexes. *Nature immunology* **3**, 61-68 (2002).
279. Stipp, C.S., Kolesnikova, T.V. & Hemler, M.E. EWI-2 is a major CD9 and CD81 partner and member of a novel Ig protein subfamily. *The Journal of biological chemistry* **276**, 40545-40554 (2001).
280. Zhang, X.A., Lane, W.S., Charrin, S., Rubinstein, E. & Liu, L. EWI2/PGRL associates with the metastasis suppressor KAI1/CD82 and inhibits the migration of prostate cancer cells. *Cancer Res* **63**, 2665-2674 (2003).
281. Kolesnikova, T.V., *et al.* EWI-2 modulates lymphocyte integrin alpha4beta1 functions. *Blood* **103**, 3013-3019 (2004).
282. Trusolino, L. & Comoglio, P.M. Scatter-factor and semaphorin receptors: cell signalling for invasive growth. *Nat Rev Cancer* **2**, 289-300 (2002).
283. Shi, W., Fan, H., Shum, L. & Derynck, R. The tetraspanin CD9 associates with transmembrane TGF-alpha and regulates TGF-alpha-induced EGF receptor activation and cell proliferation. *J Cell Biol* **148**, 591-602 (2000).
284. Yauch, R.L. & Hemler, M.E. Specific interactions among transmembrane 4 superfamily (TM4SF) proteins and phosphoinositide 4-kinase. *The Biochemical journal* **351 Pt 3**, 629-637 (2000).
285. Clayton, E.L., Minogue, S. & Waugh, M.G. Mammalian phosphatidylinositol 4-kinases as modulators of membrane trafficking and lipid signaling networks. *Progress in lipid research* **52**, 294-304 (2013).
286. Shatz, O. & Elazar, Z. ATG9 raises the BAR for PI4P in autophagy. *J Cell Biol* **218**, 1432-1433 (2019).
287. Ullah, M., Akbar, A., Ng, N.N., Concepcion, W. & Thakor, A.S. Mesenchymal stem cells confer chemoresistance in breast cancer via a CD9 dependent mechanism. *Oncotarget* **10**, 3435-3450 (2019).
288. Kohmo, S., *et al.* Cell surface tetraspanin CD9 mediates chemoresistance in small cell lung cancer. *Cancer Res* **70**, 8025-8035 (2010).
289. Zhu, R., *et al.* TSPAN8 promotes cancer cell stemness via activation of sonic Hedgehog signaling. *Nature communications* **10**, 2863 (2019).
290. Serru, V., Dessen, P., Boucheix, C. & Rubinstein, E. Sequence and expression of seven new tetraspans. *Biochim Biophys Acta* **1478**, 159-163 (2000).
291. Wang, G.L., *et al.* The effect of NET-1 on the proliferation, migration and endocytosis of the SMMC-7721 HCC cell line. *Oncol Rep* **27**, 1944-1952 (2012).
292. Hou, F.Q., Lei, X.F., Yao, J.L., Wang, Y.J. & Zhang, W. Tetraspanin 1 is involved in survival, proliferation and carcinogenesis of pancreatic cancer. *Oncol Rep* **34**, 3068-3076 (2015).
293. Lu, Z., *et al.* TSPAN1 functions as an oncogene in gastric cancer and is downregulated by miR-573. *FEBS letters* **589**, 1988-1994 (2015).
294. Zhang, J., *et al.* MicroRNA-638 inhibits cell proliferation, invasion and regulates cell cycle by targeting tetraspanin 1 in human colorectal carcinoma. *Oncotarget* **5**, 12083-12096 (2014).

References

295. Gu, T., *et al.* Expression and function of tetraspanin 1 in esophageal carcinoma. *Oncology letters* **14**, 6815-6822 (2017).
296. Tian, J., *et al.* Silencing Tspan1 inhibits migration and invasion, and induces the apoptosis of human pancreatic cancer cells. *Molecular medicine reports* **18**, 3280-3288 (2018).
297. Ji, Z.J., Wang, J.L. & Chen, L. Inhibition of skin squamous cell carcinoma proliferation and promote apoptosis by dual silencing of NET-1 and survivin. *Oncol Rep* **34**, 811-822 (2015).
298. Munkley, J., *et al.* The cancer-associated cell migration protein TSPAN1 is under control of androgens and its upregulation increases prostate cancer cell migration. *Sci Rep* **7**, 5249 (2017).
299. Duan, J., Liu, J., Liu, Y., Huang, B. & Rao, L. miR-491-3p suppresses the growth and invasion of osteosarcoma cells by targeting TSPAN1. *Molecular medicine reports* **16**, 5568-5574 (2017).
300. Chen, Y., *et al.* MiR-200a enhances the migrations of A549 and SK-MES-1 cells by regulating the expression of TSPAN1. *Journal of biosciences* **38**, 523-532 (2013).
301. Zhang, X., *et al.* TSPAN1 upregulates MMP2 to promote pancreatic cancer cell migration and invasion via PLCgamma. *Oncol Rep* **41**, 2117-2125 (2019).
302. Subrungruanga, I., *et al.* Gene expression profiling of intrahepatic cholangiocarcinoma. *Asian Pacific journal of cancer prevention : APJCP* **14**, 557-563 (2013).
303. Wang, Y., *et al.* Tetraspanin 1 promotes epithelial-to-mesenchymal transition and metastasis of cholangiocarcinoma via PI3K/AKT signaling. *Journal of experimental & clinical cancer research : CR* **37**, 300 (2018).
304. zhang, J., *et al.* Expression and function of NET-1 in human skin squamous cell carcinoma. *Archives of dermatological research* **306**, 385-397 (2014).
305. Scholz, C.J., *et al.* Tspan-1 is a tetraspanin preferentially expressed by mucinous and endometrioid subtypes of human ovarian carcinomas. *Cancer Lett* **275**, 198-203 (2009).
306. Chen, L., *et al.* Clinicopathological significance of overexpression of TSPAN1, Ki67 and CD34 in gastric carcinoma. *Tumori* **94**, 531-538 (2008).
307. Shang, H., *et al.* Evaluation of therapeutic effect of targeting nanobubbles conjugated with NET-1 siRNA by shear wave elastography: an in vivo study of hepatocellular carcinoma bearing mice model. *Drug Deliv* **26**, 944-951 (2019).
308. Li, T., *et al.* Multi-target siRNA: Therapeutic Strategy for Hepatocellular Carcinoma. *J Cancer* **7**, 1317-1327 (2016).
309. Chen, L., *et al.* Knockdown of TSPAN1 by RNA silencing and antisense technique inhibits proliferation and infiltration of human skin squamous carcinoma cells. *Tumori* **96**, 289-295 (2010).
310. Chen, L., Yuan, D., Zhao, R., Li, H. & Zhu, J. Suppression of TSPAN1 by RNA interference inhibits proliferation and invasion of colon cancer cells in vitro. *Tumori* **96**, 744-750 (2010).
311. Wu, Y.Y., *et al.* Inhibition of hepatocellular carcinoma growth and angiogenesis by dual silencing of NET-1 and VEGF. *Journal of molecular histology* **44**, 433-445 (2013).

312. Huang, Y., Sook-Kim, M. & Ratovitski, E. Midkine promotes tetraspanin-integrin interaction and induces FAK-Stat1alpha pathway contributing to migration/invasiveness of human head and neck squamous cell carcinoma cells. *Biochem Biophys Res Commun* **377**, 474-478 (2008).
313. Hannus, M., *et al.* siPools: highly complex but accurately defined siRNA pools eliminate off-target effects. *Nucleic Acids Res* **42**, 8049-8061 (2014).
314. Marques, N., *et al.* Regulation of protein translation and c-Jun expression by prostate tumor overexpressed 1. *Oncogene* **33**, 1124-1134 (2014).
315. Gulcicek, E.E., *et al.* Proteomics and the analysis of proteomic data: an overview of current protein-profiling technologies. *Current protocols in bioinformatics* **Chapter 13**, Unit 13 11 (2005).
316. Morote, J., *et al.* PTOV1 expression predicts prostate cancer in men with isolated high-grade prostatic intraepithelial neoplasia in needle biopsy. *Clin Cancer Res* **14**, 2617-2622 (2008).
317. Hermida-Prado, F., *et al.* The Differential Impact of SRC Expression on the Prognosis of Patients with Head and Neck Squamous Cell Carcinoma. *Cancers (Basel)* **11**(2019).
318. Alana, L., *et al.* Prostate tumor Overexpressed-1 (PTOV1) down-regulates HES1 and HEY1 notch targets genes and promotes prostate cancer progression. *Mol Cancer* **13**, 74 (2014).
319. Garcia-Mayea, Y., *et al.* Autophagy inhibition as a promising therapeutic target for laryngeal cancer. *Carcinogenesis* **40**, 1525-1534 (2019).
320. Salvador-Coloma, C. & Cohen, E. Multidisciplinary Care of Laryngeal Cancer. *J Oncol Pract* **12**, 717-724 (2016).
321. Nahavandipour, A., *et al.* Incidence and survival of laryngeal cancer in Denmark: a nation-wide study from 1980 to 2014. *Acta oncologica* **58**, 977-982 (2019).
322. Coskun, H., *et al.* Prognosis of subglottic carcinoma: Is it really worse? *Head & neck* **41**, 511-521 (2019).
323. Klionsky, D.J., *et al.* Guidelines for the use and interpretation of assays for monitoring autophagy. *Autophagy* **8**, 445-544 (2012).
324. Ffrench, B., *et al.* CD10(-)/ALDH(-) cells are the sole cisplatin-resistant component of a novel ovarian cancer stem cell hierarchy. *Cell Death Dis* **8**, e3128 (2017).
325. Nguyen, P.H., *et al.* Characterization of Biomarkers of Tumorigenic and Chemoresistant Cancer Stem Cells in Human Gastric Carcinoma. *Clin Cancer Res* **23**, 1586-1597 (2017).
326. Wang, S., *et al.* miR-216a-mediated upregulation of TSPAN1 contributes to pancreatic cancer progression via transcriptional regulation of ITGA2. *Am J Cancer Res* **10**, 1115-1129 (2020).
327. Bauman, J.E., *et al.* Randomized, placebo-controlled window trial of EGFR, Src, or combined blockade in head and neck cancer. *JCI Insight* **2**, e90449 (2017).
328. Herold, C.I., *et al.* Phase II trial of dasatinib in patients with metastatic breast cancer using real-time pharmacodynamic tissue biomarkers of Src inhibition to escalate dosing. *Clin Cancer Res* **17**, 6061-6070 (2011).

References

329. Chandrashekar, D.S., *et al.* UALCAN: A Portal for Facilitating Tumor Subgroup Gene Expression and Survival Analyses. *Neoplasia* **19**, 649-658 (2017).
330. Modur, V., Thomas-Robbins, K. & Rao, K. HPV and CSC in HNSCC cisplatin resistance. *Frontiers in bioscience* **7**, 58-66 (2015).
331. Sotgia, F., Fiorillo, M. & Lisanti, M.P. Mitochondrial markers predict recurrence, metastasis and tamoxifen-resistance in breast cancer patients: Early detection of treatment failure with companion diagnostics. *Oncotarget* **8**, 68730-68745 (2017).
332. Ota, I., *et al.* Snail-induced EMT promotes cancer stem cell-like properties in head and neck cancer cells. *Oncol Rep* **35**, 261-266 (2016).
333. Barrett, C.L., *et al.* Transcriptome sequencing of tumor subpopulations reveals a spectrum of therapeutic options for squamous cell lung cancer. *PLoS One* **8**, e58714 (2013).
334. Naik, P.P., *et al.* Autophagy regulates cisplatin-induced stemness and chemoresistance via the upregulation of CD44, ABCB1 and ADAM17 in oral squamous cell carcinoma. *Cell proliferation* **51**(2018).
335. Song, X., *et al.* ATG12 expression quantitative trait loci associated with head and neck squamous cell carcinoma risk in a Chinese Han population. *Mol Carcinog* **57**, 1030-1037 (2018).
336. Yang, Q., *et al.* A Prognostic Bio-Model Based on SQSTM1 and N-Stage Identifies Nasopharyngeal Carcinoma Patients at High Risk of Metastasis for Additional Induction Chemotherapy. *Clin Cancer Res* **24**, 648-658 (2018).
337. Lazova, R., *et al.* Punctate LC3B expression is a common feature of solid tumors and associated with proliferation, metastasis, and poor outcome. *Clin Cancer Res* **18**, 370-379 (2012).
338. Burdelski, C., *et al.* Cytoplasmic Accumulation of Sequestosome 1 (p62) Is a Predictor of Biochemical Recurrence, Rapid Tumor Cell Proliferation, and Genomic Instability in Prostate Cancer. *Clin Cancer Res* **21**, 3471-3479 (2015).
339. Zhu, L., *et al.* Cytoplasmic SQSTM1/ P62 Accumulation Predicates a Poor Prognosis in Patients with Malignant Tumor. *J Cancer* **9**, 4072-4086 (2018).
340. Boone, B.A., *et al.* Safety and Biologic Response of Pre-operative Autophagy Inhibition in Combination with Gemcitabine in Patients with Pancreatic Adenocarcinoma. *Annals of surgical oncology* **22**, 4402-4410 (2015).
341. Poillet-Perez, L., *et al.* Autophagy maintains tumour growth through circulating arginine. *Nature* **563**, 569-573 (2018).
342. Yang, L., *et al.* Prostate tumor overexpressed-1, in conjunction with human papillomavirus status, predicts outcome in early-stage human laryngeal squamous cell carcinoma. *Oncotarget* **7**, 31878-31891 (2016).
343. Yang, Q., *et al.* Prostate Tumor Overexpressed 1 (PTOV1) Is a Novel Prognostic Marker for Nasopharyngeal Carcinoma Progression and Poor Survival Outcomes. *PLoS One* **10**, e0136448 (2015).
344. Li, R., *et al.* Overexpressed PTOV1 associates with tumorigenesis and progression of esophageal squamous cell carcinoma. *Tumour Biol* **39**, 1010428317705013 (2017).
345. Karna, S.K.L., Ahmad, F., Lone, B.A. & Pokharel, Y.R. Knockdown of PTOV1 and PIN1 exhibit common phenotypic anti-cancer effects in MDA-MB-231 cells. *PLoS One* **14**, e0211658 (2019).

346. Behrends, C., Sowa, M.E., Gygi, S.P. & Harper, J.W. Network organization of the human autophagy system. *Nature* **466**, 68-76 (2010).
347. Adams, O., *et al.* Prognostic relevance of autophagy markers LC3B and p62 in esophageal adenocarcinomas. *Oncotarget* **7**, 39241-39255 (2016).
348. Shi, C., *et al.* Sequestosome 1 protects esophageal squamous carcinoma cells from apoptosis via stabilizing SKP2 under serum starvation condition. *Oncogene* **37**, 3260-3274 (2018).
349. Chen, S.P., *et al.* Prostate tumor overexpressed 1 is a novel prognostic marker for hepatocellular carcinoma progression and overall patient survival. *Medicine* **94**, e423 (2015).
350. Chen, Y., Hu, Z. & Chai, D. High expression of prostate tumor overexpressed 1 (PTOV1) is a potential prognostic biomarker for cervical cancer. *International journal of clinical and experimental pathology* **10**, 11044-11050 (2017).
351. Terabe, T., *et al.* Expression of autophagy-related markers at the surgical margin of oral squamous cell carcinoma correlates with poor prognosis and tumor recurrence. *Hum Pathol* **73**, 156-163 (2018).
352. Lai, K., *et al.* Differences in LC3B expression and prognostic implications in oropharyngeal and oral cavity squamous cell carcinoma patients. *BMC cancer* **18**, 624 (2018).
353. Lefort, S., *et al.* Inhibition of autophagy as a new means of improving chemotherapy efficiency in high-LC3B triple-negative breast cancers. *Autophagy* **10**, 2122-2142 (2014).
354. Ma, X.H., *et al.* Measurements of tumor cell autophagy predict invasiveness, resistance to chemotherapy, and survival in melanoma. *Clin Cancer Res* **17**, 3478-3489 (2011).
355. Dohmen, A.J., *et al.* Feasibility of Primary Tumor Culture Models and Preclinical Prediction Assays for Head and Neck Cancer: A Narrative Review. *Cancers* **7**, 1716-1742 (2015).
356. Owen, J.H., *et al.* UM-SCC-103: a unique tongue cancer cell line that recapitulates the tumorigenic stem cell population of the primary tumor. *Ann Otol Rhinol Laryngol* **123**, 662-672 (2014).
357. Pellegrini, P., *et al.* Tumor acidosis enhances cytotoxic effects and autophagy inhibition by salinomycin on cancer cell lines and cancer stem cells. *Oncotarget* **7**, 35703-35723 (2016).
358. Pei, G., *et al.* Autophagy Facilitates Metadherin-Induced Chemotherapy Resistance Through the AMPK/ATG5 Pathway in Gastric Cancer. *Cellular physiology and biochemistry : international journal of experimental cellular physiology, biochemistry, and pharmacology* **46**, 847-859 (2018).
359. Canovas, V., Lleonart, M., Morote, J. & Paciucci, R. The role of prostate tumor overexpressed 1 in cancer progression. *Oncotarget* **8**, 12451-12471 (2017).
360. Wu, Z., *et al.* Depleting PTOV1 sensitizes non-small cell lung cancer cells to chemotherapy through attenuating cancer stem cell traits. *Journal of experimental & clinical cancer research : CR* **38**, 341 (2019).
361. Zhou, Y., *et al.* Autophagy induction contributes to GDC-0349 resistance in head and neck squamous cell carcinoma (HNSCC) cells. *Biochem Biophys Res Commun* **477**, 174-180 (2016).

References

362. Zhou, F., *et al.* Down-regulation of OGT promotes cisplatin resistance by inducing autophagy in ovarian cancer. *Theranostics* **8**, 5200-5212 (2018).
363. Xing, J.J., *et al.* Ginsenoside Rb3 provides protective effects against cisplatin-induced nephrotoxicity via regulation of AMPK-/mTOR-mediated autophagy and inhibition of apoptosis in vitro and in vivo. *Cell proliferation* **52**, e12627 (2019).
364. Lee, Y.J., *et al.* Cisplatin and resveratrol induce apoptosis and autophagy following oxidative stress in malignant mesothelioma cells. *Food and chemical toxicology : an international journal published for the British Industrial Biological Research Association* **97**, 96-107 (2016).
365. Hou, N., *et al.* MicroRNA profiling in human colon cancer cells during 5-fluorouracil-induced autophagy. *PLoS One* **9**, e114779 (2014).
366. Zeng, X. & Kinsella, T.J. BNIP3 is essential for mediating 6-thioguanine- and 5-fluorouracil-induced autophagy following DNA mismatch repair processing. *Cell research* **20**, 665-675 (2010).
367. Zhang, S.F., *et al.* TXNDC17 promotes paclitaxel resistance via inducing autophagy in ovarian cancer. *Autophagy* **11**, 225-238 (2015).
368. Huang, S., Qi, P., Zhang, T., Li, F. & He, X. The HIF1alpha/miR2243p/ATG5 axis affects cell mobility and chemosensitivity by regulating hypoxia-induced protective autophagy in glioblastoma and astrocytoma. *Oncol Rep* **41**, 1759-1768 (2019).
369. Maycotte, P., *et al.* STAT3-mediated autophagy dependence identifies subtypes of breast cancer where autophagy inhibition can be efficacious. *Cancer Res* **74**, 2579-2590 (2014).
370. Levy, J.M., *et al.* Autophagy inhibition improves chemosensitivity in BRAF(V600E) brain tumors. *Cancer discovery* **4**, 773-780 (2014).
371. Mahalingam, D., *et al.* Combined autophagy and HDAC inhibition: a phase I safety, tolerability, pharmacokinetic, and pharmacodynamic analysis of hydroxychloroquine in combination with the HDAC inhibitor vorinostat in patients with advanced solid tumors. *Autophagy* **10**, 1403-1414 (2014).
372. Rangwala, R., *et al.* Combined MTOR and autophagy inhibition: phase I trial of hydroxychloroquine and temsirolimus in patients with advanced solid tumors and melanoma. *Autophagy* **10**, 1391-1402 (2014).
373. Pellegrini, P., *et al.* Acidic extracellular pH neutralizes the autophagy-inhibiting activity of chloroquine: implications for cancer therapies. *Autophagy* **10**, 562-571 (2014).
374. Basit, F., Cristofanon, S. & Fulda, S. Obatoclox (GX15-070) triggers necroptosis by promoting the assembly of the necrosome on autophagosomal membranes. *Cell death and differentiation* **20**, 1161-1173 (2013).
375. Goodall, M.L., *et al.* The Autophagy Machinery Controls Cell Death Switching between Apoptosis and Necroptosis. *Developmental cell* **37**, 337-349 (2016).
376. Kiraz, Y., Adan, A., Kartal Yandim, M. & Baran, Y. Major apoptotic mechanisms and genes involved in apoptosis. *Tumour Biol* **37**, 8471-8486 (2016).
377. Moon, J.H., *et al.* Role of integrin beta1 as a biomarker of stemness in head and neck squamous cell carcinoma. *Oral oncology* **96**, 34-41 (2019).

378. Luo, J., *et al.* 14, 15-EET induces breast cancer cell EMT and cisplatin resistance by up-regulating integrin α v β 3 and activating FAK/PI3K/AKT signaling. *Journal of experimental & clinical cancer research : CR* **37**, 23 (2018).
379. Minematsu, T., *et al.* Carrier-mediated uptake of 1-(2-methoxyethyl)-2-methyl-4,9-dioxo-3-(pyrazin-2-ylmethyl)-4,9-dihydro-1H-naphtho[2,3-d]imidazolium bromide (YM155 monobromide), a novel small-molecule survivin suppressant, into human solid tumor and lymphoma cells. *Drug metabolism and disposition: the biological fate of chemicals* **37**, 619-628 (2009).
380. Niu, T.K., Cheng, Y., Ren, X. & Yang, J.M. Interaction of Beclin 1 with survivin regulates sensitivity of human glioma cells to TRAIL-induced apoptosis. *FEBS letters* **584**, 3519-3524 (2010).
381. Cheng, S.M., *et al.* YM155 down-regulates survivin and XIAP, modulates autophagy and induces autophagy-dependent DNA damage in breast cancer cells. *British journal of pharmacology* **172**, 214-234 (2015).
382. de Bree, R., *et al.* Response assessment after induction chemotherapy for head and neck squamous cell carcinoma: From physical examination to modern imaging techniques and beyond. *Head Neck* **39**, 2329-2349 (2017).
383. Ye, J., Wu, D., Wu, P., Chen, Z. & Huang, J. The cancer stem cell niche: cross talk between cancer stem cells and their microenvironment. *Tumour Biol* **35**, 3945-3951 (2014).
384. Dudas, J., Ladanyi, A., Ingruber, J., Steinbichler, T.B. & Riechelmann, H. Epithelial to Mesenchymal Transition: A Mechanism that Fuels Cancer Radio/Chemoresistance. *Cells* **9**(2020).
385. Scholz, C.J., Sauer, G. & Deissler, H. Glycosylation of tetraspanin Tspan-1 at four distinct sites promotes its transition through the endoplasmic reticulum. *Protein and peptide letters* **16**, 1244-1248 (2009).
386. Thibodeau, B.J., *et al.* Gene Expression Characterization of HPV Positive Head and Neck Cancer to Predict Response to Chemoradiation. *Head and neck pathology* **9**, 345-353 (2015).
387. Kaufmann, A.M., Backsch, C., Schneider, A. & Durst, M. HPV induced cervical carcinogenesis: molecular basis and vaccine development. *Zentralblatt fur Gynakologie* **124**, 511-524 (2002).
388. Wollscheid, V., *et al.* Identification of a new proliferation-associated protein NET-1/C4.8 characteristic for a subset of high-grade cervical intraepithelial neoplasia and cervical carcinomas. *International journal of cancer* **99**, 771-775 (2002).
389. Nees, M., van Wijngaarden, E., Bakos, E., Schneider, A. & Durst, M. Identification of novel molecular markers which correlate with HPV-induced tumor progression. *Oncogene* **16**, 2447-2458 (1998).
390. Ke, L., *et al.* c-Src activation promotes nasopharyngeal carcinoma metastasis by inducing the epithelial-mesenchymal transition via PI3K/Akt signaling pathway: a new and promising target for NPC. *Oncotarget* **7**, 28340-28355 (2016).

ANNEXES

IX. ANNEXES

Appendix 1. List of patients with laryngeal cancer from HUVH studied by IHC for the expression of LC3, ATG5, p62 and PTOV1 proteins. The table shows the final scores of the indicated proteins in the whole database indicating the clinicopathological characteristics of the patients. ATG5, PTOV1, and p62 proteins were considered positive when scored >50, while for the protein LC3 the cut off value was zero. PN (patient number); Loc 1 (location 1: 1 glottic; 2 supraglottic; 3 subglottic); Loc 2 (location 2: 1 supraglottic, 2 other locations); CT (postsurgical chemotherapy: 0 not treated; 1 treated with CDDP); RT (postsurgical radiotherapy: 0 not treated; 1 treated); Margins (0 tumor margin non affected; 1 tumor margin affected); T (1 tumor only in the larynx; 2 tumor has expanded to the vocal cords; 3 tumor has caused that one of the vocal cords do not move; 4 tumor has grown into body tissues outside the larynx); N (0 lymph nodes don't contain cancer cells; 1 one lymph node contains cancer cells; 2a one lymph node contains cancer cells and the node is between 3cm and 6cm across; 2b more than one lymph node contain cancer cells but none of the nodes are more than 6cm across; 2c there are cancer cells in lymph nodes on the other side of the neck, or in nodes on both sides of the neck but none of the nodes are more than 6cm across; 3 at least one lymph node containing cancer cells is larger than 6cm across); G (tumor grade or histopathological grade: 1 well differentiated; 2 moderately differentiated, 3 poorly differentiated); T(S) (time survival in months); p62 n (p62 nuclear); p62 c (p62 cytoplasmic); NV (not valuable).

Annexes

	Clinical information of the patients											IHC (Scores %)				
	PN	Age	Loc 1	Loc 2	CT	RT	Margens	T	N	G	T (S)	ATG5	LC3	PTOV1	p62 n	p62 c
1	159	52	2	1	0	0	0	4	0	1	54	33	205	164	0	280
2	52	63	2	1	0	0	1	4	2a	3	212	20	0	80	140	0
3	38	67	3	2	0	0	1	2	2b	1	41	23	0	69	10	0
4	86	64	1	2	0	0	0	3	0	1	139	105	0	200	10	0
5	67	48	3	2	0	0	0	3	0	1	184	20	3	67	10	20
6	85	49	1	2	0	0	0	1	0	1	999	24	0	73	120	0
7	28	62	1	2	0	0	1	1	0	1	999	3	0	NV	NV	NV
8	84	32	1	2	0	0	0	1	0	1	999	3	0	80	50	0
9	21	77	1	2	0	0	0	1	0	1	999	40	0	50	100	0
10	41	47	1	2	0	0	0	1	0	1	999	21	0	120	280	0
11	48	58	2	1	0	1	0	3	2c	1	6	93	0	185	10	30
12	155	49	2	1	1	1	1	4	2c	1	21	113	30	200	0	154
13	142	48	2	1	0	1	0	2	1	2	53	15	0	90	40	85
14	122	55	2	1	0	1	0	3	2c	1	74	27	0	70	225	NV
15	110	57	2	1	1	1	1	3	0	1	79	0	10	20	175	0
16	157	67	2	1	1	1	0	4	2c	1	101	23	154	186	0	153
17	44	63	2	1	0	1	1	3	0	3	102	10	0	117	54	33
18	127	66	2	1	0	1	1	4	2c	1	162	120	0	207	61	26
19	30	45	2	1	1	1	0	4	2c	1	195	77	0	126	9	0
20	5	58	2	1	0	1	0	2	2c	3	49	0	20	90	0	35
21	22	54	2	1	0	1	1	3	1	2	61	NV	0	NV	NV	NV
22	46	56	2	1	1	1	0	3	2a	1	161	70	0	140	95	20
23	72	56	2	1	1	1	1	4	2c	2	162	47	0	140	15	0
24	65	60	2	1	1	1	0	4	2c	1	163	173	0	220	0	160
25	87	43	2	1	0	1	0	4	0	1	166	20	0	200	150	20
26	9	48	2	1	1	1	0	2	0	2	167	30	23	187	153	13
27	153	60	2	1	1	1	0	4	2b	3	167	50	0	20	0	55
28	162	48	2	1	0	1	0	4	1	2	169	75	0	233	40	20
29	165	55	2	1	1	1	0	3	3	1	177	25	0	30	0	255
30	126	59	2	1	0	1	0	4	2b	3	999	NV	0	NV	NV	NV
31	156	58	2	1	0	1	0	4	3	2	999	3	0	200	10	0
32	7	64	2	1	1	1	1	4	0	3	2	94	0	255	81	146
33	105	80	2	1	1	1	1	4	2c	1	4	200	0	250	71	72
34	1	42	2	1	1	1	0	2	2c	1	10	NV	0	14	NV	NV
35	151	57	2	1	0	1	0	4	0	1	999	80	3	196	81	20
36	50	41	2	1	0	1	1	4	2	1	999	20	5	105	135	20
37	51	79	2	1	0	1	1	4	1	3	999	110	0	100	0	123
38	35	48	3	2	0	1	0	3	2b	1	7	25	0	120	74	59
39	134	41	3	2	1	1	0	2	2b	1	9	20	43	90	300	300
40	49	64	3	2	0	1	0	4	2a	1	10	84	0	113	10	0
41	75	48	3	2	1	1	0	4	0	3	10	30	0	57	74	0
42	103	62	3	2	0	1	0	3	2c	1	12	43	0	150	43	0
43	17	60	3	2	0	1	1	2	2c	1	13	101	0	186	137	0
44	131	73	3	2	0	1	0	3	0	1	13	40	0	160	77	53
45	19	70	3	2	0	1	0	2	2b	1	15	57	67	109	121	196
46	66	62	3	2	0	1	1	3	2b	2	20	110	3	106	14	93
47	10	64	3	2	0	1	1	3	2a	3	22	NV	0	NV	NV	NV
48	129	47	3	2	0	1	0	4	0	2	23	25	90	200	0	132
49	161	53	3	2	0	1	0	3	0	1	30	100	0	200	160	95
50	136	69	3	2	0	1	0	3	2b	2	35	70	0	200	141	100
51	128	58	3	2	0	1	1	4	1	2	41	120	0	40	0	300
52	74	76	3	2	0	1	0	4	2c	3	43	25	0	115	114	77
53	141	51	3	2	0	1	0	3	0	2	43	93	0	123	17	33
54	55	60	3	2	1	1	0	2	2a	1	44	37	0	69	64	7
55	145	54	3	2	0	1	0	3	2b	2	47	10	0	90	165	0
56	13	69	3	2	1	1	1	3	0	2	56	103	7	106	134	23
57	205	65	3	2	0	1	1	3	2b	1	58	5	75	130	25	0
58	135	57	3	2	0	1	0	3	0	1	79	0	0	10	0	0
59	73	69	3	2	0	1	0	3	0	1	91	80	22	143	114	0
60	6	73	3	2	0	1	0	2	2c	1	94	NV	0	NV	NV	NV
61	148	73	3	2	0	1	0	3	0	2	104	30	0	150	80	20
62	133	70	3	2	1	1	0	3	2c	2	143	27	3	107	50	0
63	146	69	3	2	1	1	0	3	0	2	176	37	0	100	80	0
64	123	51	3	2	1	1	0	2	0	1	181	0	0	80	270	0
65	2	51	3	2	0	1	0	3	0	2	182	40	75	65	155	90
66	132	46	3	2	0	1	0	3	0	2	183	64	0	167	54	3
67	124	67	3	2	0	1	0	3	2b	1	189	30	40	100	180	190
68	68	57	3	2	1	1	0	4	2a	3	46	5	0	80	9	16
69	150	62	3	2	0	1	0	4	0	1	51	50	33	134	125	66
70	18	46	3	2	0	1	1	3	2b	1	59	60	0	40	0	180
71	139	57	3	2	0	1	0	3	0	1	151	NV	0	NV	0	0
72	140	43	3	2	0	1	0	3	0	1	175	33	0	186	0	90
73	144	37	3	2	0	1	0	3	0	1	175	43	7	50	152	73
74	71	59	3	2	0	1	0	3	0	1	191	60	0	80	20	85
75	143	42	3	2	0	1	0	3	2c	1	999	10	0	80	0	180
76	106	47	3	2	0	1	0	3	0	2	6	50	0	100	166	87
77	61	51	3	2	0	1	0	3	0	1	12	23	0	27	20	15
78	138	64	3	2	0	1	0	3	0	1	19	20	130	0	5	300
79	125	65	3	2	0	1	0	3	0	2	60	20	13	67	4	167
80	189	65	1	2	0	1	1	1	0	1	999	20	0	140	30	20
81	43	48	1	2	0	1	0	1	0	1	999	17	0	55	0	200
82	104	58	3	2	1	1	0	4	0	1	999	77	0	195	125	0
83	111	83	3	2	0	1	0	3	0	1	999	13	0	90	33	70
84	130	66	3	2	0	1	0	3	0	1	999	7	0	51	94	26

Appendix 2. Clinical and pathological characteristics of the 106 patients from HUCA. They were analyzed by IHC for protein quantifications of E-cadherin, active SRC and TSPAN1. E-cadherin and TSPAN1 were scored as follow: 0 (0%), 1 (1% to 10%), 2 (11% to 50%), and 3 (51% to 100 %) of the tumor cells showing cytoplasmatic staining and the staining intensity was rated as 0 (negative), 1 (weak), 2 (strong). The raw data were then converted to an Immunoreactive Score (IRS) by multiplying the quantity and staining intensity scores. For E-cadherin, an IRS equal or above the median (score 4) was considered high expression (score 1). TSPAN1 expression was dichotomized as negative (score 0) versus positive (scores 1-6) expression. In addition, nuclear expression of TSPAN1 was recorded as negative (score 0) versus positive (score 1). Active SRC staining showed a homogeneous distribution and therefore a semiquantitative scoring system based in staining intensity was applied: low (0, 1+), moderate (2+), or high expression (3+). RT post (post-surgical radiation therapy: 0 no, 1 yes); Recurrence: 0 no, 1 yes; Status: 0 live without tumor, 1 death because the tumor, 2 death from another cause, 3 no data; Survival: months from surgical; IRS: Immunoreactive Score; TSPAN1 INT: cytoplasmic TSPAN1 intensity; TSPAN1 %: percentage of positive cells showing cytoplasmatic staining; TSPAN1 NUCL: percentage of positive cells showing nuclear expression of TSPAN1; TSPAN1 01: TSPAN1 negative (0) versus positive (1).

Annexes

Patient	Age	Location	T	N	M	G	Stage	RT post	Recurrence	Status	Survival	E-Cadherin IRS	E-Cadherin Median	ActiveSRC	TSPAN1 INT	TSPAN1 %	TSPAN1 IRS	TSPAN1 NUCL	TSPAN1 01
1	52	1	3	2	0	2	4	1	0	0	80	0	0	1	1	3	3	0	1
2	52	1	3	2	0	1	4	1	1	1	22	1	0	2	0	0	0	0	0
3	65	1	4	0	0	1	4	0	0	0	80	3	0	1	0	0	0	0	0
4	57	1	4	0	0	2	4	1	0	0	89	1	0	2	1	3	3	1	1
5	37	1	4	1	0	1	4	0	1	3	29	1	0	1	1	3	3	1	1
6	81	1	3	0	0	2	3	0	0	3	46	2	0	3	2	2	4	1	1
7	74	1	4	1	0	2	4	0	1	1	32	3	0	2	2	2	4	1	1
8	70	1	4	2	0	2	4	0	0	2	36	3	0	1	2	1	2	0	1
9	36	1	4	0	0	1	4	0	1	1	32	5	1	2	0	0	0	0	0
10	63	1	3	2	0	2	4	0	1	1	18	3	0	3	1	3	3	0	1
11	53	1	1	0	0	1	1	1	0	2	24	2	0	3	1	3	3	1	1
12	65	1	3	1	0	2	3	0	0	0	72	3	0	3	1	2	2	1	1
13	85	1	3	0	0	1	3	0	0	3	44	0	0	1	0	0	0	0	0
14	61	1	3	2	0	2	4	1	1	1	6	1	0	2	0	0	0	0	0
15	67	1	1	0	0	2	1	0	0	0	82	1	0	1	0	0	0	0	0
16	73	1	2	2	0	2	4	1	0	2	51	6	1	2	0	0	0	0	0
17	75	1	3	2	0	1	4	0	1	1	19	1	0	2	2	1	2	0	1
18	53	1	3	1	0	1	3	0	0	3	25	3	0	3	0	0	0	0	0
19	68	1	4	2	0	1	4	1	1	1	11	5	1	3	0	0	0	0	0
20	62	1	1	1	0	1	3	0	0	0	66	1	0	3	1	2	2	1	1
21	56	1	3	0	0	2	3	0	0	0	68	6	1	2	0	0	0	0	0
22	44	1	3	0	0	2	3	0	0	0	62	6	1	1	0	0	0	0	0
23	71	1	3	1	0	2	3	0	0	0	37	4	1	2	0	0	0	0	0
24	50	1	3	2	0	2	4	1	1	1	4	6	1	2	2	3	6	1	1
25	80	1	3	0	0	2	3	0	1	1	12	6	1	2	0	0	0	0	0
26	44	1	2	3	0	1	4	1	0	0	80	4	1	1	0	0	0	0	0
27	66	1	3	0	0	1	3	0	0	0	62	6	1	2	0	0	0	0	0
28	86	1	3	0	0	3	3	0	0	2	15	2	0	2	0	0	0	0	0
29	54	1	3	0	0	1	3	0	0	0	61	1	0	2	1	2	2	1	1
30	74	1	4	2	0	2	4	0	1	1	9	3	0	3	1	2	2	1	1
31	50	1	4	3	0	3	4	1	1	1	26	0	0	3	2	3	6	1	1
32	48	1	4	0	0	2	4	0	0	3	2	0	0	2	0	0	0	0	0
33	67	1	3	0	0	2	3	0	1	0	59	2	0	1	2	2	4	1	1
34	72	1	4	0	0	3	4	0	1	1	14	3	0	2	1	1	1	1	1
35	39	1	4	2	0	2	4	1	1	1	15	1	0	2	0	0	0	0	0
36	59	1	3	1	0	2	3	1	0	0	55	3	0	1	2	3	6	1	1
37	77	1	4	1	0	3	4	0	0	3	35	3	0	3	1	2	2	1	1
38	56	1	3	0	0	3	3	0	0	0	52	6	1	1	0	0	0	0	0
39	59	1	1	0	0	1	1	0	0	0	75	1	0	1	0	0	0	0	0
40	58	1	1	0	0	2	1	0	0	0	72	#NULL!	#NULL!	#NULL!	1	1	1	0	1
41	42	1	1	0	0	1	1	0	0	0	66	2	0	1	0	0	0	0	0
42	79	1	2	0	0	3	2	0	0	3	1	6	1	#NULL!	0	0	0	0	0
43	72	2	4	1	0	2	4	1	0	2	68	5	1	2	0	0	0	0	0
44	69	2	2	2	0	2	4	1	1	1	48	5	1	3	0	0	0	0	0
45	61	2	3	2	0	1	4	0	1	1	21	2	0	2	0	0	0	0	0
46	49	2	4	1	0	2	4	1	1	1	10	5	1	3	0	0	0	0	0
47	52	2	3	3	0	2	4	1	0	0	73	1	0	3	0	0	0	0	0
48	45	2	2	2	0	2	4	1	1	1	9	1	0	3	1	2	2	0	1
49	56	2	1	2	0	3	4	1	1	1	12	5	1	3	0	0	0	0	0
50	49	2	3	2	0	3	4	0	1	1	5	0	0	3	1	1	1	1	1
51	49	2	3	2	0	1	4	1	0	0	63	2	0	3	0	0	0	0	0
52	43	2	4	2	0	2	4	1	1	2	33	3	0	3	2	1	2	0	1
53	52	2	3	2	0	2	4	1	0	2	28	0	0	3	1	3	3	1	1
54	51	2	3	2	0	2	4	1	1	1	11	0	0	#NULL!	0	0	0	0	0
55	63	2	2	2	0	3	4	1	1	0	58	1	0	3	1	2	2	1	1
56	68	2	3	0	0	3	3	1	0	0	77	1	0	3	1	2	2	1	1
57	53	2	2	2	0	2	4	1	0	3	5	0	0	1	2	1	2	1	1
58	60	2	4	2	0	1	4	1	1	1	45	1	0	1	0	0	0	0	0
59	78	2	3	1	0	3	3	0	0	3	1	3	0	3	0	0	0	0	0
60	68	2	3	1	0	2	3	0	0	0	54	0	0	3	0	0	0	0	0
61	59	2	4	2	0	2	4	0	0	0	51	3	0	2	0	0	0	0	0
62	56	2	2	2	0	2	4	0	0	2	71	2	0	3	0	0	0	0	0
63	46	2	4	3	0	1	4	1	1	1	18	5	1	2	0	0	0	0	0
64	57	2	2	2	0	3	4	1	1	1	19	2	0	3	2	1	2	0	1
65	47	2	2	2	0	3	4	1	1	1	13	6	1	#NULL!	0	0	0	0	0
66	52	2	4	2	0	1	4	1	1	1	6	0	0	3	1	1	1	0	1
67	52	2	4	2	0	1	4	1	0	0	83	2	0	1	0	0	0	0	0
68	73	2	3	2	0	3	4	1	0	0	88	3	0	#NULL!	1	3	3	0	1
69	58	2	4	2	0	2	4	1	1	1	12	3	0	3	1	2	2	0	1
70	62	1	3	2	0	2	4	1	1	1	59	2	0	3	1	2	2	1	1
71	64	2	1	0	0	1	1	0	1	1	27	0	0	2	1	2	2	0	1
72	71	2	1	3	0	3	4	1	1	1	12	0	0	2	1	2	2	1	1
73	63	1	4	2	1	2	4	0	1	1	9	0	0	1	0	0	0	0	0
74	50	2	4	2	0	2	4	1	1	1	0	1	0	3	0	0	0	0	0
75	62	2	2	2	0	3	4	1	1	1	30	2	0	2	0	0	0	0	0
76	59	2	4	0	0	3	4	0	1	1	50	0	0	1	1	2	2	1	1
77	65	2	3	2	0	1	4	1	1	1	48	0	0	2	1	2	2	1	1
78	55	1	4	0	0	2	4	1	1	2	97	0	0	1	0	0	0	0	0
79	62	1	4	2	0	1	4	0	1	1	12	0	0	3	0	0	0	0	0
80	47	2	4	2	0	3	4	1	1	1	18	0	0	3	1	2	2	0	1
81	62	1	3	2	0	3	4	1	1	1	9	3	0	2	2	2	4	1	1
82	64	2	3	2	0	1	4	1	1	1	9	1	0	2	0	0	0	0	0
83	61	2	3	2	0	2	4	1	1	1	43	5	1	3	0	0	0	0	0
84	61	2	4	3	0	2	4	1	1	1	7	0	0	1	0	0	0	0	0
85	66	1	4	2	0	2	4	1	1	1	49	2	0	2	1	3	3	1	1
86	53	2	3	2	0	2	4	0	1	1	8	0	0	2	0	0	0	0	0
87	80	2	3	3	1	3	4	0	1	1	4	6	1	3	2	3	6	1	1
88	72	2	4	1	0	3	4	0	1	1	3	0	0	1	0	0	0	0	0
89	70	1	3	0	0	2	3	0	1	1	60	2	0	2	2	2	4	1	1
90	62	2	4	2	0	3	4	1	1	1	30	0	0	3	1	1	1	0	1
91	52	2	3	3	0	2	4	1	1	1	21	3	0	3	1	1	1	1	1
92	49	2	4	3	0	2	4	1	1	1	27	2	0	2	0	0	0	0	0
93	79	1	2	2	0	3	4	1	1	1	11	3	0	3	2	3	6	1	1
94	58	2	3	2	0	3	4	1	1	1	9	0	0	2	0	0	0	0	0
95	52	1	3	0	0	3	3	0	1	1	14	2	0	2	2	3	6	1	1

Appendix 3. Concentrations of CDDP, 5-FU and HCQ used in the combinatorial drug assays. The cell lines JHU029, HTB-43, CCL-138, and SCC-25 were used to perform the assays.

	CDDP			5FU			HCQ		
Cell lines	C1 (μM)	C2 (μM)	C3 (μM)	C1 (μM)	C2 (μM)	C3 (μM)	C1 (μM)	C2 (μM)	C3 (μM)
JHU029	1	1.5	2	0.5	1	2	25	40	60
HTB-43	3	5	7	15	30	60	25	40	60
CCL-138	3	5	7	15	30	60	25	40	60
SCC-25	3	5	7	15	30	60	200	300	400

Appendix 4. Proteins identified in the proteomic study. The following table contains information regarding protein ID (Swiss-Prot accession number), protein name, coverage (the percentage of sequence identified), Mascot Score, protein groups, unique peptides identified, total of peptides identified, number of amino acids in the protein sequence, molecular weight and calculated isoelectric point of the 1535 proteins identified considering the 3 groups of cells (CCL-138, CCL-138-R and CCL-138 CSCs). The quantifications were performed as the ratio between each sample and the normalization sample (pool).

Supplementary table will be available in ProteomeXchange Consortium, <https://www.ebi.ac.uk/pride/>, dataset identifier PXD020159, filename “Proteins identified”. Currently, the data is private and can only be accessed with the following access data. Username: reviewer72792@ebi.ac.uk; password: Wus17VVI

Appendix 5. ANOVA test to determine proteins significantly dysregulated between CCL-138, CCL-138-R and CCL-138 CSCs. For the statistical analyses presented below, only the specific proteins present in at least 2 out of 3 replicates of each of the conditions analyzed were considered. A one-way ANOVA to find significant differences among groups with a p-value correction for multiple comparisons test of Benjamini-Hochberg was applied. This resulted in 478 significant ($p < 0.05$) proteins, which indicated that a high number of the proteins between groups could be different. Then, a Fold change of 1.1 was applied to the protein list obtained before and 476 out of 478 proteins passed the applied Fold change (FC) cut-off. Negative signs mean proteins downregulated and no signs mean proteins upregulated.

Supplementary table will be available in ProteomeXchange Consortium, <https://www.ebi.ac.uk/pride/>, dataset identifier PXD020159, filename “ANOVA”. Currently, the data is private and can only be accessed with the following access data. Username: reviewer72792@ebi.ac.uk; password: Wus17VVI

Appendix 6. Post-Hoc analysis, which shows the differences observed in protein expression between CCL-138-R and CCL-138 cells; and CCL-138 CSCs and CCL-138 cells. The proteins differentially expressed between CCL-138-R and CCL-138 cells (262 proteins), and CCL-138 CSCs and CCL-138 cells (362

proteins) were rearranged based on their Fold Change (FC), taking as cut-off those with $FC \geq 1.6$ (green color) and $FC \leq -1.4$ (blue color). For the subsequent selection of tetraspanin 1 (O60635) as a potential target protein involved in CDDP-resistance, it was considered that this protein was overexpressed in both CCL-138 CSCs and CCL-138-R cells. Furthermore, an exhaustive analysis of its potential clinical implications was carried out. Proteins were ordered from highest to lowest FC. Negative signs of FC mean downregulated proteins and no signs mean proteins upregulated. P(Corr), P corrected value.

Supplementary tables will be available in ProteomeXchange Consortium, <https://www.ebi.ac.uk/pride/>, dataset identifier PXD020159, filename “Post-Hoc (R(CDDP))” and “Post-Hoc (CSCs)” respectively. Currently, the data is private and can only be accessed with the following access data. Username: reviewer72792@ebi.ac.uk; password: Wus17VVI

Appendix 7. Proteins commonly deregulated in CCL-138-R cells and CSCs versus CCL-138 cells. The 12 upregulated proteins are highlighted in yellow and the 24 downregulated proteins are highlighted in green.

		FC ([Resistant CDDP] vs [Parentals])	FC ([CSC G1] vs [Parentals])
O43653	Prostate stem cell antigen	4,25	2,77
O00560	Syntenin-1	3,30	1,78
P25815	Protein S100-P	3,12	2,06
Q9BPW9	Dehydrogenase/reductase SDR family member 9	2,49	3,71
O60635	Tetraspanin-1	2,45	2,66
P08174	Complement decay-accelerating factor	2,22	1,67
P07476	Involucrin	2,21	2,22
P31947	14-3-3 protein sigma	2,19	2,73
O95171	Sciellin	2,06	4,07
P55786	Puromycin-sensitive aminopeptidase	1,81	1,74
P03973	Antileukoproteinase	1,74	2,45
Q8TCT9	Minor histocompatibility antigen H13	1,61	1,80
		FC ([Resistant CDDP] vs [Parentals])	FC ([CSC] vs [Parentals])
P07099	Epoxyde hydrolase 1	-1,42	-2,75
P49321	Nuclear autoantigenic sperm protein	-1,44	-1,69
P34897	Serine hydroxymethyltransferase, mitochondrial	-1,46	-1,43
P50454	Serpin H1	-1,46	-1,44
P21980	Protein-glutamine gamma-glutamyltransferase 2	-1,47	-1,51
O94875	Sorbin and SH3 domain-containing protein 2	-1,47	-2,54
P16403	Histone H1.2	-1,50	-2,13
P05023	Sodium/potassium-transporting ATPase subunit alpha-1	-1,53	-1,41
Q3LXA3	Trikinase/FMN cyclase	-1,53	-1,62
P09874	Poly [ADP-ribose] polymerase 1	-1,55	-1,49
O95810	Caveolae-associated protein 2	-1,59	-1,82
Q8N684	Cleavage and polyadenylation specificity factor subunit 7	-1,59	-1,41
P16401	Histone H1.5	-1,60	-2,10
P00326	Alcohol dehydrogenase 1C	-1,63	-4,15
Q96RQ3	Methylcrotonoyl-CoA carboxylase subunit alpha, mitochondrial	-1,64	-1,61
P35611	Alpha-adducin	-1,65	-2,24
Q9H8H3	Methyltransferase-like protein 7A	-1,70	-2,06
P52701	DNA mismatch repair protein Msh6	-1,71	-1,54
Q9UBQ5	Eukaryotic translation initiation factor 3 subunit K	-1,72	-2,20
O43175	D-3-phosphoglycerate dehydrogenase	-1,76	-2,27
P30838	Aldehyde dehydrogenase, dimeric NADP-preferring	-1,92	-1,61
Q9NPH2	Inositol-3-phosphate synthase 1	-2,60	-2,61
P43003	Excitatory amino acid transporter 1	-3,79	-5,49
P00352	Retinal dehydrogenase 1 (GEN: ALDH1A1)	-6,27	-2,83

PUBLICATIONS

X. PUBLICATIONS

Published articles:

1. J.G. Alvarez-Meythaler, **Y. Garcia-Mayea**, C. Mir, H. Kondoh and L.L. ME, Autophagy takes centre stage as a possible cancer hallmark, *Frontiers in Oncology*, (2020). DOI: 10.3389/fonc.2020.586069. **IF: 4.848** (2019).
2. A. Feliciano, L. González, **Y. Garcia-Mayea**, C. Mir, M. Artola, N. Barragán, R. Martín, A. Altés, J. Castellvi, S. Benavente, S. Ramón Y Cajal, M. Espinosa-Bravo, J. Cortes, I. T Rubio and L.L. ME, Five microRNAs in serum are able to differentiate breast cancer patients from healthy individuals, *Frontiers in Oncology*, (2020). DOI: 10.3389/fonc.2020.586268. **IF: 4.848** (2019).
3. **Y. Garcia-Mayea**, C. Mir, L. Munoz, S. Benavente, J. Castellvi, J. Temprana, V. Maggio, J. Lorente, R. Paciucci, L.L. ME, Autophagy inhibition as a promising therapeutic target for laryngeal cancer, *Carcinogenesis*, (2019). DOI: 10.1093/carcin/bgz080. **IF: 4.603** (2019).
4. **Y. Garcia-Mayea**, C. Mir, F. Masson, R. Paciucci, L.L. ME, Insights into new mechanisms and models of cancer stem cell multidrug resistance, *Seminars in cancer biology*, (2019). DOI: 10.1016/j.semcancer.2019.07.022. **IF: 11.090** (2019).
5. E. Abad, **Y. Garcia-Mayea**, C. Mir, D. Sebastian, A. Zorzano, D. Potesil, Z. Zdrahal, A. Lyakhovich, M.E. Lleonart, Common Metabolic Pathways Implicated in Resistance to Chemotherapy Point to a Key Mitochondrial Role in Breast Cancer, *Mol Cell Proteomics*, 18 (2019) 231-244. DOI: 10.1074/mcp.RA118.001102. **IF: 4.870** (2019).
6. Lorente, C. Velandia, J.A. Leal, **Y. Garcia-Mayea**, A. Lyakhovich, H. Kondoh, L.L. ME, The interplay between autophagy and tumorigenesis: exploiting autophagy as a means of anticancer therapy, *Biol Rev Camb Philos Soc*, 93 (2018) 152-165. DOI: 10.1111/brv.12337. **IF: 10.288** (2018).

Publications

7. R. Said, **Y. Garcia-Mayea**, N. Trabelsi, N. Setti Boubaker, C. Mir, A. Blel, N. Ati, R. Paciucci, J. Hernandez-Losa, S. Rammeh, A. Derouiche, M. Chebil, L.L. ME, S. Ouerhani, Expression patterns and bioinformatic analysis of miR-1260a and miR-1274a in Prostate Cancer Tunisian patients, *Mol Biol Rep*, (2018). DOI: 10.1007/s11033-018-4399-x. **IF: 2.107** (2018).
8. **Y. Garcia-Mayea**, A. Feliciano, L. Jubierre, C. Mir, M. Hummel, J. Castellvi, J. Hernandez-Losa, R. Paciucci, I. Sansano, Y. Sun, Y.C.S. Ramon, H. Kondon, A. Soriano, M. Segura, A. Lyakhovich, L.L. ME, miR-99a reveals two novel oncogenic proteins E2F2 and EMR2 and represses stemness in lung cancer, *Cell Death Dis*, 8 (2017) e3141. DOI: 10.1038/cddis.2017.544. **IF: 5.638** (2017).
9. A. Carnero, **Y. Garcia-Mayea**, C. Mir, J. Lorente, I.T. Rubio, L.L. ME, The cancer stem-cell signaling network and resistance to therapy, *Cancer Treat Rev*, 49 (2016) 25-36. DOI: 10.1016/j.ctrv.2016.07.001. **IF: 8.885** (2016).

Submitted articles:

1. **Y. Garcia-Mayea**, C. Mir, L. Carballo, J. Castellvi¹, J. Temprana-Salvador, J. Lorente, S. Benavente, J.M. Garcia-Pedrero, E. Allonca, J.P. Rodrigo, L.L. ME, TSPAN1: a novel protein involved in Head and Neck Squamous Cell Carcinoma chemoresistance. *Cancers*, (2020). Under review (Ref: cancers-942889). **IF: 6.126** (2019).